Light absorption by carbonaceous aerosols over the Amazon rain forest

Dissertation

zur Erlangung des Grades

'Doctor rerum naturalium (Dr. rer. nat.)'

im Promotionsfach Chemie

am Fachbereich Chemie, Pharmazie und Geowissenschaften

der Johannes Gutenberg-Universität in Mainz

Paul Crutzen Graduate School (PCGS)

Jorge Luis Saturno Iribarren

geb. am 27.02.1984 in San Felipe, Yaracuy, Venezuela

Mainz, 2018

I hereby declare that I wrote the dissertation submitted without any unauthorized external assistance and used only sources acknowledged in the work. All textual passages which are appropriated verbatim or paraphrased from published and unpublished texts as well as all information obtained from oral sources are duly indicated and listed in accordance with bibliographical rules. In carrying out this research, I complied with the rules of standard scientific practice as formulated in the statutes of Johannes Gutenberg-University Mainz to insure standard scientific practice.

Mainz, 16. Januar 2018.

Everything flows, nothing stands still.

–Heraclitus

Abstract

Assessing the role of atmospheric aerosol particles in the Earth system prior to the man-made perturbations of the industrial era has been a key research topic in the last decades. The climate response to direct and indirect radiative effects by aerosol particles is still not well understood. Consequently, studying the current anthropogenic perturbations to the natural aerosol cycling has become an important task. The Amazon rain forest is one of the few continental locations where the atmosphere can be near-pristine to pristine during certain periods. Man-made biomass burning (BB) due to agricultural expansion is considered the largest source of pollution to the Amazonian atmosphere. Biomass burning emits large amounts of light absorbing aerosol particles like black carbon (BC). The BB contributions to the Amazonian aerosol burden are not only regional but also transatlantic, with African savannah and woodland emissions being seasonally significant.

A comprehensive aerosol instrumentation setup has been used at the Amazon Tall Tower Observatory (ATTO) in central Amazonia to continuously measure the aerosol's physical and chemical properties. The optical measurements comprise light scattering and absorption measurements. Additionally, microscopy, chemical and particle sizing techniques have been used to characterize and measure the aerosol properties on a long-term basis. The combination of systematic field measurements at ATTO and dedicated modeling studies as presented here provides a robust long-term data set of aerosol optical properties. Specifically, the contribution of light-absorbing organic aerosol particles — so-called 'brown carbon' (BrC) — is compared to BC in the context of BB-dominated regimes. The occurrence of El Niño Southern Oscillation (ENSO) in its positive phase in 2015 caused drought in the Amazon Basin. Consequently, more frequent fire events occurred in the forest and its peripheries. The increased BB emissions affected the aerosol optical properties and near-by fire emissions allowed the observation of enhanced BrC contribution to light absorption. Long-range transport of African air masses to the Amazon rain forest was also studied by analyzing a particular volcanic emission event in the Congo. The transatlantic transport of the volcanogenic sulfur plume was traced by transport models and observed by satellite, ground-based and airborne measurements. This episode is considered an exemplary case of transatlantic aerosol transport that helps to understand the African contribution to the Amazonian aerosol population.

This dissertation provides new substantial insights into the role and relevance of atmospheric aerosols in the Amazon region. Different absorption measurement techniques are evaluated and inter-compared. The results represented here will serve as a basis for follow-up studies on particle mixing state as well as the transport and life cycle of light-absorbing aerosol particles in central Amazonia. In addition, the results contribute to a better understanding of the influence of ENSO on the Amazonian atmosphere, offering prospects to warmer and drier scenarios. Finally, this work may help to constrain the role of absorbing aerosols in the Earth's climate system.

Zusammenfassung

Die Untersuchung des natürlichen, atmosphärischen Aerosols und seiner Bedeutung für das Erdsystem vor dem Einsetzen einer anhaltenden, anthropogenen Veränderung im Zuge der Industrialisierung ist ein Forschungsschwerpunkt der letzten Jahrzehnte. Bislang sind die Auswirkungen des direkten und indirekten Strahlungseffekts durch Aerosolpartikel auf das Erdklima nicht ausreichend verstanden. Daher gewinnen Untersuchungen aktueller, anthropogener Veränderungen des natürlichen Aerosolkreislaufs zunehmend an Bedeutung. Der Amazonas-Regenwald ist einer der wenigen kontinentalen Orte, an denen die atmosphärische Zusammensetzung für gewisse Zeiträume nahezu oder gar vollständig natürlichen Ursprungs ist. Anthropogene Biomassenverbrennung (BB, biomass burning) zur Gewinnung von landwitschaftlichen Nutzflächen stellt eine der größten Quellen von Luftverschmutzung im Amazonasgebiet dar. Bei der Verbrennung von Biomasse entstehen große Mengen lichtabsorbierender Aerosolpartikel wie beispielsweise Ruß (BC, black carbon). Aerosolpartikel aus Biomassenverbrennung im Amazonas stammen jedoch nicht ausschließlich aus regionalen Quellen. Einen substanziellen sowie saisonal unterschiedlich ausgeprägten transatlantischen Beitrag liefern auch Emissionen aus afrikanischen Savannen und Waldgebieten.

Zur Untersuchung der physikalischen und chemischen Eigenschaften von Aerosolpartikeln wurde ein umfangreicher Aufbau von Aerosolmessgeräten am ‚Amazon Tall Tower' Observatorium (ATTO) eingesetzt. Die Messungen optischer Eigenschaften umfassen Lichtstreuung und Absorption. Zusätzlich wurden Langzeitmessungen der Partikeleigenschaften mit Hilfe von Mikroskopie, verschiedener chemischer Verfahren und Techniken zur Bestimmung der Partikelgröße durchgeführt. Die Kombination aus systematischen Feldmessungen an ATTO mit dedizierten Modellstudien in der hier vorliegenden Arbeit bietet eine belastbare Datengrundlage zur Charakterisierung der optischen Aerosoleigenschaften. Im speziellen wurde der Beitrag lichtabsorbierender, organischer Aerosolpartikel – sogenannter ‚brauner' Kohlenstoff (BrC, brown carbon) – mit BC-Partikeln unter Biomassenverbennung-dominierten Bedingungen verglichen. Das Auftreten eines ausgeprägten El Niño Phänomens (El Niño Southern Oscillation, ENSO) verursachte 2015 eine ausgedehnte Dürre im Amazonasbecken. Dies führte zu einer erhöhten Aktivität von athropogenen Feuern im Regenwald und seiner angrenzenden Gebiete. Die verstärkte Emission von Aerosol aus Biomassenverbrennung beeinflusste die optischen Aerosoleigenschaften. Emissionen in unmittelbarer Nähe der Messstation zeigten einen erhöhten Anteil von BrC an den lichtabsorbierenden Partikeln. Ebenfalls wurde der Ferntransport afrikanischer Luftmassen in das Gebiet des Amazonas anhand von Vulkanemissionen im Kongo untersucht. Hierbei wurde der transatlantische Transport einer durch einen Vulkan emittierten, schwefelhaltigen Abgasfahne mit Hilfe von Transportmodellen verfolgt und durch Satelliten-, Boden- und Flugzeugmessungen nachgewiesen. Dieses Ereignis steht exemplarisch für den transatlatischen Transport von Aerosol und trägt dazu bei die Bedeutung des Eintrags afrikanischen Aerosols in den Amazonas-Regenwald zu verstehen.

In dieser Dissertation werden neue, grundlegende Erkenntnisse über die Funktion und Bedeutung des atmosphärischen Aerosols im Amazonasgebiet präsentiert. Verschiedene Verfahren zur Messung von Aerosolabsorption wurden evaluiert und verglichen. Die dargestellten Ergebnisse stellen eine Grundlage für weitere Folgestudien zum Mischungszustand, Transport und Lebenszyklus von lichtabsorbierenden Aerosolpartikeln im Zentralamazonas dar. Die in dieser Arbeit gewonnen Erkenntnisse zum Einfluss von ENSO auf die Amazonasatmosphäre geben einen Ausblick auf mögliche Szenarien unter wärmeren und trockeneren Bedingungen. Abschließend können die Ergebnisse dieser Arbeit dazu beitragen die Bedeutung absorbierender Aerosolpartikel für das Erdklimasystem besser zu verstehen.

Contents

1. Introduction

1.1. The global change context

By the end of the 19th century, with the European industrialization and subsequent socio-economical transformations in many parts of the world, the natural cycles were perturbed by strong industry-related pollutants that became important inputs to the atmosphere, cryosphere, hydrosphere, lithosphere, and biosphere, affecting the interactions among these systems. The human impact on natural ecosystems has been proposed to be comparable to a geological force (Crutzen, 2002). Given the magnitude of the change and its geological implications, a change of geological epoch has been suggested. Despite the critiques that arose from social and political sciences regarding this new epoch's naming — *Anthropocene* — (Schulz, 2017; Heise, 2016), the stratigraphic marker is still a matter of debate (Finney and Edwards, 2016). Recently, 'spheroidal carbonaceous particles' have been suggested as such marker (Swindles et al., 2015) given the massive emission of this kind of particles emitted by fossil fuel (FF) combustion after the 'Great acceleration', around AD 1950. Understanding how the present-day polluted atmosphere compares to the pre-industrial conditions in terms of aerosol particles is still a pending task in climate research (Andreae, 2007). Important part of the atmospheric aerosol particles are emitted by biomass burning (BB) and can be transported long distances (Andreae and Merlet, 2001). This kind of emissions include black and brown carbon (BC and BrC, respectively), which are able to absorb radiation and warm the atmosphere (Andreae and Gelencsér, 2006). This work focuses on analyzing the role of the BC and BrC over the near-pristine Amazon rain forest, especially by studying their sources and transformations during atmospheric transport.

1.2. Aerosol optical properties

The most important light-absorbing aerosol particle is BC, or soot carbon, which is emitted by incomplete combustion of fossil fuels (FF) and biomass and consists of refractive graphitic-like particles. Usually, BC particles are emitted as very fine particles and they have the property to absorb radiation very efficiently. Black carbon is considered the second-largest anthropogenic forcing agent, just after CO_2 (Bond et al., 2013). Furthermore, biomass burning emits BC together with high amounts of organic carbon (OC). The OC mass fraction is much greater than the BC one, especially in the case of open smoldering combustion fires (Andreae and Gelencsér, 2006). The OC has been commonly considered a 'scattering aerosol', i.e., particles that cool the atmosphere.

However, a fraction of OC aerosol particles are also able to absorb radiation, being a significant contributor to light absorption (Andreae and Gelencsér, 2006). These light-absorbing OC aerosols are the so-called 'brown carbon'. Including the BrC contribution in the global or regional radiative transfer models requires a better understanding of their optical properties in ambient conditions.

Another light-absorbing aerosol is mineral dust, whose absorption is more relevant at shorter wavelengths although its contribution is small in comparison to BC (Haywood and Boucher, 2000). It has also been suggested that there is a fraction of the bio-aerosols (primary biological aerosol particles, PBAP), which could also contribute to light absorption in the coarse mode (Després et al., 2012). Partitioning the different contributions to light absorption by aerosols is not a straightforward task. The optical instruments used at present to measure light absorption coefficients by aerosols typically measure at only one wavelength, which makes it difficult to distinguish between the different contributors. However, some instruments that measure absorption at different wavelengths are available, and some approaches are being implemented to use the wavelength-dependence function of the different light-absorbing aerosols to estimate the contribution by each of them (Sandradewi et al., 2008).

Furthermore, the BC light absorption can be enhanced when the aerosol particle is internally mixed with other kinds of aerosols, like sulfate or organics. Laboratory measurements have resulted in an enhancement factor of 2 (Bond and Bergstrom, 2006). However, ambient measurements indicate that this enhancement factor is quite variable (Lack et al., 2012; Cappa et al., 2012; Pokhrel et al., 2017). This fact has been attributed to the location of the absorbing material in the aerosol particle, with a centered core-shell configuration producing the maximum absorption enhancement. An Amazonian ambient aerosol microscopy study has indicated that the BC particles are embedded in aged particles consisting of inorganic salts and secondary organic material where BC is not necessarily located at the core of the particle (Pöhlker et al., 2014).

The Absorption Ångström Exponent (AAE) is used to describe the power-law dependence of light absorption by aerosol particles. Freshly FF emitted uncoated BC has an AAE of 1 (Bond and Bergstrom, 2006). On the other hand, BrC's light absorption has been shown to be strongly wavelength dependent, with higher AAE values up to 7 (Hoffer et al., 2006). Several studies have used this difference in AAE between BC and BrC to apportion the contribution by each of these LAC types (Sandradewi et al., 2008; Favez et al., 2010). However, the assumption of a wavelength independent AAE = 1 of BC has been questioned since AAE depends on the size of the particle and its mixing state (Moosmüller et al., 2011). Given this, a novel approach that addresses this issue has been proposed (Wang et al., 2016b), which uses Mie-theory modeled data for coated and uncoated BC to retrieve a better estimate of the AAE. Further, the theoretical BC AAE is subtracted from the ambient measured AAE to retrieve the BrC contribution. This approach can be used when multi-wavelength absorption measurements are available. In the case of this PhD study, a comprehensive instrumentation has been used to attain the aerosol light absorption and its wavelength dependence. An Aethalometer has been used to measure light attenuation online at seven different wavelengths in the UV and

visible spectral regions. Additionally, a Multi-Angle Absorption Photometer (MAAP), which measures light absorption online by implementing detectors in the forward and backward hemispheres, has been useful to correct the Aethalometer measurements for multiple scattering effects. The multiple wavelength compensation of Aethalometer measurements has been done by comparing to an offline laboratory instrument, the Multi-Wavelength Absorbance Analyzer (MWAA). A descriptive diagram of the different absorption measurement techniques used in this study is presented below.

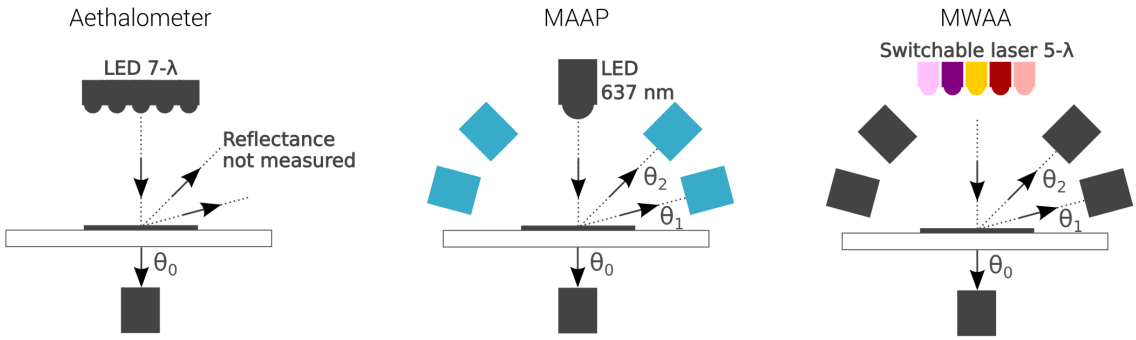

Figure 1.1.: *Simplified diagram of the Aethalometer, MAAP, and MWAA measurement techniques.*

Given the well-known absorption spectral properties of BC, the light absorption enhancement in the UV and near-UV spectral region, expressed as an increased AAE, can be used to retrieve the BrC contribution to light absorption by aerosol particles. In this study, we use a two different Aethalometer wavelength pairs (370-950 nm and 660-950 nm) to retrieve what is called the "wavelength dependence of the AAE" (WDA), and then calculate the BrC light absorption coefficient (Wang et al., 2016b). Details about these calculations and the models used in this work are presented in Appendix B.2.

1.3. Aerosol particles over the Amazon Basin

The Amazonian atmosphere is characteristically influenced by PBAP (Pöschl et al., 2010), which dominate the coarse mode fraction, and secondary organic aerosol (SOA) that is produced by photochemical reactions of precursor gases that could be biogenic (Claeys et al., 2004) or BB emitted. Therefore, the majority of aerosol particles over the Amazon rain forest are of organic composition (Pöschl et al., 2010; Andreae et al., 2015). The input of inorganic aerosol particles could also have biogenic origin (Pöhlker et al., 2012) but remote sources like Atlantic Ocean sea-salt, Saharan dust (Moran-Zuloaga et al., 2017) and biomass burning (Wang et al., 2016a) are among the most important non-biogenic aerosol sources.

The long-range transport of aerosol particles to the Amazon Basin is defined by the meteorological conditions, particularly the location of the Inter-Tropical Convergence Zone (ITCZ). Eastern trade winds bring African and oceanic aerosol particles and gas precursors to the Amazonian atmosphere. During the wet season (February to May),

winds from northern Africa can reach the Amazon Basin, when the ITCZ is located at its southernmost position in South America. These air masses episodically bring Saharan mineral dust and fire emissions from the sub-Sahelian savannahs. This season, is usually the one that offers the opportunity to study background aerosol particles under near-pristine to pristine conditions because wet scavenging efficiently removes most of the aerosol particles. When the ITCZ shifts north, between August and November (dry season), fires are initiated in the agricultural areas in South America and BB emissions from southern Africa are transported over the South Atlantic Ocean. This time of the year offers the opportunity to study the influence of BB over the background conditions and the difference between various aging states of BB aerosol particles.

The measurements presented here were done at the Amazon Tall Tower Observatory (ATTO) (S 02° 08' W 58° 59'), located in the Amazon rain forest in Brazil, 150 km northeast of the city of Manaus. The site is mostly influenced by air masses coming from untouched forest areas, especially during the wet season (Feb-May). Air masses travel over important BB emission areas in the south of the Amazon Basin during the dry season (Aug-Nov). Modelled backward air mass trajectories (Fig. 1.3) illustrate the most important source regions that feed the central Amazonia's atmosphere during the wet and the dry seasons. A detailed site description and instrumentation list can be found elsewhere (Andreae et al., 2015).

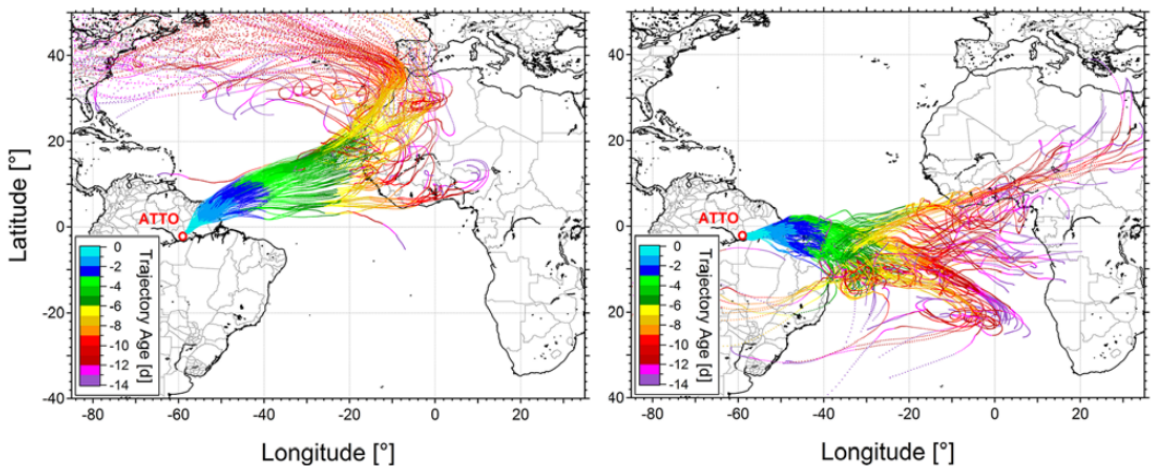

Figure 1.2.: *Fourteen-day backward air mass trajectory ensembles started at the ATTO site in central Amazonia at 1000 m above ground level. The color code indicates the trajectory age in days. The trajectories were calculated for the March 2014 (left panel), wet season, and September 2014 (right panel), dry season, using the Hybrid Single-Particle Lagrangian Integrated Trajectory Model (HYSPLIT), developed by the National Oceanic and Atmospheric Administration (NOAA), available at http://www.arl.noaa.gov/ss/models/hysplit.html. Adapted from (Pöhlker et al., 2017).*

1.4. Research objectives

The main goal of this study was to understand the optical properties of aerosol particles over the Amazon rain forest and the role that long-range transport sources play in it. The main perturbations of the Amazonian atmosphere originate from land use change — associated with increased biomass burning emissions (Artaxo et al., 2013) — and from global change, which directly affects the ecological conditions of the Amazon forest and also remote areas that are sources to the Amazonian atmosphere. The study of aerosol particles in remote Amazon forest areas is important to understand the pre-industrial behavior of atmospheric aerosols and offers the opportunity to investigate the interactions between anthropogenic and biogenic aerosols. In this context, LRT of aerosol particles needs to be addressed in order to properly characterize the natural Amazonian atmosphere aerosol cycling. Different specific goals, related to this main objective are described below.

- Improvement of the inter-comparability of different absorption measurement techniques. An algorithm to compensate Aethalometer data for different artifacts was developed and evaluated based on laboratory analysis of field collected samples.
- Determination of the BC aerosol mass absorption cross-section in the different Amazonian seasons. The refractive BC (rBC) mass was measured by means of a laser-induced incandescence technique that was used together with light absorption coefficient data to calculate the MAC of BC particles.
- Study the interannual variability of BB aerosol optical properties, especially under the influence of El Niño Southern Oscillation (ENSO).
- Estimation of the BrC contribution to light absorption by aerosol particles by using modeled BC spectral light absorption.
- Evaluation of the impact of African aerosol sources with special focus on the optical properties of these remotely emitted aerosol particles.

2. Results and conclusions

2.1. Overview

The results of this dissertation are described in three manuscripts for peer-reviewed publications in international scientific journals. The manuscripts are attached in Appendix B of this manuscript. One of them has already been published, and two others were already submitted for peer-review. The main results and conclusions of each study are summarized below.

2.2. Individual studies

2.2.1. Aethalometer measurement compensation

Aethalometer attenuation measurements require compensation for multiple scattering and filter loading effects in order to retrieve light absorption coefficients. Compensation algorithms use concomitant light scattering measurements and a reference absorption measurement for calculating the corresponding compensation factors. In this study, two different algorithms were evaluated and compared to a reference multi-wavelength technique. One of the algorithm was found to be the most appropriate to retrieve compensated absorption coefficients and AAE. The results also indicated that the raw attenuation Ångström exponent of the Aethalometer model AE31 is a good approximation to the AAE values measured by the reference absorption technique. For details see Appendix B.1: Saturno et al., *Atmospheric Measurement Techniques*, 2017.

2.2.2. Black and brown carbon over the Amazon rain forest

Regional and remotely emitted BB aerosol particles reach the Amazon Basin permanently. During the wet season (February to May), a significant part of the aerosol particles is removed by wet scavenging and fire activity in the Amazonian forest and its peripheries is at its minimum. However, during the dry season (August to November), African and South American fire emissions are observed over the Amazon rain forest. The light absorbing aerosol that reaches the ATTO site is mostly aged after atmospheric transport. This aging process enhances the absorption of BC by the lensing effect caused by different coatings that cover the BC aerosol particles. Additionally, the BrC absorption

efficiency weakens upon transport by oxidation of the chemical components responsible for its light absorption. Only under the influence of El Niño, which made drought periods last longer at the end of the dry season 2015, local fire emissions were an important source of BrC with enhanced near-UV absorption. This article provides the longest data set available of Amazon rain forest aerosol optical properties. For details see Appendix B.2: Saturno et al., *Atmospheric Chemistry and Physics Discussions*, 2017a.

2.2.3. Long-range transport of volcanogenic aerosol particles to the Amazon rain forest

Volcanogenic sulfur emissions from southern Africa have been observed by satellite measurements, especially during large explosive events at the Nyamuragira-Nyiragongo volcanic system in the Democratic Republic of Congo. Transport models indicate that the volcanic SO_2 plume was transported over the South Atlantic Ocean and reached the Amazon Basin after 10 to 15 days. Ground-based measurements at the ATTO site showed an enhanced sulfate aerosol mass concentration between 21 September and 01 October 2014 compared to the dry-season average. The arrival of the volcanogenic aerosol plume to ground-level altitudes affected the aerosol optical properties and their hygroscopicity. In addition to the ground-based measurements, airborne observations over the Amazon Basin indicated that the African volcanic plume arrived at an altitude of 4 to 5 km. Beyond the particular effects of the volcanogenic sulfur aerosol, this case study can help to understand the transatlantic transport of different aerosol particles from Africa to South America. For details see Appendix B.3: Saturno et al., *Atmospheric Chemistry and Physics Discussions*, 2017b.

2.2.4. Summary and outlook

The main findings of this study are related to the characterization of the aerosol optical properties at the ATTO site under different conditions. The present study provides a comprehensive analysis of long-term optical property measurements in central Amazonia. The seasonal and episodic conditions of the atmosphere over the Amazon rain forest from 2012 to 2017 allowed the observation of light-absorbing aerosol particles at different aging stages. The aerosol absorption wavelength dependence, expressed as the AAE, has been found to vary slightly between the seasons and to increase significantly under the influence of near-by BB emissions. This enhancement in the AAE is caused by the presence of BrC. Under the influence of El Niño, associated with intense droughts, the BrC contribution increased to its highest values at the end of 2015. Remote BB aerosol particles from southern Brazil and Africa were found to be less loaded with BrC, most likely due to the action of aging processes during transport. The African contribution to the Amazonian atmospheric aerosol burden has been found to be more important than expected. Our findings indicate that efficient transatlantic transport occurs all through the year bringing different kinds of aerosol particles to the Amazon Basin, including

savannah and woodland fire emissions, mineral dust and volcanogenic aerosol particles. The volcanogenic particles were only observed during a very strong explosive emission by the Nyamuragira-Nyiragongo volcanic system in the Congo.

Further research is required to understand the morphology and mixing state of the LAC particles over the Amazon and their interaction with PBAP and biogenic SOA. Additionally, light absorption measurement techniques can be improved by (i) measuring light absorption by suspended aerosol particles and (ii) assessing the role of coarse mode biogenic particles in light absorption. On the other hand, modeling studies should include different morphological features and conditions of the BC aggregates and their coatings.

The research presented here has led to three first-author papers and contributed to 8 further studies (published or under review in international scientific journals), which constitute the most recent and advanced studies that help to understand the aerosol cycling over the Amazon rain forest.

3. Bibliography

Andreae, M. O.: Aerosols before pollution, Science, 315, 50–51, doi:10.1126/science.1136529, 2007.

Andreae, M. O. and Gelencsér, A.: Black carbon or brown carbon? The nature of light-absorbing carbonaceous aerosols, Atmospheric Chemistry and Physics, pp. 3131–3148, 2006.

Andreae, M. O. and Merlet, P.: Emission of trace gases and aerosols from biomass burning, Global Biogeochemical Cycles, 15, 955–966, doi:10.1029/2000GB001382, 2001.

Andreae, M. O., Acevedo, O. C., Araùjo, A., Artaxo, P., Barbosa, C. G. G., Barbosa, H. M. J., Brito, J., Carbone, S., Chi, X., Cintra, B. B. L., da Silva, N. F., Dias, N. L., Dias-Júnior, C. Q., Ditas, F., Ditz, R., Godoi, A. F. L., Godoi, R. H. M., Heimann, M., Hoffmann, T., Kesselmeier, J., Könemann, T., Krüger, M. L., Lavric, J. V., Manzi, A. O., Lopes, A. P., Martins, D. L., Mikhailov, E. F., Moran-Zuloaga, D., Nelson, B. W., Nölscher, A. C., Santos Nogueira, D., Piedade, M. T. F., Pöhlker, C., Pöschl, U., Quesada, C. A., Rizzo, L. V., Ro, C.-U., Ruckteschler, N., Sá, L. D. A., de Oliveira Sá, M., Sales, C. B., dos Santos, R. M. N., Saturno, J., Schöngart, J., Sörgel, M., de Souza, C. M., de Souza, R. A. F., Su, H., Targhetta, N., Tóta, J., Trebs, I., Trumbore, S., van Eijck, A., Walter, D., Wang, Z., Weber, B., Williams, J., Winderlich, J., Wittmann, F., Wolff, S., and Yáñez-Serrano, A. M.: The Amazon Tall Tower Observatory (ATTO): Overview of pilot measurements on ecosystem ecology, meteorology, trace gases, and aerosols, Atmospheric Chemistry and Physics, 15, 10 723–10 776, doi:10.5194/acp-15-10723-2015, 2015.

Artaxo, P., Rizzo, L. V., Brito, J. F., Barbosa, H. M. J., Arana, A., Sena, E. T., Cirino, G. G., Bastos, W., Martin, S. T., and Andreae, M. O.: Atmospheric aerosols in Amazonia and land use change: from natural biogenic to biomass burning conditions, Faraday Discussions, doi:10.1039/c3fd00052d, 2013.

Bond, T. C. and Bergstrom, R. W.: Light Absorption by Carbonaceous Particles : An Investigative Review, Aerosol Science and Technology, 40, 27–67, doi:10.1080/02786820500421521, 2006.

Bond, T. C., Doherty, S. J., Fahey, D. W., Forster, P. M., Berntsen, T., DeAngelo, B. J., Flanner, M. G., Ghan, S., Kärcher, B., Koch, D., Kinne, S., Kondo, Y., Quinn, P. K., Sarofim, M. C., Schultz, M. G., Schulz, M., Venkataraman, C., Zhang, H., Zhang, S., Bellouin, N., Guttikunda, S. K., Hopke, P. K., Jacobson, M. Z., Kaiser, J. W., Klimont,

Z., Lohmann, U., Schwarz, J. P., Shindell, D., Storelvmo, T., Warren, S. G., and Zender, C. S.: Bounding the role of black carbon in the climate system: A scientific assessment, Journal of Geophysical Research: Atmospheres, 118, 5380–5552, doi: 10.1002/jgrd.50171, 2013.

Cappa, C. D., Onasch, T. B., Massoli, P., Worsnop, D. R., Bates, T. S., Cross, E. S., Davidovits, P., Hakala, J., Hayden, K. L., Jobson, B. T., Kolesar, K. R., Lack, D. a., Lerner, B. M., Li, S.-M., Mellon, D., Nuaaman, I., Olfert, J. S., Petäjä, T., Quinn, P. K., Song, C., Subramanian, R., Williams, E. J., and Zaveri, R. a.: Radiative absorption enhancements due to the mixing state of atmospheric black carbon., Science, 337, 1078–81, doi:10.1126/science.1223447, 2012.

Claeys, M., Graham, B., Vas, G., Wang, W., Vermeylen, R., Pashynska, V., Cafmeyer, J., Guyon, P., Andreae, M. O., Artaxo, P., and Maenhaut, W.: Formation of Secondary Organic Aerosols Through Photooxidation of Isoprene, Science, 303, 1173–1176, doi:10.1126/science.1092805, 2004.

Crutzen, P. J.: Geology of mankind, Nature, 415, 23–23, doi:10.1038/415023a, 2002.

Després, V., Huffman, J., Burrows, S. M., Hoose, C., Safatov, A., Buryak, G., Fröhlich-Nowoisky, J., Elbert, W., Andreae, M., Pöschl, U., and Jaenicke, R.: Primary biological aerosol particles in the atmosphere: a review, Tellus B: Chemical and Physical Meteorology, 64, 15 598, doi:10.3402/tellusb.v64i0.15598, 2012.

Favez, O., El Haddad, I., Piot, C., Boréave, A., Abidi, E., Marchand, N., Jaffrezo, J.-L., Besombes, J.-L., Personnaz, M.-B., Sciare, J., Wortham, H., George, C., and D'Anna, B.: Inter-comparison of source apportionment models for the estimation of wood burning aerosols during wintertime in an Alpine city (Grenoble, France), Atmospheric Chemistry and Physics, 10, 5295–5314, doi:10.5194/acp-10-5295-2010, 2010.

Finney, S. C. and Edwards, L. E.: The "Anthropocene" epoch: Scientific decision or political statement?, GSA Today, 26, 4–10, doi:10.1130/GSATG270A.1, 2016.

Haywood, J. and Boucher, O.: Estimates of the direct and indirect radiative forcing due to tropospheric aerosols: A review, Reviews of Geophysics, 38, 513, doi:10.1029/1999RG000078, 2000.

Heise, U. K.: The Environmental Humanities and the Futures of the Human, New German Critique, 43, 21–31, doi:10.1215/0094033X-3511847, 2016.

Hoffer, A., Gelencsér, A., Guyon, P., Kiss, G., Schmid, O., Frank, G. P., Artaxo, P., and Andreae, M. O.: Optical properties of humic-like substances (HULIS) in biomass-burning aerosols, Atmospheric Chemistry and Physics, 6, 3563–3570, doi:10.5194/acp-6-3563-2006, 2006.

Lack, D. a., Richardson, M. S., Law, D., Langridge, J. M., Cappa, C. D., McLaughlin, R. J., and Murphy, D. M.: Aircraft Instrument for Comprehensive Characterization of Aerosol Optical Properties, Part 2: Black and Brown Carbon Absorption and Absorption Enhancement Measured with Photo Acoustic Spectroscopy, Aerosol Science and Technology, 46, 555–568, doi:10.1080/02786826.2011.645955, 2012.

Moosmüller, H., Chakrabarty, R. K., Ehlers, K. M., and Arnott, W. P.: Absorption Ångström coefficient, brown carbon, and aerosols: basic concepts, bulk matter, and spherical particles, Atmospheric Chemistry and Physics, 11, 1217–1225, doi:10.5194/acp-11-1217-2011, 2011.

Moran-Zuloaga, D., Ditas, F., Walter, D., Araùjo, A. C., Brito, J., Carbone, S., Chi, X., Hrabe de Angelis, I., Lavrič, J. V., Ming, J., Pöhlker, M. L., Ruckteschler, N., Saturno, J., Wang, Y., Wang, Q., Weber, B., Wolff, S., Artaxo, P., Pöschl, U., Andreae, M. O., and Pöhlker, C.: Long-term study on coarse mode aerosols in the Amazon rain forest with the frequent intrusion of Saharan dust plumes, Atmospheric Chemistry and Physics Discussions, 2017.

Pöhlker, C., Wiedemann, K. T., Sinha, B., Shiraiwa, M., Gunthe, S. S., Smith, M., Su, H., Artaxo, P., Chen, Q., Cheng, Y., Elbert, W., Gilles, M. K., Kilcoyne, A. L. D., Moffet, R. C., Weigand, M., Martin, S. T., Pöschl, U., and Andreae, M. O.: Biogenic Potassium Salt Particles as Seeds for Secondary Organic Aerosol in the Amazon, Science, 337, 1075–1078, doi:10.1126/science.1223264, 2012.

Pöhlker, C., Saturno, J., Krüger, M. L., Förster, J.-D., Weigand, M., Wiedemann, K. T., Bechtel, M., Artaxo, P., and Andreae, M. O.: Efflorescence upon humidification? X-ray microspectroscopic in-situ observation of changes in aerosol microstructure and phase state upon hydration, Geophysical Research Letters, 41, 3681–3689, doi:10.1002/2014GL059409, 2014.

Pöhlker, C., Walter, D., Paulsen, H., Könemann, T., Moran-Zuloaga, D., Pickersgill, D., Ditas, F., Saturno, J., Lammel, G., Després, V. R., Artaxo, P., and Andreae, M. O.: Technical Note: Back trajectory analysis, land cover footprints, and future perturbation trends in the upwind fetch of the ATTO site in the central Amazon, Atmospheric Chemistry and Physics Discussions (in preparation), 2017.

Pokhrel, R. P., Beamesderfer, E. R., Wagner, N. L., Langridge, J. M., Lack, D. A., Jayarathne, T., Stone, E. A., Stockwell, C. E., Yokelson, R. J., and Murphy, S. M.: Relative importance of black carbon, brown carbon, and absorption enhancement from clear coatings in biomass burning emissions, Atmospheric Chemistry and Physics, 17, 5063–5078, doi:10.5194/acp-17-5063-2017, 2017.

Pöschl, U., Martin, S. T., Sinha, B., Chen, Q., Gunthe, S. S., Huffman, J. A., Borrmann, S., Farmer, D. K., Garland, R. M., Helas, G., Jimenez, J. L., King, S. M., Manzi, A., Mikhailov, E., Pauliquevis, T., Petters, M. D., Prenni, A. J., Roldin, P., Rose, D.,

Schneider, J., Su, H., Zorn, S. R., Artaxo, P., and Andreae, M. O.: Rainforest Aerosols as Biogenic Nuclei of Clouds and Precipitation in the Amazon, Science, 329, 1513–1516, doi:10.1126/science.1191056, 2010.

Sandradewi, J., Prévôt, A. S. H., Szidat, S., Perron, N., Alfarra, M. R., Lanz, V. a., Weingartner, E., and Baltensperger, U.: Using aerosol light absorption measurements for the quantitative determination of wood burning and traffic emission contributions to particulate matter., Environmental science & technology, 42, 3316–23, 2008.

Schulz, K.: Decolonising the Anthropocene: The Mytho-Politics of Human Mastery, in: Critical Epistemologies of Global Politics, edited by Woons, M. and Weier, S., p. 46, E-International Relations Publishing, Bristol, England, 2017.

Swindles, G. T., Watson, E., Turner, T. E., Galloway, J. M., Hadlari, T., Wheeler, J., and Bacon, K. L.: Spheroidal carbonaceous particles are a defining stratigraphic marker for the Anthropocene, Scientific Reports, 5, 10 264, doi:10.1038/srep10264, 2015.

Wang, Q., Saturno, J., Chi, X., Walter, D., Lavric, J. V., Moran-Zuloaga, D., Ditas, F., Pöhlker, C., Brito, J., Carbone, S., Artaxo, P., and Andreae, M. O.: Modeling investigation of light-absorbing aerosols in the Amazon Basin during the wet season, Atmospheric Chemistry and Physics, 16, 14 775–14 794, doi:10.5194/acp-16-14775-2016, 2016a.

Wang, X., Heald, C. L., Sedlacek, A. J., de Sá, S. S., Martin, S. T., Alexander, M. L., Watson, T. B., Aiken, A. C., Springston, S. R., and Artaxo, P.: Deriving brown carbon from multiwavelength absorption measurements: method and application to AERONET and Aethalometer observations, Atmospheric Chemistry and Physics, 16, 12 733–12 752, doi:10.5194/acp-16-12733-2016, 2016b.

A. Personal list of publications and presentations

A.1. Journal articles

1. Saturno, J., Ditas, F., Penning de Vries, M., Holanda, B. A., Pöhlker, M. L., Carbone, S., Walter, D., Bobrowski, N., Brito, J., Chi, X., Gutmann, A., Hrabe de Angelis, I., Machado, L. A. T., Moran-Zuloaga, D., Rüdiger, J., Schneider, J., Schulz, C., Wang, Q., Wendisch, M., Artaxo, P., Wagner, T., Pöschl, U., Andreae, M. O. and Pöhlker, C.: African volcanic emissions influencing atmospheric aerosol particles over the Amazon rain forest, ***Atmos. Chem. Phys. Discuss.***, 2017. https://doi.org/10.5194/acp-2017-1152.

2. Saturno, J., Holanda, B. A., Pöhlker, C., Ditas, F., Wang, Q., Moran-Zuloaga, D., Brito, J., Carbone, S., Cheng, Y., Chi, X., Ditas, J., Hoffmann, T., Hrabe de Angelis, I., Könemann, T., Lavrič, J. V., Ma, N., Ming, J., Paulsen, H., Pöhlker, M. L., Rizzo, L. V., Schlag, P., Su, H., Walter, D., Wolff, S., Zhang, Y., Artaxo, P., Pöschl, U. and Andreae, M. O.: Black and brown carbon over central Amazonia: Long-term aerosol measurements at the ATTO site, ***Atmos. Chem. Phys. Discuss.***, 2017. https://doi.org/10.5194/acp-2017-1097.

3. Moran-Zuloaga, D., Ditas, F., Walter, D., Saturno, J., Brito, J., Carbone, S., Chi, X., Hrabe de Angelis, I., Baars, H., Godoi, R. H. M., Heese, B., Holanda, B. A., Lavrič, J. V., Martin, S. T., Ming, J., Pöhlker, M. L., Ruckteschler, N., Su, H., Wang, Y., Wang, Q., Wang, Z., Weber, B., Wolff, S., Artaxo, P., Pöschl, U., Andreae, M. O. and Pöhlker, C.: Long-term study on coarse mode aerosols in the Amazon rain forest with the frequent intrusion of Saharan dust plumes, ***Atmos. Chem. Phys. Discuss.***, 2017. https://doi.org/10.5194/acp-2017-1043.

4. Pöhlker, M. L., Ditas, F., Saturno, J., Klimach, T., Hrabe de Angelis, I., Araùjo, A., Brito, J., Carbone, S., Cheng, Y., Chi, X., Ditz, R., Gunthe, S. S., Kandler, K., Kesselmeier, J., Könemann, T., Lavrič, J. V., Martin, S. T., Mikhailov, E., Moran-Zuloaga, D., Rizzo, L. V., Rose, D., Su, H., Thalman, R., Walter, D., Wang, J., Wolff, S., Barbosa, H. M. J., Artaxo, P., Andreae, M. O., Pöschl, U. and Pöhlker, C.: Long-term observations of cloud condensation nuclei in the Amazon rain forest – Part 2: Variability and characteristic differences under near-pristine, biomass burning, and long-range transport conditions, ***Atmos. Chem. Phys. Discuss.***, 2017. https://doi.org/10.5194/acp-2017-847.

5. Saturno, J., Pöhlker, C., Massabò, D., Brito, J., Carbone, S., Cheng, Y., Chi, X., Ditas, F., Hrabě de Angelis, I., Morán-Zuloaga, D., Pöhlker, M. L., Rizzo, L. V, Walter, D., Wang, Q., Artaxo, P., Prati, P. and Andreae, M. O.: Comparison of different Aethalometer correction schemes and a reference multi-wavelength absorption technique for ambient aerosol data, ***Atmos. Meas. Tech.***, $10(8), 2837-2850, 2017$. https://doi.org/10.5194/amt-10-2837-2017.

6. Rizzolo, J. A., Barbosa, C. G. G., Borillo, G. C., Godoi, A. F. L., Souza, R. A. F., Andreoli, R. V, Alves, E. G., Angelis, I. H., Ditas, F., Saturno, J., Moran-Zuloaga, D., Rizzo, L. V, Pauliquevis, T., Santos, R. M. N., Yamamoto, C. I., Andreae, M. O., Artaxo, P., Taylor, P. E. and Godoi, R. H. M.: Soluble iron nutrients in Saharan dust over the central Amazon rainforest, ***Atmos. Chem. Phys.***, $17, 2673-2687, 2017$. https://doi.org/10.5194/acp-17-2673-2017.

7. Wang, Q., Saturno, J., Chi, X., Walter, D., Lavric, J. V., Moran-Zuloaga, D., Ditas, F., Pöhlker, C., Brito, J., Carbone, S., Artaxo, P. and Andreae, M. O.: Modeling investigation of light-absorbing aerosols in the Amazon Basin during the wet season, ***Atmos. Chem. Phys.***, $16(22), 14775-14794, 2016$. https://doi.org/10.5194/acp-16-14775-2016.

8. Wang, J., Krejci, R., Giangrande, S., Kuang, C., Barbosa, H. M. J., Brito, J., Carbone, S., Chi, X., Comstock, J., Ditas, F., Lavric, J., Manninen, H. E., Mei, F., Moran-Zuloaga, D., Pöhlker, C., Pöhlker, M. L., Saturno, J., Schmid, B., Souza, R. A. F., Springston, S. R., Tomlinson, J. M., Toto, T., Walter, D., Wimmer, D., Smith, J. N., Kulmala, M., Machado, L. A. T., Artaxo, P., Andreae, M. O., Petäjä, T. and Martin, S. T.: Amazon boundary layer aerosol concentration sustained by vertical transport during rainfall, ***Nature***, $1-17, 2016$. https://doi.org/10.1038/nature19819.

9. Pöhlker, M. L., Pöhlker, C., Ditas, F., Klimach, T., Hrabe de Angelis, I., Araújo, A., Brito, J., Carbone, S., Cheng, Y., Chi, X., Ditz, R., Gunthe, S. S., Kesselmeier, J., Könemann, T., Lavrič, J. V., Martin, S. T., Mikhailov, E., Moran-Zuloaga, D., Rose, D., Saturno, J., Su, H., Thalman, R., Walter, D., Wang, J., Wolff, S., Barbosa, H. M. J., Artaxo, P., Andreae, M. O. and Pöschl, U.: Long-term observations of cloud condensation nuclei in the Amazon rain forest – Part 1: Aerosol size distribution, hygroscopicity, and new model parametrizations for CCN prediction, ***Atmos. Chem. Phys.***, $16(24), 15709-15740, 2016$. https://doi.org/10.5194/acp-16-15709-2016.

10. Andreae, M. O., Acevedo, O. C., Araùjo, A., Artaxo, P., Barbosa, C. G. G., Barbosa, H. M. J., Brito, J., Carbone, S., Chi, X., Cintra, B. B. L., da Silva, N. F., Dias, N. L., Dias-Júnior, C. Q., Ditas, F., Ditz, R., Godoi, A. F. L., Godoi, R. H. M., Heimann, M., Hoffmann, T., Kesselmeier, J., Könemann, T., Krüger, M. L., Lavric, J. V, Manzi, A. O., Lopes, A. P., Martins, D. L., Mikhailov, E. F., Moran-Zuloaga, D., Nelson, B. W., Nölscher, A. C., Santos Nogueira, D., Piedade, M. T. F., Pöhlker, C., Pöschl, U., Quesada, C. A., Rizzo, L. V, Ro, C.-U., Ruckteschler, N., Sá, L. D. A., de Oliveira Sá, M., Sales, C. B., dos Santos, R. M. N., Saturno, J., Schöngart,

J., Sörgel, M., de Souza, C. M., de Souza, R. A. F., Su, H., Targhetta, N., Tóta, J., Trebs, I., Trumbore, S., van Eijck, A., Walter, D., Wang, Z., Weber, B., Williams, J., Winderlich, J., Wittmann, F., Wolff, S. and Yáñez-Serrano, A. M.: The Amazon Tall Tower Observatory (ATTO): Overview of pilot measurements on ecosystem ecology, meteorology, trace gases, and aerosols, ***Atmos. Chem. Phys.***, $15(18), 10723 - 10776, 2015$. https://doi.org/10.5194/acp-15-10723-2015.

11. Pöhlker, C., Saturno, J., Krüger, M. L., Förster, J.-D., Weigand, M., Wiedemann, K. T., Bechtel, M., Artaxo, P. and Andreae, M. O.: Efflorescence upon humidification? X-ray microspectroscopic in-situ observation of changes in aerosol microstructure and phase state upon hydration, ***Geophys. Res. Lett.***, $41, 3681 - 3689, 2014$. https://doi.org/10.1002/2014GL059409.

A.2. Oral presentations

1. Saturno, J., Pöhlker, C., Ditas, F., Wang, Q., Carbone, S., Cheng, Y., Chi, X., Holanda, B. A., Moran-Zuloaga, D., Pöhlker, M. L., Walter, D., Artaxo, P., Pöschl, U. and Andreae, M. O., Long-term aerosol observations at the Amazon Tall Tower Observatory (ATTO): The influence of African emissions, Guest talk at the Laboratoire Interuniversitaire des Systèmes Atmosphériques (LISA), 2017, Paris, France.

2. Saturno, J., Chi, X., Pöhlker, C., Morán, D., Ditas, F., Massabò, D., Prati, P., Rizzo, L., Artaxo, P. and Andreae, M. O., Multi-wavelength aerosol light absorption measurements in the Amazon rainforest, European Geosciences Union General Assembly, 2015, Vienna, Austria.

A.3. Poster presentations

1. Saturno, J., Chi, X., Pöhlker, C., Morán-Zuloaga, D., Ditas, F., Hrabe de Angelis, I., Fermo, P., Corbella, L., González, R., Rizzo, L., Artaxo, P., Massabò, D., Prati, P. and Andreae, M. O., Optical properties of aerosol particles over the Amazon rain forest: From background to biomass burning conditions, European Aerosol Conference, 2015, Milan, Italy.

2. Saturno, J., Chi, X., Pöhlker, C., Massabò, D., Prati, P. and Andreae, M. O., Absorption enhancement of internally and externally mixed black carbon, European Research Course on Atmospheres, 2014, Université Joseph Fourier, Grenoble, France.

B. Selected List of Publications

1. Saturno, J., Pöhlker, C., Massabò, D., Brito, J., Carbone, S., Cheng, Y., Chi, X., Ditas, F., Hrabě de Angelis, I., Morán-Zuloaga, D., Pöhlker, M. L., Rizzo, L. V, Walter, D., Wang, Q., Artaxo, P., Prati, P. and Andreae, M. O.: Comparison of different Aethalometer correction schemes and a reference multi-wavelength absorption technique for ambient aerosol data, ***Atmos. Meas. Tech.***, $10(8), 2837 - 2850, 2017$. https://doi.org/10.5194/amt-10-2837-2017.

2. Saturno, J., Holanda, B. A., Pöhlker, C., Ditas, F., Wang, Q., Moran-Zuloaga, D., Brito, J., Carbone, S., Cheng, Y., Chi, X., Ditas, J., Hoffmann, T., Hrabe de Angelis, I., Könemann, T., Lavrič, J. V., Ma, N., Ming, J., Paulsen, H., Pöhlker, M. L., Rizzo, L. V., Schlag, P., Su, H., Walter, D., Wolff, S., Zhang, Y., Artaxo, P., Pöschl, U. and Andreae, M. O.: Black and brown carbon over central Amazonia: Long-term aerosol measurements at the ATTO site, ***Atmos. Chem. Phys. Discuss.***, 2017. https://doi.org/10.5194/acp-2017-1097.

3. Saturno, J., Ditas, F., Penning de Vries, M., Holanda, B. A., Pöhlker, M. L., Carbone, S., Walter, D., Bobrowski, N., Brito, J., Chi, X., Gutmann, A., Hrabe de Angelis, I., Machado, L. A. T., Moran-Zuloaga, D., Rüdiger, J., Schneider, J., Schulz, C., Wang, Q., Wendisch, M., Artaxo, P., Wagner, T., Pöschl, U., Andreae, M. O. and Pöhlker, C.: African volcanic emissions influencing atmospheric aerosol particles over the Amazon rain forest, ***Atmos. Chem. Phys. Discuss.***, 2017. https://doi.org/10.5194/acp-2017-1152.

B.1. Saturno et al., Atmos. Meas. Tech., 2017

Comparison of different Aethalometer correction schemes and a reference multi-wavelength absorption technique for ambient aerosol data

Jorge Saturno[1], Christopher Pöhlker[1], Dario Massabò[2], Joel Brito[3], Samara Carbone[4], Yafang Cheng[1], Xuguang Chi[5], Florian Ditas[1], Isabella Hrabě de Angelis[1], Daniel Morán-Zuloaga[1], Mira L. Pöhlker[1], Luciana V. Rizzo[6], David Walter[1], Qiaoqiao Wang[1], Paulo Artaxo[7], Paolo Prati[2], and Meinrat O. Andreae[1,8,9]

[1] *Biogeochemistry and Multiphase Chemistry Departments, Max Planck Institute for Chemistry, P.O. Box 3060, 55020 Mainz, Germany*
[2] *Department of Physics & INFN, University of Genoa, via Dodecaneso 33, 16146, Genoa, Italy*
[3] *Laboratory for Meteorological Physics, University Blaise Pascal, Clermont-Ferrand, France*
[1] *Institute of Agrarian Sciences, Federal University of Uberlândia, Uberlândia, Minas Gerais, Brazil*
[5] *Institute for Climate and Global Change and School of Atmospheric Sciences, Nanjing University, Nanjing, China*
[6] *Department of Earth and Exact Sciences, Institute of Environmental, Chemical and Pharmaceutics Sciences, Federal University of São Paulo, São Paulo, Brazil*
[7] *Department of Applied Physics, Institute of Physics, University of São Paulo, Rua do Matão, Travessa R, 187, CEP 05508-900, São Paulo, SP, Brazil*
[8] *Scripps Institution of Oceanography, University of California San Diego, La Jolla, CA 92098, USA*
[9] *Geology and Geophysics Department, King Saud University, Riyadh, Saudi Arabia*

Atmospheric Measurement Techniques, $10(8), 2837 - 2850, 2017$.

Atmos. Meas. Tech., 10, 2837–2850, 2017
https://doi.org/10.5194/amt-10-2837-2017

Atmospheric Measurement Techniques
Open Access
EGU

Comparison of different Aethalometer correction schemes and a reference multi-wavelength absorption technique for ambient aerosol data

Jorge Saturno[1], Christopher Pöhlker[1], Dario Massabò[2], Joel Brito[3], Samara Carbone[4], Yafang Cheng[1], Xuguang Chi[5], Florian Ditas[1], Isabella Hrabě de Angelis[1], Daniel Morán-Zuloaga[1], Mira L. Pöhlker[1], Luciana V. Rizzo[6], David Walter[1], Qiaoqiao Wang[1], Paulo Artaxo[7], Paolo Prati[2], and Meinrat O. Andreae[1,8,9]

[1]Biogeochemistry and Multiphase Chemistry Departments, Max Planck Institute for Chemistry, P.O. Box 3060, 55020 Mainz, Germany
[2]Department of Physics & INFN, University of Genoa, via Dodecaneso 33, 16146, Genoa, Italy
[3]Laboratory for Meteorological Physics, University Blaise Pascal, Clermont-Ferrand, France
[4]Institute of Agrarian Sciences, Federal University of Uberlândia, Uberlândia, Minas Gerais, Brazil
[5]Institute for Climate and Global Change and School of Atmospheric Sciences, Nanjing University, Nanjing, China
[6]Department of Earth and Exact Sciences, Institute of Environmental, Chemical and Pharmaceutics Sciences, Federal University of São Paulo, São Paulo, Brazil
[7]Department of Applied Physics, Institute of Physics, University of São Paulo, Rua do Matão, Travessa R, 187, CEP 05508-900, São Paulo, SP, Brazil
[8]Scripps Institution of Oceanography, University of California San Diego, La Jolla, CA 92098, USA
[9]Geology and Geophysics Department, King Saud University, Riyadh, Saudi Arabia

Correspondence to: Jorge Saturno (j.saturno@mpic.de)

Received: 31 October 2016 – Discussion started: 13 December 2016
Revised: 19 February 2017 – Accepted: 12 July 2017 – Published: 9 August 2017

Abstract. Deriving absorption coefficients from Aethalometer attenuation data requires different corrections to compensate for artifacts related to filter-loading effects, scattering by filter fibers, and scattering by aerosol particles. In this study, two different correction schemes were applied to seven-wavelength Aethalometer data, using multi-angle absorption photometer (MAAP) data as a reference absorption measurement at 637 nm. The compensation algorithms were compared to five-wavelength offline absorption measurements obtained with a multi-wavelength absorbance analyzer (MWAA), which serves as a multiple-wavelength reference measurement. The online measurements took place in the Amazon rainforest, from the wet-to-dry transition season to the dry season (June–September 2014). The mean absorption coefficient (at 637 nm) during this period was $1.8 \pm 2.1\,\mathrm{Mm}^{-1}$, with a maximum of $15.9\,\mathrm{Mm}^{-1}$. Under these conditions, the filter-loading compensation was negligible. One of the correction schemes was found to artificially increase the short-wavelength absorption coefficients. It was found that accounting for the aerosol optical properties in the scattering compensation significantly affects the absorption Ångström exponent ($å_{\mathrm{ABS}}$) retrievals. Proper Aethalometer data compensation schemes are crucial to retrieve the correct $å_{\mathrm{ABS}}$, which is commonly implemented in brown carbon contribution calculations. Additionally, we found that the wavelength dependence of uncompensated Aethalometer attenuation data significantly correlates with the $å_{\mathrm{ABS}}$ retrieved from offline MWAA measurements.

1 Introduction

Aerosol particles scatter and absorb solar radiation in the atmosphere and thus have an important impact on the Earth's radiative budget and climate (Andreae and Ramanathan, 2013; IPCC, 2013; Penner et al., 1992; Yu et al., 2006).

Light absorption by atmospheric aerosols is dominated by black carbon (BC), an aerosol species that is emitted by incomplete combustion of biomass or fossil fuels (Bond and Bergstrom, 2006). Black carbon absorbs radiation from infrared to near-UV wavelengths and leads to positive radiative forcing (IPCC, 2013). Other light-absorbing aerosols include a class of organics called *brown carbon* (BrC) (Andreae and Gelencsér, 2006), mineral dust (Myhre and Stordal, 2001), and *primary biological aerosol particles* (PBAPs) (Després et al., 2012). High uncertainties still remain regarding the aerosol interactions with solar radiation (Andreae and Ramanathan, 2013; Bond et al., 2013), especially because ambient aerosol absorption is often measured over a limited wavelength range or at only one wavelength.

The wavelength dependence of aerosol light absorption is expressed by the absorption Ångström exponent ($\mathring{a}_{\mathrm{ABS}}$) (Ångström, 1929). The $\mathring{a}_{\mathrm{ABS}}$ of fresh fossil-fuel-derived BC is typically around 1.0 – i.e., the absorption changes as a function of λ^{-1} (Bergstrom et al., 2002). However, when BC particle size is larger than 50 nm or becomes coated by non-absorbing materials, the $\mathring{a}_{\mathrm{ABS}}$ can decrease below 1.0 (Lack and Langridge, 2013). Moreover, the bulk aerosol wavelength dependence can significantly increase in the presence of other light absorbers, such as BrC (Andreae and Gelencsér, 2006; Kirchstetter et al., 2004), reaching high values between 3.5 and 7.0. Assuming a fixed spectral dependence of 1 for BC, several studies have estimated the BrC contribution as a function of $\mathring{a}_{\mathrm{ABS}}$ (Favez et al., 2010; Sandradewi et al., 2008). However, given the uncertainties associated with the $\mathring{a}_{\mathrm{ABS}}$ of BC, these methods could potentially provide erroneous BrC estimations (Garg et al., 2016; Schuster et al., 2016a, b; Wang et al., 2016).

Absorption coefficients and BC mass concentrations are related by the mass absorption cross section (MAC) (Bond et al., 2013). Ground-based continuous measurements of BC mass concentrations and absorption coefficients are required to retrieve the appropriate ambient aerosol MAC values, since this relationship and its wavelength dependence are affected by the mixing state and physical and chemical conditions of the aerosol particles (Flowers et al., 2010; Lack and Cappa, 2010; Moosmüller et al., 2011). Moreover, retrieving the wavelength dependence of ambient aerosol optical properties requires absorption measurements at two or more wavelengths.

Only a few commercially available techniques offer multi-wavelength absorption measurements. The most commonly used methods are filter-based techniques, including a modified version of the particle soot absorption photometer (PSAP) (Virkkula, 2010; Virkkula et al., 2005), which measures at three different wavelengths in the visible spectral region, and the Aethalometer (Hansen et al., 1984), which measures the attenuation of light at two or seven different wavelengths (2λ vs. 7λ instrument). The above-mentioned instruments are filter-based techniques that determine attenuation and suffer from various artifacts (detailed discussion below), converting attenuation coefficients to absorption coefficients requires several corrections (Arnott et al., 2005; Collaud Coen et al., 2010; Schmid et al., 2006; Virkkula et al., 2007; Weingartner et al., 2003) that generally need concomitant scattering and additional absorption measurements. The correction process of filter-based measurement artifacts introduces uncertainties in the $\mathring{a}_{\mathrm{ABS}}$ that are difficult to determine (Collaud Coen et al., 2010).

Two well-known artifacts affect filter-based absorption measurements by enhancing or reducing the effective optical path length. One of them is related to the multiple-scattering effects, which induces a positive bias of light attenuation. The multiple-scattering effects are caused by the *scattering by the filter fibers* and the *scattering by aerosol particles on the filter*. The scattering by aerosol particles depends on the optical properties and size distribution of the measured aerosol particles. On the other hand, the second effect is related to the *shadowing* that deposited aerosol particles cause on each other. This effect, called *filter-loading effect*, reduces the optical path length in the filter and depends on the amount and optical properties of the deposited particles.

The bias related to multiple-scattering effects can be reduced by measuring the radiation reflected by the filter at different angles and simulating the radiation transfer. This principle was incorporated in the design of the multi-angle absorption photometry (MAAP) technique (Petzold and Schönlinner, 2004). The design consists of a single-wavelength instrument (637 nm LED light source) that measures the transmitted radiation through a glass-fiber filter and the reflectance at two different angles (130° and 165°). Using this configuration and a radiation transfer model, the instrument is able to account for the mentioned artifacts related to multiple scattering and provides approximately "corrected" absorption coefficients (Petzold et al., 2005).

For accurate estimation of absorption coefficients and their spectral dependency, Aethalometer measurements rely on a number of correction procedures; a compilation of different correction schemes can be found in Collaud Coen et al. (2010). The first systematic correction scheme that deals with the different artifacts affecting Aethalometer measurements was proposed by Weingartner et al. (2003). This correction scheme uses a comparison with an indirect light absorption measurement (extinction minus scattering) to estimate a multiple-scattering compensation. In addition, a filter-loading correction was estimated by empirically calculating a "shadowing factor". This correction consists of the following empirical equation that converts attenuation coefficients, σ_{ATN}, into absorption coefficients, σ_{ap},

$$\sigma_{\mathrm{ap}} = \frac{\sigma_{\mathrm{ATN}}}{C \cdot R\,(\mathrm{ATN})}, \quad (1)$$

where C accounts for multiple-scattering effects on the filter, due to (a) scattering by the filter fibers and (b) scattering by aerosol particles embedded on the filter. The factor R(ATN) accounts for the filter-loading effect.

Later, Virkkula et al. (2007) proposed another filter-loading correction through calculating the average attenuation before and after a filter change. This correction applied a compensation factor in the form of $(1 + k \times \mathrm{ATN})$, where k is calculated for each filter change and ATN corresponds to the attenuation. A similar approach was used to design the dual-spot technology Aethalometer (model AE33) that intrinsically compensates for filter-loading effects using a two beam system with different flow rates (Drinovec et al., 2015).

In a detailed study, Arnott et al. (2005) introduced a scattering correction factor that accounts for the aerosol particle scattering artifact. In a similar way, Schmid et al. (2006) proposed a correction algorithm that included a parameterization of the scattering by filter fibers and scattering by aerosol particles as a function of $\mathring{a}_{\mathrm{ABS}}$ and an iteration procedure to obtain corrected absorption coefficients. Both correction schemes used photoacoustic spectroscopy (PAS) measurements at 532 nm as a reference absorption measurement. Later, by using MAAP absorption measurements as a reference, Collaud Coen et al. (2010) evaluated the abovementioned correction algorithms and proposed two new ones based on the Schmid and Arnott corrections. Their algorithms, among several changes to the previous ones, included a new scattering correction parameterization that uses measured optical properties of the aerosol particles instead of the "standard" ones implemented in Schmid and Arnott correction algorithms. The comparison made by Collaud Coen et al. (2010) resulted in a good agreement between MAAP and Aethalometer BC measurements when using the "Schmid-like" correction algorithm. On the other hand, the "Arnott-like" algorithm lead to many negative σ_{ap} values, especially under low absorption conditions (Collaud Coen et al., 2010).

Previous studies on Aethalometer compensation schemes have evaluated corrected absorption coefficients in comparison to reference absorption measurements (PAS or MAAP), which were done at only one wavelength. In this study, we use a multi-wavelength absorbance analyzer (MWAA), introduced by Massabò et al. (2013, 2015), to conduct a systematic multi-wavelength evaluation of ambient data. This way we can estimate the impact of the most common and reliable Aethalometer correction schemes on the $\mathring{a}_{\mathrm{ABS}}$ uncertainties. We used collected MAAP filter samples from long-term aerosol measurements in central Amazonia to perform offline multi-wavelength absorption measurements using the MWAA. The results presented here are relevant for the study of valuable multi-wavelength data provided by the widely used Aethalometers.

2 Materials and methods

2.1 Sampling site and selected data period

Field measurements were carried out at the Amazon Tall Tower Observatory (ATTO) (08.602′02° S, 00.033′59° W), located in the Uatumã Sustainable Development Reserve, Amazonas State, Brazil, in the central Amazon Basin. The site is located 150 km NE of the city of Manaus, upwind of the urban plume. A detailed description of the site can be found in Andreae et al. (2015).

The atmospheric aerosol was collected by using a 60 m long, 1 in. diameter stainless steel inlet tube without size cut-off, installed on a triangular mast since early 2014. The laminar flow rate in the inlet was constant at $30\,\mathrm{L\,min^{-1}}$. The aerosol stream relative humidity was decreased down to 30–40 % by using diffusion driers. In this study, we corrected the data for standard temperature and pressure (273.15 K and 1013.25 hPa) and did not apply any correction to compensate for particle losses. The sampling period analyzed here comprises the wet-to-dry transition time (June–July 2014) and part of the dry season (August–September 2014). In the beginning of the measurement period (beginning of June), aerosol particle number concentrations were very low, in the order of 100–400 $\mathrm{cm^{-3}}$, measured by a condensation particle counter (CPC) (Andreae et al., 2015). These typical wet-season conditions slightly changed during the transition season until the end of August, when particle number concentrations increased to around 500–2000 $\mathrm{cm^{-3}}$ (Andreae et al., 2015). The selected measurement period was a good opportunity to evaluate the Aethalometer performance under different conditions. During this period, the aerosol absorption coefficients increased from near detection limit values to the highest values measured at the ATTO site during the dry season.

2.2 Instrumentation

A 7λ Aethalometer (model AE31, Magee Scientific Company, Berkeley, USA; nominal wavelengths: 370, 470, 520, 590, 660, 880, and 950 nm) was used to measure attenuation coefficients σ_{ATN}, which are reported by the instrument as equivalent black carbon ($\mathrm{BC_e}$) mass concentrations. Details about the measurement principle and the different corrections to the data are explained in the next section.

Scattering coefficients, σ_{sp}, were measured by a 3λ nephelometer (model Aurora 3000, Ecotech Pty Ltd., Knoxfield, Australia; nominal wavelengths: 450, 525, and 635 nm). The instrument was manually calibrated using $\mathrm{CO_2}$ as span gas. Zero tests and spans were conducted periodically. The scattering coefficients measured by the instrument were corrected for truncation errors following the method proposed by Müller et al. (2011), using the sub-micrometer correction factors as function of the scattering Ångström exponents. The detection limits, calculated as 3 standard deviations of 1 min resolution particle-free air measurements, were 1.1, 0.9, and $0.7\,\mathrm{Mm^{-1}}$ at 450, 525, and 635 nm, respectively. Due to a malfunction of the 635 nm channel, we excluded those data from our calculations.

A multi-angle absorption photometer, MAAP (model 5012, Thermo Electron Group, Waltham, USA)

was used to measure the absorption coefficient at 637 nm. The instrument uses a glass-fiber filter tape, where the aerosol particles are collected on a sample spot. Light transmission (at 0°) and reflectance at two different angles (130° and 165°) are measured every 5 min (Petzold et al., 2005). A radiative model calculation provides the light absorption coefficient derived from the absorbance measurements and accounts for the light scattering by filter fibers and aerosol particles deposited on the filter. The instrument reports BC_e mass concentrations calculated by assuming a mass absorption cross section (MAC) of $6.6\,m^2\,g^{-1}$, based on Bond et al. (2006). A measurement bias after every filter change can occur if the absorption coefficients exceed $\sim 20\,Mm^{-1}$ (Hyvärinen et al., 2013), which was not the case during the period of this study. The instrument sampled at a flow rate of $500\,L\,h^{-1}$ in series with the nephelometer and was configured to trigger a filter change when transmission reached a minimum of 60 % or after 24 h. Therefore, more samples were collected during the dry season, when the aerosol particle concentration was higher and the transmission threshold was reached quickly. All data obtained from the online measurements (nephelometer, Aethalometer, and MAAP) were aggregated to 30 min means. MAAP data below the detection limit ($0.132\,Mm^{-1}$ with 30 min resolution) were excluded from the analysis.

The MWAA was used to measure the light absorption coefficients on MAAP-collected filter samples. This instrument was developed by Massabò et al. (2013) and measures the light transmitted through a filter sample (forward hemisphere) and the light reflected at two different angles (backward hemisphere) in a similar configuration to the MAAP. By using a radiative transfer model, the light absorption coefficients can be calculated. The instrument design offers the advantage of accounting for the multiple-scattering effects and is able to measure absorption coefficients at three different wavelengths, as initially introduced, and was later upgraded to measure at five different wavelengths (375, 407, 532, 635, and 850 nm) (Massabò et al., 2015). The MAAP aerosol-laden filter tape was collected at the ATTO site and analyzed by MWAA at the University of Genoa, Genoa, Italy. During transport of the samples, they could be affected by aging of the organic aerosol, microbial processes, and/or loss of semivolatile material (Laskin et al., 2015; Saleh et al., 2014). In order to avoid these issues, the samples were collected everyday directly from the MAAP and kept frozen (−4 °C) during the campaign time and transported in a cool bag with blue ice (~ 72 h) to the laboratory in Genoa. We reanalyzed some samples after they were stored at room temperature during 3 days to investigate the potential aging of carbonaceous material collected on the filters and found no significant differences in the absorbance results measured by the MWAA.

2.3 Aethalometer measurements and corrections

The Aethalometer continuously measures light attenuation on an aerosol-laden filter. The attenuation is defined, according to the Lambert–Beer law, as

$$\mathrm{ATN} = -100 \cdot \ln\left(\frac{I}{I_0}\right), \tag{2}$$

where I and I_0 are the light intensity transmitted through an aerosol loaded and an original area of the filter tape, respectively. A list of symbols and abbreviations is provided in Table 1. The instrument is programmed to calculate the BC_e mass concentration by assuming that a change in attenuation (ΔATN) is caused by an increase in the BC mass deposited on the filter substrate during an interval Δt (min), as follows:

$$\mathrm{BC}\left(\mathrm{ng\,m^{-3}}\right) = \frac{A \cdot \Delta\mathrm{ATN}}{\alpha_{\mathrm{ATN}} \cdot Q \cdot \Delta t}, \tag{3}$$

where A is the filter area ($1.67\,cm^2$), α_{ATN} is the λ-dependent BC mass attenuation cross section ($14\,625\,nm\,m^2\,g^{-1}\lambda^{-1}$), and Q is the volumetric flow rate in $L\,min^{-1}$. By using the α_{ATN} recommended by the manufacturer, we reversed the calculation to convert reported mass concentrations back to attenuation coefficients, as

$$\sigma_{\mathrm{ATN}} = \mathrm{BC}\left(\mathrm{ng\,m^{-3}}\right) \cdot \alpha_{\mathrm{ATN}}. \tag{4}$$

Two different correction schemes were applied to our dataset, including the Schmid et al. (2006) and the Collaud Coen et al. (2010) algorithms. These two correction schemes were chosen because both of them compensate for the three artifacts that affect Aethalometer measurements. The Arnott and Collaud Coen's Arnott-like corrections were excluded due to their limitations when dealing with low-absorption data. Both the Collaud Coen and the Schmid correction require concomitant scattering measurements and a reference absorption measurement, which in our case was the MAAP. Moreover, we present and discuss a comparison of corrected Aethalometer data to the multi-wavelength light absorption measurement obtained from the MWAA.

2.3.1 Schmid correction algorithm

The Schmid correction consists of an iterative procedure, which is applied to each measured attenuation spectrum. The compensated absorption coefficients, σ_{ap}, are calculated from attenuation coefficients, σ_{ATN}, by accounting for the different artifacts,

$$\begin{aligned}\sigma_{\mathrm{ap}} &= \frac{\sigma_{\mathrm{ATN}}}{(C_{\mathrm{ref}} + C_{\mathrm{sca}}) \cdot R} \\ &= \frac{\sigma_{\mathrm{ATN}}}{\left(C_{\mathrm{ref}} + m_{\mathrm{s}}\frac{\omega_0}{1-\omega_0}\right)\left[\left(\frac{1}{f}-1\right)\left(\frac{\ln \mathrm{ATN} - \ln 10}{\ln 50 - \ln 10}\right)+1\right]},\end{aligned} \tag{5}$$

where C_{ref} compensates for the scattering effects in comparison with a reference absorption measurement, C_{sca} accounts

Table 1. List of symbols and abbreviations used.

Description	Abbreviation	Symbol	Units
Instruments			
Aethalometer	AE		
Multi-angle absorption photometer	MAAP		
Multi-wavelength absorbance analyzer	MWAA		
Parameters			
Attenuation	ATN	ATN	
Absorption Ångström exponent	AAE	$\mathring{a}_{\mathrm{ABS}}$	
Scattering Ångström exponent	SAE	$\mathring{a}_{\mathrm{SCA}}$	
Attenuation Ångström exponent		$\mathring{a}_{\mathrm{ATN}}$	
Attenuation coefficient		σ_{ATN}	m^{-1}
Absorption coefficient		σ_{ap}	m^{-1}
Scattering coefficient		σ_{sp}	m^{-1}
Mass attenuation cross section		α_{ATN}	$\mathrm{m}^2\,\mathrm{g}^{-1}$
Mass absorption cross section	MAC	α_{ABS}	$\mathrm{m}^2\,\mathrm{g}^{-1}$
Scattering proportionality constant		β_{SCA}	m^{-1}
Filter-loading correction factor		R	
Shadowing factor		f	
Multiple scattering correction factor		C_{ref}	
Scattering correction factor		C_{sca}	
Scattering effect parameter		m_{s}	

for the scattering effect of non-absorbing aerosol particles and R, for the filter-loading effect. The Schmid formulation uses the scattering factor m_{s} and ω_0 to calculate C_{sca} and the filter loading correction proposed by Weingartner et al. (2003), which takes ATN = 10 % as a reference point and includes the shadowing factor parameter, f, which describes the slope between σ_{ATN} and ln(ATN).

As a first step, C_{ref} is calculated for attenuation coefficients corresponding to attenuation values lower than 10 %, when the filter-loading correction is considered negligible (ATN < 10 %; $R \approx 1$). By using MAAP absorption coefficient measurements, it is possible to obtain C_{ref} as follows:

$$C_{\mathrm{ref}} = \frac{\sigma_{\mathrm{ATN,10}}}{\sigma_{\mathrm{MAAP}}}, \tag{6}$$

where σ_{MAAP} is the absorption coefficient measured by the MAAP at 637 nm and $\sigma_{\mathrm{ATN,\,10}}$ is the attenuation coefficient at 637 nm when ATN < 10 %.

Attenuation coefficients at 590 nm were interpolated to 637 nm assuming a power-law relationship as,

$$\sigma_{\mathrm{ATN}}(637\,\mathrm{nm}) = \sigma_{\mathrm{ATN}}(590\,\mathrm{nm}) \cdot \left(\frac{637\,\mathrm{nm}}{590\,\mathrm{nm}}\right)^{-\mathring{a}_{\mathrm{ATN}}}. \tag{7}$$

The attenuation Ångström exponent $\mathring{a}_{\mathrm{ATN}}$ used in this step was calculated by applying a log–log fit to σ_{ATN} vs. λ , where $\mathring{a}_{\mathrm{ATN}}$ was obtained from the slope as follows:

$$\ln\sigma_{\mathrm{ATN}} = -\mathring{a}_{\mathrm{ATN}} \ln(\lambda) + \ln(\mathrm{constant}). \tag{8}$$

Absorption Ångström exponents ($\mathring{a}_{\mathrm{ABS}}$) were obtained in a similar way in further calculations.

The multiple-scattering correction factor, C_{ref}, obtained from Eq. (6) was averaged over the sampling period to calculate the measured filter-loading correction factor, R_{meas}, as

$$R_{\mathrm{meas}} = \frac{\sigma_{\mathrm{ATN}}}{\sigma_{\mathrm{MAAP}} \cdot \overline{C}_{\mathrm{ref}}}. \tag{9}$$

Weingartner et al. (2003) found that the linear relationship between σ_{ATN} and ln(ATN) can be used to parameterize the filter-loading effect. The slope of this relationship was given by the shadowing factor parameter, f. By applying a linear fit to the R_{meas} values obtained from Eq. (9) and the attenuation data, as shown in Eq. (10), the term $(1/f - 1)$ can be obtained from the slope.

$$R = \left(\frac{1}{f} - 1\right)\left(\frac{\ln\mathrm{ATN} - \ln 10}{\ln 50 - \ln 10}\right) + 1 \tag{10}$$

Assuming f is wavelength-independent, the averaged f is then used to calculate R at different wavelengths.

In the next step, C, understood as the overall multiple-scattering correction factor ($C_{\mathrm{ref}} + C_{\mathrm{sca}}$), is parameterized as a function of λ. The single-scattering albedo, ω_0, at 637 nm is used in the following equation to calculate C as

$$C = C^* + m_{\mathrm{s}} \frac{\omega_0}{1 - \omega_0}, \tag{11}$$

where C^* corresponds to the multiple-scattering effect by filter fibers and m_{s} to the aerosol scattering factor found

by Arnott et al. (2005) (see Table S1). The implemented approach is useful to examine any wavelength dependence on C. The values of ω_0 were interpolated to the different Aethalometer wavelengths by using the Eq. (12), assuming that absorption and scattering coefficients follow a power-law wavelength dependence described by $å_{ABS}$ and $å_{SCA}$, respectively.

$$\omega_0(\lambda) = \frac{\sigma_{sp}}{\sigma_{sp}+\sigma_{ap}} = \frac{\omega_{0,ref}\left(\frac{\lambda}{\lambda_{ref}}\right)^{-å_{SCA}}}{\omega_{0,ref}\left(\frac{\lambda}{\lambda_{ref}}\right)^{-å_{SCA}} + (1-\omega_{0,ref})\left(\frac{\lambda}{\lambda_{ref}}\right)^{-å_{ABS}}} \quad (12)$$

Different $å_{ABS}$ values (1; 1.25; 1.5; 1.75; 2) are then used to generate different correlation factors between $\ln(C)$ vs. $\ln(\lambda)$. The coefficients resulting from a quadratic fit are used to parameterize C as a function of $å_{ABS}$ (see Fig. 4 in Schmid et al., 2006). An iteration procedure is used to force the convergence of $å_{ABS}$. In our calculations, the data converged after seven iterations.

2.3.2 Collaud Coen correction algorithm

In this study we implemented the Collaud Coen correction algorithm that resembles the Schmid correction (see Eq. 14b in Collaud Coen et al., 2010). This algorithm is different from the original Schmid algorithm in the calculations of the filter-loading effect and the multiple-scattering correction factor. As shown in Eq. (6), the Schmid algorithm filters the data for ATN < 10 % in order to account only for the scattering by filter fibers in the C_{ref} calculation. On the other hand, the Collaud Coen algorithm applies a prior filter-loading correction and then, by dividing the reference absorption data (MAAP) by the Aethalometer attenuation coefficients, C_{ref} is obtained, which accounts for both scattering by filter fibers and scattering by embedded aerosol particles.

Regarding the filter-loading effect, Collaud Coen et al. used the linear dependency of the shadowing factor, f, on the single-scattering albedo, ω_0, expressed by Eq. (12), to calculate f using measured ω_0 and assuming m was constant ($m = 0.74$).

$$f = m \cdot (1-\omega_0) + 1 \quad (13)$$

Additionally, they found statistically better results by correlating σ_{ATN} vs. ATN, instead of the logarithmic correlation proposed by Weingartner et al. (2003), which was implemented by Schmid et al. (2010). Considering no filter-loading artifact for ATN = 0, they proposed the following equation, which replaces Eq. (10):

$$R = \left(\frac{1}{m(1-\overline{\omega}_0)+1} - 1\right)\left(\frac{ATN}{50}\right) + 1. \quad (14)$$

In this case, ω_0 was averaged for every filter spot period (from one filter spot change to the next) and this average

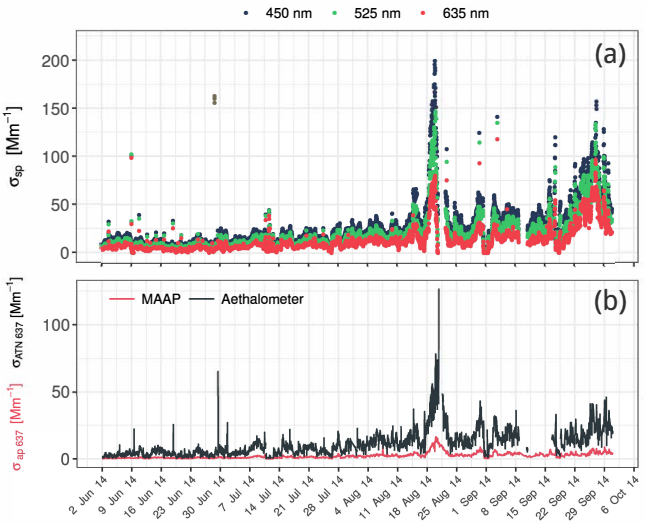

Figure 1. Time series (June–September 2014) of **(a)** scattering by aerosol particles measured by the nephelometer and **(b)** Aethalometer attenuation and MAAP absorption coefficient measurements at 637 nm during the sampling period.

was used for calculating every measurement included in the corresponding filter spot period. The ω_0 values at different wavelengths were calculated by using Eq. (12) but including attenuation Ångström exponents ($å_{ATN}$) because $å_{ABS}$ is not known yet.

Filter-loading corrected data are then divided by the MAAP absorption coefficients to obtain an average C_{ref}. Regarding the embedded aerosol scattering effects, the Collaud Coen correction includes a change in the aerosol scattering effect parameter expressed as m_s in Eq. (11). The constant m_s values used by Schmid et al. (2010) correspond to ammonium sulfate. Collaud Coen substituted them by the measured aerosol scattering properties by using the following equation

$$m_s = \beta_{SCA}^{(d-1)} \cdot c \cdot \lambda^{(-å_{SCA}(d-1))}; \quad (15)$$
$$d = 0.564;$$
$$c = 0.00032910 \ (\sigma_{sp} \text{ in } \mathrm{Mm^{-1}} \text{ units}),$$

where β_{SCA} is the scattering proportionality constant and c and d are constants corresponding to the power-law relation between σ_{ATN} and σ_{sp}, previously reported by Arnott et al. (2005).

Finally, the corrected absorption coefficients are calculated in a similar way to Eq. (5) but using m_s from Eq. (15) and averaging C_{ref}, m_s, ω_0 and R over a filter spot period, i.e., from a filter change time to the subsequent one.

3 Results and discussion

The beginning of the sampling period is characterized by low scattering coefficients compared to the second half of the

period when scattering increases significantly. Several scattering peaks can be observed after the beginning of August (see Fig. 1a). Occasionally, local or regional biomass burning plumes reach the site during the dry season and scattering by aerosol particles increases significantly due to enhanced concentration of fine mode aerosol particles, which are more efficient in scattering light in the visible range. The major effect of multiple-scattering artifacts is evident when comparing MAAP measured absorption coefficients and Aethalometer measured attenuation coefficients (see Fig. 1b). The absorption coefficients averaged $1.8 \pm 2.1\,\mathrm{Mm}^{-1}$, with the minimum values occurring in the beginning of the sampling period, whereas a maximum of absorption (up to $15.9\,\mathrm{Mm}^{-1}$, measured by MAAP) took place between 18 and 23 August 2014. Calculated back-trajectories using the HYSPLIT model (Draxler and Hess, 1998) confirmed that air masses on the days of maximum absorption and scattering were coming from south and southeast, an area with intense fire activity; see Fig. S1 in the Supplement. Levoglucosan measurements further confirmed the predominance of biomass-burning-originated aerosol particles (not shown). From 1 June to 1 August 2014, the attenuation coefficient at 637 nm had a median of $5.1\,\mathrm{Mm}^{-1}$ (3.2–7.9, interquartile range, IQR). Then, during the first days of August, it increased slightly until the biomass burning event took place on 18–23 August 2014. The maximum attenuation coefficient during this event reached $115\,\mathrm{Mm}^{-1}$. Details about this event, regarding chemical composition and CCN activity, are presented in Pöhlker et al. (2016, 2017). The observed absorption and attenuation coefficients represent typical conditions at the ATTO site for the wet, transition and dry periods. In the next sections, we present data compensated to account for the different filter artifacts and study the influence of the applied compensation algorithms on the $\mathring{a}_{\mathrm{ABS}}$. The artifacts that affect the $\mathring{a}_{\mathrm{ABS}}$ retrieval from filter-based multi-wavelength absorption measurements could be avoided by using PAS methods that have been successfully implemented to measure light absorption by suspended aerosol particles (e.g., Ajtai et al., 2010). However, PAS measurements have high detection limits and have only been implemented at near-source measurement sites (Cappa et al., 2012; Cheng et al., 2016; Lewis et al., 2008) and not in clean environments like central Amazonia.

3.1 Aethalometer corrections

Immediately after every Aethalometer filter change, aerosol particles are collected on a clean new spot. Under these conditions, the filter-loading effect is considered to be negligible because there is not enough aerosol on the filter to "darken" the substrate (Virkkula et al., 2007). Therefore, the only bias to the Aethalometer response is given by the scattering effects by filter fibers. The scattering by filter fibers, expressed as C_{ref}, was calculated by using Eq. (6), assuming $R \approx 1$ for data corresponding to ATN < 10 %. The C_{ref} time series

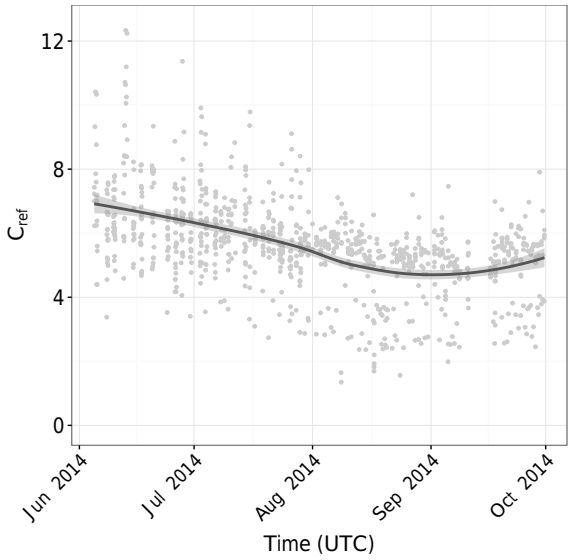

Figure 2. Multiple scattering correction calculated by using MAAP absorption coefficients as reference ($\lambda = 637$ nm). Light-gray points represent all calculated C_{ref} values. The black line and shaded area represent a conditional non-parametric mean estimation and its confidence limits, respectively.

is shown in Fig. 2. We observed that C_{ref} decreased somewhat from June–July to August–September, when the average $\pm$ 1SD values were 6.3 ± 1.5 and 4.9 ± 1.1, respectively. Additionally, we observed a larger C_{ref} variability during the transition period, which may increase the uncertainty of the corrected absorption coefficients. This seasonal effect on the multiple-scattering compensation parameter could be related to the condensation or adsorption of semi-volatile organic compounds or liquid organic aerosol particles on the filter fibers, inducing a change in the filter matrix optical properties (Collaud Coen et al., 2010; Subramanian et al., 2007; Weingartner et al., 2003). The Schmid algorithm uses an average C_{ref} for further calculation of the filter-loading correction factor, R. We found that using an overall average C_{ref} significantly affects the calculation of the shadowing factor (f). Therefore, two different averages of C_{ref} were implemented in this work for the two above-mentioned periods, transition (June–July) and dry season (August–September). Subsequent multiple-scattering correction calculations were conducted using real-time C_{ref} values.

The measured filter-loading calibration factor (R_{meas}) was obtained by using Eq. (9). Then, by following the Schmid algorithm, the shadowing factor was calculated by applying a fit to Eqs. (9) and (10) (Rizzo et al., 2011; Schmid et al., 2006). The calculated average shadowing factors were 1.10 ± 0.10 and 1.04 ± 0.08 for June–July and August–September, respectively. These values were lower compared to those obtained for darker aerosols ($f = 1.23$–1.89) (Weingartner et al., 2003) and for biomass burning aerosol ($f = 1.2$) (Schmid et al., 2006). At 660 nm, the Aethalometer

wavelength that is closer to the MAAP measurement wavelength, the filter-loading correction calculation resulted in R correction factors of 0.98 ± 0.02 and 1.01 ± 0.01 for June–July and August–September, respectively. A slight wavelength dependence was observed; the R values were up to 4 % higher at 370 nm compared to those calculated at 950 nm during the cleanest period of this study (June–July). A similar behavior was observed during August–September. As explained by Schmid et al. (2006), this wavelength dependency is related to the fact that R depends on ATN, which increases with decreasing wavelength. The obtained R correction factors were very close to 1 – i.e., the filter loading effect barely affected the conversion from attenuation to absorption coefficients, even during the most polluted period, August–September. A filter-loading correction factor close to 1 was expected since the average ω_0 measured during the campaign was 0.88 ± 0.04 at 637 nm. A high ω_0 is related to the predominance of scattering aerosol particles, which diminishes the shadowing effect of dark aerosol particles embedded in the filter matrix (Weingartner et al., 2003).

To compare both correction schemes in terms of the filter-loading correction, C_{ref} was recalculated after compensating all the data for filter loading by (1) following the Schmid et al. correction and (2) the Collaud Coen et al. correction, which includes ω_0 in the shadowing factor calculation and the relationship σ_{ATN} vs. ATN. We found no statistical difference between the two correction algorithms in terms of the filter-loading compensation because this effect was generally low over the sampling period. More information about the effect of increasing attenuation on the calculated C_{ref} after applying the filter-loading correction can be found in the Supplement (Fig. S2).

As already mentioned, the multiple-scattering effects significantly affect the correction of Aethalometer data by a factor of 5 to 7. According to previous studies, the multiple-scattering correction is the most important one in ambient aerosol with a high ω_0 (Collaud Coen et al., 2010; Rizzo et al., 2011; Schmid et al., 2006; Segura et al., 2014). The seasonal variability of C can be explained by the different scattering properties of the aerosol particles in the different seasons (Collaud Coen et al., 2010). In order to compare the different scattering contributions to C, we calculated C_{ref} and C_{sca} by using the Collaud Coen algorithm. C_{sca} was calculated using Eq. (5) in this case. We observed that a lower ω_0 during the biomass burning period was related to a decrease in the scattering correction factor, C_{sca}. The relative contribution of C_{sca} was examined and it was found that the relative contribution from the scattering correction decreases with decreasing ω_0 and increasing β_{sca}; see Fig. 3. No correlation was found between C_{sca} and $\mathring{a}_{\mathrm{SCA}}$ since the scattering Ångström exponent was quite stable during the sampling period with the exception of the few days influenced by regional biomass burning (see Fig. S3). In other words, the C_{sca} relative contribution was only affected by variations on β_{sca} and ω_0. Given that R is almost negligible in our dataset, the comparison between both algorithms was done in terms of their different ways to treat the multiple-scattering effects.

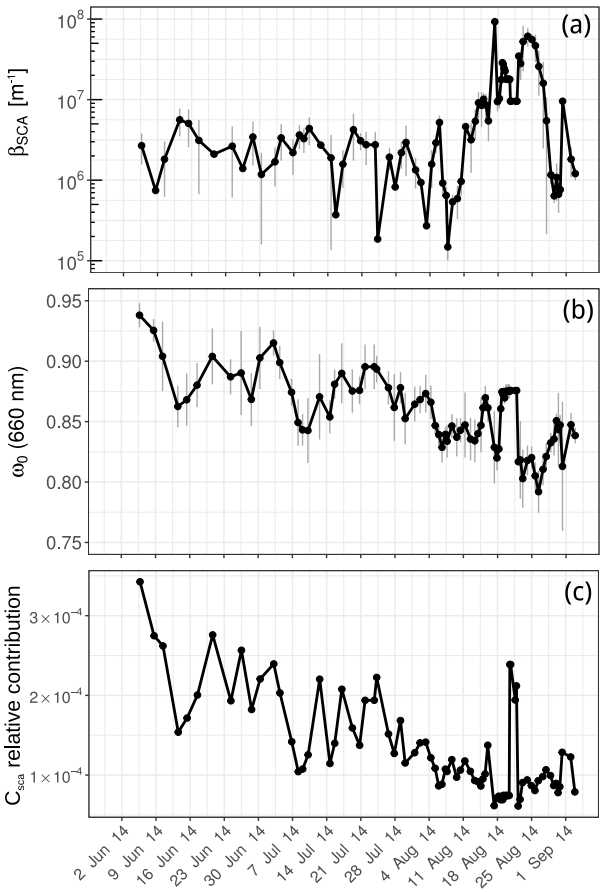

Figure 3. Filter cycle averaged data corresponding to **(a)** scattering proportionality constant, **(b)** single-scattering albedo at 660 nm, and **(c)** relative contribution of C_{sca} to the total multiple-scattering compensation ($C_{\mathrm{ref}} + C_{\mathrm{sca}}$) at 660 nm. Vertical bars in **(a)** and **(b)** correspond to 1 standard deviation.

A scatter plot of both corrections' outputs vs. MAAP measurements is shown in Fig. 4. We found that corrected AE data fitted very well the MAAP measurements for both correction algorithms. The slopes were 1.05 (1.04–1.06) and 1.03 (1.02–1.03) for the Schmid and Collaud Coen corrections, respectively, with significant correlation factors. The slight difference between both correction schemes in terms of the comparison to MAAP measurements can be related to the parameterization of C applied by Schmid et al., which is not implemented by Collaud Coen et al., and the way Collaud Coen et al. estimate C_{ref}.

3.2 Absorption Ångström exponent

The MWAA was used as a reference multi-wavelength measurement since it accounts for multiple-scattering effects by means of a similar configuration to the MAAP. Light absorp-

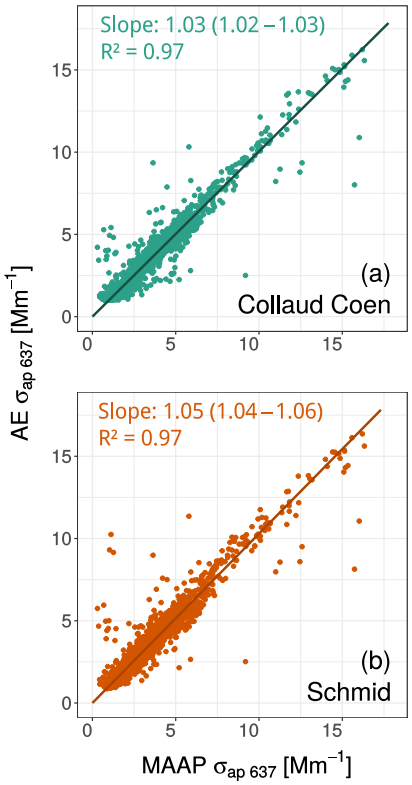

Figure 4. Scatter plot of **(a)** Collaud Coen and **(b)** Schmid corrections results vs. MAAP absorption coefficients (all data at 637 nm). The fit was obtained by applying a standardized major axis regression.

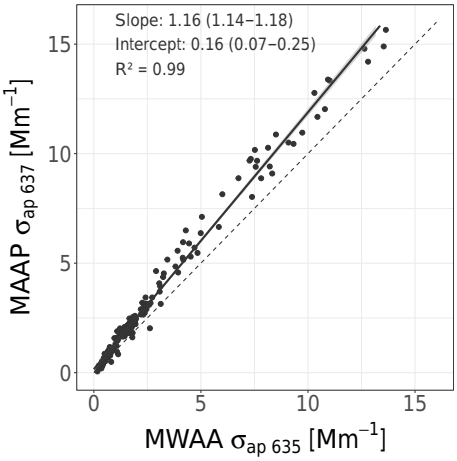

Figure 5. Scatter plot and linear regression of MWAA and MAAP absorption coefficient data. The 1 : 1 relationship is represented by a dashed line. The fit was obtained by applying a standardized major axis regression.

tion coefficients obtained from the MWAA (at 635 nm) and from the MAAP (at 637 nm) were compared by applying an linear regression to both datasets after integrating the MAAP data over the filter total sampling times, as shown in Fig. 5. The fit resulted in a MWAA underestimation of 14 to 18 % when fitting the whole dataset. In general, all values measured by the MWAA at 635 nm were below the MAAP measurements at 637 nm with a decreasing offset towards lower absorption coefficients. This could be associated with a significant volatilization of the absorbing aerosol collected during the polluted period. The comparison of Aethalometer and MWAA at different wavelengths was based on the assumption that these losses are wavelength-independent.

MWAA data measured at five different wavelengths was used to retrieve $\mathring{a}_{ABS}$ by applying a log–log fit as expressed in Eq. (8). Figure 6 shows the MWAA Ångström exponents and their uncertainty intervals, together with the values obtained from the two different Aethalometer corrections and the original $\mathring{a}_{ATN}$. The MWAA $\mathring{a}_{ABS}$ retrieved from each filter were not all statistically optimal; 30 out of 175 had a $R^2 < 0.85$. All the values below this R^2 limit were excluded from the results shown in Fig. 6. Absorption Ångström exponents obtained using the Schmid correction were mostly higher than the MWAA results. On the other hand, the Collaud Coen correction resulted in a better approach to reproduce the MWAA data, with most of the results in the MWAA uncertainty range. During the biomass burning period, from 18 to 23 August 2014, the BrC contribution became more important and caused an increase in the $\mathring{a}_{ABS}$ and both algorithms' results became similar to each other and slightly higher than the MWAA $\mathring{a}_{ABS}$. After the biomass burning episode, when the scattering and absorption coefficients fell down to background levels, the offset between both algorithms, in terms of $\mathring{a}_{ABS}$, widened again. In this regard, the Collaud Coen algorithm, which includes a modified scattering correction, seems to be more appropriate to retrieve the $\mathring{a}_{ABS}$ for a broader range of absorption coefficients.

A scatter plot of the $\mathring{a}_{ABS}$ data, including the corresponding linear fits, is shown in Fig. 7. The data analyzed in this comparison include only filters that had a σ_{ap} vs. λ log–log fit with $R^2 > 0.85$. Although both algorithms overestimate the $\mathring{a}_{ABS}$ retrieved from the MWAA measurements, the Collaud Coen algorithm produces a lower offset and a better linear fit, with a $R^2 = 0.72$. On the other hand, the Schmid algorithm seems to be artificially enhancing the absorption at lower wavelengths. When applying linear regressions forced through the origin, the overall tendency showed a statistically significant $\mathring{a}_{ABS}$ overestimation by the Schmid algorithm and a better fit for the Collaud Coen algorithm (not shown). The original attenuation Ångström exponent ($\mathring{a}_{ATN}$, without applying any compensation) was also found to fit the MWAA-retrieved $\mathring{a}_{ABS}$ quite well (slope IQR: 0.89–1.10 with $R^2 = 0.75$, not shown). This finding is in accordance with Ajtai et al. (2011), who found a good agreement between 4λ PAS measurements and the Aethalometer raw wavelength dependence at a suburban site.

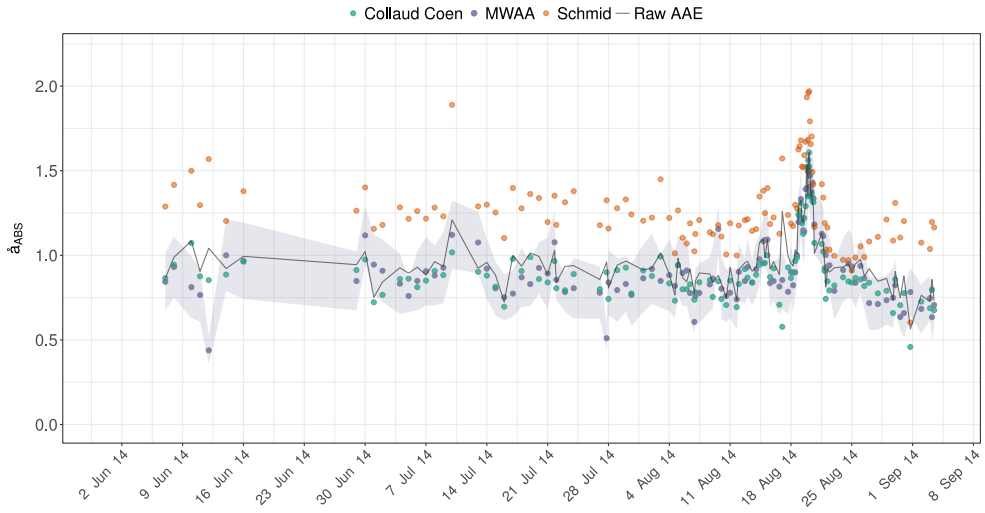

Figure 6. Wavelength dependence retrieved from MWAA absorption data and its standard error (purple points and shaded area), raw attenuation data (gray line), and Schmid (orange points) and Collaud Coen (green points) corrected absorption data, all averaged over MWAA sample intervals. Error lines were removed to improve visualization.

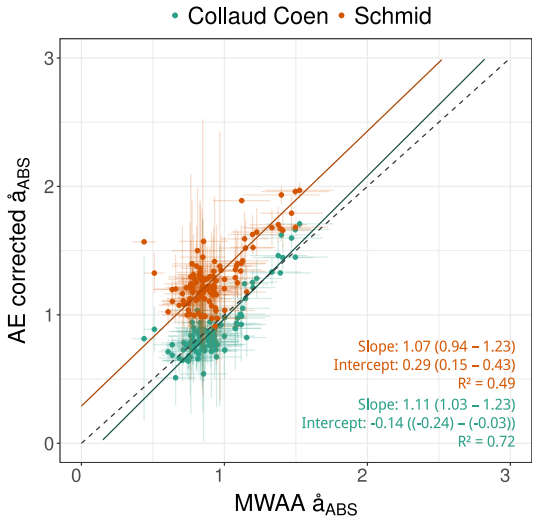

Figure 7. Scatter plot of AAE values obtained by Aethalometer corrections vs. AAE obtained from MWAA measurements. The dark-colored lines correspond to the standardized major axis linear fits and light-colored lines correspond to 1 standard deviation of the retrieved AAE data. The dashed gray line represents a 1 : 1 relationship.

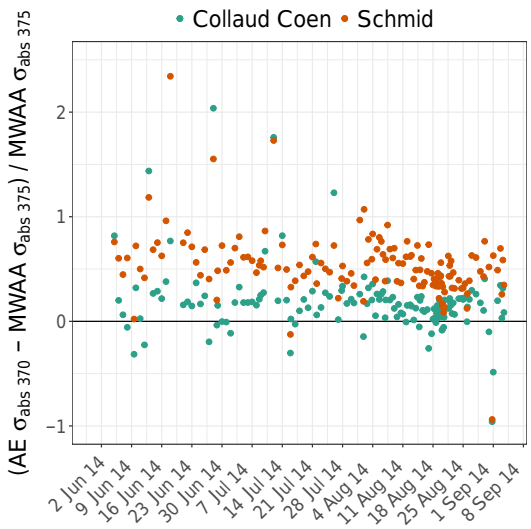

Figure 8. Overestimation of Aethalometer corrected absorption coefficients relative to MWAA at 370 nm. Values above zero are related to an overestimation of σ_{ap} and, below zero, to an underestimation of σ_{ap} at this given wavelength.

3.3 Overestimation of near-UV absorption by AE corrections

The unexpectedly high $\mathring{a}_{ABS}$, especially that obtained by applying the Schmid algorithm, is probably caused by an artificial enhancement of the near-UV absorption. Figure 8 shows the relative enhancement of the absorption coefficients at 370 nm, compared to the MWAA absorption at 375 nm. No interpolation was applied to match both wavelengths since they are close enough that the differences were negligible ($\sim 3\,\%$ for a $\mathring{a}_{ABS}$ of 2.0). It is clear that the Schmid algorithm almost always overestimated the absorption at 370 nm. Only a few filters showed a difference close to or below zero. On average, the Schmid algorithm overestimation relative to MWAA was a factor of 0.46 ± 0.31. In the case of the Collaud Coen algorithm, the average difference was slightly positive, being a factor of 0.19 ± 0.32, and reaching an average of 0.12 ± 0.12 for $\sigma_{ap} > 5\,Mm^{-1}$, during the biomass burn-

ing event. A near-UV over- or underestimation of the data will substantially affect brown carbon calculations if apportionment algorithms based on the wavelength dependence of absorption are used. More details on the effects of inaccurate $å_{ABS}$ on the BrC / BC apportionment are discussed in Garg et al. (2016), Schuster et al. (2016a, b), Wang et al. (2016), and references therein. A BrC estimation is beyond the scope of this paper.

4 Conclusions

We applied two different correction algorithms to compensate for the various Aethalometer absorption measurement artifacts. The compensated data were compared to an offline multi-wavelength reference absorption measurement technique. This comparison allowed studying the effects of the correction schemes on the absorption at lower wavelengths and showed how this affects the $å_{ABS}$ retrieval. We found that both analyzed algorithms efficiently reproduce the reference MAAP absorption coefficients from Aethalometer data. However, the Schmid algorithm overestimates the $å_{ABS}$ compared to that obtained by the multiple wavelength measurement (MWAA). On the other hand, the Collaud Coen algorithm as well as the "raw" Aethalometer attenuation spectral dependence reproduced the $å_{ABS}$ values obtained from MWAA measurements quite well. The under- or overestimation of short-wavelength absorption coefficients by compensation algorithms is a factor that has to be considered when using corrected Aethalometer data to apportion the black and brown carbon contributions to total absorption. When comparing the absorption coefficients obtained from the different correction algorithms to the reference measurement at 370 nm, we found that the Collaud Coen algorithm is more appropriate to achieve the best comparison at this wavelength, especially for data with $\sigma_{ap} > 5\,Mm^{-1}$. The Schmid algorithm resulted in high enhancements of the absorption coefficients at 370 nm over the sampling period.

Data availability. The data presented in this paper can be accessed via e-mail request to Jorge Saturno (j.saturno@mpic.de).

The Supplement related to this article is available online at https://doi.org/10.5194/amt-10-2837-2017-supplement.

Competing interests. The authors declare that they have no conflict of interest.

Acknowledgements. This work has been supported by the Max Planck Society (MPG) and the Max Planck Graduate School (MPGS). For the operation of the ATTO site, we acknowledge the support by the German Federal Ministry of Education and Research (BMBF contract 01LB1001A) and the Brazilian Ministério da Ciência, Tecnologia e Inovação (MCTI/FINEP contract 01.11.01248.00) as well as the Amazon State University (UEA), FAPEAM, LBA/INPA and SDS/CEUC/RDS-Uatumã. Paulo Artaxo acknowledges support from FAPESP – Fundação de Amparo à Pesquisa do Estado de São Paulo. Jorge Saturno is grateful for a PhD scholarship from the Fundación Gran Mariscal de Ayacucho (Fundayacucho). We acknowledge Paola Fermo, Raquel Gonzalez and Lorenza Corbella for the levoglucosan analysis. This paper contains results of research conducted under the Technical/Scientific Cooperation Agreement between the National Institute for Amazonian Research, the State University of Amazonas, and the Max-Planck-Gesellschaft e.V.; the opinions expressed are the entire responsibility of the authors and not of the participating institutions. We highly acknowledge the support by the Instituto Nacional de Pesquisas da Amazônia (INPA). We would like to especially thank all the people involved in the technical, logistical, and scientific support of the ATTO project, in particular Reiner Ditz, Jürgen Kesselmeier, Niro Higuchi, Matthias Sörgel, Stefan Wolff, Thomas Disper, Andrew Crozier, Uwe Schulz, Steffen Schmidt, Antonio Ocimar Manzi, Alcides Camargo Ribeiro, Hermes Braga Xavier, Elton Mendes da Silva, Nagib Alberto de Castro Souza, Adi Vasconcelos Brandão, Amaury Rodrigues Pereira, Antonio Huxley Melo Nascimento, Thiago de Lima Xavier, Josué Ferreira de Souza, Roberta Pereira de Souza, Bruno Takeshi, Ana María Yáñez-Serrano and Wallace Rabelo Costa. Moreover, we thank Thorsten Hoffmann, Ulrich Pöschl, Arthur Sedlacek, Jeannine Ditas, Su Hang, Jian Wang, Sachin Gunthe, Jan-David Förster, Ming Jing, Tobias Könemann, Maria Praß, Andrea Arangio and Bruna Amorim Holanda for support and stimulating discussions.

The authors gratefully acknowledge the NOAA Air Resources Laboratory (ARL) for the provision of the HYSPLIT transport and dispersion model and READY website (http://www.ready.noaa.gov) used in this publication.

The article processing charges for this open-access publication were covered by the Max Planck Society.

Edited by: Paolo Laj
Reviewed by: two anonymous referees

References

Ajtai, T., Filep, Á., Schnaiter, M., Linke, C., Vragel, M., Bozóki, Z., Szabó, G., and Leisner, T.: A novel multi−wavelength photoacoustic spectrometer for the measurement of the UV–vis-NIR spectral absorption coefficient of atmospheric aerosols, J. Aerosol Sci., 41, 1020–1029, https://doi.org/10.1016/j.jaerosci.2010.07.008, 2010.

Ajtai, T., Filep, Á., Utry, N., Schnaiter, M., Linke, C., Bozóki, Z., Szabó, G., and Leisner, T.: Inter-comparison of optical absorption coefficients of atmospheric aerosols determined by a multiwavelength photoacoustic spectrometer and an Aethalometer under sub-urban wintry conditions, J. Aerosol Sci., 42, 859–866, https://doi.org/10.1016/j.jaerosci.2011.07.008, 2011.

Andreae, M. O. and Gelencsér, A.: Black carbon or brown carbon? The nature of light-absorbing carbonaceous aerosols, Atmos. Chem. Phys., 6, 3131–3148, https://doi.org/10.5194/acp-6-3131-2006, 2006.

Andreae, M. O. and Ramanathan, V.: Climate's Dark Forcings, Science, 340, 280–281, https://doi.org/10.1126/science.1235731, 2013.

Andreae, M. O., Acevedo, O. C., Araùjo, A., Artaxo, P., Barbosa, C. G. G., Barbosa, H. M. J., Brito, J., Carbone, S., Chi, X., Cintra, B. B. L., da Silva, N. F., Dias, N. L., Dias-Júnior, C. Q., Ditas, F., Ditz, R., Godoi, A. F. L., Godoi, R. H. M., Heimann, M., Hoffmann, T., Kesselmeier, J., Könemann, T., Krüger, M. L., Lavrič, J. V, Manzi, A. O., Lopes, A. P., Martins, D. L., Mikhailov, E. F., Moran-Zuloaga, D., Nelson, B. W., Nölscher, A. C., Santos Nogueira, D., Piedade, M. T. F., Pöhlker, C., Pöschl, U., Quesada, C. A., Rizzo, L. V, Ro, C.-U., Ruckteschler, N., Sá, L. D. A., de Oliveira Sá, M., Sales, C. B., dos Santos, R. M. N., Saturno, J., Schöngart, J., Sörgel, M., de Souza, C. M., de Souza, R. A. F., Su, H., Targhetta, N., Tóta, J., Trebs, I., Trumbore, S., van Eijck, A., Walter, D., Wang, Z., Weber, B., Williams, J., Winderlich, J., Wittmann, F., Wolff, S., and Yáñez-Serrano, A. M.: The Amazon Tall Tower Observatory (ATTO): overview of pilot measurements on ecosystem ecology, meteorology, trace gases, and aerosols, Atmos. Chem. Phys., 15, 10723–10776, https://doi.org/10.5194/acp-15-10723-2015, 2015.

Ångström, A.: On the Atmospheric Transmission of Sun Radiation and on Dust in the Air, Geogr. Ann., 11, 156–166, 1929.

Arnott, W. P., Hamasha, K., Moosmüller, H., Sheridan, P. J., and Ogren, J. A.: Towards Aerosol Light-Absorption Measurements with a 7-Wavelength Aethalometer: Evaluation with a Photoacoustic Instrument and 3-Wavelength Nephelometer, Aerosol Sci. Technol., 39, 17–29, https://doi.org/10.1080/027868290901972, 2005.

Bergstrom, R. W., Russell, P. B., and Hignett, P.: Wavelength Dependence of the Absorption of Black Carbon Particles?: Predictions and Results from the TARFOX Experiment and Implications for the Aerosol Single Scattering Albedo, J. Atmos. Sci., 59, 567–577, 2002.

Bond, T. C. and Bergstrom, R. W.: Light Absorption by Carbonaceous Particles?: An Investigative Review, Aerosol Sci. Technol., 40, 27–67, https://doi.org/10.1080/02786820500421521, 2006.

Bond, T. C., Doherty, S. J., Fahey, D. W., Forster, P. M., Berntsen, T., DeAngelo, B. J., Flanner, M. G., Ghan, S., Kärcher, B., Koch, D., Kinne, S., Kondo, Y., Quinn, P. K., Sarofim, M. C., Schultz, M. G., Schulz, M., Venkataraman, C., Zhang, H., Zhang, S., Bellouin, N., Guttikunda, S. K., Hopke, P. K., Jacobson, M. Z., Kaiser, J. W., Klimont, Z., Lohmann, U., Schwarz, J. P., Shindell, D., Storelvmo, T., Warren, S. G., and Zender, C. S.: Bounding the role of black carbon in the climate system: A scientific assessment, J. Geophys. Res.-Atmos., 118, 5380–5552, https://doi.org/10.1002/jgrd.50171, 2013.

Cappa, C. D., Onasch, T. B., Massoli, P., Worsnop, D. R., Bates, T. S., Cross, E. S., Davidovits, P., Hakala, J., Hayden, K. L., Jobson, B. T., Kolesar, K. R., Lack, D. a, Lerner, B. M., Li, S.-M., Mellon, D., Nuaaman, I., Olfert, J. S., Petäjä, T., Quinn, P. K., Song, C., Subramanian, R., Williams, E. J., and Zaveri, R. A.: Radiative absorption enhancements due to the mixing state of atmospheric black carbon, Science, 337, 1078–1081, https://doi.org/10.1126/science.1223447, 2012.

Cheng, Y., Engling, G., Moosmüller, H., Arnott, W. P., Chen, A. L. W., Wold, C. E., Hao, W. M., and He, K.: Light absorption by biomass burning source emissions, Atmos. Environ., 127, 347–354, https://doi.org/10.1016/j.atmosenv.2015.12.045, 2016.

Collaud Coen, M., Weingartner, E., Apituley, A., Ceburnis, D., Fierz-Schmidhauser, R., Flentje, H., Henzing, J. S., Jennings, S. G., Moerman, M., Petzold, A., Schmid, O., and Baltensperger, U.: Minimizing light absorption measurement artifacts of the Aethalometer: evaluation of five correction algorithms, Atmos. Meas. Tech., 3, 457–474, https://doi.org/10.5194/amt-3-457-2010, 2010.

Després, V. R., Alex Huffman, J., Burrows, S. M., Hoose, C., Safatov, A. S., Buryak, G., Fröhlich-Nowoisky, J., Elbert, W., Andreae, M. O., Pöschl, U., and Jaenicke, R.: Primary biological aerosol particles in the atmosphere: a review, Tellus B, 64, 15598, https://doi.org/10.3402/tellusb.v64i0.15598, 2012.

Draxler, R. R. and Hess, G. D.: An overview of the HYSPLIT 4 modelling system for trajectories, dispersion and deposition, Aust. Met. Mag., 47, 295–308, 1998.

Drinovec, L., Močnik, G., Zotter, P., Prévôt, A. S. H., Ruckstuhl, C., Coz, E., Rupakheti, M., Sciare, J., Müller, T., Wiedensohler, A., and Hansen, A. D. A.: The "dual-spot" Aethalometer: an improved measurement of aerosol black carbon with real-time loading compensation, Atmos. Meas. Tech., 8, 1965–1979, https://doi.org/10.5194/amt-8-1965-2015, 2015.

Favez, O., El Haddad, I., Piot, C., Boréave, A., Abidi, E., Marchand, N., Jaffrezo, J.-L., Besombes, J.-L., Personnaz, M.-B., Sciare, J., Wortham, H., George, C., and D'Anna, B.: Intercomparison of source apportionment models for the estimation of wood burning aerosols during wintertime in an Alpine city (Grenoble, France), Atmos. Chem. Phys., 10, 5295–5314, https://doi.org/10.5194/acp-10-5295-2010, 2010.

Flowers, B. A., Dubey, M. K., Mazzoleni, C., Stone, E. A., Schauer, J. J., Kim, S.-W., and Yoon, S. C.: Optical-chemical-microphysical relationships and closure studies for mixed carbonaceous aerosols observed at Jeju Island; 3-laser photoacoustic spectrometer, particle sizing, and filter analysis, Atmos. Chem. Phys., 10, 10387–10398, https://doi.org/10.5194/acp-10-10387-2010, 2010.

Garg, S., Chandra, B. P., Sinha, V., Sarda-Esteve, R., Gros, V., and Sinha, B.: Limitation of the Use of the Absorption Angstrom Exponent for Source Apportionment of Equivalent Black Carbon: a Case Study from the North West Indo-Gangetic Plain, Environ. Sci. Technol., 50, 814–824, https://doi.org/10.1021/acs.est.5b03868, 2016.

Hansen, A. D. A., Rosen, H., and Novakov, T.: The aethalometer – An instrument for the real-time measurement of optical absorption by aerosol particles, Sci. Total Environ., 36, 191–196, https://doi.org/10.1016/0048-9697(84)90265-1, 1984.

Hyvärinen, A.-P., Vakkari, V., Laakso, L., Hooda, R. K., Sharma, V. P., Panwar, T. S., Beukes, J. P., van Zyl, P. G., Josipovic, M., Garland, R. M., Andreae, M. O., Pöschl, U., and Petzold, A.: Correction for a measurement artifact of the Multi-Angle Absorption Photometer (MAAP) at high black carbon mass concentration levels, Atmos. Meas. Tech., 6, 81–90, https://doi.org/10.5194/amt-6-81-2013, 2013.

IPCC: Climate Change 2013: The Physical Science Basis. Contribution of Working Group I to the Fifth Assessment Report of the

Intergovernmental Panel on Climate Change, Cambridge, UK, 1535 pp., 2013.

Kirchstetter, T. W., Novakov, T., and Hobbs, P. V.: Evidence that the spectral dependence of light absorption by aerosols is affected by organic carbon, J. Geophys. Res.-Atmos., 109, D21208, https://doi.org/10.1029/2004JD004999, 2004.

Lack, D. A. and Cappa, C. D.: Impact of brown and clear carbon on light absorption enhancement, single scatter albedo and absorption wavelength dependence of black carbon, Atmos. Chem. Phys., 10, 4207–4220, https://doi.org/10.5194/acp-10-4207-2010, 2010.

Lack, D. A. and Langridge, J. M.: On the attribution of black and brown carbon light absorption using the Ångström exponent, Atmos. Chem. Phys., 13, 10535–10543, https://doi.org/10.5194/acp-13-10535-2013, 2013.

Laskin, A., Laskin, J., and Nizkorodov, S. A.: Chemistry of Atmospheric Brown Carbon, Chem. Rev., 115, 4335–4382, https://doi.org/10.1021/cr5006167, 2015.

Lewis, K., Arnott, W. P., Moosmüller, H., and Wold, C. E.: Strong spectral variation of biomass smoke light absorption and single scattering albedo observed with a novel dual-wavelength photoacoustic instrument, J. Geophys. Res., 113, D16203, https://doi.org/10.1029/2007JD009699, 2008.

Massabò, D., Bernardoni, V., Bove, M. C., Brunengo, A., Cuccia, E., Piazzalunga, A., Prati, P., Valli, G., and Vecchi, R.: A multi-wavelength optical set-up for the characterization of carbonaceous particulate matter, J. Aerosol Sci., 60, 34–46, https://doi.org/10.1016/j.jaerosci.2013.02.006, 2013.

Massabò, D., Caponi, L., Bernardoni, V., Bove, M. C., Brotto, P., Calzolai, G., Cassola, F., Chiari, M., Fedi, M. E., Fermo, P., Giannoni, M., Lucarelli, F., Nava, S., Piazzalunga, A., Valli, G., Vecchi, R., and Prati, P.: Multi-wavelength optical determination of black and brown carbon in atmospheric aerosols, Atmos. Environ., 108, 1–12, https://doi.org/10.1016/j.atmosenv.2015.02.058, 2015.

Moosmüller, H., Chakrabarty, R. K., Ehlers, K. M., and Arnott, W. P.: Absorption Ångström coefficient, brown carbon, and aerosols: basic concepts, bulk matter, and spherical particles, Atmos. Chem. Phys., 11, 1217–1225, https://doi.org/10.5194/acp-11-1217-2011, 2011.

Müller, T., Laborde, M., Kassell, G., and Wiedensohler, A.: Design and performance of a three-wavelength LED-based total scatter and backscatter integrating nephelometer, Atmos. Meas. Tech., 4, 1291–1303, https://doi.org/10.5194/amt-4-1291-2011, 2011.

Myhre, G. and Stordal, F.: Global sensitivity experiments of the radiative forcing due to mineral aerosols, J. Geophys. Res.-Atmos., 106, 18193–18204, https://doi.org/10.1029/2000JD900536, 2001.

Penner, J. E., Dickinson, R. E., and O'Neill, C. A.: Effects of Aerosol from Biomass Burning on the Global Radiation Budget, Science, 256, 1432–1434, https://doi.org/10.1126/science.256.5062.1432, 1992.

Petzold, A. and Schönlinner, M.: Multi-angle absorption photometry – a new method for the measurement of aerosol light absorption and atmospheric black carbon, J. Aerosol Sci., 35, 421–441, https://doi.org/10.1016/j.jaerosci.2003.09.005, 2004.

Petzold, A., Schloesser, H., Sheridan, P. J., Arnott, W. P., Ogren, J. A., and Virkkula, A.: Evaluation of Multiangle Absorption Photometry for Measuring Aerosol Light Absorption, Aerosol Sci. Technol., 39, 40–51, https://doi.org/10.1080/027868290901945, 2005.

Pöhlker, M. L., Pöhlker, C., Klimach, T., Hrabe de Angelis, I., Barbosa, H. M. J., Brito, J., Carbone, S., Cheng, Y., Chi, X., Ditas, F., Ditz, R., Gunthe, S. S., Kesselmeier, J., Könemann, T., Lavrič, J. V., Martin, S. T., Moran-Zuloaga, D., Rose, D., Saturno, J., Su, H., Thalman, R., Walter, D., Wang, J., Wolff, S., Artaxo, P., Andreae, M. O. and Pöschl, U.: Long-term observations of cloud condensation nuclei in the Amazon rain forest – Part 1: Aerosol size distribution, hygroscopicity, and new model parametrizations for CCN prediction, Atmos. Chem. Phys., 16, 15709–15740, https://doi.org/10.5194/acp-16-15709-2016, 2016.

Pöhlker, M. L., Pöhlker, C., Klimach, T., Hrabe de Angelis, I., Barbosa, H. M. J., Brito, J., Carbone, S., Chi, X., Cheng, Y., Ditas, F., Ditz, R., Gunthe, S. S., Kesselmeier, J., Könemann, T., Lavrič, J. V., Martin, S. T., Moran-Zuloaga, D., Rose, D., Saturno, J., Su, H., Thalman, R., Walter, D., Wang, J., Wolff, S., Artaxo, P., Andreae, M. O., and Pöschl, U.: Long-term observations of atmospheric aerosol, cloud condensation nuclei concentration and hygroscopicity in the Amazon rain forest – Part 2: Ultrafine particle bursts, biomass burning and long range transport events, Atmos. Chem. Phys., in preparation, 2017.

Rizzo, L. V., Correia, A. L., Artaxo, P., Procópio, A. S., and Andreae, M. O.: Spectral dependence of aerosol light absorption over the Amazon Basin, Atmos. Chem. Phys., 11, 8899–8912, https://doi.org/10.5194/acp-11-8899-2011, 2011.

Saleh, R., Robinson, E. S., Tkacik, D. S., Ahern, A. T., Liu, S., Aiken, A. C., Sullivan, R. C., Presto, A. a, Dubey, M. K., Yokelson, R. J., Donahue, N. M., and Robinson, A. L.: Brownness of organics in aerosols from biomass burning linked to their black carbon content, Nat. Geosci., 7, 2–5, https://doi.org/10.1038/ngeo2220, 2014.

Sandradewi, J., Prévôt, A. S. H., Szidat, S., Perron, N., Alfarra, M. R., Lanz, V. A., Weingartner, E., and Baltensperger, U.: Using aerosol light absorption measurements for the quantitative determination of wood burning and traffic emission contributions to particulate matter, Environ. Sci. Technol., 42, 3316–23, 2008.

Schmid, O., Artaxo, P., Arnott, W. P., Chand, D., Gatti, L. V., Frank, G. P., Hoffer, A., Schnaiter, M., and Andreae, M. O.: Spectral light absorption by ambient aerosols influenced by biomass burning in the Amazon Basin. I: Comparison and field calibration of absorption measurement techniques, Atmos. Chem. Phys., 6, 3443–3462, https://doi.org/10.5194/acp-6-3443-2006, 2006.

Schuster, G. L., Dubovik, O., and Arola, A.: Remote sensing of soot carbon – Part 1: Distinguishing different absorbing aerosol species, Atmos. Chem. Phys., 16, 1565–1585, https://doi.org/10.5194/acp-16-1565-2016, 2016a.

Schuster, G. L., Dubovik, O., Arola, A., Eck, T. F., and Holben, B. N.: Remote sensing of soot carbon – Part 2: Understanding the absorption Ångström exponent, Atmos. Chem. Phys., 16, 1587–1602, https://doi.org/10.5194/acp-16-1587-2016, 2016b.

Segura, S., Estellés, V., Titos, G., Lyamani, H., Utrillas, M. P., Zotter, P., Prévôt, A. S. H., Močnik, G., Alados-Arboledas, L., and Martínez-Lozano, J. A.: Determination and analysis of in situ spectral aerosol optical properties by a multi-instrumental approach, Atmos. Meas. Tech., 7, 2373–2387, https://doi.org/10.5194/amt-7-2373-2014, 2014.

Subramanian, R., Roden, C. A., Boparai, P., and Bond, T. C.: Yellow Beads and Missing Particles: Trouble Ahead for Filter-Based

Absorption Measurements, Aerosol Sci. Technol., 41, 630–637, https://doi.org/10.1080/02786820701344589, 2007.

Virkkula, A.: Correction of the Calibration of the 3-wavelength Particle Soot Absorption Photometer (3λ PSAP), Aerosol Sci. Technol., 44, 706–712, https://doi.org/10.1080/02786826.2010.482110, 2010.

Virkkula, A., Ahlquist, N. C., Covert, D. S., Arnott, W. P., Sheridan, P. J., Quinn, P. K., and Coffman, D. J.: Modification, Calibration and a Field Test of an Instrument for Measuring Light Absorption by Particles, Aerosol Sci. Technol., 39, 68–83, https://doi.org/10.1080/027868290901963, 2005.

Virkkula, A., Mäkelä, T., Hillamo, R., Yli-Tuomi, T., Hirsikko, A., Hämeri, K., and Koponen, I. K.: A simple procedure for correcting loading effects of aethalometer data, J. Air Waste Manag. Assoc., 57, 1214–1222, https://doi.org/10.3155/1047-3289.57.10.1214, 2007.

Wang, X., Heald, C. L., Sedlacek, A. J., de Sá, S. S., Martin, S. T., Alexander, M. L., Watson, T. B., Aiken, A. C., Springston, S. R., and Artaxo, P.: Deriving brown carbon from multiwavelength absorption measurements: method and application to AERONET and Aethalometer observations, Atmos. Chem. Phys., 16, 12733–12752, https://doi.org/10.5194/acp-16-12733-2016, 2016.

Weingartner, E., Saathoff, H., Schnaiter, M., Streit, N., Bitnar, B., and Baltensperger, U.: Absorption of light by soot particles: determination of the absorption coefficient by means of aethalometers, J. Aerosol Sci., 34, 1445–1463, https://doi.org/10.1016/S0021-8502(03)00359-8, 2003.

Yu, H., Kaufman, Y. J., Chin, M., Feingold, G., Remer, L. A., Anderson, T. L., Balkanski, Y., Bellouin, N., Boucher, O., Christopher, S., DeCola, P., Kahn, R., Koch, D., Loeb, N., Reddy, M. S., Schulz, M., Takemura, T., and Zhou, M.: A review of measurement-based assessments of the aerosol direct radiative effect and forcing, Atmos. Chem. Phys., 6, 613–666, https://doi.org/10.5194/acp-6-613-2006, 2006.

Supplement of Atmos. Meas. Tech., 10, 2837–2850, 2017
https://doi.org/10.5194/amt-10-2837-2017-supplement

Atmospheric Measurement Techniques
Open Access
EGU

Supplement of

Comparison of different Aethalometer correction schemes and a reference multi-wavelength absorption technique for ambient aerosol data

Jorge Saturno et al.

Correspondence to: Jorge Saturno (j.saturno@mpic.de)

Supplementary material

Table S1. Constants C^* and m_s taken from Arnott et al. (2005)

Wavelength (nm)	C^*	m_s
370	1.813	0.0335
470	2.073	0.0457
520	2.076	0.0523
590	2.104	0.0616
660	2.182	0.0713
880	2.226	0.1038
950	2.199	0.1148

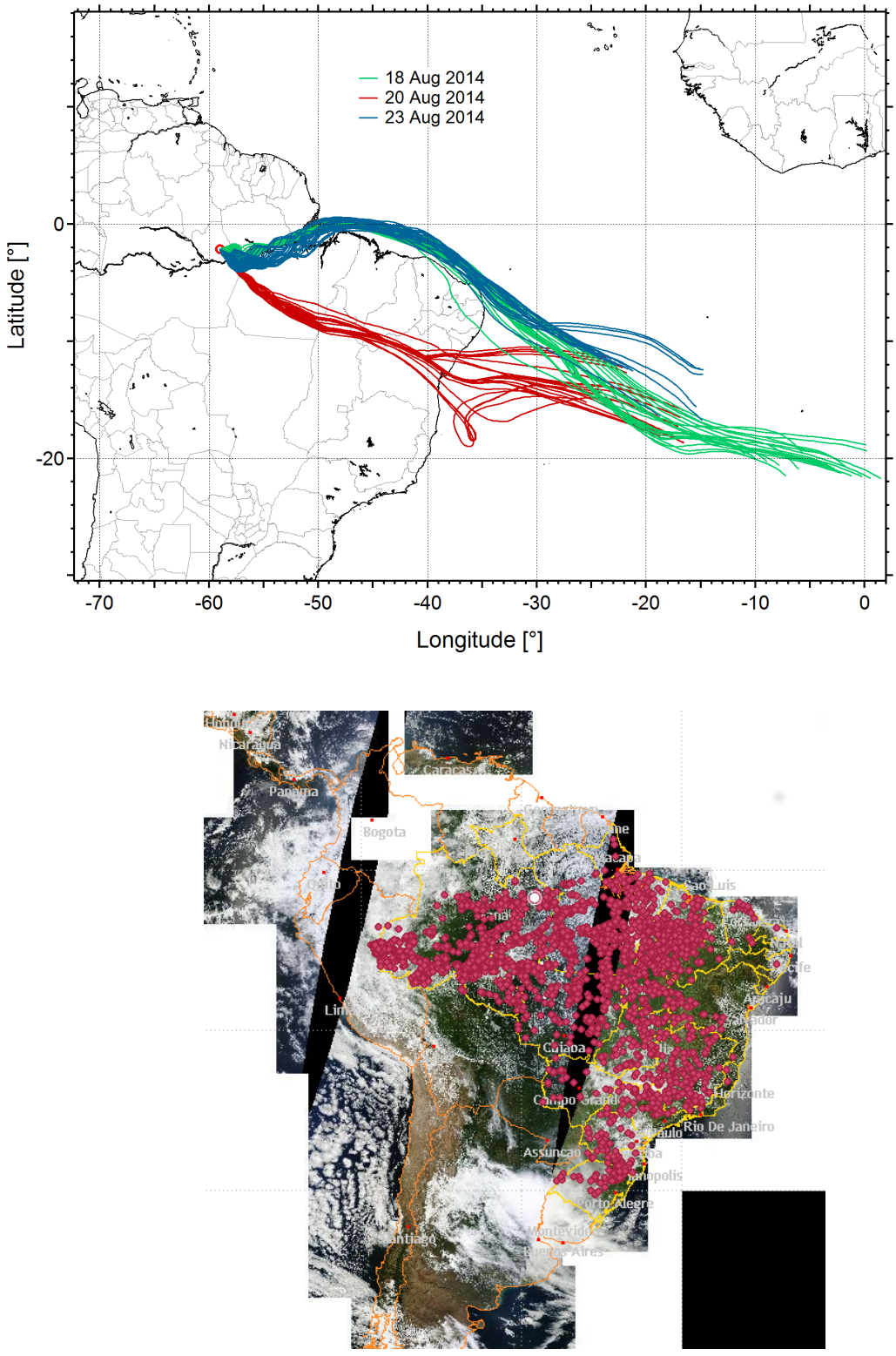

Figure S1. HYPSLIT 200-m high 9-days backward trajectories calculated for 18, 20 and 23 August 2014. Fire spots shown in the bottom picture were remotely detected by NOAA-12 between 19 August 2014 00:00:00 and 21 August 2014 23:59:59, ATTO site location is shown as a white circle.

Filter loading correction

Comparison between Schmid et al. and Collaud Coen et al.

The ration between attenuation coefficients and the MAAP absorption coefficients (expressed as C_{ref}) should not depend on ATN after applying the filter-loading correction. Figure S2 shows C_{ref} as a function of ATN, after applying both filter-loading corrections. The result of both corrections is quite similar and the slopes obtained by orthogonal fits are statistically equivalent. The drop observed in C_{ref} for ATN > 30% in the Schmid correction was also obtained by Collaud Coen et al. (2010) in a sampling site located far from the sources, where the aerosol was characteristically aged and SSA was close to 1.

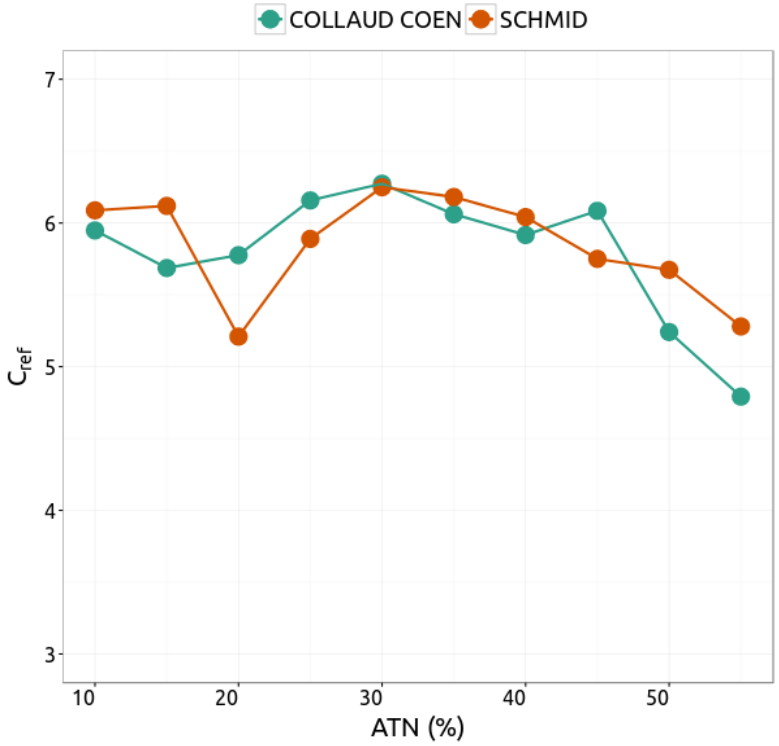

Figure S2. C_{ref} obtained by following Schmid and Collaud Coen corrections as a function of 5%-wide attenuation bins.

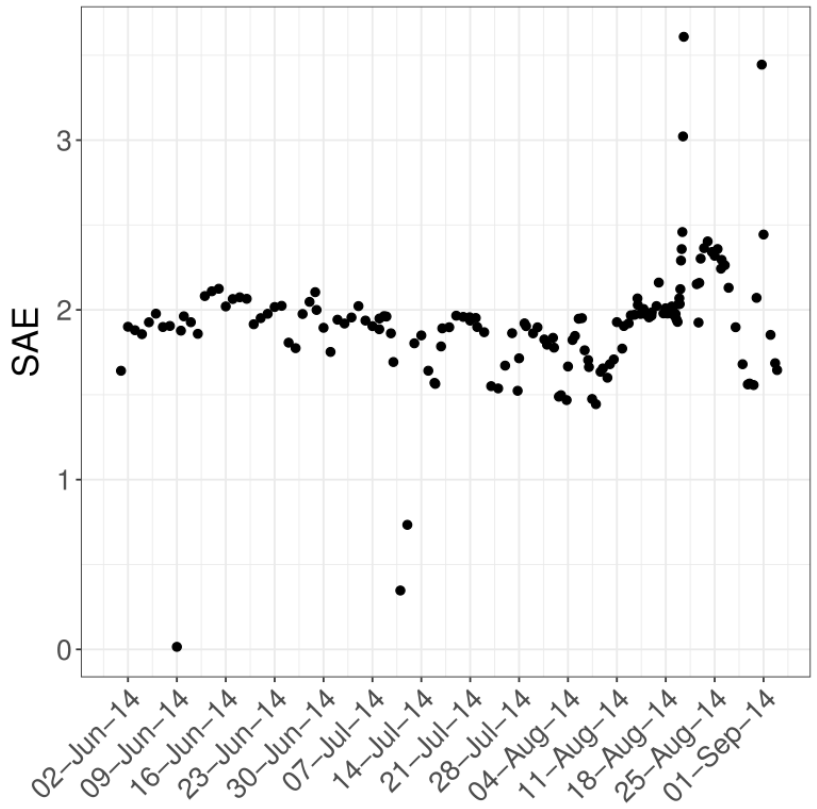

Figure S3. Scattering Ångström exponent, $å_{SCA}$, averaged over MAAP filter sampling times.

Software

We used the statistical software environment R (R Development Core Team, 2009) to process the data presented in this work. When comparing two different datasets, resulting from different instruments or different corrections, we used the package SMATR (Falster et al., 2006; Warton et al., 2012) to apply standardized major axis (SMA) estimations.

The scripts used in this work are available under GPLv3 license at:
https://dx.doi.org/10.6084/m9.figshare.c.3501153.v3

References

Falster, D. S., Warton, D. I. and Wright, I. J.: SMATR: Standardised major axis tests and routines, ver 2.0, 2006.

R Development Core Team: R: A language and environment for statistical computing, [online] Available from: http://www.r-project.org, 2009.

Warton, D. I., Duursma, R. A., Falster, D. S. and Taskinen, S.: smatr 3- an R package for estimation and inference about allometric lines, Methods Ecol. Evol., 3(2), 257–259, doi:10.1111/j.2041-210X.2011.00153.x, 2012.

B.2. Saturno et al., Atmos. Chem. Phys. Discuss., 2017a

Black and brown carbon over central Amazonia: Long-term aerosol measurements at the ATTO site

Jorge Saturno[1], Bruna A. Holanda[1], Christopher Pöhlker[1], Florian Ditas[1], Qiaoqiao Wang[1,2], Daniel Moran-Zuloaga[1], Joel Brito[3,4], Samara Carbone[3,5], Yafang Cheng[1], Xuguang Chi[6], Jeannine Ditas[1], Thorsten Hoffmann[7], Isabella Hrabe de Angelis[1], Tobias Könemann[1], Jost V. Lavrič[8], Nan Ma[1], Jing Ming[1], Hauke Paulsen[9], Mira L. Pöhlker[1], Luciana V. Rizzo[10], Patrick Schlag[3], Hang Su[1], David Walter[1], Stefan Wolff[1], Yuxuan Zhang[1], Paulo Artaxo[3], Ulrich Pöschl[1], and Meinrat O. Andreae[1,11]

[1] *Biogeochemistry & Multiphase Chemistry Departments, Max Planck Institute for Chemistry, P.O. Box 3060, 55020 Mainz, Germany*
[2] *Jinan University Institute for Environmental and Climate Research, Guangzhou, China*
[3] *Department of Applied Physics, Institute of Physics, University of São Paulo (USP), Rua do Matão, Travessa R, 187, CEP 05508-900, São Paulo, SP, Brazil*
[4] *Laboratory for Meteorological Physics, Université Clermont Auvergne, Clermont-Ferrand, France*
[5] *Institute of Agrarian Sciences, Federal University of Uberlândia, Uberlândia, Minas Gerais, Brazil*
[6] *Institute for Climate and Global Change Research & School of Atmospheric Sciences, Nanjing University, Nanjing, 210093, China*
[7] *Department of Chemistry, Johannes Gutenberg University, Mainz, Germany*
[8] *Department of Biogeochemical Systems, Max Planck Institute for Biogeochemistry, 07701 Jena, Germany.*
[9] *Institute of General Botany, Johannes Gutenberg University, Mainz, Germany*
[10] *Departamento de Ciencias Ambientais, Universidade Federal de Sao Paulo, Diadema, SP, Brasil*
[11] *Scripps Institution of Oceanography, University of California San Diego, La Jolla, CA 92098, USA*

Atmospheric Chemistry and Physics Discussions, in review, 2017.

Atmos. Chem. Phys. Discuss., https://doi.org/10.5194/acp-2017-1097
Manuscript under review for journal Atmos. Chem. Phys.
This is just a preview and not the published paper.

Atmospheric Chemistry and Physics Discussions

Black and brown carbon over central Amazonia: Long-term aerosol measurements at the ATTO site

Jorge Saturno[1], Bruna A. Holanda[1], Christopher Pöhlker[1], Florian Ditas[1], Qiaoqiao Wang[1,2], Daniel Moran-Zuloaga[1], Joel Brito[3,4], Samara Carbone[3,5], Yafang Cheng[1], Xuguang Chi[6], Jeannine Ditas[1,2], Thorsten Hoffmann[7], Isabella Hrabe de Angelis[1], Tobias Könemann[1], Jošt V. Lavrič[8], Nan Ma[1,2], Jing Ming[1], Hauke Paulsen[9], Mira L. Pöhlker[1], Luciana V. Rizzo[10], Patrick Schlag[3], Hang Su[1], David Walter[1], Stefan Wolff[1], Yuxuan Zhang[1], Paulo Artaxo[3], Ulrich Pöschl[1], and Meinrat O. Andreae[1,11]

[1]Biogeochemistry & Multiphase Chemistry Departments, Max Planck Institute for Chemistry, P. O. Box 3060, 55020 Mainz, Germany.
[2]Jinan University Institute for Environmental and Climate Research, Guangzhou, China.
[3]Department of Applied Physics, Institute of Physics, University of São Paulo (USP), Rua do Matão, Travessa R, 187, CEP 05508-900, São Paulo, SP, Brazil.
[4]Laboratory for Meteorological Physics, Université Clermont Auvergne, Clermont-Ferrand, France.
[5]Institute of Agrarian Sciences, Federal University of Uberlândia, Uberlândia, Minas Gerais, Brazil.
[6]Institute for Climate and Global Change Research & School of Atmospheric Sciences, Nanjing University, Nanjing, 210093, China.
[7]Department of Chemistry, Johannes Gutenberg University, Mainz, Germany.
[8]Department of Biogeochemical Systems, Max Planck Institute for Biogeochemistry, 07701 Jena, Germany.
[9]Institute of General Botany, Johannes Gutenberg University, Mainz, Germany.
[10]Departamento de Ciencias Ambientais, Universidade Federal de Sao Paulo, Diadema, SP, Brasil.
[11]Scripps Institution of Oceanography, University of California San Diego, La Jolla, CA 92098, USA.

Correspondence to: Jorge Saturno (j.saturno@mpic.de) and Christopher Pöhlker (c.pohlker@mpic.de)

Abstract. The Amazon rain forest is considered a very sensitive ecosystem that could be significantly affected by a changing climate. It is still one of the few places on Earth where the atmosphere in the continent approaches near-pristine conditions for some periods of the year. The Amazon Tall Tower Observatory (ATTO) has been built in central Amazonia to monitor the atmospheric and forest ecosystem conditions. The atmospheric conditions at the ATTO site oscillate between biogenic and biomass burning (BB) dominated states. By using a comprehensive ground-based aerosol measurement setup, we studied the physical and chemical properties of aerosol particles at the ATTO site. This paper presents results from 2012 to 2017, with special focus on light absorbing aerosol particles. The aerosol

Atmos. Chem. Phys. Discuss., https://doi.org/10.5194/acp-2017-1097
Manuscript under review for journal Atmos. Chem. Phys.
This is just a preview and not the published paper.

Atmospheric Chemistry and Physics Discussions

absorption wavelength dependence (expressed as the absorption Ångström exponent, $å_{abs}$) was usually below 1.0 and increased during the presence of smoke transported from fires in the southern and eastern regions of the Amazon or advected from savanna fires in Africa. In this study, the brown carbon (BrC) contribution to light absorption at 370 nm was obtained by calculating the theoretical wavelength dependence of $å_{abs}$ (WDA). Our calculations resulted in BrC contributions of 17 – 29 % (25th and 75th percentiles) to total light absorption at 370 nm ($\sigma_{ap\,370}$) during the measurement period (2012 – 2017). The BrC contribution increased up to 27 – 47 % during fire events occurring under the influence of El Niño, between September and November 2015. An extended time series of ATTO and ZF2 (another Amazon rain forest sampling site) data showed enhanced light scattering and absorption coefficients during El Niño periods in 2009 and 2015. Long-range transport (LRT) aerosol particles that reached the central Amazon Basin from Africa or from southern Amazon exhibited a wide range of black carbon (BC) to carbon monoxide (CO) enhancement ratios (ER_{BC}) (between 4 and 15 ng m^{-3} ppb^{-1}) reflecting the variability of fuels, combustion phase, and removal processes in the atmosphere. Higher ER_{BC} were measured during the dry season when we observed values up to 15 ng m^{-3} ppb^{-1}, which were related to the lowest single scattering albedo (ω_0) measured during the studied period, (0.86 – 0.93). A parameterization of $å_{abs}$ as a function of the BC to OA mass ratio was investigated and was found applicable to tropical forest emissions but further investigation is required, especially by segregating fuel types. Additionally, important enhancements of the BC mass absorption cross-section (α_{abs}) were found over the measurement period. This enhancement could be linked to heavy coating of the BC aerosol particles. In the future, the BC mixing state should be systematically investigated by using different instrumental approaches.

1 Introduction

Atmospheric aerosol particles affect the Earth's climate through different mechanisms. Direct mechanisms include the aerosol particle interaction with radiation by scattering and absorption. The balance between scattering and absorption can lead to warming or cooling of the atmosphere (IPCC, 2013). Moreover, aerosol-cloud interactions related to cloud formation and cloud microphysical

Atmos. Chem. Phys. Discuss., https://doi.org/10.5194/acp-2017-1097
Manuscript under review for journal Atmos. Chem. Phys.
This is just a preview and not the published paper.

Atmospheric Chemistry and Physics Discussions

modification, are related to high uncertainties, especially due to the lack of knowledge of pre-industrial cloud condensation nuclei (CCN) availability (Carslaw et al., 2013) and aerosol particles spatial distribution in the atmosphere (Andreae, 2007).

Continuous aerosol measurements at remote continental locations are crucial to understand atmospheric conditions prior to industrialization and reduce the uncertainties in climate models (Seinfeld et al., 2016). The Amazon Basin is one of the few continental areas in the world where the atmosphere can be studied in near-pristine conditions during some periods of the year (Andreae et al., 2015). However, measuring under near-pristine to pristine conditions is quite challenging even in very remote places because anthropogenic pollution is rather persistent and, thus, reaches almost every continental place on the planet (Andreae, 2007; Chi et al., 2013; Hamilton et al., 2014). The Amazon rain forest has been impacted by intensified agriculture and associated deforestation in the southern and eastern areas and infrastructural development in the last 50 years (Artaxo et al., 2013; Davidson et al., 2012). Given these circumstances, only when air masses travel over clean marine areas and the rain-related scavenging is significant, the observations approach near-pristine aerosol particle levels (Andreae et al., 2012, 2015).

Biogenic primary and secondary organic aerosol particles over the Amazon rain forest are ubiquitous throughout the year (Martin et al., 2010). During the dry season (August – November), when fires are frequent in the forest and its peripheries, the background biogenic aerosol is overwhelmed by BB smoke. Despite the occurrence of natural tropical forest fires, most of the fire episodes in the Amazon rain forest peripheries occur due to human activity, including land use change, brush clearing for agricultural activities and burning of agricultural waste (Andreae, 1991; Crutzen and Andreae, 1990). Additionally, cooperative burning of savannas is a common practice by indigenous communities in the region and it helps to prevent larger wildfires when burned areas can act as “firebreaks” (Bilbao et al., 2010). Starting in August, the dry season is characterized by aerosol number concentrations of 1000 – 3000 cm^{-3} (Andreae et al., 2015). Another characteristic of this period is the abundance of black carbon (BC). This type of aerosol particles are primarily emitted by flaming and smoldering fires together with large amounts of organic aerosol (OA) (Andreae and Merlet, 2001) and are considered an important short-lived climate forcing agent (Bond et al., 2004, 2013). The BC co-emitted light absorbing fraction of OA is called *brown carbon* (BrC) (Andreae and Gelencsér, 2006). The BC + BrC

Atmos. Chem. Phys. Discuss., https://doi.org/10.5194/acp-2017-1097
Manuscript under review for journal Atmos. Chem. Phys.
This is just a preview and not the published paper.

Atmospheric Chemistry and Physics Discussions

aerosol fraction is commonly defined as *light-absorbing carbonaceous matter* (LAC). The mentioned nomenclature is in accordance with the one compiled by Petzold et al. (2013). A list of frequently used acronyms and symbols can be found in Table 1.

During combustion, aerosol particles are co-emitted with carbon monoxide (CO). The ratio between aerosol mass or number concentrations and CO has been used to trace air masses origin and age (Guyon et al., 2005; Janhäll et al., 2010). Enhancement ratios (ER_{BC}) for open biomass burning measured for boreal forest smoldering fires have an average ER_{BC} of 1.7 ng m^{-3} ppb^{-1} (Kondo et al., 2011). On the other hand, agricultural fires exhibit higher ER_{BC} compared to forest fires, with reported values varying between 2.2 and 29.8 ng m^{-3} ppb^{-1}, see Mikhailov et al. (2017) and references therein.

Biomass burning plumes are usually dominated by accumulation mode aerosol particles, which are efficient to scatter radiation and also rich in BC. In the absence of BB aerosol particles, the biological coarse mode particles become dominant in terms of mass and the aerosol optical properties are affected. Therefore, clear seasonal trends in scattering and absorption have been observed by long-term measurements in the Amazon region (Rizzo et al., 2013).

The light absorption of BC has a wavelength dependence that is conditioned by the BC mixing state, its size distribution and the composition of co-emitted particles (Andreae and Gelencsér, 2006; Kirchstetter et al., 2004; Lack et al., 2013; Schuster et al., 2016). The wavelength dependence is described by the absorption Ångström exponent ($å_{abs}$) (Ångström, 1929), which can vary from low values ($å_{abs} = 1.0 \pm 0.1$, weak spectral dependence), usually associated to fossil fuel emitted BC (Bond and Bergstrom, 2006), up to high values ($å_{abs}$ = 6-7, strong spectral dependence) for organic-rich aerosol, e.g., humic-like substances (HULIS) (Hoffer et al., 2006). Measurements at an Amazonian forest site during the dry season resulted in $å_{abs}$ average values below 1.0 for absorption coefficients lower than 15 Mm^{-1} at 450 nm (Rizzo et al., 2011). For BB aerosol particles, the $å_{abs}$ is usually higher than 1.0. However, it depends on the burning conditions, its BC to OA ratio (Saleh et al., 2014), and the BC-BrC size distributions and morphologies (Womack et al., ref needed). Several studies have used the absorption spectral dependence to apportion the fossil fuel and BB contributions to total absorption (Favez et al., 2010; Massabò et al., 2015; Sandradewi et al., 2008). However, the $å_{abs}$ values do not

Atmos. Chem. Phys. Discuss., https://doi.org/10.5194/acp-2017-1097
Manuscript under review for journal Atmos. Chem. Phys.
This is just a preview and not the published paper.

Atmospheric Chemistry and Physics Discussions

always reflect the combustion type and using it as a source apportionment parameter could lead to erroneous results (Garg et al., 2016; Lack and Langridge, 2013; Lewis et al., 2008; Wang et al., 2016b). Several measurement studies assume a BC $å_{abs}$ of 1.0 but models show that pure BC could exhibit a broader range of $å_{abs}$ values (Moosmüller et al., 2011). In order to retrieve the ambient BC wavelength dependence, Wang et al. (2016b) proposed the use of the wavelength dependence of $å_{abs}$ instead of $å_{abs}$ itself. The so-called *wavelength dependence of* $å_{abs}$ (WDA) is calculated as the difference of two wavelength pairs; one for shorter to long wavelengths (e.g., 440 – 870 nm) and another for medium to long wavelengths (e.g., 675 – 880 nm).

Precise BC mass measurements are required to retrieve the correct relationship between absorptivity and BC mass, defined as the mass absorption cross-section (MAC or α_{abs}). The BC mass concentration has been traditionally measured by using thermal or thermal-optical techniques. However, these methods suffer from several bias, like organic carbon charring that increases the apparent BC concentration, especially when high organic fractions are present (Andreae and Gelencsér, 2006). More recently, laser-induced incandescence (LII) techniques have been introduced (Snelling et al., 2005). These techniques measure the volume-equivalent mass of refractory black carbon (rBC) that vaporizes at temperatures of 2800-4000 K. The MAC is used by atmospheric radiative transfer models to obtain absorption coefficients from mass concentration data. The MAC of BC varies between 4 and 11 $m^2\ g^{-1}$ at 550 nm (Bond and Bergstrom, 2006), having an average of 6.5 $m^2\ g^{-1}$ at 637 nm for fresh soot. In case of condensation of non-BC material on the BC particles, the MAC can be enhanced due to the well-known 'lensing effect' (Fuller et al., 1999). This commonly happens when BC is emitted by BB, since it is co-emitted with large amounts of organic vapors that would condense on BC particles (Saleh et al., 2014). Black carbon particles can also obtain a secondary organic aerosol (SOA) coating during advection over the rain forest (Pöschl et al., 2010) as well as inorganic coatings, which has been previously observed at the ATTO site (Pöhlker et al., 2014). It has been found that the coating mass significantly affects the absorption enhancement of BC cores but no significant changes are caused by a different coating's O:C ratio (Tasoglou et al., 2017). A wide range of MAC can be found in the literature for different fire conditions (smoldering and flaming).

Atmos. Chem. Phys. Discuss., https://doi.org/10.5194/acp-2017-1097
Manuscript under review for journal Atmos. Chem. Phys.
This is just a preview and not the published paper.

Atmospheric Chemistry and Physics Discussions

Commonly, the absorption properties of an aerosol population are reported as the single scattering albedo (SSA, ω_0), which is defined as total scattering divided by total extinction (absorption + scattering). Therefore, a lower ω_0 is associated with a stronger absorption. Tropical Amazonian forest fires have moderately high ω_0 values (0.93 ± 0.02 at 670 nm), given the high amount of scattering aerosols which are co-emitted with LAC, compared to African savanna fires that have lower ω_0 values (0.84 ± 0.015 at 670 nm) (Reid et al., 2005). In the Amazon rain forest, long-term measurements by Rizzo et al. (2013) have found similar values for ω_0 during the dry and the wet season, 0.87 ± 0.06 and 0.86 ± 0.09, respectively. The low ω_0 in the wet season is attributed to long-range transport aerosol masses that include mineral dust and aged BB aerosol particles. Aged BB aerosol is proven to have increased MAC, and therefore lower ω_0 (Reid et al., 2005). Moreover, part of the biogenic aerosol can contribute up to 35 % of total light absorption (Guyon et al., 2004).

When present in large mass amounts in the atmosphere, mineral dust can significantly absorb light, with a MAC of 0.02 – 0.1 $m^2\ g^{-1}$ at 550 nm (Clarke and Charlson, 1985). It is mobilized from soils and suspended in the atmosphere by windstorms in areas like the Saharan desert in Africa. Dust aerosol particles in the atmosphere efficiently scatter visible radiation and are able to absorb infrared radiation (Andreae, 1996), having a $\mathring{a}_{abs} >> 1.0$ (Caponi et al., 2017; Denjean et al., 2016). Mineral dust plumes travel over the Atlantic Ocean and are able to reach the American continent. Depending on the circulation patterns over the tropical Atlantic, the African dust plumes will be transported to South America or to the Caribbean Sea and Central America (Prospero et al., 1981). The average transport time from emission to deposition in the Amazon basin during winter is ~10 days (Gläser et al., 2015). Ground measurements of aerosol physical and chemical properties have confirmed that between January and April mineral dust plumes from Africa episodically dominate the aerosol load over the Amazon rain forest (Formenti et al., 2001; Guyon et al., 2004; Moran-Zuloaga et al., 2017; Talbot et al., 1990; Wang et al., 2016a). Moreover, the dust-enriched aerosol usually arrives together with BB aerosol emitted by fires in the sub-Sahelian west Africa and also aerosol particles emitted by industrial activities in Morocco and the western Sahara coast (Pöhlker et al., 2017a; Salvador et al., 2016). In spite of anthropogenic disturbance of soils in Africa that could enhance the flux of mineral dust to the

Atmos. Chem. Phys. Discuss., https://doi.org/10.5194/acp-2017-1097
Manuscript under review for journal Atmos. Chem. Phys.
This is just a preview and not the published paper.

atmosphere (Andreae, 1991), a decreasing trend in mineral dust emissions since the 1980s has been observed and is mainly caused by a reduction of surface winds in the Sahel region (Ridley et al., 2014).

This study provides a comprehensive and in-depth analysis of the aerosol optical properties in the Amazonian atmosphere. A continuous long-term dataset (2012 – 2017) of different optical properties is provided. We especially focus on the impact of BB emissions from long-range transport and from regional/local open fires during the dry season. By using data from another central Amazonia remote sampling site, we extend our time series back to 2008 and provide the longest optical properties dataset measured in the Amazon rain forest. By this means, we are able to study the perturbations caused by El Niño Southern Oscillation (ENSO), which has been reported to cause drought all over the Amazon Basin (see Fig. S1), with increasing fire activity and forest degradation (Aragão et al., 2008; Lewis et al., 2011).

2 Materials and methods

2.1 Sampling site and measurement period

Aerosol particles and trace gases are being measured at the Amazon Tall Tower Observatory (ATTO) site, located in the Uatumã Sustainable Development Reserve, Amazonas State, Brazil, in central Amazonia since 2012 (Andreae et al., 2015). The large-scale meteorological conditions of the site are determined by the seasonal shifts of the Inter-Tropical Convergence Zone (ITCZ) location (Pöhlker et al., 2017a). From August to November, during the *dry season*, the ITCZ is located in the north of South America, and mostly Southern Hemisphere air masses reach the ATTO site bringing BB emissions from deforestation hotspots in Southeastern Brazil (i.e., so called arc of deforestation) as well as transcontinental emissions from Southern Africa. During the *wet season*, from February to May, when the ITCZ shifts to southern latitudes, the air masses generally come from the northern hemisphere, following a path over the Atlantic Ocean from the African continent and then, over mostly untouched forest areas upwind of the ATTO site. The transition seasons, *dry to wet* and *wet to dry*, occur in December – January and June – July, respectively.

At the ATTO site, aerosol measurements were started in March 2012, being continuously extended and intensified since then. In the course of this process, the aerosol inlet system was modified and upgraded stepwise. A detailed list of the different inlet configurations and locations can be found in Table S1. On 04 May 2014, a PM_1 cyclone was installed in the common inlet line for the aerosol optical measurements. The rest of the instrumentation kept sampling total suspended particles (TSP). The sampled aerosol was dried by diffusion driers filled with silica gel to guarantee a relative humidity around 40 % or below. An automatic regenerating adsorption aerosol dryer (Tuch et al., 2009) was installed in January 2015.

Another sampling site, ZF2 / TT34 tower, located 60 km NNW of Manaus (Fig. S2) has been the location of long-term aerosol observations and intensive measurement campaigns (Rizzo et al., 2013). Given that most of the air masses that reach the ZF2 site are the same that are transported over the ATTO site (Pöhlker et al., 2017a), the ZF2 data is usually comparable to the ATTO data and the time series presented in this study can complement previous ZF2 time series already reported for the period 2008 – 2011 (Rizzo et al., 2013). Additionally, two intensive observation periods (IOP) and long-term measurements of the GoAmazon2014/5 experiment took place at several measurement sites in the Amazon Basin, including the ATTO site. More details can be found in Martin et al. (2016, 2017).

2.2 Instrumentation

2.2.1 Aerosol light scattering measurements

Scattering coefficients at ATTO were measured using different nephelometers. Figure S3 shows the measurement periods of the different instruments. The first one was a 3-wavelength integrating nephelometer (Model 3563, TSI, St. Paul, USA) (14 Aug 2012 to 24 Nov 2013). The instrument measures aerosol scattering (σ_{sp}) and backscattering (σ_{bsp}) at 450, 550 and 700 nm (Anderson et al., 1996). Calibrations were periodically done by using CO_2 as span gas. Given the optical configuration of the instrument, the truncation of forward scattered radiation constitutes the largest source of error and was corrected by following the procedure described by Anderson et al. (1996). The estimated error of the nephelometer measurements is 8 % for scattering coefficients in the order of 10 Mm^{-1} (Rizzo et al.,

2013). Using an averaging time of 30 min, the detection limit at 550 nm was 0.14 Mm^{-1} (Rizzo et al., 2013).

Later, in February 2014, the TSI nephelometer was replaced by an Aurora 3000 (Ecotech Pty Ltd., Knoxfield, Australia), which measures at 450, 525, and 635 nm wavelength. Over the measurement period studied in this work, we used two different Aurora instruments, with and without backscattering. The instrument was set up to work with an integration time of 1 min. Similar to the TSI nephelometer, CO_2 calibrations were periodically performed. Uncertainty in scattering measurements by the Aurora nephelometers was estimated to be 5 % (Müller et al., 2011).

2.2.2 Aerosol light attenuation and absorption measurements

Light absorption coefficients at 637 nm wavelength, $\sigma_{ap\,637}$, were measured by a multi-angle absorption photometer, (MAAP, model 5012, Thermo Electron Group, Waltham, USA). This instrument measures the transmission of light through a glass-fiber filter on which aerosol particles are collected. Additionally to the forward hemisphere transmission measurement, the MAAP measures the light back scattering at 130° and 165°. By using a radiative transfer model (Petzold and Schönlinner, 2004), the instrument is able to provide absorption coefficients with a time resolution of 5 min. The provided data are 1-min running averages. By averaging the data at 30-min intervals, the MAAP detection limit is 0.132 Mm^{-1}, which corresponds to a BC_e mass concentration of 20 ng m^{-3} (calculated with a MAC of 6.6 $m^2\ g^{-1}$). The MAAP was generally operated at a flow rate of 10 L min^{-1}, but for some periods the flow rate was reduced to 8.3 L min^{-1}. According to Müller et al. (2011), the MAAP measures at a wavelength of 637 ± 1 nm, instead of the 670 nm reported in the instrument's manual. In our calculations, we use 637 nm as the default MAAP wavelength and do not apply any interpolation factor to scale up the data from 670 to 637 nm since it would be in the ~5 % range, which is within the instrument uncertainty. The total uncertainty of the MAAP absorption measurements is of the order of 10 % for 30-min average times (Rizzo et al., 2013).

An Aethalometer was used to measure attenuation of light by aerosol particles at different wavelengths. This instrument uses a LED light source to irradiate an aerosol-laden quartz-fiber filter and a detector,

located in the forward hemisphere, to measure the light transmission (Hansen et al., 1984). The measured transmission is compared to a blank measurement in order to obtain a change in light transmission (attenuation). This attenuation is then converted to BC mass concentration by using a mass attenuation cross section that depends on the instrument model (14625 and 6837.6 $m^2\ g^{-1}\ \lambda^{-1}$ for the AE31 and AE33 Aethalometer models, respectively).

Aethalometer measurements started at the ATTO site in April 2012 using an Aethalometer model AE31 (Magee Scientific, Berkeley, USA). The instrument was operated at different flow rates during the measurement period (varying from 2.0 to 3.7 L min^{-1}) and measured attenuation every 15 min. In January 2015, a new Aethalometer, model AE33 (Aerosol d.o.o., Ljubljana, Slovenia), was installed. The overlapping measurement time of the AE31 and the AE33 models (27 Nov to 15 Dec 2014) enabled the comparison of both datasets. We found a good agreement between both models (difference < 10 %) for measurements at 470, 520, 590, and 660 nm. However, the wavelength dependence did not fit very well during this intercomparison period. Similar deviations in the wavelength dependence of AE31 and AE33 have been reported previously (ACTRIS, 2014). Nevertheless, it is still not clear if the higher wavelength dependence of the AE33 compared to the AE31 is the result of an artifact of the instrument. An independent multi-wavelength absorption measurement can help to clarify the aforementioned AE31/AE33 deviation in $\mathring{a}_{abs}$ (Saturno et al., 2017b). The comparison between compensated AE31 and AE33 data was used to correct the AE33 wavelength dependence deviation by applying intercomparison factors to AE33 data. The obtained AE31-AE33 intercomparison fits are shown in Fig. S4.

Aethalometer data require several corrections to account for different artifacts related to multiple scattering by the filter fibers, scattering by embedded aerosol particles and filter loading effects. The correction applied in this study has been described in a previous article (Saturno et al., 2016). The compensation algorithm is based on the correction scheme proposed by Collaud Coen et al. (2010). It uses MAAP data as a reference absorption measurement, which could introduce uncertainties related to the modification that aerosol particles can suffer by being deposited on a filter matrix. We retrieved the $\mathring{a}_{abs}$ from applying a log-log fit to Aethalometer data corrected for filter-loading and multiple scattering effects. In the case of the Aethalometer AE33, the measurements do not require a filter-loading

Atmos. Chem. Phys. Discuss., https://doi.org/10.5194/acp-2017-1097
Manuscript under review for journal Atmos. Chem. Phys.
This is just a preview and not the published paper.

Atmospheric Chemistry and Physics Discussions

correction because this model uses the dual-spot technology which accounts for this artifact (Drinovec et al., 2015).

2.2.3 rBC mass measurements and MAC calculations

Refractory black carbon (rBC) was measured using a single particle soot photometer (SP2) revision C (Droplet Measurement Technologies, Longmont, USA). Initially, the measurements were done with a 4-channel SP2 and the instrument was upgraded on 19 January 2015 to the 8-channel configuration. Figure S3 shows the different measurement periods of this instrument. The SP2 uses a high-intensity Nd:YAG laser beam (1 MW cm^{-2}, λ = 1064 nm) to irradiate aerosol particles that are provided by an air jet at 90°, with a flow rate of 0.12 L min^{-1}. All particles scatter the light from the laser beam and some of them, which are able to absorb radiation at the given wavelength (e.g., rBC), will incandesce and vaporize at high temperatures (Moteki and Kondo, 2008; Stephens et al., 2003). Four avalanche photo-diode (APD) detectors are installed in the instrument to measure a) scattering, b) broadband incandescence (350 – 800 nm), c) narrowband incandescence (630 – 880 nm) and d) scattering with a split detector. Time dependent data is recorded from each particle as it passes through the laser beam. The ratio between broadband and narrowband signals can provide information on the particle's composition since it is related to the boiling point temperature of the sampled particles (Schwarz et al., 2006). The instrument was periodically calibrated using fullerene soot (Alfa Aesar Inc.) as rBC reference material. A quadratic fit was applied to the recorded incandescence peak heights vs. the mass of mobility size-selected fullerene particles. The fullerene effective densities were taken from Gysel et al. (2011). The scattering detector was calibrated using polystyrene latex spheres (PSL) by relating the scattering signal to the PSL scattering cross-section. The SP2 rBC dynamic ranges were 80 – 280 nm and 80 – 450 nm for the 4-channel and the 8-channel configurations, respectively.

The narrow dynamic range of the 4-channel SP2 was preventing us from measuring rBC mass concentration values comparable to MAAP measurements. In a comparison with another 8-channel instrument during the GoAmazon2014/5 experiment we found that the 4-channel instrument was underestimating the rBC mass concentration by a factor of 40 %. This factor was stable during the wet

season 2014 but we could not guarantee or measure its stability during the dry season. Due to instability of this factor over the sampling period, a proper data correction was not possible. Therefore, in this paper we use only the 8-channel instrument's data, which were available from 09 February 2015 until 31 July 2016 with some interruptions due to hardware failures. The 8-channel SP2 rBC mass measurement was underestimated by a factor of 5 %, related to the size-dependent detection efficiency of the instrument, which is below 100 % in the 80 to 150 nm diameter range. Therefore, a scaling factor of 1.05 was applied to rBC mass concentration data to account for this systematic error.

The BC mass absorption cross-section, α_{abs}, was calculated by running daily fits of 30-min averaged MAAP $\sigma_{ap\,637}$ vs. SP2 rBC mass concentration data, using a standardized major axis estimation (as explained in section 2.6). Fits with $R^2 < 0.9$ were filtered out resulting in a total of 106 out of 220 days included in the final result. The obtained α_{abs} values (shown in section 3.1) were used to convert MAAP absorption measurements into BC_e mass concentrations.

2.2.4 Complementary measurements

Online chemical composition of aerosol particles has been measured since August 2014 using an aerosol chemical speciation monitor (ACSM) (Aerodyne Research Inc., Billerica, USA). Initial results on non-refractory aerosol chemical composition at the ATTO site have already been reported by Andreae et al. (2015) and a detailed paper on the long-term ACSM observations is being prepared by Carbone et al. (2017). This online mass spectrometry technique detects organics, nitrate, sulfate, ammonium and chloride in the sub-micron (< 1 μm) aerosol size range (Ng et al., 2011).

A Picarro cavity ring-down spectrometer G1302 analyzer (Picarro Inc., Santa Clara, USA) measured CO_2 and CO at the ATTO site. Three calibration tanks were used to calibrate the instrument every 100 h. A Nafion dryer was installed in front of the instrument in order to reduce the noise in the CO measurements, which are affected by the high relative humidity of the tropical forest air. Calibration and performance checks will be reported in an upcoming paper. The instrument samples at five different heights but we restrict our analysis to the data measured at 79 m. All CO measurements have been conducted on the walk-up tower. More details on the measurement setup can be found in Winderlich et

Atmos. Chem. Phys. Discuss., https://doi.org/10.5194/acp-2017-1097
Manuscript under review for journal Atmos. Chem. Phys.
This is just a preview and not the published paper.

Atmospheric Chemistry and Physics Discussions

al. (2010). In order to calculate the BC enhancement ratios with respect to CO (ER_{BC}), we used a major axis estimation fit that was applied to the bivariate data (Falster et al., 2006) where the slope represents the enhancement ratio. The 5th percentiles were used as background values.

Condensation nuclei (CN) number concentrations, N_{CN}, and size distributions from 10 nm to 10 µm were continuously measured using several instruments including mobility and optical particle sizers (more details can be found in Andreae et al. (2015)). In this study, we used coarse mode (> 1 µm) number and mass concentrations obtained by means of an optical particle sizer (OPS) model 3330 (TSI Inc., Shoreview, USA) to identify mineral dust transport events. A detailed analysis of the Saharan dust plumes arrivals at the ATTO site can be found in Moran-Zuloaga et al. (2017). Aerosol particle size distributions (10 – 430 nm diameter) were measured with a scanning mobility particle sizer (SMPS) models 3080 and 3081 (TSI Inc., Shoreview, USA) using a condensation particle counter (CPC), model 3772 (TSI Inc., Shoreview, USA).

2.3 Wavelength dependence calculations

Light scattering and absorption wavelength dependence are represented by the Ångström exponents, $å_{sca}$ and $å_{abs}$, respectively. The Ångström exponent can be retrieved when measurements at two different wavelengths are available, for example, the $å_{abs}$ can be calculated as

$$å_{abs} = -\frac{\ln\left(\frac{\sigma_{ap}(\lambda_1)}{\sigma_{ap}(\lambda_2)}\right)}{\ln\left(\frac{\lambda_1}{\lambda_2}\right)} \quad , \qquad (1)$$

where σ_{ap} is the absorption coefficient at two different wavelengths, λ_1 and λ_2.

When measurements at more than two wavelengths are available, a linear fit can be used to retrieve the Ångström exponent from the logarithm of the absorption (or scattering) coefficients vs. the logarithm of the wavelength, as follows

$$\ln \sigma_{ap} = -å_{abs} \ln(\lambda) + \ln(\text{constant}) \quad , \qquad (2)$$

Atmos. Chem. Phys. Discuss., https://doi.org/10.5194/acp-2017-1097
Manuscript under review for journal Atmos. Chem. Phys.
This is just a preview and not the published paper.

Atmospheric Chemistry and Physics Discussions

Black carbon is commonly taken to be wavelength-independent with $å_{abs} = 1$. However, this assumption is theoretically wrong and the BC-related $å_{abs}$ is very sensitive to the size of the particles (Moosmüller et al., 2011). Wang et al. (2016b) proposed a method to calculate the *wavelength dependence of the Ångström exponent* (WDA) in order to estimate the BrC contribution to total light absorption by aerosol particles. They use the difference between two $å_{abs}$ calculated for two different wavelength pairs (440 – 870 nm, and 675 – 880 nm) using aerosol robotic network (AERONET) and Aethalometer data. We use a similar approach to retrieve WDA using Aethalometer data from the ATTO site. In this study the WDA is calculated as follows:

$$\mathrm{WDA} = å_{\mathrm{abs\ 370\text{-}950}} - å_{\mathrm{abs\ 660\text{-}950}} \quad , \qquad (3)$$

where $å_{\mathrm{abs\ 370\text{-}950}}$ and $å_{\mathrm{abs\ 660\text{-}950}}$ correspond to the absorption Ångström exponents calculated for the 370 – 950 and 660 – 950 nm wavelength pairs, respectively.

Theoretical WDA values were calculated following conceptual Mie theory models for (i) polydisperse BC particles (Mishchenko et al., 1999), and (ii) core-shell internally mixed monodisperse BC (Bohren and Huffman, 1983). Calculated BC WDA thresholds, presented in Fig. S5, were compared to the ambient data in order to retrieve the BrC contribution to light absorption. Characteristic BC core size distributions measured by the SP2 during the wet and dry season were used in the polydisperse BC-only model to retrieve extinction efficiency and single scattering albedo. The refractive indices used were 1.95 - 0.79i for BC (Bond and Bergstrom, 2006) and 1.55 - 0.001i for the coating material (Liu et al., 2015). The latter value was only used for the internally mixed BC case. The BC core diameters used in the internally mixed case were 100, 125, 150, 175, 200, 225, and 250 nm, with coating thickness to core size ratio from 0.1 to 1. Black carbon density was set to 1.8 g cm^{-3} (Schkolnik et al., 2007). Brown carbon absorption at 370 nm was calculated by using the WDA approach, as follows:

$$\mathrm{BC}\,å_{\mathrm{abs\ 370\text{-}950}} = å_{\mathrm{abs\ 660\text{-}950}} + \mathrm{WDA} \quad , \qquad (4)$$

$$\mathrm{BC}\,\sigma_{\mathrm{ap\ 370}} = \sigma_{\mathrm{ap\ 950}} \times \left(\frac{370}{950}\right)^{-\mathrm{BC}\,å_{\mathrm{abs\ 370\text{-}950}}} \quad , \qquad (5)$$

$$\mathrm{BrC}\,\sigma_{\mathrm{ap\ 370}} = \sigma_{\mathrm{ap\ 370}} - \mathrm{BC}\,\sigma_{\mathrm{ap\ 370}} \quad . \qquad (6)$$

The uncertainties of the BrC contribution to total absorption at 370 nm were calculated using the theoretical minimum and maximum WDA values. They were below 37 % overall, and decreased to below 19 % when the BrC contribution was higher than 30 % at 370 nm. The relative overestimation of the BrC contribution obtained by using different BC core sizes and different refractive indices in the Mie model calculations can be found in Table S2.

2.4 HYSPLIT backward trajectories and clustering

The systematic back trajectory analysis used here is described in Pöhlker et al. (2017a). Briefly summarized: Three-days backward trajectories were calculated by running the NOAA hybrid single-particle Lagrangian integrated trajectory (HYSPLIT) model (Draxler and Hess, 1998) using 1-degree resolution meteorological data from the global data assimilation system (GDAS1). The trajectories were calculated for 1000 m above ground level at 1 hour intervals for the period January 2008 to June 2016. The entire trajectory ensemble was classified into 15 backward trajectory (BT) clusters using a k-means cluster analysis. The clusters represent different air mass transport tracks and velocities. The different cluster average trajectories and their frequency of occurrence are shown in Fig. 1a and 1b, respectively. The clusters are classified as north-easterly ("NE1", "NE2", and "NE3"), east-north-easterly ("ENE1", "ENE2", "ENE3", and "ENE4"), easterly ("E1", "E2", "E3", and "E4), south-easterly ("ESE1", "ESE2", and "ESE3"), and south-westerly ("SW1") trajectory clusters.

South American fire count data were retrieved from the satellite observations database available online by the Instituto Nacional de Pesquisas Espaciais (INPE), Brazil, at https://prodwww-queimadas.dgi.inpe.br/bdqueimadas/, last access on 04 Apr 2017. The fire data covered the same period as the HYSPLIT clustering analysis period, January 2008 to June 2016. Fire counts were classified according to the corresponding BT cluster where they occurred at hourly resolution. The fire counts reported in this study were weighted according to the trajectory density as (trajectory counts) / 100 km^2. Since the fire count number depends on the amount of satellite data available, we use these data with caution and only as a qualitative reference. For an extended discussion on fire geographical locations and land cover types, see Pöhlker et al. (2017).

2.5 Satellite data

The aerosol optical depth (AOD) at 550 nm, measured by the moderate resolution imaging spectroradiometers (MODIS) on board of the satellites Terra and Aqua, was retrieved for two domains of interest (see Fig. 2a):

- DOI1: Over the Atlantic Ocean. Used to monitor the westward transport of BB aerosol particles from southern Africa, which is mostly emitted during the Amazon dry season, especially between August and September (Das et al., 2017). There is no guarantee that the observed aerosol over this area will necessarily reach the ATTO site, but it is used as an indication of LRT events from southern Africa that will likely reach the Amazon Basin.
  Boundaries: 30 W; 20 S; 10 W; 0 S.
- DOI2: Over the southern Amazon. Used to monitor BB in this region where fire activity is related to deforestation and agriculture-related activities.
  Boundaries: 58 W; 14 S; 40 W; 8 S.

The MODIS products can be found online on the Goddard Earth Science Data and Information Services Center at https://giovanni.gsfc.nasa.gov/giovanni/, last access on 17 Jul 2017, (GES-DISC, 2017).

Terra and Aqua data were averaged over the two different domains. The averaged AOD at 550 nm time series corresponding to DOI1 and DOI2 can be found in Fig. 2b. The seasonality observed for both datasets is similar but AOD for DOI1 (Atlantic Ocean) generally increased in August and decreased after the end of September with some peaks in January – February, especially in 2016. On the other hand, high AOD values in DOI2 (South Amazon), increased sharply in the beginning of September and decreased continuously until the middle of December with the exception of the dry season 2015 when high AOD was observed until February 2016.

2.6 Data treatment

The analyzed data were averaged to 30-min intervals and corrected to standard temperature and pressure (STP, 273.15 K and 1013.25 hPa). Furthermore, the scattering data were interpolated to 637 nm to compare directly to the absorption data obtained by the MAAP, in order to avoid the

uncertainty associated with the absorption spectral dependence calculation. The time periods of major and medium dust influence were taken from a study by Moran-Zuloaga et al. (2017). During the dry season, BB pulses were segregated by using the 75th percentile of $\sigma_{ap\ 637}$ as a threshold. When examining correlations between independent measurements, we applied standardized major-axis estimations (SMA) by using the SMATR package (Falster et al., 2006) in the statistical software environment R (R Development Core Team, 2009). This method minimizes the error on the *x* and *y* axes and not only at the *y* axis, like a linear regression does. Therefore, it provides unbiased estimates of the slope (Warton et al., 2006).

3 Results and discussion

3.1 Overview of aerosol optical properties (2012 – 2017)

This section summarizes the aerosol optical properties from five years of continuous measurements at the ATTO site. The corresponding time series are shown in Fig. 3 and descriptive statistics can be found in Table 2. The wet and dry season statistics were calculated excluding the transition periods.

The scattering coefficients, σ_{sp}, shown in Fig. 3a, averaged 7.5 ± 9.3 Mm^{-1} and 33 ± 25 Mm^{-1} at 550 nm during the wet and the dry season, respectively (see Table 2). These values agree well with previously reported results at ZF2 of 8.1 ± 7.2 Mm^{-1} and 36 ± 48 Mm^{-1} at 550 nm during the wet and dry season, respectively (Rizzo et al., 2013). The same is valid for our results at 450 nm and 700 nm (not shown) and the ones presented by Rizzo et al. (2003). The proximity of both sites, ATTO and ZF2, frequently allows probing comparable air masses of similar origin and atmospheric history. The long-term measurements show also a pronounced year-to-year variability in σ_{sp} (compare e.g., 2014 and 2015). The largest observed deviations from the dry-season average were found during the dry season 2015 with an average increase of 38 % in σ_{sp} at 550 nm. Similar increases were observed in σ_{sp} at 450 and 637 nm. These increases can be directly related to the higher occurrence of fire episodes during the strong ENSO period 2015/6 with its negative precipitation anomaly, as discussed in more detail in sections 3.5 and 3.6.

The absorption coefficients, σ_{ap}, at 637 nm (MAAP) are shown in Fig. 3b, and averaged 0.68 ± 0.91 Mm^{-1} and 4.0 ± 2.2 Mm^{-1} during the wet and the dry season, respectively. Also for this parameter, comparable values were measured at the ZF2 site, with averages of 1.0 ± 1.4 Mm^{-1} and 3.9 ± 3.6 Mm^{-1} at 637 nm during the wet and the dry season, respectively (Rizzo et al., 2013). The higher increase of the absorption coefficient (factor of 5.9) from wet to dry season compared to the increase in scattering (factor of 4.4) affected the ω_0 (see Fig. 3c). Lower values were observed during the dry season (0.87 ± 0.03 at 637 nm, 0.81 ± 0.08 at 550 nm) compared to the averages observed in the wet season (0.93 ± 0.04 at 637 nm, 0.88 ± 0.08 at 550 nm). At the ZF2 site, Rizzo et al. (2013) have found small differences between ω_0 values during the dry and wet seasons (0.87 ± 0.06, and 0.86 ± 0.09 at 637 nm, respectively) for over 2 years (2008 – 2011) measurements. However, measurements during the wet season in 1998 at a sampling site closer to the ATTO site (Balbina, 60 km NW of ATTO and 140 km NE of Manaus) showed higher ω_0 values: 0.92 – 0.95 at 550 nm (Formenti et al., 2001). These values are within our measurement range for the same season (0.88 ± 0.08 at 550 nm). Single scattering albedo retrieved from multi-year ground-based radiometer measurements in the Amazonian forest had an average of 0.93 ± 0.02 (Dubovik et al., 2002). Given that we sampled dried aerosol particles, our average ω_0 are expected to be lower than these ambient-humidity values during the entire measurement period and the dry season. Measurements close to BB sources in Brazil have shown a wide range of ω_0; e.g., Chand et al. (2006) found a ω_0 of 0.92 ± 0.02 (550 nm) for dried aerosol over Rondônia, whereas Guyon et al. (2003) calculated lower ω_0 values during BB events at the end of the LBA-EUSTACH 1 campaign in Rondônia, reaching 0.85 ± 0.02 at 550 nm. Fresh smoke fires have been reported to have lower ω_0, of 0.79 ± 0.05 at 550 nm (Reid et al., 1998).

The scattering Ångström exponent, $å_{sca}$, is a function of the aerosol particle size distribution. Rizzo et al. (2013), however, pointed out that this relationship is only evident for surface and volume mean diameters and was not clearly valid between $å_{sca}$ and count mean diameters. We obtained higher $å_{sca}$ values during the dry season (1.71 ± 0.24) compared to the wet season (1.29 ± 0.50) as shown in Fig. 3d. This is an indication of the dominance of fine mode aerosol (mostly BB related) during the dry season over the coarse mode aerosols that become more important in the wet season (i.e., PBAP, Saharan dust and sea salt), as previously observed at the ATTO site (Andreae et al., 2015;

Atmos. Chem. Phys. Discuss., https://doi.org/10.5194/acp-2017-1097
Manuscript under review for journal Atmos. Chem. Phys.
This is just a preview and not the published paper.

Atmospheric Chemistry and Physics Discussions

Moran-Zuloaga et al., 2017). A similar seasonal trend has been observed at the ZF2 site, where $å_{sca}$ was 1.70 ± 1.41 and 1.48 ± 1.12 (30-min averages) for the dry and the wet season, respectively (Rizzo et al., 2013). A detailed analysis of the coarse mode aerosol abundance and properties measured at the ATTO site is presented elsewhere (Moran-Zuloaga et al., 2017).

Regarding the absorption Ångström exponent, $å_{abs}$, the overall average during the whole sampling period was 0.93 ± 0.16 (see Fig. 3e). Although no significant difference was found between dry and wet season averaged values, the $å_{abs}$ was slightly higher during the dry season, reaching an average of 0.94 ± 0.16 compared to a wet season average of 0.91 ± 0.19. The Aethalometer compensation calculation could potentially affect the retrieved $å_{abs}$ values. It has been shown that the raw attenuation Ångström exponent can represent a good approximation to the real $å_{abs}$ (Saturno et al., 2017b). High absorption and scattering coefficients coincide with ESE and E trajectories, which are mostly dominant, but not exclusively, during the dry season, see Fig. 1. On the other hand, the "cleanest" periods in the wet season, when light absorption reaches its minimum and ω_0 its maximum, the dominant trajectories are ENE and NE.

Accurate MAC values are required to retrieve BC mass concentrations from absorption measurements. During the entire measurement period, the calculated MAC was 11.9 ± 1.4 m² g^{-1} (mean ± standard deviation) at λ = 637 nm. Daily calculated MAC values in the wet season were slightly lower on average compared to the dry season values (11.4 ± 1.2 and 12.3 ± 1.3 m² g^{-1}, respectively, see Table 2). As an illustration of the different MAC values obtained in the wet and the dry season, $\sigma_{ap\ 637}$ vs. M_{rBC} scatter plots are presented as supplementary information in Fig. S6. Lower MAC values measured in the wet season 2016 could be associated with less coated BC compared to more aged particles in the dry season, which could have thicker coatings. Nevertheless, both values are much higher than the 6.6 m² g^{-1} suggested by Bond and Bergstrom (2006), especially considering that mineral dust and BrC do not strongly absorb at this wavelength and would therefore have little influence on the apparent MAC. However, they are in agreement with a modelled absorption enhancement of 1.6 calculated for open biomass burning in Brazil (Liu et al., 2017). In any case, there are large discrepancies that make it difficult to compare different MAC values obtained from ambient measurements due to systematic analytical uncertainties that dominate over the natural variability (Zanatta et al., 2016). These

uncertainties are introduced by filter-based absorption measurement biases and BC mass over- or underestimation when thermal optical methods are used. In the case of the SP2, the rBC mass measurements are free of the different biases that affect thermal-optical techniques and are a wavelength independent measurement. In the case of absorption measurements, a positive bias is introduced when organic aerosol deposits on the filter, enhancing the scattering by the filter fibers and the absorption by previously deposited BC particles when coating them. This artifact can be between 12 and 70 % for particle soot absorption photometer (PSAP) measurements and will depend on the OA to BC ratio and the aging state of the organic aerosol particles (Lack et al., 2008). We expect a lower artifact for the MAAP since the scattering by filter fibers is accounted by the reflectance measurements, but using our instrumentation we are not able to estimate the artifact coming from embedded BC absorption being modified by organic aerosol deposition. There are only few field studies that present comparisons of rBC measurements and light absorption measurements, like MAAP, photoacoustic spectrometry (PAS), or Aethalometer, and especially long-term measurements are scarce. Raatikainen et al. (2015) reported SP2 (8-channel) and MAAP measurements in the Finnish Arctic and found that SP2 rBC mass concentrations were 5 times lower than MAAP BC_e mass concentration measurements, which is equivalent to MAC values of ~30 $m^2\ g^{-1}$ at 637 nm. Some other studies have found values in closer agreement with our ATTO MAC results. For example, Laborde et al. (2013) found that air masses over Paris had an average MAC of 11.9 and 10.8 $m^2\ g^{-1}$ (interpolated to 637 nm), for aged and fresh BB aerosol, respectively. Additionally, Liu et al. (2010) calculated a median MAC of 10.2 ± 3.2 $m^2\ g^{-1}$ during a measurement campaign at the Jungfraujoch research station in Switzerland. Another study in Mexico City, using PSAP for absorption measurements at λ = 660 nm, found a MAC of 11.2 $m^2\ g^{-1}$ (interpolated to 637 nm) (Subramanian et al., 2010).

3.2 Variability of optical properties during the dry season

The Amazonian dry season is generally impacted by BB aerosol particles that cause an increase in scattering and absorption coefficients (see Fig. 3a-b). However, the aerosol optical properties vary with the burning material (and region), as well as the aging process prior to reaching the ATTO site. In order to study the dry season variability of BB aerosol particles, multi-year (2012 – 2017) weekly averages

were analyzed. The air mass trajectories, presented as BT clusters in Fig. 4a, show a decreasing dominance of ESE winds from August to November, whereas from October to November there is an increasing influence of ENE winds, indicating the south-to-north air mass trajectory shift that occurs during the transition from the dry to the wet season. It is important to note that southerly and easterly winds are most likely to bring BB aerosol to the ATTO site during the dry season, given that very active open fire areas during this period are located in the southern Amazon and the Cerrado region (Andreae et al., 2012; Guyon et al., 2005) and, more remotely, in southern Africa (Andreae et al., 1994; Barbosa et al., 1999; Das et al., 2017). Aerosol optical depth at 550 nm is used in this study as a parameter to study the seasonal pattern of BB emission transport from both areas. In section 2.5, we defined two domains of interest to study the aerosol seasonal patterns in these two areas: DOI1 for the LRT of South African smoke over the Atlantic Ocean, and DOI2 for the fires occurring in the southern Amazon. For the case of southern Africa fires (DOI1), the seasonal pattern shows an important influence during August – October, slightly decreasing towards the end of the Amazonian dry season (see Fig. 4d). For the southern Amazon region (DOI2), the typical fire seasonality during the dry season is observed in the AOD over this area (Fig. 4d) with the highest values observed during September and October. A second increase in AOD is observed in the middle of November over DOI2. It is important to note that August seems to be the period when African LRT is a more important source than regional emissions and could be considered as the main contributor of BB aerosol to the ATTO site during this time. For the rest of the dry season, it is likely that the aerosol properties are defined by South American BB emissions. In fact, the shift in air mass trajectories and variation of BB sources drive the BrC contribution to $\sigma_{ap\ 370}$, as can be seen in Fig. 4b. The BrC contribution (associated with high $\mathring{a}_{abs}$) is more important at the end of the dry season and is lower during August, when the aerosol particles likely arrive from Zambian woodland savanna fires (Barbosa et al., 1999), which burn more efficiently and emit aerosol particles with lower ω_0, 0.84 ± 0.015 at 670 nm in average (Dubovik et al., 2002). Additionally, on average, high $\sigma_{ap\ 637}$ events (see increasing circle size in Fig. 4b) are more likely to bring high BrC containing aerosol, which is another indication that closer fires have higher probability to provide BrC-rich aerosol particles to the ATTO site. The absorption wavelength dependence and BrC contribution are discussed in detail in section 3.6. The differences between both identified BB sources in terms of BrC can be explained by

Atmos. Chem. Phys. Discuss., https://doi.org/10.5194/acp-2017-1097
Manuscript under review for journal Atmos. Chem. Phys.
This is just a preview and not the published paper.

Atmospheric Chemistry and Physics Discussions

two reasons: (i) the BrC photochemical oxidation during transport that would strongly affect LRT aerosol, and (ii) a lower wet scavenging rate for BC during transport, which would lead to an increased BC fraction in the aerosol population. In terms of the single scattering albedo (ω_0, Fig. 4c), its increase towards the end of the dry season confirms that the aerosol particles during this time are scattering more radiation, not only due to higher BrC presence but also due to an increased sulfate concentration.

3.3 Diel cycles

Figure 5 presents the different diel cycles observed during the dry and the wet season for selected aerosol properties and some meteorological parameters (N_{acc}, $\sigma_{ap\ 637}$, $\sigma_{ap\ BrC\ 370}$, P_{ATTO}, and θ_e). In order to study the typical diel cycles in each season, extreme events like mineral dust transport in the wet season and nearby BB during El Niño in 2015 – 2016 have been excluded. The diel cycle of the equivalent potential temperature (Fig. 6i-j) reflects the evolution of the planetary boundary layer. Shortly before sunrise (~ 10:00 UTC), θ_e exhibits its minimum and increases afterwards reaching its maximum values in the early afternoon hours. The pronounced temperature increase in the early morning hours is connected to the initiation of vertical mixing, leading to the evolution of the convective boundary layer. After sunset, a stable nocturnal boundary layer is formed close to the forest canopy. A detailed analysis of the planetary boundary layer of the Amazon can be found in Fisch et al. (2004). Figures 5a-b (dry and the wet season, respectively) show diel cycles of accumulation mode (particle diameter between 100 – 430 nm) particle number concentration, N_{acc}. The diel patterns are similar during both seasons, with a minimum at sunrise, and an increase that starts in the morning at 12:00 UTC (8:00 LT) and maximum concentrations between 17:00 and 18:00 UTC (13:00 – 14:00 LT). This diel pattern observed in N_{acc} is driven by the diurnal evolution of the planetary boundary layer. On the one hand, the stable nocturnal layer leads to a concentration of particles and gases close to the canopy. On the other hand, the canopy acts as an effective particle sink, resulting in a concentration decrease towards the early morning (Ahlm et al., 2009). After sunrise, vertical mixing breaks up the stable nocturnal boundary layer. While the subsequent increase in N_{acc} is likely due to entrainment of particles from the residual layer, the decrease in the afternoon hours can be attributed to effective deposition in the forest canopy, as also discussed in Ahlm et al. (2009). The absorption coefficient at 637 nm, $\sigma_{ap\ 637}$, which is mostly

Atmos. Chem. Phys. Discuss., https://doi.org/10.5194/acp-2017-1097
Manuscript under review for journal Atmos. Chem. Phys.
This is just a preview and not the published paper.

Atmospheric Chemistry and Physics Discussions

related to BC, follows a diel pattern (Fig. 5c-d) similar to the N_{acc} trend for both seasons. Since BC is usually not emitted by near-by sources and it is generally transported in the accumulation mode, the similarities with N_{acc} diel patterns were expected. However, the wet season diel cycle of $\sigma_{ap\ 637}$ exhibits a decreasing tendency that starts two hours earlier than the decrease in N_{acc}. This difference can be explained by the fact that $\sigma_{ap\ 637}$ and N_{acc} are mass and number-related measurements, respectively. Therefore, a size-dependent deposition would affect mass and number-related aerosol properties in a different way. This difference was more evident in the wet season when BC concentrations were not as dominant as in the dry season. The diel pattern of BrC contribution during the dry season is significantly different from the $\sigma_{ap\ 637}$ (BC) pattern. Brown carbon absorption at 370 nm, $\sigma_{ap\ BrC\ 370}$, shows its highest values between 12:00 and 14:00 UTC (08:00 – 10:00 LT) in the dry season and starts decreasing at 14:00 UTC (10:00 LT), earlier than $\sigma_{ap\ 637}$ and N_{acc} (Fig. 5e). This observation implies that the BrC aerosol particles measured at the ATTO site are mixed down into the boundary layer in the early morning and are then quickly photo-degraded during the day (Forrister et al., 2015; Wang et al., 2016b; Wong et al., 2017). This pattern is not observed during the wet season, when $\sigma_{ap\ BrC\ 370}$ exhibits no significant diel variability.

Other remote site observations have found no significant diel variation of the absorption coefficient, due to efficient mixing of the planetary boundary layer (PBL) and low anthropogenic emissions (Chi et al., 2013). However, the high convectivity at tropical latitudes makes possible the entrainment of high altitude air masses that bring regional and/or LRT emissions, as observed before at an Amazonian site during the dry season (Brito et al., 2014).

3.4 BC to CO enhancement ratio

Agricultural clearing fires, like savanna fires, are dominated by the flaming combustion phase, in contrast to deforestation fires, where less than 50 % of the biomass is burned in the flaming phase (Dubovik et al., 2002). An important part of forest fires occurs in the form of smoldering combustion due to higher fuel moisture (Guyon et al., 2005). Under smoldering fire regimes, when the combustion is less efficient and thus, tends to emit more CO, observations tend to show lower ER_{BC} and higher single scattering albedo, ω_0, as well as higher organic carbon (OC) enhancement ratio, ER_{OC}. On the

other hand, flaming fires, which produce abundant BC aerosol particles, tend to exhibit lower ω_0 and higher ER_{BC} (Akagi et al., 2011). The smoke that arrives at the ATTO site during the dry season is a mixture of smoldering and flaming emissions with varying relative fractions. The air mass origin, (i.e., the back trajectories) largely defines if emissions are advected from regions with predominantly smoldering or flaming fires (Pöhlker et al., 2017a).

The calculated ER_{BC} values and ω_0 allow us to distinguish between flaming and smoldering smoke and locate the different sources. Figure 6 shows the ER_{BC} and ω_0 values measured at the ATTO site classified by grouped BT clusters. It can be observed that mainly the ESE and E trajectory clusters have ER_{BC} higher than 8 ng m^{-3} ppb^{-1}. From the two predominant BT cluster groups in the dry season (ESE and E), the ESE trajectories seem to be the more influenced by flaming fires since the measurements are more shifted to high ER_{BC} and lower ω_0. In fact, the ESE clusters are dominated by the 0.80 – 0.90 ω_0-range, which means they are highly loaded with light-absorbing aerosol. This evidence is supported by the land cover information, which indicates that agricultural lands account for 6 – 20 % of the ESE clusters total land cover, 3 – 5 % of the E clusters, and < 1 % of the ENE and NE clusters (Pöhlker et al., 2017a). The eastern clusters (E) are more equally distributed in the ω_0 range and tend to be lower in terms of ER_{BC} compared to the ESE clusters. Therefore, we expect E trajectories to be more influenced by smoldering fires during the dry season compared to the ESE trajectories, even though, as already mentioned, the arrival of African savanna fire smoke from easterly trajectories in August-September provides BB aerosol particles that have lower ω_0 and higher ER_{BC}.

During the wet season, when ENE and NE BT clusters are dominant, we observed a trend towards lower ER_{BC} and higher ω_0 than expected, since the frequency of regional fires is much lower than in the dry season. Actually, when including data from the beginning of 2016, under the influence of ENSO, we observed a shift towards higher ER_{BC} in the NE directions due to the occurrence of fires in the Guyanas area. These atypical data were excluded from Fig. 6 to improve the contrast between the different air mass trajectory clusters. The NE and ENE trajectories were very similar in terms of ω_0 and ER_{BC}. Occasional dust transport events from the Sahara, mixed with BB aerosol from the Sahel region, brought aerosol particles with lower ω_0 compared to the wet season average.

Atmos. Chem. Phys. Discuss., https://doi.org/10.5194/acp-2017-1097
Manuscript under review for journal Atmos. Chem. Phys.
This is just a preview and not the published paper.

Atmospheric Chemistry and Physics Discussions

The lower ER_{BC} observed in the wet season was likely due to aerosol scavenging during the transatlantic advection (Moran-Zuloaga et al., 2017), while CO is not affected by wet deposition (Liu et al., 2010). One important aspect worth mentioning is the fact that ER_{BC} decreased more steeply with increasing ω_0 and their correlation was closer during the dry season (E and ESE BT clusters) in comparison to the wet season. This feature might be related to the age of the aerosol particles, because aging would make the BC become less hydrophobic (Pöhlker et al., 2017b) so that it can be more efficiently removed by wet scavenging.

3.5 El Niño impact on aerosol optical properties

The aerosol optical properties measured at ATTO changed during the El Niño period at the end of 2015 and the beginning of 2016 (Fig. 3). To have a broader view on how this phenomenon affected the Amazon rain forest aerosol, we added scattering and absorption data from ZF2 published in Rizzo et al. (2013) and extended with recent data to the current ATTO time series in Fig. 7a-b. Overlapping data in 2013 (Fig. 7a and 7b) are statistically equivalent with only a few days affected by probable near-site sources. Positive Oceanic Niño Index (ONI) values (Fig. 7c) were found to be related to higher scattering and absorption coefficients in the dry season. However, the ENSO is not the only cause of precipitation anomalies in the Amazon Basin. The Atlantic Multi-Decadal Oscillation (AMO) has also been found to be causing droughts (Aragão et al., 2008). The non-ENSO average (ZF2 and ATTO) scattering coefficient at 637 nm during the dry seasons was 24 ± 18 Mm^{-1}. This average increased up to 54 ± 39 Mm^{-1} and 42 ± 24 Mm^{-1} during the dry seasons 2009 and 2015, respectively. The wet season scattering coefficient average was also affected during El Niño, increasing from a non-ENSO average of 7 ± 7 Mm^{-1} to 10 ± 11 Mm^{-1} during the wet season 2016. A similar pattern was observed for $\sigma_{ap\ 637}$, which increased from a non-ENSO average in the dry seasons of 3.8 ± 2.8 Mm^{-1} to 5.5 ± 2.8 Mm^{-1} and 5.2 ± 2.1 Mm^{-1} during the dry seasons in 2009 and 2015, respectively. It is remarkable that high absorption coefficients were also measured during the dry season 2010 (5.6 ± 4.7 Mm^{-1}), a year with mostly negative ONI. However, it has been shown that an increased sea surface temperature in the Atlantic Ocean (not ENSO related) in 2010 caused a special drought period in the Amazon rain forest (Lewis et al., 2011).

Atmos. Chem. Phys. Discuss., https://doi.org/10.5194/acp-2017-1097
Manuscript under review for journal Atmos. Chem. Phys.
This is just a preview and not the published paper.

Atmospheric Chemistry and Physics Discussions

3.6 Absorption wavelength dependence and BrC contribution

Open biomass burning emits a mixture of BC and OA with high absorption wavelength dependence (Andreae and Gelencsér, 2006; Hoffer et al., 2006; Kirchstetter et al., 2004). However, our observations show that sometimes LAC measured at the ATTO site can fall in the BC-only regime, with $å_{abs} \approx 1$. To understand this pattern, we have analyzed the relationship between the WDA and other parameters, like the OA-to-sulfate ratio and ω_0. In Fig. 8a, WDA is presented as a function of the OA-to-sulfate mass ratio. According to the result of an orthogonal fit (not shown), there is a significant correlation between these variables ($R^2 = 0.61$), and the aerosol light absorption is in the BC-only regime (shaded area in Fig. 8a) when the OA-to-sulfate ratio is lower than ~6.5, which occurred 15 % of the time in the high-absorption periods ($\sigma_{ap\ 637}$ higher than the 75th percentile). On the other hand, higher OA-to-sulfate ratios correspond to likely BrC-rich aerosol masses, which were the majority of the cases. The ω_0 at 637 nm of the BC-only regime (inter-quartile range, IQR: 0.82 – 0.86) was clearly lower than the one corresponding to the BrC-rich regime (IQR: 0.85 – 0.90).

In Fig. 8b, the BC-only regime data has been segregated by trajectory cluster. The air masses that are more likely to bring wavelength independent BC to the site are those with the faster wind speed: E3, E4, and ESE3. These emissions could be related to ship traffic in the Atlantic Ocean, BB in southern Africa, or power plant emissions from the west African coast. Low OA-to-sulfate ratios with high ω_0 occurred a few times and could be explained by high sulfate input from volcanic emissions in the Congo (Fioletov et al., 2016; Saturno et al., 2017a), rather than fossil fuel emissions, which are typically rich in BC.

In an effort to identify the BrC-rich trajectories, the WDA was studied for the different BT clusters that are mostly active during the dry season. Boxplots corresponding to each trajectory cluster, together with the average fire counts in the geographical cluster area, are presented in Fig. 9. From the group of ESE trajectory clusters (ESE1, ESE2, and ESE3), the ESE1 trajectories exhibit the highest WDA values, with a decreasing tendency towards faster trajectories, ESE3 being the one with lowest WDA values. Even though ESE3 is the trajectory cluster with more fire counts, the fact that those fires occur farther from the ATTO site compared to the ones in the slowest trajectory, ESE1, could be related to a decrease in absorption wavelength dependence during transport. A similar pattern is observed for the easterly

Atmos. Chem. Phys. Discuss., https://doi.org/10.5194/acp-2017-1097
Manuscript under review for journal Atmos. Chem. Phys.
This is just a preview and not the published paper.

Atmospheric Chemistry and Physics Discussions

trajectory clusters (E1, E2, E3, and E4), where the slowest air mass trajectories comprised by the E1 cluster exhibit the highest WDA median compared to the rest of the E clusters. In the case of E4, the WDA 25th percentile is lower than the rest of the E trajectories, but it shows an increased median that can not be explained by the occurrence of fire events, which is lower than the observations for the other clusters (E2, E3, and E4). The E4 weighted fire counts is anyhow in the same order magnitude as E2 and E3 and the wavelength dependence differences could be related to different fuel types or combustion phase. Actually, the long E clusters (E3 and E4) cover more southern areas than the shorter ones (E1 and E2) and have some overlap with ESE3. By comparing grouped E and ESE clusters, it can be observed that WDA in the E clusters has higher variability compared to the ESE ones. This pattern could be associated with a wider range of sources in the E trajectories compared to ESE. The E trajectories travel over the Amazon River where ship traffic is quite significant. In fact, as can be observed in Fig. 9, for the E3 and E4 trajectories, there is a significant amount (> 25th percentile) of measurements that fall in the BC-only regime. Something similar is only observed for the ESE3 trajectories among the ESE group. Most of the agricultural land is located along the southern margins of the Amazon rain forest (Pöhlker et al., 2017a). This area is within the ESE clusters footprint. The narrower range of WDA values measured for the ESE trajectories compared to the E ones, indicates that sources in the ESE footprint are more homogeneous compared to the sources located in the E footprint. These WDA tendencies could be useful to understanding the BrC emissions and atmospheric transformations in the context of the Amazon rain forest and its surroundings.

Using the calculated BC-only WDA thresholds, we were able to estimate the BrC contribution to total absorption during the measurement period (2012 – 2017) (Fig. 10). We found that BrC contributes 24 % (IQR: 17 – 29 %) of total light absorption at 370 nm wavelength. A slight seasonal variability was observed for the BrC relative contribution, with the medians and IQR during the wet and dry season being 27 % (19 – 34) and 22 % (16 – 27), respectively. However, most of the wet season data had to be excluded, because they were from air masses rich in mineral dust, which introduces large uncertainties in the WDA method. During El Niño, at the end of 2015, open fire events were more frequent (with weighted fire counts of 1756 km^{-2} compared to the 2008 – 2016 average of 1076 km^{-2}), and the CO 95th percentile was exceeded several times. In this period, the BrC contribution had a median of 37 % (IQR:

Atmos. Chem. Phys. Discuss., https://doi.org/10.5194/acp-2017-1097
Manuscript under review for journal Atmos. Chem. Phys.
This is just a preview and not the published paper.

Atmospheric Chemistry and Physics Discussions

27 – 47) and showed a significant correlation with CO ($R^2 = 0.47$). This significant increase of the BrC contribution could be related to the relatively short distance between the fire spots and the ATTO site. It can be observed in Fig. 10 that the El Niño influence continued during the dry season 2016 but not as strongly as in 2015. Previous observations have shown that the atmospheric lifetime of BB-emitted BrC is ~1 day due to photolysis and oxidation, which destroy the chromophores (Forrister et al., 2015; Wang et al., 2016b; Wong et al., 2017). Therefore, BrC emitted from fires in the southern borders of the Amazon rain forest, which require ~3 days to be transported to the ATTO site, is likely to be significantly photodegraded and to contribute only weakly to total aerosol light absorption after atmospheric processing.

The BC to OA mass ratio during the sampling time had a median of 0.06 (IQR: 0.04 – 0.10). The ratio BC to OA has been used before to parameterize $å_{abs}$ and ω_0 (Pokhrel et al., 2016; Saleh et al., 2014), but little is known about this relationship for tropical forest emissions. A broader range of BC to OA mass ratio between 2014 and 2016 was observed during the dust episodes in the wet season, including those periods when regional fires were active (IQR: 0.08 – 0.24). Other periods, like the dry season, with higher BC mass concentrations, exhibited a narrower and lower BC to OA mass ratio range (IQR: 0.03 – 0.08). A scatter plot of the absorption wavelength dependence, $å_{abs}$, as a function of the BC to OA mass ratio during the North African LRT events in the wet season can be found in Fig. 11. We have found a trend where $å_{abs}$ increases with decreasing BC to OA mass ratio following an exponential function. These results are comparable to those presented by Pokhrel et al. (2016) and Saleh et al. (2014), with slightly lower $å_{abs}$ values in our study, however. This pattern could be related to a dominant presence of primary organic aerosol (POA) that has characteristically lower absorption wavelength dependence compared to SOA (Saleh et al., 2013). However, more experimental studies are required to investigate the optical properties of aerosol produced by burning different tropical forest fuels.

Summary and conclusions

The optical properties of aerosol particles sampled at the ATTO site have been presented for a measurement period of 5 years (2012 – 2017). Seasonal trends affected light scattering and absorption

by aerosol particles, showing a significant increase during the dry season due to a higher frequency of regional open fires. The wet season was dominated by background biogenic aerosol, occasionally disrupted by LRT dust and BB aerosol transported from Africa to the ATTO site, which lead to decreased $å_{sca}$ and ω_0 (637 nm). The average ω_0 during the wet season was 0.93 ± 0.04, higher than the dry season average of 0.87 ± 0.03. The absorption wavelength dependence, $å_{abs}$, was relatively low with an average of 0.93 ± 0.16, and only slight variations between seasons. The highest $å_{abs}$ were measured in the presence of BB events but no effect on $å_{abs}$ was observed due to the presence of dust, most likely due to a size effect, given that absorption coefficients were measured only for sub-micron aerosol particles after May 2014. Black carbon MAC at 637 nm calculated from MAAP and SP2 measurements was comparable to other studies, although higher than "typical" values commonly used in the literature to convert σ_{ap} into BC mass concentrations. The calculated wet season MAC average was 11.4 ± 1.2 $m^2\ g^{-1}$, while during the dry season the MAC average was increased slightly to an average of 12.3 ± 1.3 $m^2\ g^{-1}$ at 637 nm. These values are consistent with a strong "lensing effect" by organic coatings attached to BC aerosol particles. High OA amounts in the Amazonian atmosphere resulted in low BC to OA mass ratios, which were in the range of 0.04 to 0.10 (IQR). A significant correlation between BC to OA mass ratio and $å_{abs}$ was observed during the wet season under the influence of regional and remote BB emissions. The ΔBC/ΔCO enhancement ratios (ER_{BC}) were mostly lower than 8 ng m^{-3} ppb^{-1}, mainly due to the aging of BB aerosol particles during transport to the site. A higher and wider range of ER_{BC} values was observed during the dry season due to the influence of different biomass combustion phases that varied from smoldering to flaming fires.

Theoretical wavelength-dependent BC $å_{abs}$ were calculated and used to estimate the BrC contribution to near-UV (370 nm) light absorption. This approach resulted in medians of 27 and 22 % BrC contributions in the wet and dry season, respectively. Higher BrC contributions were measured during the El Niño season at the end of 2015. During this period, the BrC absorption at 370 nm increased to a median of 37 %. We observed that winds coming from ESE directions in the dry season were more likely to bring aerosols with a high absorption wavelength dependence, implying a higher BrC content.

In the case of prolonged drought periods in the Amazon Basin, significant increases of BrC absorption contribution could be expected due to increased fire occurrence. Long-term monitoring of light

absorbing aerosol particles is required to reduce uncertainty in global climate models. The data presented here provide a contribution in this direction and can help to understand how different climatic phenomena, like El Niño, can affect the Amazon atmospheric aerosol cycling. Further investigations on the BC mixing state and morphology will be required to improve modeled calculations and BrC retrievals.

Acknowledgements

This work has been supported by the Max Planck Society (MPG) and the Max Planck Graduate School (MPGS). For the operation of the ATTO site, we acknowledge the support by the German Federal Ministry of Education and Research (BMBF contract 01LB1001A) and the Brazilian Ministério da Ciência, Tecnologia e Inovação (MCTI/FINEP contract 01.11.01248.00) as well as the Amazon State University (UEA), FAPEAM, LBA/INPA and SDS/CEUC/RDS-Uatumã. P. A. acknowledges support from FAPESP – Fundação de Amparo à Pesquisa do Estado de São Paulo. J. S. is grateful for the PhD scholarship from the Fundación Gran Mariscal de Ayacucho (Fundayacucho). This paper contains results of research conducted under the Technical/Scientific Cooperation Agreement between the National Institute for Amazonian Research, the State University of Amazonas, and the Max-Planck-Gesellschaft e.V.; the opinions expressed are the entire responsibility of the authors and not of the participating institutions. We highly acknowledge the support by the Instituto Nacional de Pesquisas da Amazônia (INPA). We would like to especially thank all the people involved in the technical, logistical, and scientific support of the ATTO project, in particular Reiner Ditz, Jürgen Kesselmeier, Alberto Quesada, Niro Higuchi, Susan Trumbore, Matthias Sörgel, Thomas Disper, Andrew Crozier, Uwe Schulz, Steffen Schmidt, Antonio Ocimar Manzi, Alcides Camargo Ribeiro, Hermes Braga Xavier, Elton Mendes da Silva, Nagib Alberto de Castro Souza, Adi Vasconcelos Brandão, Amaury Rodrigues Pereira, Antonio Huxley Melo Nascimento, Feliciano de Souza Coehlo, Thiago de Lima Xavier, Josué Ferreira de Souza, Roberta Pereira de Souza, Bruno Takeshi, and Wallace Rabelo Costa.

Atmos. Chem. Phys. Discuss., https://doi.org/10.5194/acp-2017-1097
Manuscript under review for journal Atmos. Chem. Phys.
This is just a preview and not the published paper.

Atmospheric Chemistry and Physics Discussions

References

ACTRIS: ACTRIS Intercomparison Workshop for Integrating Nephelometer and Absorption Photometers, Leipzig, Germany, 2014.

Ahlm, L., Nilsson, E. D., Krejci, R., Mårtensson, E. M., Vogt, M. and Artaxo, P.: Aerosol number fluxes over the Amazon rain forest during the wet season, Atmos. Chem. Phys. Discuss., 9(4), 17335–17383, doi:10.5194/acpd-9-17335-2009, 2009.

Akagi, S. K., Yokelson, R. J., Wiedinmyer, C., Alvarado, M. J., Reid, J. S., Karl, T., Crounse, J. D. and Wennberg, P. O.: Emission factors for open and domestic biomass burning for use in atmospheric models, Atmos. Chem. Phys., 11(9), 4039–4072, doi:10.5194/acp-11-4039-2011, 2011.

Anderson, T. L., Covert, D. S., Marshall, S. F., Laucks, M. L., Charlson, R. J., Waggoner, A. P., Ogren, J. A., Caldow, R., Holm, R. L., Quant, F. R., Sem, G. J., Wiedensohler, A., Ahlquist, N. A. and Bates, T. S.: Performance Characteristics of a High-Sensitivity, Three-Wavelength, Total Scatter/Backscatter Nephelometer, J. Atmos. Ocean. Technol., 13(5), 967–986, doi:10.1175/1520-0426(1996)013<0967:PCOAHS>2.0.CO;2, 1996.

Andreae, M. O., Biomass burning: Its history, use and distribution and its impact on environmental quality and global climate, in *Global Biomass Burning: Atmospheric, Climatic and Biospheric Implications*, edited by J. S. Levine, pp. 3-21, MIT Press, Cambridge, Mass., 1991.

Andreae, M. O.: Raising dust in the greenhouse, Nature, 380(6573), 389–390, doi:10.1038/380389a0, 1996.

Andreae, M. O.: Aerosols before pollution, Science, 315(5808), 50–51, doi:10.1126/science.1136529, 2007.

Andreae, M. O. and Gelencsér, A.: Black carbon or brown carbon? The nature of light-absorbing carbonaceous aerosols, Atmos. Chem. Phys., 3131–3148, 2006.

Andreae, M. O. and Merlet, P.: Emission of trace gases and aerosols from biomass burning, Global Biogeochem. Cycles, 15(4), 955–966, doi:10.1029/2000GB001382, 2001.

Andreae, M. O., Anderson, B. E., Blake, D. R., Bradshaw, J. D., Collins, J. E., Gregory, G. L., Sachse, G. W. and Shipham, M. C.: Influence of plumes from biomass burning on atmospheric chemistry

over the equatorial and tropical South Atlantic during CITE 3, J. Geophys. Res., 99(D6), 12793, doi:10.1029/94JD00263, 1994.

Andreae, M. O., Artaxo, P., Beck, V., Bela, M., Freitas, S., Gerbig, C., Longo, K., Munger, J. W., Wiedemann, K. T. and Wofsy, S. C.: Carbon monoxide and related trace gases and aerosols over the Amazon Basin during the wet and dry seasons, Atmos. Chem. Phys., 12(13), 6041–6065, doi:10.5194/acp-12-6041-2012, 2012.

Andreae, M. O., Acevedo, O. C., Araùjo, A., Artaxo, P., Barbosa, C. G. G., Barbosa, H. M. J., Brito, J., Carbone, S., Chi, X., Cintra, B. B. L., da Silva, N. F., Dias, N. L., Dias-Júnior, C. Q., Ditas, F., Ditz, R., Godoi, A. F. L., Godoi, R. H. M., Heimann, M., Hoffmann, T., Kesselmeier, J., Könemann, T., Krüger, M. L., Lavric, J. V, Manzi, A. O., Lopes, A. P., Martins, D. L., Mikhailov, E. F., Moran-Zuloaga, D., Nelson, B. W., Nölscher, A. C., Santos Nogueira, D., Piedade, M. T. F., Pöhlker, C., Pöschl, U., Quesada, C. A., Rizzo, L. V, Ro, C.-U., Ruckteschler, N., Sá, L. D. A., de Oliveira Sá, M., Sales, C. B., dos Santos, R. M. N., Saturno, J., Schöngart, J., Sörgel, M., de Souza, C. M., de Souza, R. A. F., Su, H., Targhetta, N., Tóta, J., Trebs, I., Trumbore, S., van Eijck, A., Walter, D., Wang, Z., Weber, B., Williams, J., Winderlich, J., Wittmann, F., Wolff, S. and Yáñez-Serrano, A. M.: The Amazon Tall Tower Observatory (ATTO): Overview of pilot measurements on ecosystem ecology, meteorology, trace gases, and aerosols, Atmos. Chem. Phys., 15(18), 10723–10776, doi:10.5194/acp-15-10723-2015, 2015.

Ångström, A.: On the Atmospheric Transmission of Sun Radiation and on Dust in the Air, Geogr. Ann., 11, 156–166, 1929.

Aragão, L. E. O. ., Malhi, Y., Barbier, N., Lima, A., Shimabukuro, Y., Anderson, L. and Saatchi, S.: Interactions between rainfall, deforestation and fires during recent years in the Brazilian Amazonia, Philos. Trans. R. Soc. B Biol. Sci., 363(1498), 1779–1785, doi:10.1098/rstb.2007.0026, 2008.

Artaxo, P., Rizzo, L. V., Brito, J. F., Barbosa, H. M. J., Arana, A., Sena, E. T., Cirino, G. G., Bastos, W., Martin, S. T. and Andreae, M. O.: Atmospheric aerosols in Amazonia and land use change: from natural biogenic to biomass burning conditions, Faraday Discuss., doi:10.1039/c3fd00052d, 2013.

Barbosa, P. M., Stroppiana, D., Grégoire, J.-M. and Cardoso Pereira, J. M.: An assessment of vegetation fire in Africa (1981-1991): Burned areas, burned biomass, and atmospheric emissions, Global Biogeochem. Cycles, 13(4), 933–950, doi:10.1029/1999GB900042, 1999.

Bilbao, B. A., Leal, A. V. and Méndez, C. L.: Indigenous Use of Fire and Forest Loss in Canaima National Park, Venezuela. Assessment of and Tools for Alternative Strategies of Fire Management in Pemón Indigenous Lands, Hum. Ecol., 38(5), 663–673, doi:10.1007/s10745-010-9344-0, 2010.

Bohren, C. F. and Huffman, D. R.: Absorption and scattering of light by small particles, Wiley, Hoboken, N. J., 1983.

Bond, T. C. and Bergstrom, R. W.: Light Absorption by Carbonaceous Particles : An Investigative Review, Aerosol Sci. Technol., 40, 27–67, doi:10.1080/02786820500421521, 2006.

Bond, T. C., Streets, D. G., Yarber, K. F., Nelson, S. M., Woo, J.-H. and Klimont, Z.: A technology-based global inventory of black and organic carbon emissions from combustion, J. Geophys. Res., 109(D14), D14203, doi:10.1029/2003JD003697, 2004.

Bond, T. C., Doherty, S. J., Fahey, D. W., Forster, P. M., Berntsen, T., DeAngelo, B. J., Flanner, M. G., Ghan, S., Kärcher, B., Koch, D., Kinne, S., Kondo, Y., Quinn, P. K., Sarofim, M. C., Schultz, M. G., Schulz, M., Venkataraman, C., Zhang, H., Zhang, S., Bellouin, N., Guttikunda, S. K., Hopke, P. K., Jacobson, M. Z., Kaiser, J. W., Klimont, Z., Lohmann, U., Schwarz, J. P., Shindell, D., Storelvmo, T., Warren, S. G. and Zender, C. S.: Bounding the role of black carbon in the climate system: A scientific assessment, J. Geophys. Res. Atmos., 118(11), 5380–5552, doi:10.1002/jgrd.50171, 2013.

Brito, J., Rizzo, L. V., Morgan, W. T., Coe, H., Johnson, B., Haywood, J., Longo, K., Freitas, S., Andreae, M. O. and Artaxo, P.: Ground-based aerosol characterization during the South American Biomass Burning Analysis (SAMBBA) field experiment, Atmos. Chem. Phys., 14(22), 12069–12083, doi:10.5194/acp-14-12069-2014, 2014.

Caponi, L., Formenti, P., Massabó, D., Di Biagio, C., Cazaunau, M., Pangui, E., Chevaillier, S., Landrot, G., Andreae, M. O., Kandler, K., Piketh, S., Saeed, T., Seibert, D., Williams, E., Balkanski, Y., Prati, P. and Doussin, J.-F.: Spectral- and size-resolved mass absorption efficiency of mineral dust aerosols in the shortwave spectrum: a simulation chamber study, Atmos. Chem. Phys., 17(11), 7175–7191, doi:10.5194/acp-17-7175-2017, 2017.

Carbone, S., Brito, J. F., Xu, L., Ng, N. L., Rizzo, L. V., Stern, R., Cirino, G. G., Holanda, B. A., Senna, E., Wolff, S., Saturno, J., Chi, X., Souza, R. A. F., Arana, A., de Sá, M., Pöhlker, M. L., Andreae, M. O., Pöhlker, C., Barbosa, H. M. J. and Artaxo, P.: Long-term chemical composition and source apportionment of submicron aerosol particles in the central Amazon basin (ATTO), Atmos. Chem. Phys. Discuss., in preparation, 2017.

Carslaw, K. S., Lee, L. A., Reddington, C. L., Pringle, K. J., Rap, A., Forster, P. M., Mann, G. W., Spracklen, D. V., Woodhouse, M. T., Regayre, L. A. and Pierce, J. R.: Large contribution of natural aerosols to uncertainty in indirect forcing, Nature, 503(7474), 67–71, doi:10.1038/nature12674, 2013.

Chand, D., Guyon, P., Artaxo, P., Schmid, O., Frank, G. P., Rizzo, L. V., Mayol-Bracero, O. L., Gatti, L. V. and Andreae, M. O.: Optical and physical properties of aerosols in the boundary layer and free troposphere over the Amazon Basin during the biomass burning season, Atmos. Chem. Phys., 6(10), 2911–2925, doi:10.5194/acp-6-2911-2006, 2006.

Chi, X., Winderlich, J., Mayer, J.-C., Panov, a. V., Heimann, M., Birmili, W., Heintzenberg, J., Cheng, Y. and Andreae, M. O.: Long-term measurements of aerosol and carbon monoxide at the ZOTTO tall tower to characterize polluted and pristine air in the Siberian taiga, Atmos. Chem. Phys., 13(24), 12271–12298, doi:10.5194/acp-13-12271-2013, 2013.

Clarke, A. D. and Charlson, R. J.: Radiative Properties of the Background Aerosol: Absorption Component of Extinction, Science, 229(4710), 263–265, doi:10.1126/science.229.4710.263, 1985.

Collaud Coen, M., Weingartner, E., Apituley, A., Ceburnis, D., Fierz-Schmidhauser, R., Flentje, H., Henzing, J. S., Jennings, S. G., Moerman, M., Petzold, A., Schmid, O. and Baltensperger, U.: Minimizing light absorption measurement artifacts of the Aethalometer: evaluation of five correction algorithms, Atmos. Meas. Tech., 3, 457–474, doi:10.5194/amt-3-457-2010, 2010.

Crutzen, P. J. and Andreae, M. O.: Biomass burning in the tropics: Impact on atmospheric chemistry and biogeochemical cycles, Science, 250(4988), 1669–1678, 1990.

Das, S., Harshvardhan, H., Bian, H., Chin, M., Curci, G., Protonotariou, A. P., Mielonen, T., Zhang, K., Wang, H. and Liu, X.: Biomass burning aerosol transport and vertical distribution over the South African-Atlantic region, J. Geophys. Res. Atmos., 6391–6415, doi:10.1002/2016JD026421, 2017.

Davidson, E. a., de Araújo, A. C., Artaxo, P., Balch, J. K., Brown, I. F., C. Bustamante, M. M., Coe, M. T., DeFries, R. S., Keller, M., Longo, M., Munger, J. W., Schroeder, W., Soares-Filho, B. S., Souza, C. M. and Wofsy, S. C.: The Amazon basin in transition, Nature, 481(7381), 321–328, doi:10.1038/nature10717, 2012.

Denjean, C., Cassola, F., Mazzino, A., Triquet, S., Chevaillier, S., Grand, N., Bourrianne, T., Momboisse, G., Sellegri, K., Schwarzenbock, A., Freney, E., Mallet, M. and Formenti, P.: Size distribution and optical properties of mineral dust aerosols transported in the western Mediterranean, Atmos. Chem. Phys., 16(2), 1081–1104, doi:10.5194/acp-16-1081-2016, 2016.

Draxler, R. R. and Hess, G. D.: An overview of the HYSPLIT 4 modelling system for trajectories, dispersion and deposition, Aust. Met. Mag., 47(4), 295–308, 1998.

Drinovec, L., Močnik, G., Zotter, P., Prévôt, A. S. H., Ruckstuhl, C., Coz, E., Rupakheti, M., Sciare, J., Müller, T., Wiedensohler, A. and Hansen, A. D. A.: The "dual-spot" Aethalometer: an improved measurement of aerosol black carbon with real-time loading compensation, Atmos. Meas. Tech., 8(5), 1965–1979, doi:10.5194/amt-8-1965-2015, 2015.

Dubovik, O., Holben, B., Eck, T. F., Smirnov, A., Kaufman, Y. J., King, M. D., Tanré, D. and Slutsker, I.: Variability of Absorption and Optical Properties of Key Aerosol Types Observed in Worldwide Locations, J. Atmos. Sci., 59, 590–608, 2002.

Falster, D. S., Warton, D. I. and Wright, I. J.: SMATR: Standardised major axis tests and routines, ver 2.0, 2006.

Favez, O., El Haddad, I., Piot, C., Boréave, A., Abidi, E., Marchand, N., Jaffrezo, J.-L., Besombes, J.-L., Personnaz, M.-B., Sciare, J., Wortham, H., George, C. and D'Anna, B.: Inter-comparison of source apportionment models for the estimation of wood burning aerosols during wintertime in an Alpine city (Grenoble, France), Atmos. Chem. Phys., 10(12), 5295–5314, doi:10.5194/acp-10-5295-2010, 2010.

Fioletov, V. E., McLinden, C. A., Krotkov, N., Li, C., Joiner, J., Theys, N., Carn, S. and Moran, M. D.: A global catalogue of large SO2 sources and emissions derived from the Ozone Monitoring Instrument, Atmos. Chem. Phys., 16(18), 11497–11519, doi:10.5194/acp-16-11497-2016, 2016.

Fisch, G., Tota, J., Machado, L. A. T., Silva Dias, M. A. F., da F. Lyra, R. F., Nobre, C. A., Dolman, A. J. and Gash, J. H. C.: The convective boundary layer over pasture and forest in Amazonia, Theor. Appl. Climatol., 78(1–3), 47–59, doi:10.1007/s00704-004-0043-x, 2004.

Formenti, P., Andreae, M. O., Lange, L., Roberts, G., Cafmeyer, J., Rajta, I., Maenhaut, W., Holben, B. N., Artaxo, P. and Lelieveld, J.: Saharan dust in Brazil and Suriname during the Large-Scale Biosphere-Atmosphere Experiment in Amazonia (LBA) - Cooperative LBA Regional Experiment (CLAIRE) in March 1998, J. Geophys. Res. Atmos., 106(D14), 14919–14934, doi:10.1029/2000JD900827, 2001.

Forrister, H., Liu, J., Scheuer, E., Dibb, J., Ziemba, L., Thornhill, K. L., Anderson, B., Diskin, G., Perring, A. E., Schwarz, J. P., Campuzano-Jost, P., Day, D. A., Palm, B. B., Jimenez, J. L., Nenes, A. and Weber, R. J.: Evolution of brown carbon in wildfire plumes, Geophys. Res. Lett., 42(11), 4623–4630, doi:10.1002/2015GL063897, 2015.

Fuller, K. A., Malm, W. C. and Kreidenweis, S. M.: Effects of mixing on extinction by carbonaceous particles, J. Geophys. Res. Atmos., 104(D13), 15941–15954, doi:10.1029/1998JD100069, 1999.

Garg, S., Chandra, B. P., Sinha, V., Sarda-Esteve, R., Gros, V. and Sinha, B.: Limitation of the Use of the Absorption Angstrom Exponent for Source Apportionment of Equivalent Black Carbon: a Case Study from the North West Indo-Gangetic Plain, Environ. Sci. Technol., 50(2), 814–824, doi:10.1021/acs.est.5b03868, 2016.

GES-DISC: Goddard Earth Sciences Data and Information Services Center, [online] Available from: https://giovanni.gsfc.nasa.gov/giovanni/ (Accessed 1 June 2017), 2017.

Gläser, G., Wernli, H., Kerkweg, A. and Teubler, F.: The transatlantic dust transport from North Africa to the Americas-Its characteristics and source regions, J. Geophys. Res. Atmos., 120(21), 11,231-11,252, doi:10.1002/2015JD023792, 2015.

Guyon, P., Boucher, O., Graham, B., Beck, J., Mayol-Bracero, O. L., Roberts, G. C., Maenhaut, W., Artaxo, P. and Andreae, M. O.: Refractive index of aerosol particles over the Amazon tropical forest during LBA-EUSTACH 1999, J. Aerosol Sci., 34(7), 883–907, doi:10.1016/S0021-8502(03)00052-1, 2003.

Guyon, P., Graham, B., Roberts, G. C., Mayol-Bracero, O. L., Maenhaut, W., Artaxo, P. and Andreae, M. O.: Sources of optically active aerosol particles over the Amazon forest, Atmos. Environ., 38(7), 1039–1051, doi:10.1016/j.atmosenv.2003.10.051, 2004.

Guyon, P., Frank, G. P., Welling, M., Chand, D., Artaxo, P., Rizzo, L., Nishioka, G., Kolle, O., Fritsch, H., Silva Dias, M. A. F., Gatti, L. V., Cordova, A. M. and Andreae, M. O.: Airborne measurements of trace gas and aerosol particle emissions from biomass burning in Amazonia, Atmos. Chem. Phys., 5(11), 2989–3002, doi:10.5194/acp-5-2989-2005, 2005.

Gysel, M., Laborde, M., Olfert, J. S., Subramanian, R. and Gröhn, a. J.: Effective density of Aquadag and fullerene soot black carbon reference materials used for SP2 calibration, Atmos. Meas. Tech., 4(12), 2851–2858, doi:10.5194/amt-4-2851-2011, 2011.

Hamilton, D. S., Lee, L. A., Pringle, K. J., Reddington, C. L., Spracklen, D. V. and Carslaw, K. S.: Occurrence of pristine aerosol environments on a polluted planet, Proc. Natl. Acad. Sci., 111(52), 18466–18471, doi:10.1073/pnas.1415440111, 2014.

Hansen, A. D. A., Rosen, H. and Novakov, T.: The aethalometer — An instrument for the real-time measurement of optical absorption by aerosol particles, Sci. Total Environ., 36, 191–196, doi:10.1016/0048-9697(84)90265-1, 1984.

Hoffer, A., Gelencsér, A., Guyon, P., Kiss, G., Schmid, O., Frank, G. P., Artaxo, P. and Andreae, M. O.: Optical properties of humic-like substances (HULIS) in biomass-burning aerosols, Atmos. Chem. Phys., 6(11), 3563–3570, doi:10.5194/acp-6-3563-2006, 2006.

Janhäll, S., Andreae, M. O. and Pöschl, U.: Biomass burning aerosol emissions from vegetation fires: particle number and mass emission factors and size distributions, Atmos. Chem. Phys., 10(3), 1427–1439, doi:10.5194/acp-10-1427-2010, 2010.

Kirchstetter, T. W., Novakov, T. and Hobbs, P. V.: Evidence that the spectral dependence of light absorption by aerosols is affected by organic carbon, J. Geophys. Res. Atmos., 109(D21), D21208, doi:10.1029/2004JD004999, 2004.

Kondo, Y., Matsui, H., Moteki, N., Sahu, L., Takegawa, N., Kajino, M., Zhao, Y., Cubison, M. J., Jimenez, J. L., Vay, S., Diskin, G. S., Anderson, B., Wisthaler, a., Mikoviny, T., Fuelberg, H. E., Blake, D. R., Huey, G., Weinheimer, a. J., Knapp, D. J. and Brune, W. H.: Emissions of black carbon, organic, and inorganic aerosols from biomass burning in North America and Asia in 2008, J. Geophys. Res., 116(D8), D08204, doi:10.1029/2010JD015152, 2011.

Laborde, M., Crippa, M., Tritscher, T., Jurányi, Z., Decarlo, P. F., Temime-Roussel, B., Marchand, N., Eckhardt, S., Stohl, A., Baltensperger, U., Prévôt, a. S. H., Weingartner, E. and Gysel, M.: Black carbon physical properties and mixing state in the European megacity Paris, Atmos. Chem. Phys., 13(11), 5831–5856, doi:10.5194/acp-13-5831-2013, 2013.

Lack, D. a., Bahreni, R., Langridge, J. M., Gilman, J. B. and Middlebrook, a. M.: Brown carbon absorption linked to organic mass tracers in biomass burning particles, Atmos. Chem. Phys., 13(5), 2415–2422, doi:10.5194/acp-13-2415-2013, 2013.

Lack, D. A. and Langridge, J. M.: On the attribution of black and brown carbon light absorption using the Ångström exponent, Atmos. Chem. Phys., 13(20), 10535–10543, doi:10.5194/acp-13-10535-2013, 2013.

Lack, D. A., Cappa, C. D., Covert, D. S., Baynard, T., Massoli, P., Sierau, B., Bates, T. S., Quinn, P. K., Lovejoy, E. R. and Ravishankara, A. R.: Bias in Filter-Based Aerosol Light Absorption Measurements Due to Organic Aerosol Loading: Evidence from Ambient Measurements, Aerosol Sci. Technol., 42(12), 1033–1041, doi:10.1080/02786820802389277, 2008.

Lewis, K., Arnott, W. P., Moosmüller, H. and Wold, C. E.: Strong spectral variation of biomass smoke light absorption and single scattering albedo observed with a novel dual-wavelength photoacoustic instrument, J. Geophys. Res., 113(D16), D16203, doi:10.1029/2007JD009699, 2008.

Lewis, S. L., Brando, P. M., Phillips, O. L., van der Heijden, G. M. F. and Nepstad, D.: The 2010 Amazon Drought, Science, 331(6017), 554–554, doi:10.1126/science.1200807, 2011.

Liu, D., Flynn, M., Gysel, M., Targino, A., Crawford, I., Bower, K., Choularton, T., Jurányi, Z., Steinbacher, M., Hüglin, C., Curtius, J., Kampus, M., Petzold, A., Weingartner, E., Baltensperger, U. and Coe, H.: Single particle characterization of black carbon aerosols at a tropospheric alpine site in Switzerland, Atmos. Chem. Phys., 10(15), 7389–7407, doi:10.5194/acp-10-7389-2010, 2010.

Liu, D., Taylor, J. W., Young, D. E., Flynn, M. J., Coe, H. and Allan, J. D.: The effect of complex black carbon microphysics on the determination of the optical properties of brown carbon, Geophys. Res. Lett., 42(2), 613–619, doi:10.1002/2014GL062443, 2015.

Liu, D., Whitehead, J., Alfarra, M. R., Reyes-Villegas, E., Spracklen, D. V., Reddington, C. L., Kong, S., Williams, P. I., Ting, Y.-C., Haslett, S., Taylor, J. W., Flynn, M. J., Morgan, W. T., McFiggans, G., Coe, H. and Allan, J. D.: Black-carbon absorption enhancement in the atmosphere determined by particle mixing state, Nat. Geosci., 10(3), 184–188, doi:10.1038/ngeo2901, 2017.

Martin, S. T., Andreae, M. O., Artaxo, P., Baumgardner, D., Chen, Q., Goldstein, A. H., Guenther, A., Heald, C. L., Mayol-Bracero, O. L., McMurry, P. H., Pauliquevis, T., Pöschl, U., Prather, K. A., Roberts, G. C., Saleska, S. R., Silva Dias, M. A., Spracklen, D. V., Swietlicki, E. and Trebs, I.: Sources and properties of Amazonian aerosol particles, Rev. Geophys., 48(2), RG2002, doi:10.1029/2008RG000280, 2010.

Martin, S. T., Artaxo, P., Machado, L. A. T., Manzi, A. O., Souza, R. A. F., Schumacher, C., Wang, J., Andreae, M. O., Barbosa, H. M. J., Fan, J., Fisch, G., Goldstein, A. H., Guenther, A., Jimenez, J. L., Pöschl, U., Silva Dias, M. A., Smith, J. N. and Wendisch, M.: Introduction: Observations and Modeling of the Green Ocean Amazon (GoAmazon2014/5), Atmos. Chem. Phys., 16(8), 4785–4797, doi:10.5194/acp-16-4785-2016, 2016.

Martin, S. T., Artaxo, P., Machado, L., Manzi, A. O., Souza, R. A. F., Schumacher, C., Wang, J., Biscaro, T., Brito, J., Calheiros, A., Jardine, K., Medeiros, A., Portela, B., de Sá, S. S., Adachi, K., Aiken, A. C., Albrecht, R., Alexander, L., Andreae, M. O., Barbosa, H. M. J., Buseck, P., Chand, D., Comstock, J. M., Day, D. A., Dubey, M., Fan, J., Fast, J., Fisch, G., Fortner, E., Giangrande, S., Gilles, M., Goldstein, A. H., Guenther, A., Hubbe, J., Jensen, M., Jimenez, J. L., Keutsch, F. N., Kim, S., Kuang, C., Laskin, A., McKinney, K., Mei, F., Miller, M., Nascimento, R., Pauliquevis, T., Pekour, M., Peres, J., Petäjä, T., Pöhlker, C., Pöschl, U., Rizzo, L., Schmid, B., Shilling, J. E., Dias, M. A. S., Smith, J. N., Tomlinson, J. M., Tóta, J. and Wendisch, M.: The

Green Ocean Amazon Experiment (GoAmazon2014/5) Observes Pollution Affecting Gases, Aerosols, Clouds, and Rainfall over the Rain Forest, Bull. Am. Meteorol. Soc., 98(5), 981–997, doi:10.1175/BAMS-D-15-00221.1, 2017.

Massabò, D., Caponi, L., Bernardoni, V., Bove, M. C., Brotto, P., Calzolai, G., Cassola, F., Chiari, M., Fedi, M. E., Fermo, P., Giannoni, M., Lucarelli, F., Nava, S., Piazzalunga, A., Valli, G., Vecchi, R. and Prati, P.: Multi-wavelength optical determination of black and brown carbon in atmospheric aerosols, Atmos. Environ., 108, 1–12, doi:10.1016/j.atmosenv.2015.02.058, 2015.

Mikhailov, E., Mironova, S., Mironov, G., Vlasenko, S., Panov, A., Chi, X., Walter, D., Carbone, S., Artaxo, P., Pöschl, U. and Andreae, M.: Long-term measurements (2010-2014) of carbonaceous aerosol and carbon monoxide at the Zotino Tall Tower Observatory (ZOTTO) in central Siberia, Atmos. Chem. Phys. Discuss., (May), 1–60, doi:10.5194/acp-2017-409, 2017.

Mishchenko, M. I., Dlugach, J. M., Yanovitskij, E. G. and Zakharova, N. T.: Bidirectional reflectance of flat, optically thick particulate layers: an efficient radiative transfer solution and applications to snow and soil surfaces, J. Quant. Spectrosc. Radiat. Transf., 63(2–6), 409–432, doi:10.1016/S0022-4073(99)00028-X, 1999.

Moosmüller, H., Chakrabarty, R. K., Ehlers, K. M. and Arnott, W. P.: Absorption Ångström coefficient, brown carbon, and aerosols: basic concepts, bulk matter, and spherical particles, Atmos. Chem. Phys., 11(3), 1217–1225, doi:10.5194/acp-11-1217-2011, 2011.

Moran-Zuloaga, D., Ditas, F., Walter, D., Saturno, J., Brito, J., Carbone, S., Chi, X., Hrabe de Angelis, I., Baars, H., Godoi, R. H. M., Heese, B., Holanda, B. A., Lavrič, J. V., Martin, S. T., Ming, J., Pöhlker, M. L., Ruckteschler, N., Su, H., Wang, Y., Wang, Q., Wang, Z., Weber, B., Wolff, S., Artaxo, P., Pöschl, U., Andreae, M. O. and Pöhlker, C.: Long-term study on coarse mode aerosols in the Amazon rain forest with the frequent intrusion of Saharan dust plumes, Atmos. Chem. Phys. Discuss., submitted, 2017.

Moteki, N. and Kondo, Y.: Method to measure time-dependent scattering cross sections of particles evaporating in a laser beam, J. Aerosol Sci., 39(4), 348–364, doi:10.1016/j.jaerosci.2007.12.002, 2008.

Müller, T., Laborde, M., Kassell, G. and Wiedensohler, A.: Design and performance of a three-wavelength LED-based total scatter and backscatter integrating nephelometer, Atmos. Meas. Tech., 4(6), 1291–1303, doi:10.5194/amt-4-1291-2011, 2011.

Ng, N. L., Herndon, S. C., Trimborn, A., Canagaratna, M. R., Croteau, P. L., Onasch, T. B., Sueper, D., Worsnop, D. R., Zhang, Q., Sun, Y. L. and Jayne, J. T.: An Aerosol Chemical Speciation Monitor

(ACSM) for Routine Monitoring of the Composition and Mass Concentrations of Ambient Aerosol, Aerosol Sci. Technol., 45(7), 780–794, doi:10.1080/02786826.2011.560211, 2011.

Petzold, A. and Schönlinner, M.: Multi-angle absorption photometry—a new method for the measurement of aerosol light absorption and atmospheric black carbon, J. Aerosol Sci., 35(4), 421–441, doi:10.1016/j.jaerosci.2003.09.005, 2004.

Petzold, a., Ogren, J. a., Fiebig, M., Laj, P., Li, S.-M., Baltensperger, U., Holzer-Popp, T., Kinne, S., Pappalardo, G., Sugimoto, N., Wehrli, C., Wiedensohler, a. and Zhang, X.-Y.: Recommendations for reporting "black carbon" measurements, Atmos. Chem. Phys., 13(16), 8365–8379, doi:10.5194/acp-13-8365-2013, 2013.

Pöhlker, C., Saturno, J., Krüger, M. L., Förster, J., Weigand, M., Wiedemann, K. T., Bechtel, M., Artaxo, P. and Andreae, M. O.: Efflorescence upon humidification? X-ray microspectroscopic in situ observation of changes in aerosol microstructure and phase state upon hydration, Geophys. Res. Lett., 41, 3681–3689, doi:10.1002/2014GL059409, 2014.

Pöhlker, C., Walter, D., Paulsen, H., Könemann, T., Moran-Zuloaga, D., Pickersgill, D., Ditas, F., Saturno, J., Lammel, G., Després, V. R., Artaxo, P. and Andreae, M. O.: Technical Note: Back trajectory analysis, land cover footprints, and future perturbation trends in the upwind fetch of the ATTO site in the central Amazon, Atmos. Chem. Phys. Discuss., in preparation, 2017a.

Pöhlker, M. L., Pöhlker, C., Klimach, T., Hrabe de Angelis, I., Barbosa, H. M. J., Brito, J., Carbone, S., Chi, X., Cheng, Y., Ditas, F., Ditz, R., Gunthe, S. S., Kesselmeier, J., Könemann, T., Lavric, J. V., Martin, S. T., Moran, D., Rose, D., Saturno, J., Su, H., Thalman, R., Walter, D., Wang, J., Wolff, S., Artaxo, P., Andreae, M. O. and Pöschl, U.: Long-term observations of cloud condensation nuclei in the Amazon rain forest – Part 2: Variability and characteristic differences under near-pristine, biomass burning, and long-range transport conditions, Atmos. Chem. Phys. Discuss., doi:10.5194/acp-2017-847, 2017b.

Pokhrel, R. P., Wagner, N. L., Langridge, J. M., Lack, D. A., Jayarathne, T., Stone, E. A., Stockwell, C. E., Yokelson, R. J. and Murphy, S. M.: Parameterization of single-scattering albedo (SSA) and absorption Ångström exponent (AAE) with EC / OC for aerosol emissions from biomass burning, Atmos. Chem. Phys., 16(15), 9549–9561, doi:10.5194/acp-16-9549-2016, 2016.

Pöschl, U., Martin, S. T., Sinha, B., Chen, Q., Gunthe, S. S., Huffman, J. A., Borrmann, S., Farmer, D. K., Garland, R. M., Helas, G., Jimenez, J. L., King, S. M., Manzi, A., Mikhailov, E., Pauliquevis, T., Petters, M. D., Prenni, A. J., Roldin, P., Rose, D., Schneider, J., Su, H., Zorn, S. R., Artaxo, P.

and Andreae, M. O.: Rainforest Aerosols as Biogenic Nuclei of Clouds and Precipitation in the Amazon, Science, 329(5998), 1513–1516, doi:10.1126/science.1191056, 2010.

Prospero, J. M., Glaccum, R. A. and Nees, R. T.: Atmospheric transport of soil dust from Africa to South America, Nature, 289(5798), 570–572, doi:10.1038/289570a0, 1981.

Raatikainen, T., Brus, D., Hyvärinen, A.-P., Svensson, J., Asmi, E. and Lihavainen, H.: Black carbon concentrations and mixing state in the Finnish Arctic, Atmos. Chem. Phys., 15(11), 10057–10070, doi:10.5194/acpd-15-15621-2015, 2015.

R Development Core Team: R: A language and environment for statistical computing, [online] Available from: http://www.r-project.org, 2009.

Reid, J. S., Hobbs, P. V, Ferek, R. J., Blake, D. R., Martins, J. V., Dunlap, M. R. and Liousse, C.: Physical, chemical, and optical properties of regional hazes dominated by smoke in Brazil, J. Geophys. Res. Atmos., 103(D24), 32059–32080, doi:10.1029/98JD00458, 1998.

Reid, J. S., Eck, T. F., Christopher, S. a., Koppmann, R., Dubovik, O., Eleuterio, D. P., Holben, B. N., Reid, E. a. and Zhang, J.: A review of biomass burning emissions part III: intensive optical properties of biomass burning particles, Atmos. Chem. Phys., 5, 827–849, doi:10.5194/acpd-4-5201-2004, 2005.

Ridley, D. a., Heald, C. L. and Prospero, J. M.: What controls the recent changes in African mineral dust aerosol across the Atlantic?, Atmos. Chem. Phys., 14(11), 5735–5747, doi:10.5194/acp-14-5735-2014, 2014.

Rizzo, L. V., Correia, A. L., Artaxo, P., Procópio, A. S. and Andreae, M. O.: Spectral dependence of aerosol light absorption over the Amazon Basin, Atmos. Chem. Phys., 11, 8899–8912, doi:10.5194/acp-11-8899-2011, 2011.

Rizzo, L. V., Artaxo, P., Müller, T., Wiedensohler, A., Paixão, M., Cirino, G. G., Arana, A., Swietlicki, E., Roldin, P., Fors, E. O., Wiedemann, K. T., Leal, L. S. M. and Kulmala, M.: Long term measurements of aerosol optical properties at a primary forest site in Amazonia, Atmos. Chem. Phys., 13, 2391–2413, doi:10.5194/acp-13-2391-2013, 2013.

Saleh, R., Hennigan, C. J., McMeeking, G. R., Chuang, W. K., Robinson, E. S., Coe, H., Donahue, N. M. and Robinson, a. L.: Absorptivity of brown carbon in fresh and photo-chemically aged biomass-burning emissions, Atmos. Chem. Phys., 13(15), 7683–7693, doi:10.5194/acp-13-7683-2013, 2013.

Saleh, R., Robinson, E. S., Tkacik, D. S., Ahern, A. T., Liu, S., Aiken, A. C., Sullivan, R. C., Presto, A. a, Dubey, M. K., Yokelson, R. J., Donahue, N. M. and Robinson, A. L.: Brownness of organics in aerosols from biomass burning linked to their black carbon content, Nat. Geosci., 7(August), 2–5, doi:10.1038/ngeo2220, 2014.

Salvador, P., Almeida, S. M., Cardoso, J., Almeida-Silva, M., Nunes, T., Cerqueira, M., Alves, C., Reis, M. A., Chaves, P. C., Artíñano, B. and Pio, C.: Composition and origin of PM10 in Cape Verde: Characterization of long-range transport episodes, Atmos. Environ., 127, 326–339, doi:10.1016/j.atmosenv.2015.12.057, 2016.

Sandradewi, J., Prévôt, A. S. H., Szidat, S., Perron, N., Alfarra, M. R., Lanz, V. a, Weingartner, E. and Baltensperger, U.: Using aerosol light absorption measurements for the quantitative determination of wood burning and traffic emission contributions to particulate matter., Environ. Sci. Technol., 42(9), 3316–23, 2008.

Saturno, J., Ditas, F., Penning de Vries, M., Holanda, B. A., Pöhlker, M. L., Carbone, S., Walter, D., Bobrowski, N., Brito, J., Chi, X., Dinger, F., Gutmann, A., Hrabe de Angelis, I., Machado, L. A. T., Moran-Zuloaga, D., Rüdiger, J., Schneider, J., Schulz, C., Wang, Q., Wendisch, M., Artaxo, P., Wagner, T., Pöschl, U., Andreae, M. O. and Pöhlker, C.: African volcanic emissions influencing atmospheric aerosol particles over the Amazon rain forest, Atmos. Chem. Phys. Discuss., in preparation, 2017a.

Saturno, J., Pöhlker, C., Massabò, D., Brito, J., Carbone, S., Cheng, Y., Chi, X., Ditas, F., Hrabě de Angelis, I., Morán-Zuloaga, D., Pöhlker, M. L., Rizzo, L. V, Walter, D., Wang, Q., Artaxo, P., Prati, P. and Andreae, M. O.: Comparison of different Aethalometer correction schemes and a reference multi-wavelength absorption technique for ambient aerosol data, Atmos. Meas. Tech., 10(8), 2837–2850, doi:10.5194/amt-10-2837-2017, 2017b.

Schkolnik, G., Chand, D., Hoffer, A., Andreae, M. O., Erlick, C., Swietlicki, E. and Rudich, Y.: Constraining the density and complex refractive index of elemental and organic carbon in biomass burning aerosol using optical and chemical measurements, Atmos. Environ., 41(5), 1107–1118, doi:10.1016/j.atmosenv.2006.09.035, 2007.

Schuster, G. L., Dubovik, O., Arola, A., Eck, T. F. and Holben, B. N.: Remote sensing of soot carbon – Part 2: Understanding the absorption Ångström exponent, Atmos. Chem. Phys., 16(3), 1587–1602, doi:10.5194/acp-16-1587-2016, 2016.

Schwarz, J. P., Gao, R. S., Fahey, D. W., Thomson, D. S., Watts, L. a., Wilson, J. C., Reeves, J. M., Darbeheshti, M., Baumgardner, D. G., Kok, G. L., Chung, S. H., Schulz, M., Hendricks, J., Lauer,

A., Kärcher, B., Slowik, J. G., Rosenlof, K. H., Thompson, T. L., Langford, A. O., Loewenstein, M. and Aikin, K. C.: Single-particle measurements of midlatitude black carbon and light-scattering aerosols from the boundary layer to the lower stratosphere, J. Geophys. Res., 111(D16), D16207, doi:10.1029/2006JD007076, 2006.

Seinfeld, J. H., Bretherton, C., Carslaw, K. S., Coe, H., DeMott, P. J., Dunlea, E. J., Feingold, G., Ghan, S., Guenther, A. B., Kahn, R., Kraucunas, I., Kreidenweis, S. M., Molina, M. J., Nenes, A., Penner, J. E., Prather, K. A., Ramanathan, V., Ramaswamy, V., Rasch, P. J., Ravishankara, A. R., Rosenfeld, D., Stephens, G. and Wood, R.: Improving our fundamental understanding of the role of aerosol−cloud interactions in the climate system, Proc. Natl. Acad. Sci., 113(21), 5781–5790, doi:10.1073/pnas.1514043113, 2016.

Snelling, D. R., Smallwood, G. J., Liu, F., Gülder, Ö. L. and Bachalo, W. D.: A calibration-independent laser-induced incandescence technique for soot measurement by detecting absolute light intensity, Appl. Opt., 44(31), 6773, doi:10.1364/AO.44.006773, 2005.

Stephens, M., Turner, N. and Sandberg, J.: Particle Identification by Laser-Induced Incandescence in a Solid-State Laser Cavity, Appl. Opt., 42(19), 3726, doi:10.1364/AO.42.003726, 2003.

Subramanian, R., Kok, G. L., Baumgardner, D., Clarke, A., Shinozuka, Y., Campos, T. L., Heizer, C. G., Stephens, B. B., de Foy, B., Voss, P. B. and Zaveri, R. A.: Black carbon over Mexico: the effect of atmospheric transport on mixing state, mass absorption cross-section, and BC/CO ratios, Atmos. Chem. Phys., 10(1), 219–237, doi:10.5194/acp-10-219-2010, 2010.

Talbot, R. W., Andreae, M. O., Berresheim, H., Artaxo, P., Garstang, M., Harriss, R. C., Beecher, K. M. and Li, S. M.: Aerosol chemistry during the wet season in central Amazonia: The influence of long-range transport, J. Geophys. Res., 95(D10), 16955, doi:10.1029/JD095iD10p16955, 1990.

Tasoglou, A., Saliba, G., Subramanian, R. and Pandis, S. N.: Absorption of chemically aged biomass burning carbonaceous aerosol, J. Aerosol Sci., 113, 141–152, doi:10.1016/j.jaerosci.2017.07.011, 2017.

Tuch, T. M., Haudek, A., Müller, T., Nowak, A., Wex, H. and Wiedensohler, A.: Design and performance of an automatic regenerating adsorption aerosol dryer for continuous operation at monitoring sites, Atmos. Meas. Tech., 2(2), 417–422, doi:10.5194/amt-2-417-2009, 2009.

Wang, Q., Saturno, J., Chi, X., Walter, D., Lavric, J. V., Moran-Zuloaga, D., Ditas, F., Pöhlker, C., Brito, J., Carbone, S., Artaxo, P. and Andreae, M. O.: Modeling investigation of light-absorbing aerosols in the Amazon Basin during the wet season, Atmos. Chem. Phys., 16(22), 14775–14794, doi:10.5194/acp-16-14775-2016, 2016a.

Wang, X., Heald, C. L., Sedlacek, A. J., de Sá, S. S., Martin, S. T., Alexander, M. L., Watson, T. B., Aiken, A. C., Springston, S. R. and Artaxo, P.: Deriving brown carbon from multiwavelength absorption measurements: method and application to AERONET and Aethalometer observations, Atmos. Chem. Phys., 16(19), 12733–12752, doi:10.5194/acp-16-12733-2016, 2016b.

Warton, D. I., Wright, I. J., Falster, D. S. and Westoby, M.: Bivariate line-fitting methods for allometry., Biol. Rev. Camb. Philos. Soc., 81(2), 259–91, doi:10.1017/S1464793106007007, 2006.

Winderlich, J., Chen, H., Gerbig, C., Seifert, T., Kolle, O., Lavrič, J. V., Kaiser, C., Höfer, A. and Heimann, M.: Continuous low-maintenance CO_2/CH_4/H_2O measurements at the Zotino Tall Tower Observatory (ZOTTO) in Central Siberia, Atmos. Meas. Tech., 3(4), 1113–1128, doi:10.5194/amt-3-1113-2010, 2010.

Wong, J. P. S., Nenes, A. and Weber, R. J.: Changes in Light Absorptivity of Molecular Weight Separated Brown Carbon Due to Photolytic Aging, Environ. Sci. Technol., 51(15), 8414–8421, doi:10.1021/acs.est.7b01739, 2017.

Zanatta, M., Gysel, M., Bukowiecki, N., Müller, T., Weingartner, E., Areskoug, H., Fiebig, M., Yttri, K. E., Mihalopoulos, N., Kouvarakis, G., Beddows, D., Harrison, R. M., Cavalli, F., Putaud, J. P., Spindler, G., Wiedensohler, A., Alastuey, A., Pandolfi, M., Sellegri, K., Swietlicki, E., Jaffrezo, J. L., Baltensperger, U. and Laj, P.: A European aerosol phenomenology-5: Climatology of black carbon optical properties at 9 regional background sites across Europe, Atmos. Environ., 145, 346–364, doi:10.1016/j.atmosenv.2016.09.035, 2016.

Atmos. Chem. Phys. Discuss., https://doi.org/10.5194/acp-2017-1097
Manuscript under review for journal Atmos. Chem. Phys.
This is just a preview and not the published paper.

Atmospheric Chemistry and Physics Discussions

Table 1. List of frequently used symbols and acronyms

Description	Acronym	Symbol	Units
Black carbon	BC		
Brown carbon	BrC		
Equivalent black carbon	BC_e		
Refractory black carbon	rBC		
Organic carbon	OC		
Organic aerosol	OA		
Light-absorbing carbonaceous matter	LAC		
ΔBC/ΔCO enhancement ratio	ER_{BC}		
Attenuation coefficient	ATN	σ_{ATN}	m^{-1}
Absorption coefficient		σ_{ap}	m^{-1}
Scattering coefficient		σ_{sp}	m^{-1}
Absorption Ångström exponent	AAE	$å_{abs}$	
Scattering Ångström exponent	SAE	$å_{sca}$	
Wavelength dependence of $å_{abs}$	WDA		
Mass attenuation cross-section		α_{atn}	$m^2 g^{-1}$
(BC) Mass absorption cross-section	MAC	α_{abs}	$m^2 g^{-1}$
Backscattering coefficient		σ_{bsp}	m^{-1}
Single scattering albedo	SSA	ω_0	
Aerosol optical depth	AOD		
Condensation nuclei number concentration (> 10 nm)		N_{CN}	cm^{-3}
Accumulation mode particle number concentration (100 to 430 nm)		N_{acc}	cm^{-3}
Precipitation at ATTO region of interest (ROI), Fig. 1a		P_{ATTO}	mm
Equivalent potential temperature		θ_e	K
Amazon Tall Tower Observatory	ATTO		
Backward trajectory	BT		
Long-range transport	LRT		
El Niño Southern Oscillation	ENSO		
Oceanic Niño Index	ONI		
Biomass burning	BB		
Fossil fuel	FF		
Coordinated universal time	UTC		
Local time	LT		
Inter-quartile range	IQR		
Domain of interest, Fig. 2a	DOI		

Atmos. Chem. Phys. Discuss., https://doi.org/10.5194/acp-2017-1097
Manuscript under review for journal Atmos. Chem. Phys.
This is just a preview and not the published paper.

Atmospheric Chemistry and Physics Discussions

Table 2. Descriptive statistics (mean ± standard deviation and interquartile range, IQR) of daily-averaged aerosol optical properties over the Amazon rain forest during the different seasons and the entire measurement period.

	Wavelength	Wet season (Feb – Mar – Apr – May)		Dry season (Aug – Sep – Oct – Nov)		Entire period (2012 – 2017)	
		Mean ± SD	IQR	Mean ± SD	IQR	Mean ± SD	IQR
Scattering coefficient σ_{sp} [Mm^{-1}]	450 nm	9 ± 11	(5.1 – 11)	47 ± 35	(24 – 64)	31 ± 35	(10 – 39)
	550 nm	7.5 ± 9.3	(3.8 – 8.7)	33 ± 25	(17 – 46)	22 ± 25	(7 – 28)
	637 nm	6.4 ± 8.9	(3.0 – 7.4)	26 ± 19	(13 – 35)	17 ± 19	(6 – 23)
Absorption coefficient σ_{ap} [Mm^{-1}]	637 nm	0.68 ± 0.91	(0.17 – 0.72)	4.0 ± 2.2	(2.4 – 5.1)	2.1 ± 2.2	(0.43 – 3.2)
Single scattering albedo ω_0	637 nm	0.93 ± 0.04	(0.91 – 0.96)	0.87 ± 0.03	(0.84 – 0.89)	0.89 ± 0.04	(0.86 – 0.93)
Scattering Ångström exp. * $å_{sca}$		1.29 ± 0.50	(0.98 – 1.65)	1.71 ± 0.24	(1.53 – 1.89)	1.54 ± 0.42	(1.32 – 1.84)
Absorption Ångström exp. * $å_{abs}$		0.91 ± 0.19	(0.80 – 0.98)	0.94 ± 0.16	(0.84 – 1.03)	0.93 ± 0.16	(0.83 – 1.01)
Mass absorption cross-section α_{abs} [$m^2 g^{-1}$] **	637 nm	11.4 ± 1.2	(10.8 – 12.0)	12.3 ± 1.3 [a]	(11.4 – 13.3) [a]	11.9 ± 1.4	(11.0 – 13.0)

* Calculated by applying a log-log linear fit to measurements at all available wavelengths.
** Calculated by fitting 8-channel SP2 and MAAP data.
[a] Including data from July 2015/16 (wet-to-dry transition season).

Atmos. Chem. Phys. Discuss., https://doi.org/10.5194/acp-2017-1097
Manuscript under review for journal Atmos. Chem. Phys.
This is just a preview and not the published paper.

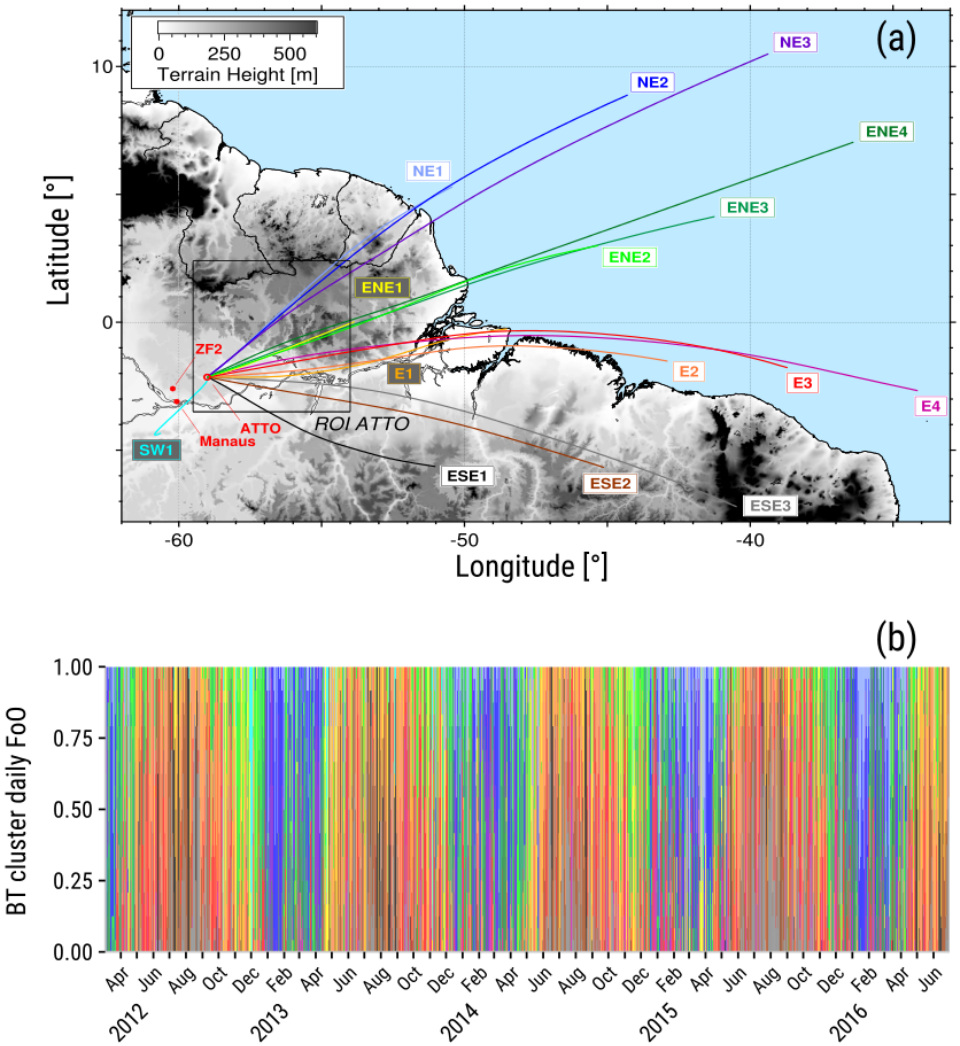

Figure 1. (a) Map of the northeastern Amazon Basin including averaged backward trajectory clusters and the region of interest (ROI) (59° W to 54° W; 3.5° S to 2.4° N), as a black rectangle, used to retrieve precipitation in the ATTO area. (b) Time series of the frequency of occurrence (FoO) of each BT cluster during the sampling period. Adapted from Pöhlker et al. (2017).

Atmos. Chem. Phys. Discuss., https://doi.org/10.5194/acp-2017-1097
Manuscript under review for journal Atmos. Chem. Phys.
This is just a preview and not the published paper.

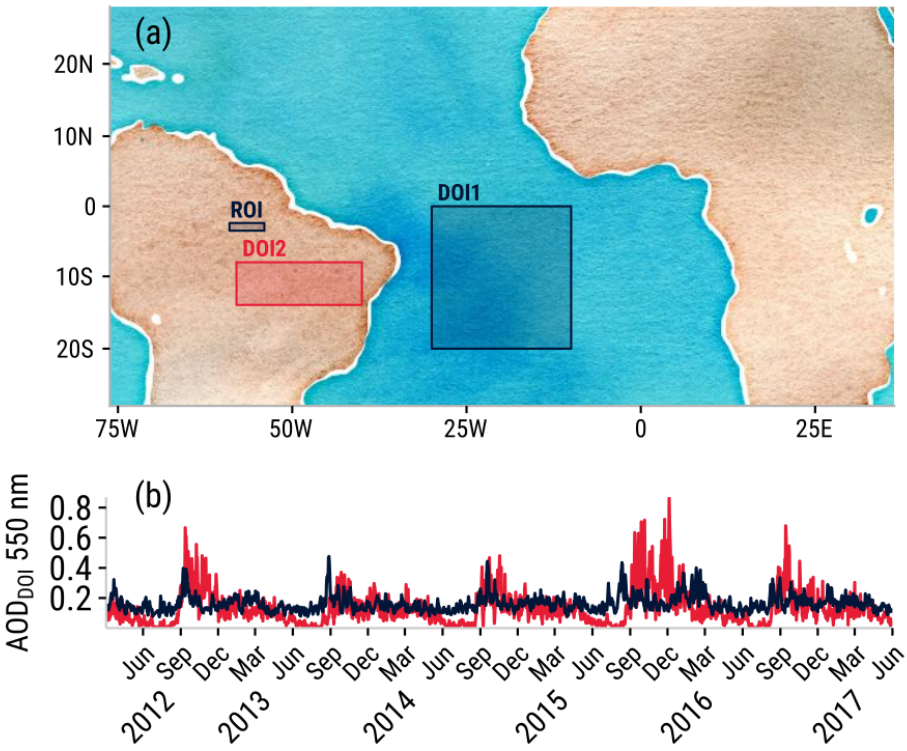

Figure 2. Aerosol optical depth (550 nm) observations in two different domains of interest (DOI1 and DOI2), as shown in (a). Time series of area-averaged AOD are shown in (b) for DOI1 (dark blue) and DOI2 (red). The ATTO region of interest (ROI) is shown as a black rectangle in (a).

Atmos. Chem. Phys. Discuss., https://doi.org/10.5194/acp-2017-1097
Manuscript under review for journal Atmos. Chem. Phys.
This is just a preview and not the published paper.

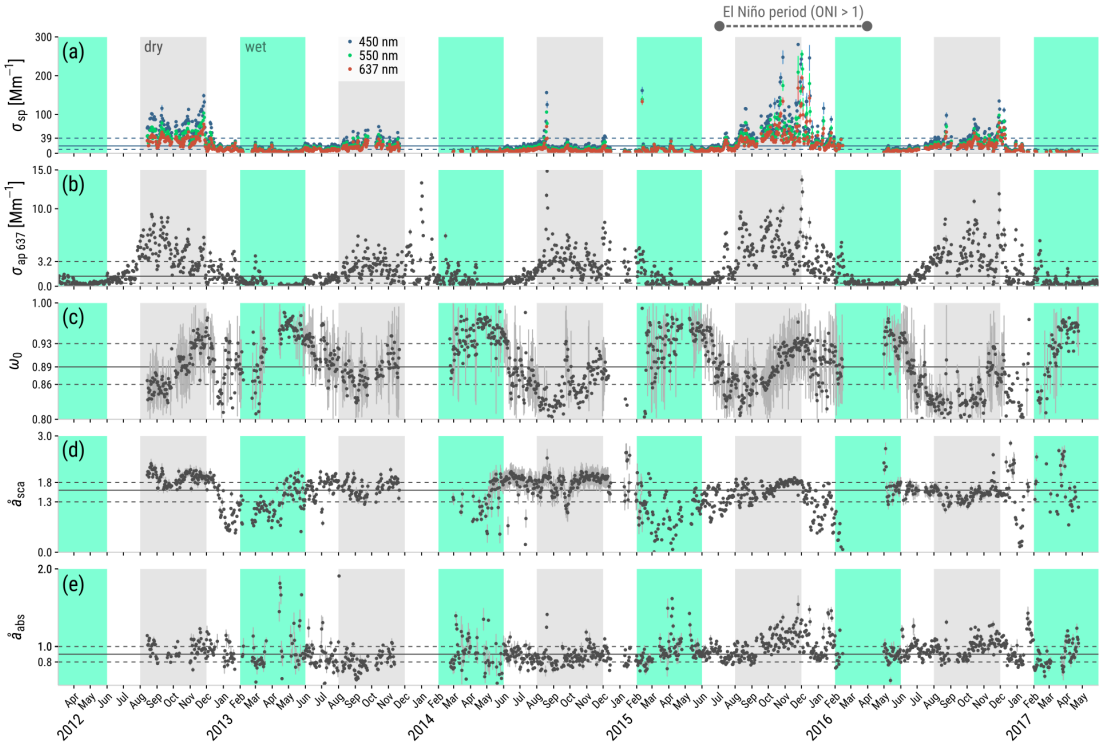

Figure 3. Overview of aerosol optical properties during the measurement period. (a) Scattering coefficient, (b) absorption coefficient at 637 nm, (c) single scattering albedo at 637 nm, (d) scattering Ångström exponent, and (e) absorption Ångström exponent. All data were averaged on 24-h intervals and standard errors are presented as vertical gray bars. Green and gray shaded areas correspond to the wet and dry seasons, respectively. First and third quartiles are represented as horizontal dashed lines, and medians as horizontal solid lines.

Atmos. Chem. Phys. Discuss., https://doi.org/10.5194/acp-2017-1097
Manuscript under review for journal Atmos. Chem. Phys.
This is just a preview and not the published paper.

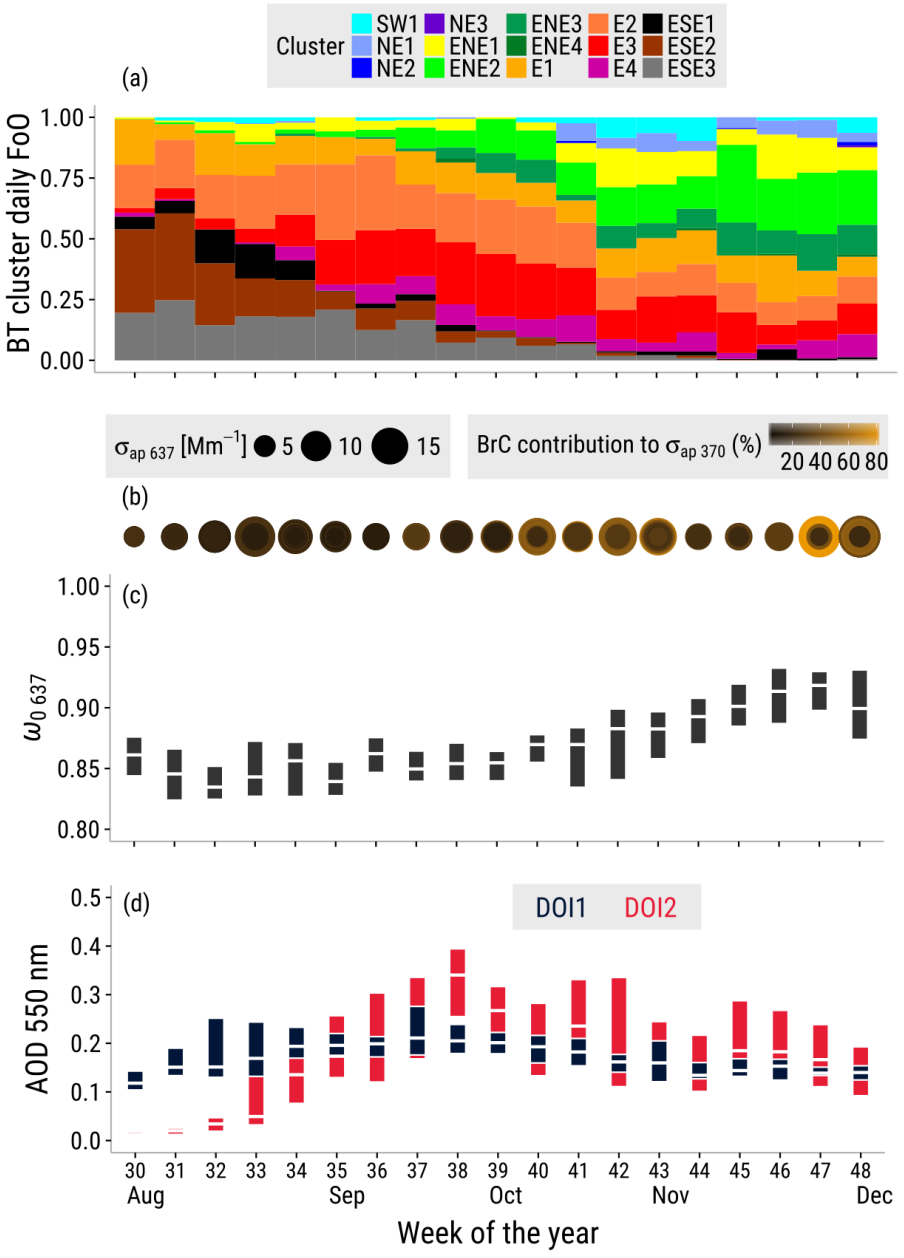

Figure 4. Multi-year (2012 – 2017) weekly averages over the dry season corresponding to (a) frequency of occurrence of BT clusters, (b) absorption coefficients at 637 nm ($\sigma_{ap\,637}$) shown as circles with increasing diameters, the color scale corresponds to the relative BrC contribution to $\sigma_{ap\,370}$, (c) single scattering albedo at 637 nm ($\omega_{0\,637}$), and (d) aerosol optical depth at 550 nm (AOD) for the different domains of interest, DOI1 and DOI2, which cover regions of the South Atlantic Ocean and the southern Amazon, respectively. Boxplots in (c) and (d) represent the median (white segment) and the 25th and 75th percentiles (lower and upper box edges, respectively).

Atmos. Chem. Phys. Discuss., https://doi.org/10.5194/acp-2017-1097
Manuscript under review for journal Atmos. Chem. Phys.
This is just a preview and not the published paper.

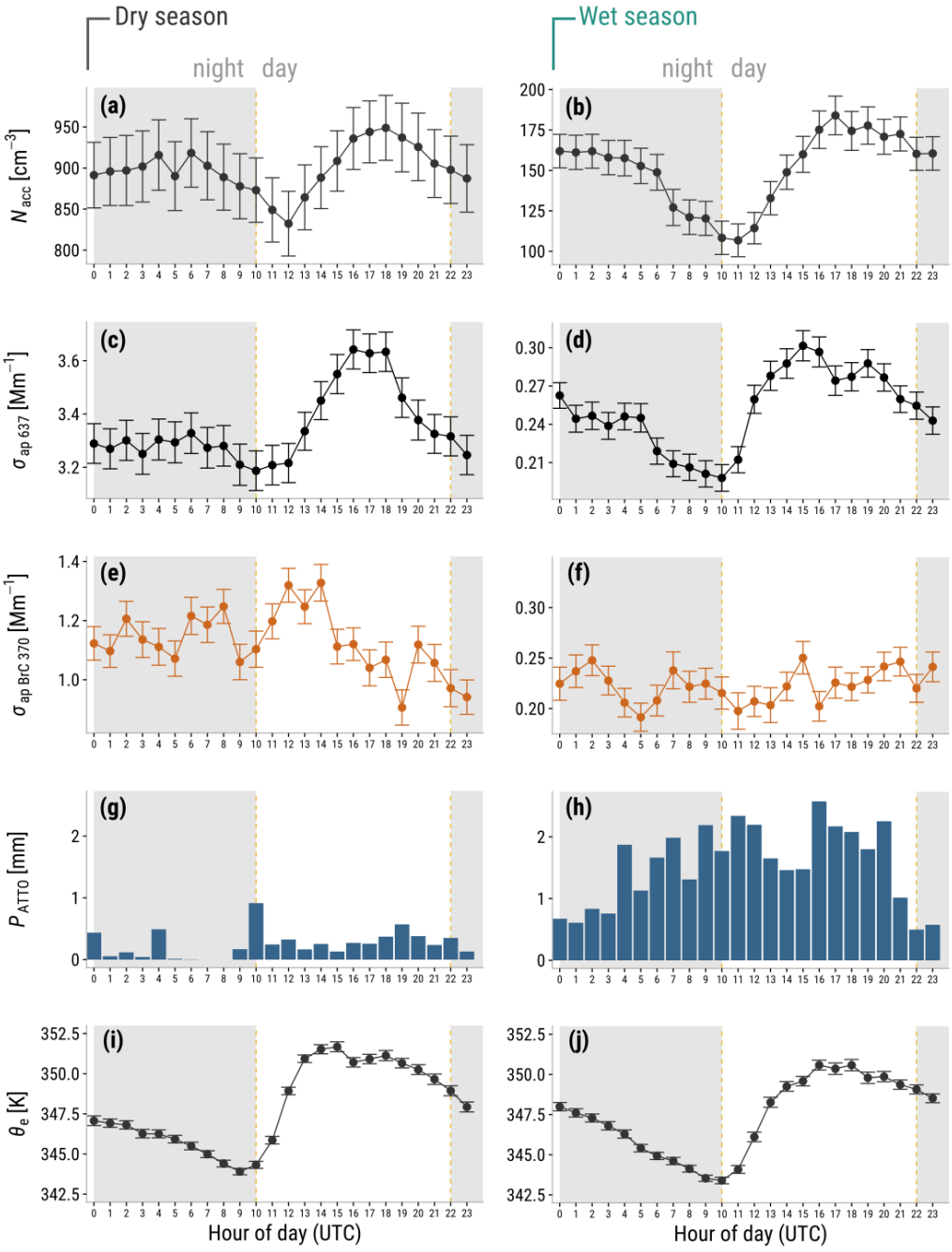

Figure 5. Diel variation of (a, b) median of the accumulation mode particle number concentration, N_{acc}, (c, d) median of the absorption coefficient at 637 nm, (e, f) median of the BrC absorption coefficient at 370 nm, (g, h) precipitation rate, and (i, j) median of the equivalent potential temperature. Gray and white backgrounds correspond to the night and day times, respectively. Error bars correspond to the standard error. Please note the different *y*-axis scales in (a-f).

Atmos. Chem. Phys. Discuss., https://doi.org/10.5194/acp-2017-1097
Manuscript under review for journal Atmos. Chem. Phys.
This is just a preview and not the published paper.

Atmospheric Chemistry and Physics Discussions

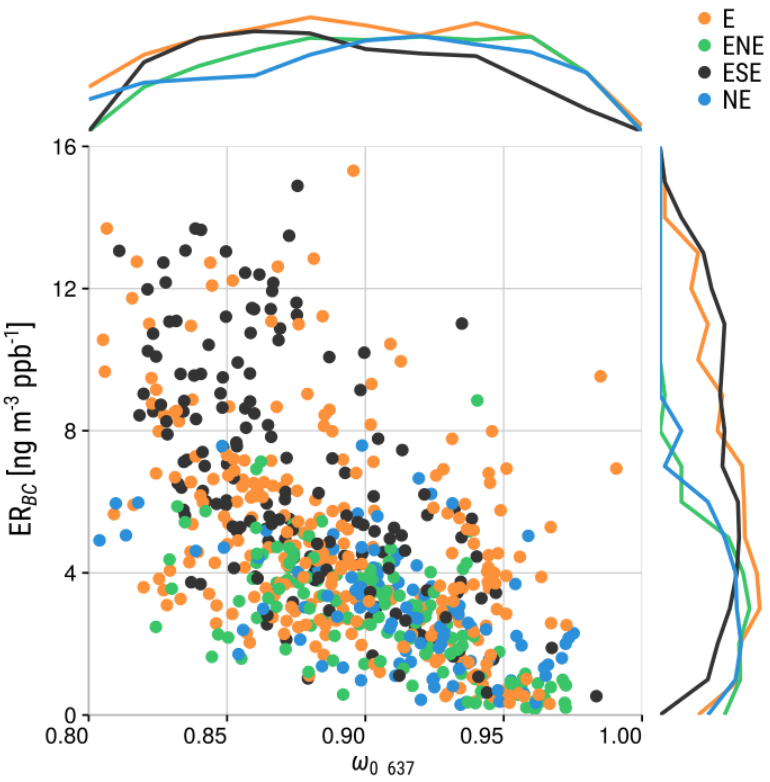

Figure 6. Scatter plot of the black carbon to CO enhancement ratio (ER_{BC}) vs. single scattering albedo at 637 nm ($\omega_{0\ 637}$) with marginal probability density plots (normalized counts in log-scale) for data corresponding to grouped back-trajectory clusters. Each point represent a 24-h average.

Atmos. Chem. Phys. Discuss., https://doi.org/10.5194/acp-2017-1097
Manuscript under review for journal Atmos. Chem. Phys.
This is just a preview and not the published paper.

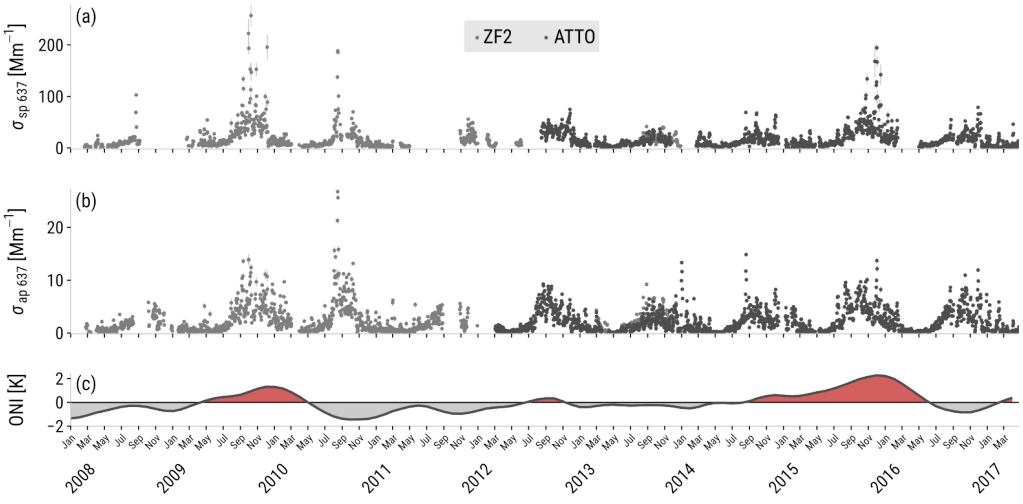

Figure 7. Scattering (a) and absorption (b) coefficient (637 nm) time series measured at the ZF2 and the ATTO sites from 2008 to 2016 (24-h averaged data). Increased scattering and absorption coefficients were observed under the influence of El Niño. (c) High ONI indicates active ENSO periods, shown as red shaded areas.

Atmos. Chem. Phys. Discuss., https://doi.org/10.5194/acp-2017-1097
Manuscript under review for journal Atmos. Chem. Phys.
This is just a preview and not the published paper.

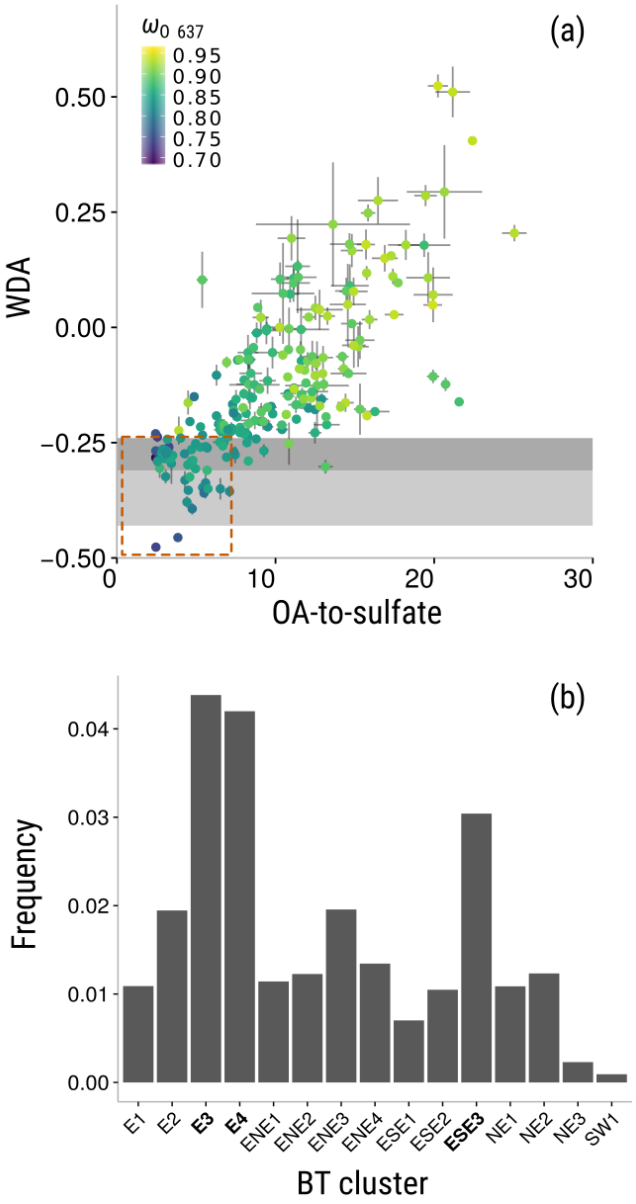

Figure 8. (a) Absorption wavelength dependence (WDA) as function of the OA-to-sulfate mass ratio during high-absorption periods in the dry season. The color scale indicates the ω_0 at 637nm. Gray shaded areas correspond to theoretical WDA for internally mixed BC (light gray), and externally mixed BC (dark gray). The data inside the dashed rectangle in (a) is used in (b) to identify the BT clusters that are more likely to bring BC to the ATTO site.

Atmos. Chem. Phys. Discuss., https://doi.org/10.5194/acp-2017-1097
Manuscript under review for journal Atmos. Chem. Phys.
This is just a preview and not the published paper.

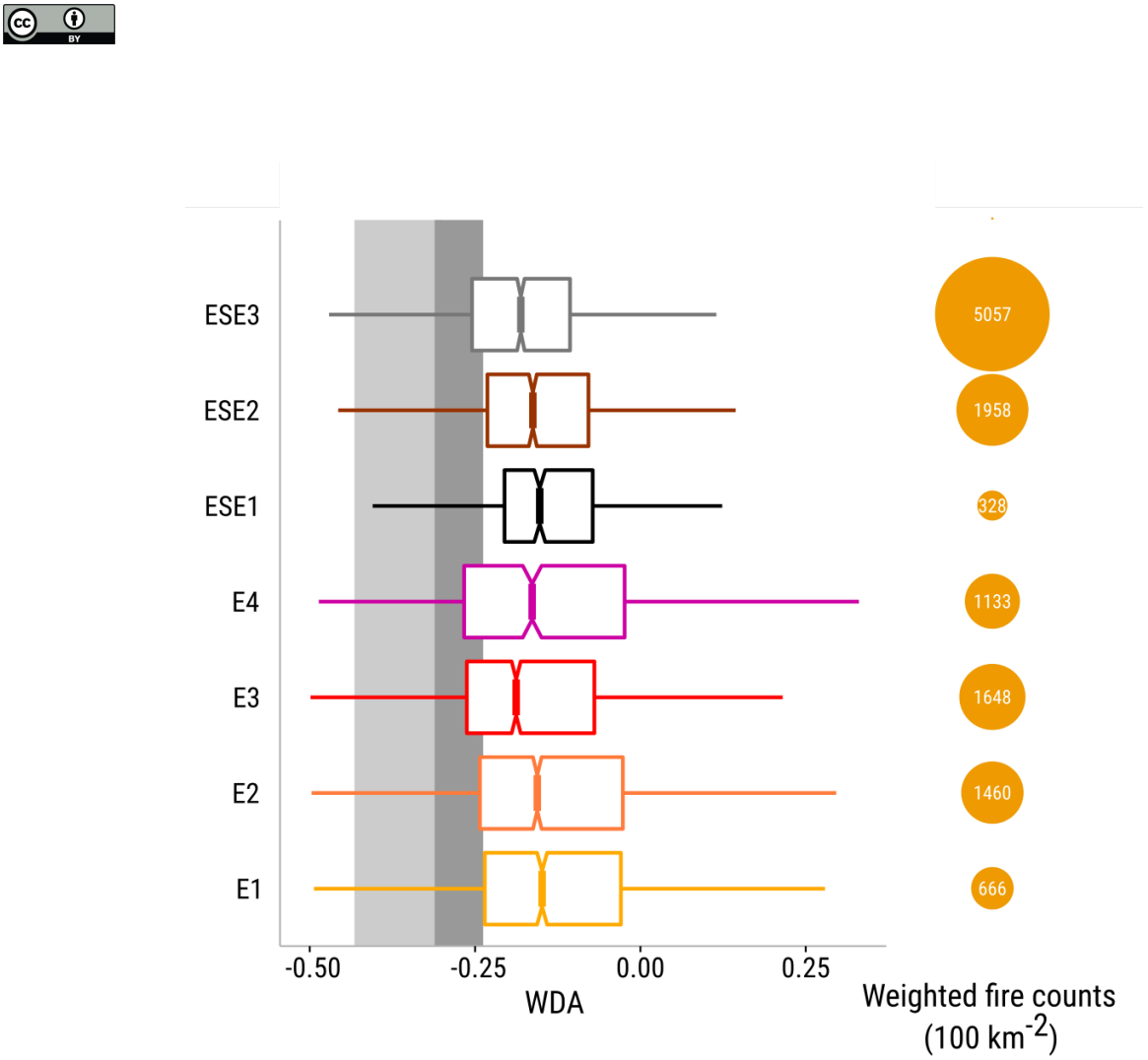

Figure 9. Wavelength dependence of $å_{abs}$ (WDA) for different trajectories in the dry season presented as box and whisker plots (left). The light and dark gray shaded areas correspond to the pure BC and internally mixed BC regimes, respectively. Notches correspond to 1.58 IQR $n^{-½}$. If notch ranges do not overlap, the medians are statistically different (95% confidence). The trajectory weighted fire counts for each BT cluster are shown as circles on the right side. The data presented here correspond to 1-h averages.

Atmos. Chem. Phys. Discuss., https://doi.org/10.5194/acp-2017-1097
Manuscript under review for journal Atmos. Chem. Phys.
This is just a preview and not the published paper.

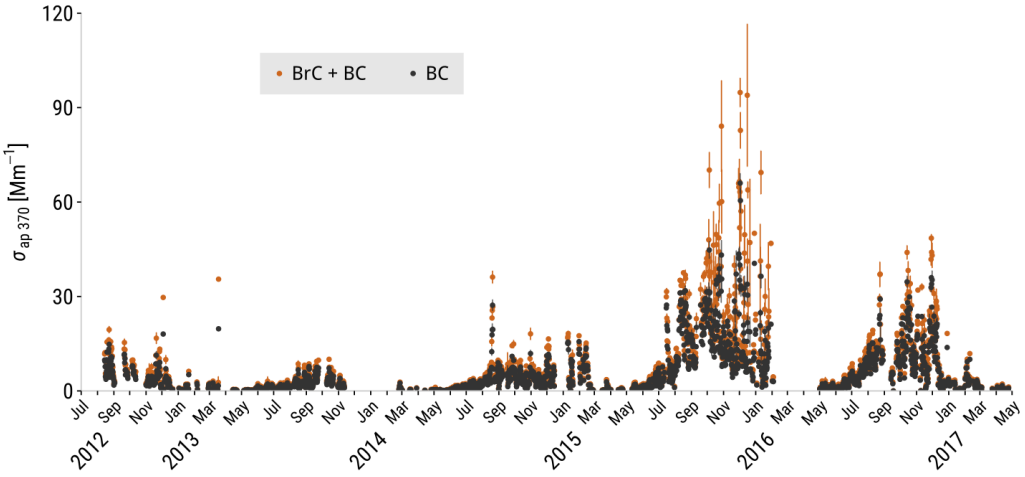

Figure 10. Total absorption at 370 nm (12-h average data) segregated by BC only (gray points) and BrC + BC (brown points). Error bars are equivalent to ± 1 standard error. Long-range transport dust events have been excluded from the analysis.

Atmos. Chem. Phys. Discuss., https://doi.org/10.5194/acp-2017-1097
Manuscript under review for journal Atmos. Chem. Phys.
This is just a preview and not the published paper.

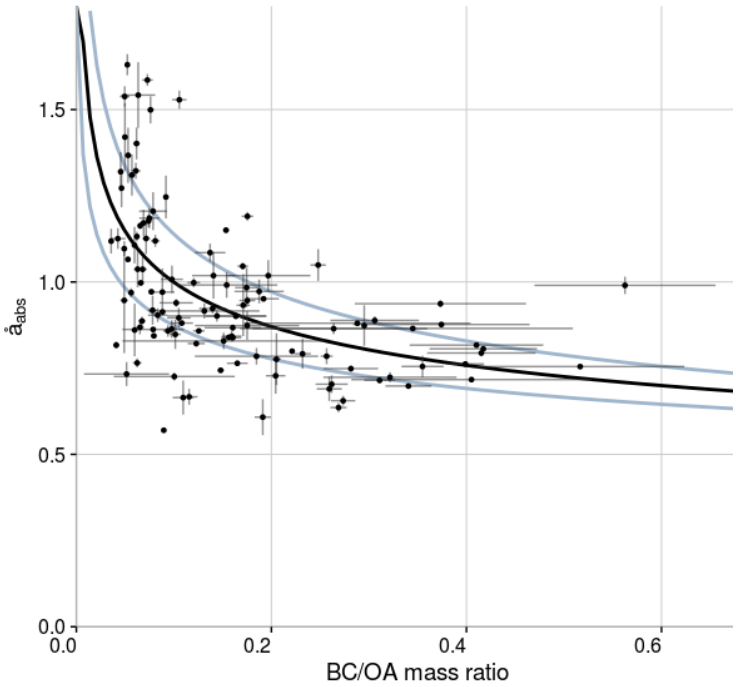

Figure 11. Absorption Ångström exponent ($å_{abs}$) as a function of the BC/OA mass ratio for selected dust events in the wet season. The black line corresponds to a non-linear least squares fit applied to the data ($y = x^{-0.199} \times 0.632$). The light blue lines correspond to the standard error of the fit.

Supplement to

Black and brown carbon over central Amazonia: Long-term aerosol measurements at the ATTO site

Jorge Saturno[1], Bruna A. Holanda[1], Christopher Pöhlker[1], Florian Ditas[1], Qiaoqiao Wang[1,2], Daniel Moran-Zuloaga[1], Joel Brito[3,4], Samara Carbone[3,5], Yafang Cheng[1], Xuguang Chi[6], Jeannine Ditas[1,2], Thorsten Hoffmann[7], Isabella Hrabe de Angelis[1], Tobias Könemann[1], Jošt V. Lavrič[8], Nan Ma[1,2], Jing Ming[1], Hauke Paulsen[9], Mira L. Pöhlker[1], Luciana V. Rizzo[10], Patrick Schlag[3], Hang Su[1], David Walter[1], Stefan Wolff[1], Yuxuan Zhang[1], Paulo Artaxo[3], Ulrich Pöschl[1], and Meinrat O. Andreae[1,11]

[1]Biogeochemistry & Multiphase Chemistry Departments, Max Planck Institute for Chemistry, P. O. Box 3060, 55020 Mainz, Germany.
[2]Jinan University Institute for Environmental and Climate Research, Guangzhou, China.
[3]Department of Applied Physics, Institute of Physics, University of São Paulo (USP), Rua do Matão, Travessa R, 187, CEP 05508-900, São Paulo, SP, Brazil.
[4]Laboratory for Meteorological Physics, Université Clermont Auvergne, Clermont-Ferrand, France.
[5]Institute of Agrarian Sciences, Federal University of Uberlândia, Uberlândia, Minas Gerais, Brazil.
[6]Institute for Climate and Global Change Research & School of Atmospheric Sciences, Nanjing University, Nanjing, 210093, China.
[7]Department of Chemistry, Johannes Gutenberg University, Mainz, Germany.
[8]Department of Biogeochemical Systems, Max Planck Institute for Biogeochemistry, 07701 Jena, Germany.
[9]Institute of General Botany, Johannes Gutenberg University, Mainz, Germany.
[10]Departamento de Ciencias Ambientais, Universidade Federal de Sao Paulo, Diadema, SP, Brasil.
[11]Scripps Institution of Oceanography, University of California San Diego, La Jolla, CA 92098, USA.

Correspondence to: Jorge Saturno (j.saturno@mpic.de) and Christopher Pöhlker (c.pohlker@mpic.de)

This file includes:

Tables S1 to S2.
Figures S1 to S6.

Table S1. Aerosol sampling conditions and locations at the ATTO site.

Time period	**Location**	**Inlet tube dimensions**	**Approx. flow rate (L min^{-1})**	**Drying system**	**1 µm cyclone cut for BC (y/n)**
Mar 2012 – Sep 2012	Mast *	60 m height 17 mm (0.685 ″) inner diameter	13	Diffusion dryers	n
Sep 2012 – Dec 2013	Walk-up tower **	60 m height 17 mm (0.685 ″) inner diameter	13	Diffusion dryers	n
Dec 2013 – May 2014	Mast *	60 m height 24 mm (0.935 ″) inner diameter	18	Diffusion dryers	n
May 2014 – Jan 2015	Mast *	60 m height 24 mm (0.935 ″) inner diameter	30	Diffusion dryers	y
Jan 2015 – present	Mast *	60 m height 24 mm (0.935 ″) inner diameter	30	Automatic regenerating adsorption aerosol dryer	y

* S 02° 08.602’; W 59° 00.033’, 130 m a.s.l.
** S 02° 08.647’; W 58° 59.992’, 130 m a.s.l.

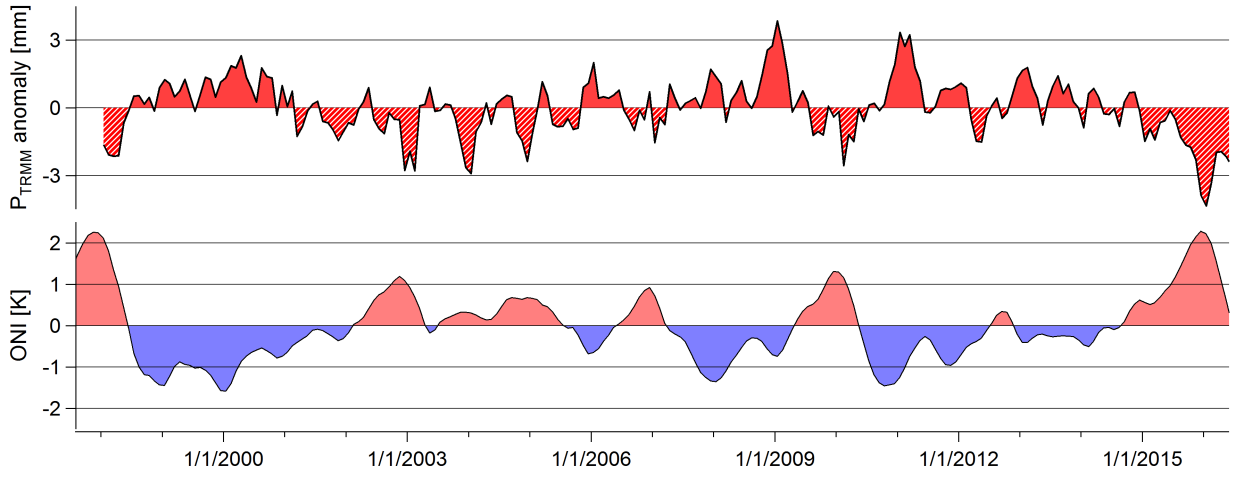

Figure S1. Precipitation anomalies calculated from the Tropical Rainfall Measurement Mission (TRMM) observations along the BT tracks in the ROI ATTO area (top) (see Fig. 1), and Oceanic Niño Index (ONI) (bottom) time series from 1998 to 2016.

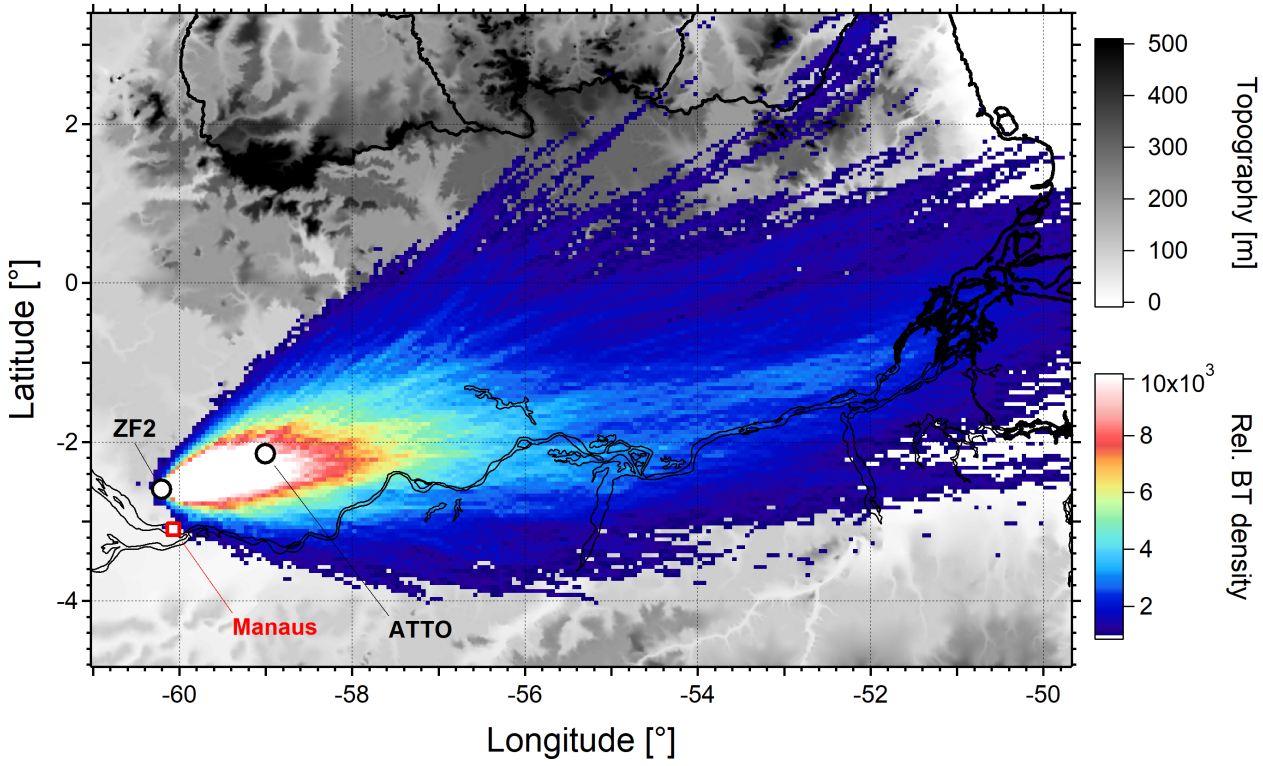

Figure S2. HYPSLIT backward trajectory footprint of the ZF2 site (01 Jan 2014 to 31 Dec 2015) calculated every hour with a starting height of 1000 m. Adapted from Pöhlker et al. (2017).

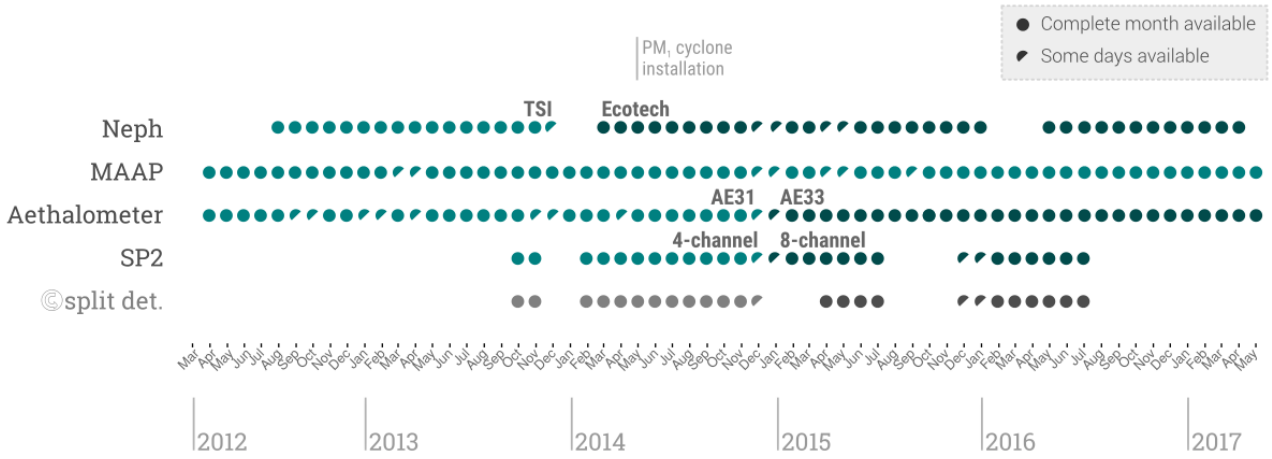

Figure S3. Nephelometer, MAAP, Aethalometer, and SP2 (+ split detector) measurement periods at the ATTO site.

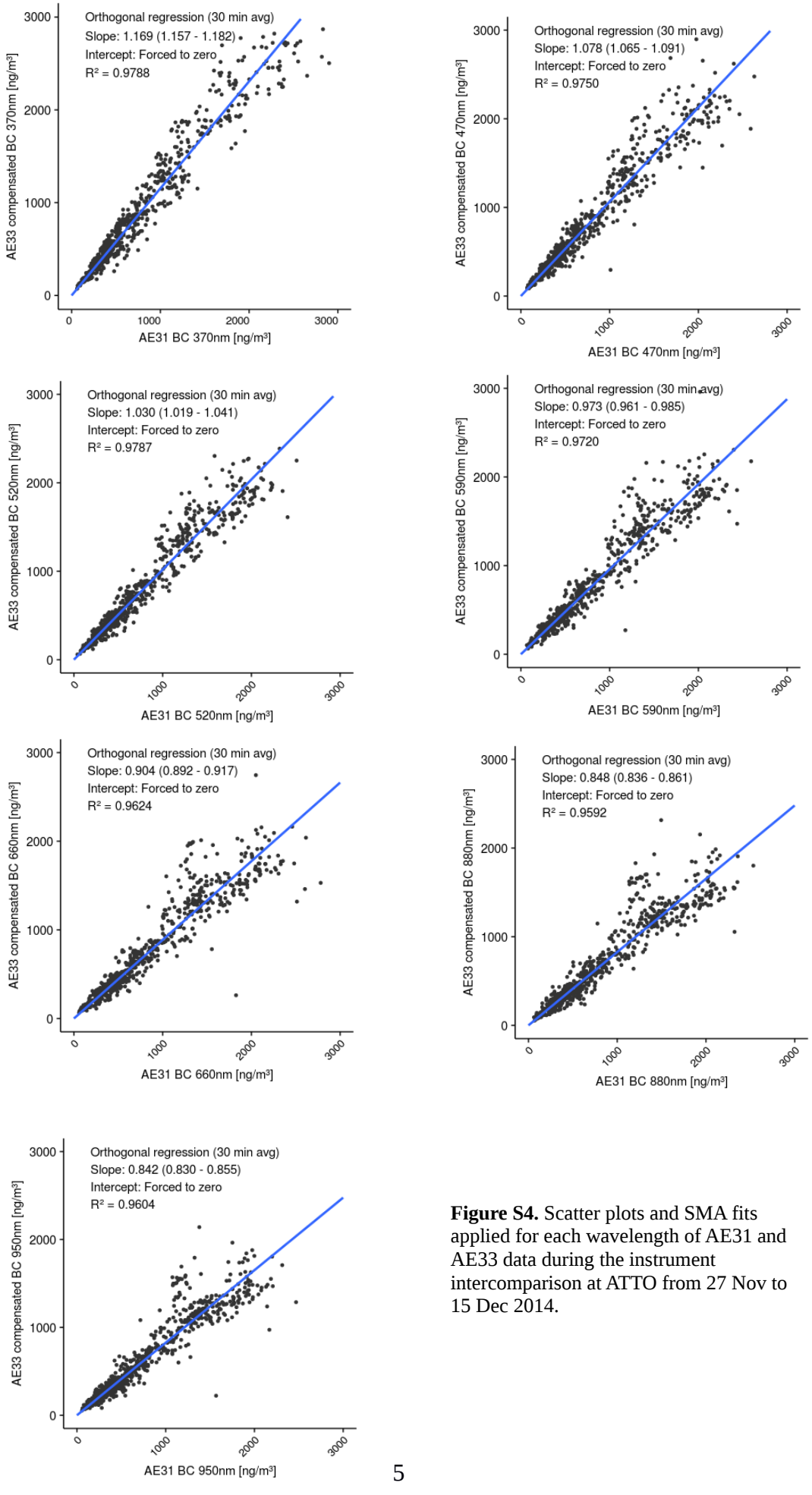

Figure S4. Scatter plots and SMA fits applied for each wavelength of AE31 and AE33 data during the instrument intercomparison at ATTO from 27 Nov to 15 Dec 2014.

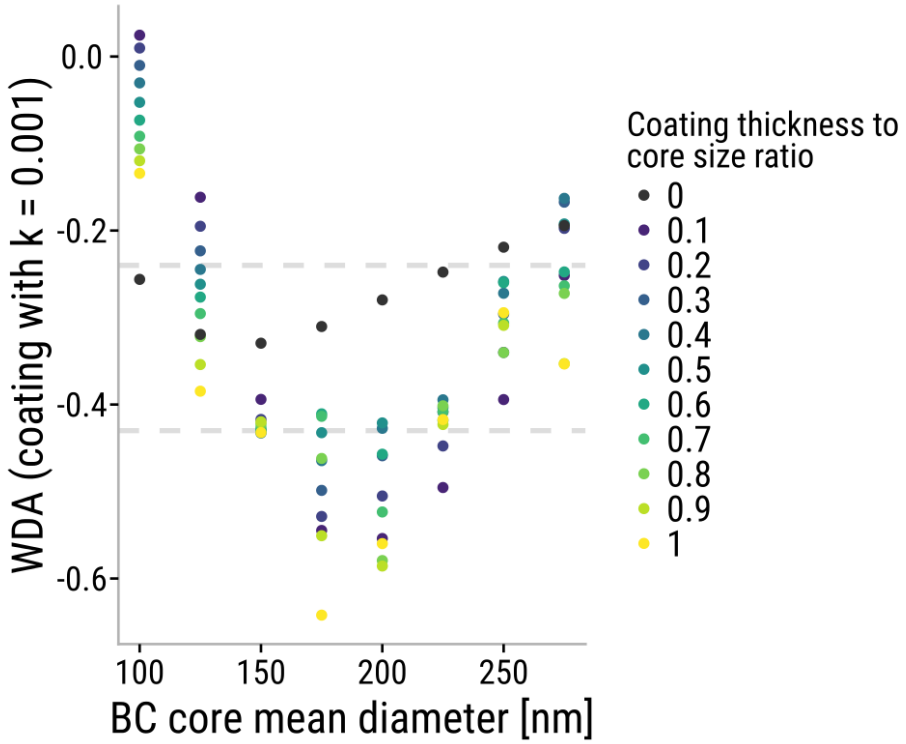

Figure S5. Results of Mie model calculations for pure BC, using a log-normal size distribution with mean = BC geometric mean diameter (GMD), and a standard deviation of 1.45, and internally mixed BC using the core-shell model for monodisperse BC cores with a coating's refractive index of 1.55 - 0.001i. The horizontal dashed lines show the boundaries of the inter-quartile range.

Table S2. Relative overestimation of the BrC contribution to light absorption at 370 nm obtained from Mie model calculations by considering different BC core size ranges and different refractive indices of the coating material. The parameters used in this study are shown in bold letters.

BC core size range [nm]	Refractive index of the coating material	Relative overestimation of BrC contribution to σ_{370} (%)
100 – 275	1.55 - 0i	0
100 – 275	**1.55 - 0.001i**	**0**
100 – 275	1.55 - 0.1i	33
100 – 275	1.55 - 0.2i	46
80 – 275	1.55 - 0i	18
80 – 275	1.55 - 0.001i	18
80 – 275	1.55 - 0.1i	44
80 – 275	1.55 - 0.2i	56

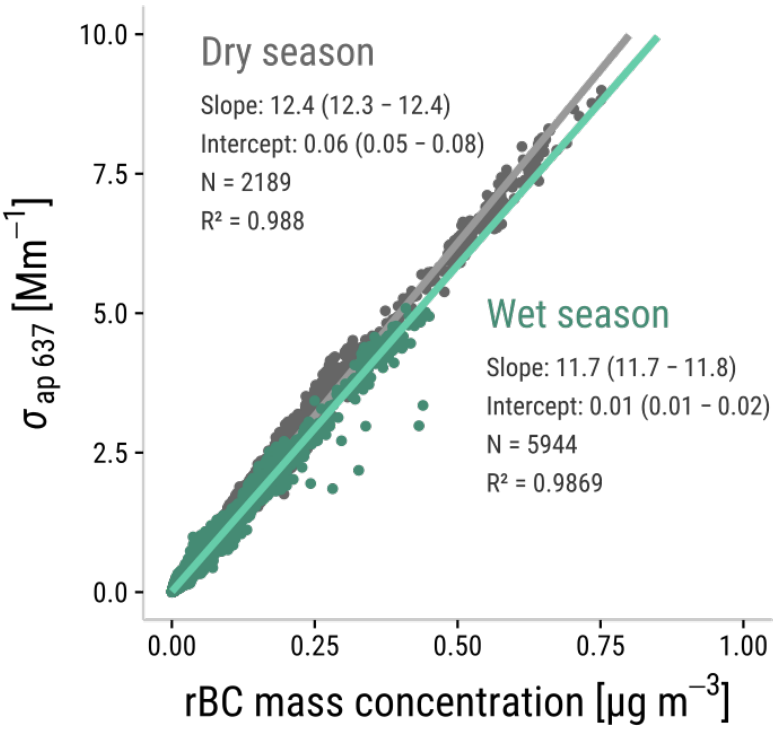

Figure S6. Light absorption coefficient at 637 nm ($\sigma_{ap\ 637}$) vs. rBC mass concentration (30-min averaged data) corresponding to the wet and the dry seasons, in green and gray, respectively. The slopes of the SMA fits correspond to the BC mass absorption cross-section at 637 nm ($\alpha_{abs\ 637}$), inter-quartile ranges are indicated in brackets.

106

B.3. Saturno et al., Atmos. Chem. Phys. Discuss., 2017b

African volcanic emissions influencing atmospheric aerosol particles over the Amazon rain forest

Jorge Saturno[1], Florian Ditas[1], Marloes Penning de Vries[1], Bruna A. Holanda[1], Mira L. Pöhlker[1], Samara Carbone[2,3], David Walter[1], Nicole Bobrowski[4], Joel Brito[2,5], Xuguang Chi[6], Alexandra Gutmann[7], Isabella Hrabe de Angelis[1], Luiz A. T. Machado[8], Daniel Moran-Zuloaga[1], Julian Rüdiger[9], Johannes Schneider[1], Christiane Schulz[1], Qiaoqiao Wang[10], Manfred Wendisch[11], Paulo Artaxo[2], Thomas Wagner[1], Ulrich Pöschl[1], Meinrat O. Andreae[1,12], and Christopher Pöhlker[1]

[1] *Biogeochemistry, Multiphase Chemistry, and Particle Chemistry Departments, and Satellite Research Group, Max Planck Institute for Chemistry, P.O. Box 3060, 55020 Mainz, Germany*
[2] *Department of Applied Physics, Institute of Physics, University of São Paulo (USP), Rua do Matão, Travessa R, 187, CEP 05508-900, São Paulo, SP, Brazil*
[3] *Institute of Agrarian Sciences, Federal University of Uberlândia, Uberlândia, Minas Gerais, Brazil*
[4] *Universität Heidelberg, IUP, Heidelberg, Germany*
[5] *Laboratory for Meteorological Physics, Université Clermont Auvergne, Clermont-Ferrand, France.*
[6] *Institute for Climate and Global Change Research & School of Atmospheric Sciences, Nanjing University, Nanjing, 210093, China*
[7] *Department of Chemistry, Johannes Gutenberg University, Mainz, Germany*
[8] *Centro de Previsão de Tempo e Estudos Climáticos, Instituto Nacional de Pesquisas Espaciais, Cachoeira Paulista, Brasil*
[9] *University of Bayreuth, Atmospheric Chemistry, Dr.-Hans-Frisch-Straße 1–3, 95448 Bayreuth, Germany*
[10] *Institute for Environmental and Climate Research, Jinan University, Guangzhou, 511443, China*
[11] *Leipziger Institut für Meteorologie (LIM), Universität Leipzig, Stephanstr. 3, 04103 Leipzig, Germany*
[12] *Scripps Institution of Oceanography, University of California San Diego, La Jolla, CA 92098, USA*

Atmospheric Chemistry and Physics Discussions, in review, 2017.

Atmos. Chem. Phys. Discuss., https://doi.org/10.5194/acp-2017-1152
Manuscript under review for journal Atmos. Chem. Phys.
This is just a preview and not the published paper.

Atmospheric Chemistry and Physics Discussions

African volcanic emissions influencing atmospheric aerosol particles over the Amazon rain forest

Jorge Saturno[1], Florian Ditas[1], Marloes Penning de Vries[1], Bruna A. Holanda[1], Mira L. Pöhlker[1], Samara Carbone[2,3], David Walter[1], Nicole Bobrowski[4,1], Joel Brito[2,5], Xuguang Chi[6], Alexandra Gutmann[7], Isabella Hrabe de Angelis[1], Luiz A. T. Machado[8], Daniel Moran-Zuloaga[1], Julian Rüdiger[9], Johannes Schneider[1], Christiane Schulz[1], Qiaoqiao Wang[10], Manfred Wendisch[11], Paulo Artaxo[2], Thomas Wagner[1], Ulrich Pöschl[1], Meinrat O. Andreae[1,12], and Christopher Pöhlker[1]

[1]Biogeochemistry, Multiphase Chemistry, and Particle Chemistry Departments, and Satellite Research Group, Max Planck Institute for Chemistry, P. O. Box 3060, 55020 Mainz, Germany
[2]Department of Applied Physics, Institute of Physics, University of São Paulo (USP), Rua do Matão, Travessa R, 187, CEP 05508-900, São Paulo, SP, Brazil
[3]Institute of Agrarian Sciences, Federal University of Uberlândia, Uberlândia, Minas Gerais, Brazil
[4]Institute for Environmental Physics, University of Heidelberg, Heidelberg, Germany
[5]Laboratory for Meteorological Physics, Université Clermont Auvergne, Clermont-Ferrand, France
[6]Institute for Climate and Global Change Research & School of Atmospheric Sciences, Nanjing University, Nanjing, 210093, China
[7]Department of Chemistry, Johannes Gutenberg University, Mainz, Germany
[8]Centro de Previsão de Tempo e Estudos Climáticos, Instituto Nacional de Pesquisas Espaciais, Cachoeira Paulista, Brazil
[9]Atmospheric Chemistry, University of Bayreuth, Dr.-Hans-Frisch-Straße 1–3, 95448 Bayreuth, Germany
[10]Institute for Environmental and Climate Research, Jinan University, Guangzhou, 511443, China
[11]Leipziger Institut für Meteorologie (LIM), Universität Leipzig, Stephanstr. 3, 04103 Leipzig, Germany
[12]Scripps Institution of Oceanography, University of California San Diego, La Jolla, CA 92098, USA

Correspondence to: Jorge Saturno (j.saturno@mpic.de) and Christopher Pöhlker (c.pohlker@mpic.de)

Abstract.

Long-range transport (LRT) plays an important role in the Amazon rain forest by bringing in different primary and secondary aerosol particles from distant sources. The atmospheric oxidation of dimethyl sulfide (DMS), emitted from marine plankton, is considered an important sulfate source over the Amazon rain forest, with a lesser contribution from terrestrial soil and vegetation sulfur emissions. Volcanic sulfur emissions from Africa could be a source of particulate sulfate to the Amazonian atmosphere upon transatlantic transport but no observations have been published. By using satellite observations, together with ground-based and airborne aerosol particle observations, this paper provides evidence of the influence that volcanic emissions have on the aerosol properties that have been observed

Atmos. Chem. Phys. Discuss., https://doi.org/10.5194/acp-2017-1152
Manuscript under review for journal Atmos. Chem. Phys.
This is just a preview and not the published paper.

Atmospheric Chemistry and Physics Discussions

in central Amazonia. Under the volcanic influence, sulfate mass concentrations reached up to 3.6 µg m^{-3} (hourly mean) at ground level, the highest value ever reported in the Amazon region. The hygroscopicity parameter was higher than the characteristic dry-season average, reaching a maximum of 0.36 for accumulation mode aerosol particles. Airborne measurements and satellite data indicated the transport of two different volcanic plumes reaching the Amazon Basin in September 2014 with a sulfate-enhanced layer at an altitude between 4 and 5 km. These observations show that remote volcanic sources can episodically affect the aerosol cycling over the Amazon rain forest and perturb the background conditions. Further studies should address the long-term effect of volcanogenic aerosol particles over the Amazon Basin by running long-term and intensive field measurements in the Amazon region and by monitoring African emissions and their transatlantic transport.

1 Introduction

Sulfate aerosol particles are produced in the atmosphere by oxidation of sulfur dioxide (SO_2), emitted by fossil fuel (FF) combustion, volcanic emissions, and by oxidation of DMS (Andreae and Rosenfeld, 2008). These particles scatter solar radiation and act as efficient cloud condensation nuclei (CCN) (Stevens and Feingold, 2009). Anthropogenic SO_2 emissions have increased over the 20th century to a maximum around the year 1980 and declined somewhat thereafter to around 100 Tg SO_2 per year, but they are still the most important source of sulfur to the atmosphere (Boucher et al., 2013; http://edgar.jrc.ec.europa.eu/overview.php?v=431, last accessed 6 Sep 2017). Volcanic emissions are the predominant natural source of SO_2 and account for about 5 % of total SO_2 emissions (Yang et al., 2017). Sulfur dioxide is oxidized in the atmosphere to gaseous sulfuric acid, which is quickly converted to sulfate aerosol particles (Chin et al., 1996; Reiner and Arnold, 1994). Volcanic sulfur emissions can account for 20 – 40 % of sulfate aerosol particle mass concentrations in the middle troposphere at 650 hPa (Chin and Jacob, 1996). Volcanic eruptions can change the atmospheric composition (gas and particle phase) drastically in large areas (Mather et al., 2003). Two prominent examples are the Pinatubo eruption in 1991 (Kirchner et al., 1999) and the 2014 – 2015 eruption of the Holuhraun volcano in Iceland (Ilyinskaya et al., 2017), where the emissions affected the cloud-drop effective radius

Atmos. Chem. Phys. Discuss., https://doi.org/10.5194/acp-2017-1152
Manuscript under review for journal Atmos. Chem. Phys.
This is just a preview and not the published paper.

Atmospheric Chemistry and Physics Discussions

(r_{eff}) while other cloud properties like the cloud optical depth and the cloud liquid water path remained unaffected (Malavelle et al., 2017; Yuan et al., 2011). Moreover, a connection between tropical volcanic explosive eruptions and El Niño-like events has been described recently (Khodri et al., 2017). Besides explosive-effusive eruptions, small eruptions and passive degassing account for relatively stable SO_2 fluxes (23.0 ± 2.3 Tg yr^{-1}, 2005–2015), and approximately one order of magnitude higher than explosive eruptive SO_2 fluxes (Carn et al., 2017). To what extent volcanic passive sulfur emissions can affect cloud properties is still debated (Ebmeier et al., 2014; Malavelle et al., 2017). There are several active volcanoes in Africa. The Nyamuragira-Nyiragongo neighboring volcanoes in the Democratic Republic of the Congo (DRC) were among the most persistent passively degassing volcanoes worldwide between 2004 and 2014, with around 150 days with detected degassing in 2014 and the highest average SO_2 index observed in the period 2004 – 2014 (Carn et al., 2016). The strong passive degassing activity of Nyamuragira starting in 2011 and culminating in a formation of a lava lake in late 2014 (Campion, 2014) lead to enhanced SO_2 emission from the Nyiragongo-Nyamuragira complex for several years (Bobrowski et al., 2017).

In the Amazon rain forest, biogenic sulfate aerosol is sustained by oceanic DMS emission, and to a lesser degree by hydrogen sulfide (H_2S), methanethiol (MeSH), and DMS emissions from soils and vegetation (Andreae and Andreae, 1988; Jardine et al., 2015; Martin et al., 2010). Occasional anthropogenic sulfur injections have been attributed to open biomass burning and fossil fuel combustion emissions, either from Brazil or, via LRT, from Africa (Andreae et al., 1990; Talbot et al., 1988). A recent study suggests that fossil fuel sources (e.g., ship traffic, power plants) do not significantly influence aerosol particles measured in the remote Amazon forest (Saturno et al., 2017) but can be important downwind of populated areas like Manaus, Brazil (Kuhn et al., 2010; Martin et al., 2016). Recent measurements during the South AMerican Biomass Burning Analysis (SAMBBA) campaign, which focused on biomass burning (BB) emissions, found no correlation between sulfate aerosol and various kinds of BB aerosol particles (Brito et al., 2014). On the other hand, aircraft observations of haze layers at 2 – 4 km altitude over the Amazon rain forest have shown high sulfate enrichment in comparison to the boundary layer and the free troposphere concentrations and indicated these haze layers to be linked to LRT of aerosol particles from Africa (Andreae et al., 1988; Holanda et al., 2017).

Atmos. Chem. Phys. Discuss., https://doi.org/10.5194/acp-2017-1152
Manuscript under review for journal Atmos. Chem. Phys.
This is just a preview and not the published paper.

A modeled global sulfate source attribution study showed that southern Africa peak sulfate concentrations occur between June and August. For this three-month period, estimated emissions were 0.81 Tg S and decreased in the following three months to 0.66 Tg S (Yang et al., 2017).

Northeasterly and southeasterly trade winds (north and south of the inter-tropical convergence zone (ITCZ), respectively) are able to transport aerosols over large distances given the typically weak wet deposition in this latitude band (Wang et al., 2016). During the Amazonian dry season (August – November), the transport of African smoke from southern Africa savanna and shrubland fires is an important source of aerosol in addition to the emissions by regional fires in South America (Andreae et al., 1994). When the ITCZ shifts north in the dry season, south-east trade winds originating from southern Africa are more likely to reach the central Amazon rain forest. Even though the potential impact of transatlantic transport of volcanic sulfur emission has been suggested (Yang et al., 2017), no ground-based evidence has been reported previously in the literature concerning the impact of African volcanic sources.

In this paper, we present satellite observations that show volcanic SO_2 emissions in central Africa that have been transported over the South Atlantic Ocean and reach the Amazon rain forest after being oxidized to particulate sulfate. Satellite, airborne, and ground-based observations are used to show that volcanogenic sulfate can significantly affect the aerosol physical and optical properties over the Amazon Basin during the dry season.

2 Data and methods

2.1 Ground-based instrumentation

The ground-based aerosol data presented here have been collected at the Amazon Tall Tower Observatory (ATTO) site (called *T0a* in the GoAmazon2014/5 experiment, (Martin et al., 2016)), located in the Uatumã Sustainable Development Reserve, Amazonas, Brazil. Details about the ATTO site infrastructure, instrumentation and an overview of running measurements can be found elsewhere (Andreae et al., 2015). Figure 1 shows the ATTO site location and the place of the Nyamuragira

Atmos. Chem. Phys. Discuss., https://doi.org/10.5194/acp-2017-1152
Manuscript under review for journal Atmos. Chem. Phys.
This is just a preview and not the published paper.

Atmospheric Chemistry and Physics Discussions

volcano in the DRC located at 1.41° S, 29.2° E, 3058 m a.s.l. The long-term measurements at ATTO started in 2012. A systematic backward trajectory (BT) analysis of air masses arriving at ATTO can be found in Pöhlker et al. (2017a). The ATTO aerosol measurements were taken on a triangular mast (02° 08.602' S, 59° 00.033' W, 130 m above sea level, a.s.l.) using a 25 mm diameter, 60 m high stainless steel tube with a laminar sampling flow rate of 30 L min^{-1}. The instruments were installed inside an air-conditioned container where the temperature was kept between 29 and 31 °C.

Equivalent black carbon (BC_e) mass concentrations, M_{BCe}, were calculated from absorption measurements by a multi-angle absorption photometer, MAAP (Model 5012, Thermo Electron Group, Waltham, USA). The details of the instrument are described elsewhere (Petzold and Schönlinner, 2004). The BC mass absorption cross-section (MAC) was retrieved from fitting MAAP absorption coefficients at 637 nm wavelength and refractory black carbon (rBC) mass concentrations measured by using a single-particle soot photometer (SP2) revision D (Droplet Measurement Technologies, Boulder, USA). Details of the technique can be found in Stephens et al. (2003). The MAC calculations are described in Saturno et al. (2017). Light scattering coefficients were measured using a three-wavelength integrating nephelometer (Aurora 3000, Ecotech Pty Ltd., Knoxfield, Australia). For details of the instrument, see Müller et al. (2011). Absorption and interpolated scattering measurements at 637 nm wavelength were used to calculate the single scattering albedo of dry aerosol particles, ω_0, at this wavelength, which is defined as the ratio of scattering to extinction coefficients (extinction = scattering + absorption). A detailed study of aerosol optical properties measured at the ATTO site can be found in Saturno et al. (2017).

An aerosol chemical speciation monitor (ACSM) (Aerodyne Research Inc., Billerica, USA) was used to measure online non-refractory aerosol chemical composition (Carbone et al., 2017). These measurements started in February 2014 at the ATTO site. The technique resolves the sub-micron aerosol chemical species in the following categories: Organics, sulfate, nitrate, ammonium and chloride (Ng et al., 2011). In this paper, we only use organics and sulfate mass concentration data, M_{org} and $M_{sulfate}$, respectively.

Atmos. Chem. Phys. Discuss., https://doi.org/10.5194/acp-2017-1152
Manuscript under review for journal Atmos. Chem. Phys.
This is just a preview and not the published paper.

Cloud condensation nuclei (CCN) number concentrations, N_{CCN}, were measured with a CCN counter (CCNC, model CCN-100, Droplet Measurement Technologies, Boulder, USA), which was deployed at the ATTO site starting in March 2014. The instrument scanned over a range of different supersaturations and particle diameters; more details can be found elsewhere (Pöhlker et al., 2016). The hygroscopicity parameter, κ, retrieved for a CCN activation ratio of 50 % is used in this study. Condensation nuclei number concentrations (> 10 nm), N_{CN}, were measured with a condensation particle counter (CPC, model 3022A, TSI, USA).

2.2 Airborne *in-situ* measurements

Chemical species of sub-micron aerosol particles were measured using a compact time-of-flight aerosol mass spectrometer (C-ToF-AMS) installed on board of the German High-Altitude and Long Range Research Aircraft (HALO, http://www.halo.dlr.de, last visited 13 September 2017), a modified business jet G550 (Gulfstream, Savannah, USA). The C-ToF-MS details are presented elsewhere (Drewnick et al., 2005). The measurements took place between 6 September and 1 October 2014, during the "Aerosol, Cloud, Precipitation, and Radiation Interactions and Dynamics of Convective Cloud Systems" (ACRIDICON) - "Cloud Processes of the Main Precipitation Systems in Brazil: A Contribution to Cloud Resolving Modeling and to the GPM (Global Precipitation Measurement)" (CHUVA) campaign over the Amazon rain forest (Machado et al., 2014). More details on the flight trajectories and instrumentation can be found elsewhere (Wendisch et al., 2016). In this study, only data up to 7 km altitude have been used.

2.3 Air mass trajectories

To investigate the probability of the volcanic sulfate plume reaching the ATTO site, trajectories were calculated using the National Oceanic and Atmospheric Administration (NOAA) hybrid single-particle Lagrangian integrated trajectory HYSPLIT model (Draxler and Hess, 1997, 1998; Stein et al., 2015). NOAA Global Data Assimilation System (GDAS) (Kleist et al., 2009) data at 1° × 1° resolution were used as meteorological input for HYSPLIT.

Atmos. Chem. Phys. Discuss., https://doi.org/10.5194/acp-2017-1152
Manuscript under review for journal Atmos. Chem. Phys.
This is just a preview and not the published paper.

Atmospheric Chemistry and Physics Discussions

2.4 Satellite SO_2 VCD data

As one of the most abundant gases in a volcanic plume, SO_2 is often used as a tracer for volcanic emissions by a variety of spectroscopic remote sensing techniques. The strong characteristic absorption features in the UV spectral range allow the quantification of SO_2 using differential optical absorption spectroscopy (DOAS, see e.g. Platt and Stutz, 2008; Richter and Wagner, 2011), both from the ground (e.g. Bobrowski and Platt, 2007; Galle et al., 2003) and from space (e.g., Eisinger and Burrows, 1998; Khokhar et al., 2005; Krueger and J., 1985).

The ozone monitoring instrument (OMI) on board of the National Aeronautics and Space Administration (NASA) Aura satellite, launched in 2004, detects backscattered solar radiation in the UV-visible range (Levelt et al., 2006). The polar-orbiting instrument crosses the equator at 13:30 local time. DOAS analysis of OMI spectra yields column densities of trace gases such as NO_2, SO_2, and HCHO with a spatial resolution of about 13 × 24 km^2 away from the swath edges. OMI's wide swath of 2600 km allowed daily global coverage until the first occurrence of the so-called row anomaly in June 2007, an instrumental problem that causes grievous radiance errors in up to half of OMI's ground pixels (Van Hoek and Claas, 2010). The row anomaly strongly affects the reliability of observations; therefore all affected pixels were removed from the data set prior to analysis.

The OMI SO_2 vertical column density (VCD) data presented in this paper were retrieved using the NASA's principal-component based algorithm with an a-priori vertical profile representative of a volcanic plume in the middle troposphere (TRM, Li et al., 2013, 2017). The assumption that the volcanic plume is located in the mid–troposphere is justified by the elevation of the volcano (3 km), the strength of the eruption, and, particularly, the HYSPLIT trajectory analysis presented later in this paper. It is, however, important to note that the sensitivity of the satellite measurements depends systematically on plume altitude. Thus, the absolute values of the SO_2 VCD derived from the satellite observations over- or underestimate the true values if the plume is located at a higher or lower altitude, respectively. Fortunately, this does not influence our study, as the focus of this paper is on the spatial pattern of the SO_2 plumes, and not on SO_2 amount.

The level-2 data were downloaded from: https://mirador.gsfc.nasa.gov/ (last visited 27 October 2017) and gridded to a regular, 0.1° × 0.1° grid for easily handling.

Multi-year OMI SO_2 VCD daily averages from 11° S to 17° N are summarized in Fig. S1 as a function of time and longitude. The figure shows observations during the ATTO measurement period (March 2012 to July 2017) and a snapshot of September 2014. Given that the Nyamuragira and Nyiragongo volcanoes are so close to each other (within ~15 km), their emissions detected by remote sensors are often treated as a paired source (Carn et al., 2017). Hereafter, the term "Nyamuragira" refers to the couple Nyamuragira-Nyiragongo in this text. Time series of area-averaged OMI SO_2 observations are shown in Fig. 2a. Nyamuragira produced frequent intensive SO_2 emission events especially from 2012 to the end of 2015. The area where the average was calculated (Fig. 2b) corresponds to approximately 200,000 km^2 around Nyamuragira. Emissions from Nyamuragira were often transported westward, as can be observed in HYSPLIT forward trajectories calculated for 2014 (Fig. S2).

3 Results and discussion

3.1 Satellite measurements and trajectory analysis of the volcanic plume

The most important activity at the Nyamuragira volcano since 2011 occurred in September 2014 (Global Volcanism Program, 2017), coinciding with ground and airborne measurement campaigns in the Amazon Basin (Andreae et al., 2015; Wendisch et al., 2016; Martin et al., 2017). Satellite SO_2 VCD observations over central Africa and the Atlantic Ocean were examined during this period in order to precisely identify the volcanic eruptive period and the plume trajectory. A map of gridded OMI SO_2 TRM VCD observations from 7 to 17 September 2014, is available as supplementary material (Fig. S3). Two important emission events were observed at the Nyamuragira location, one on 7 September and another on 12 September. The latter one exhibits a clear westward transport of the SO_2 plume starting from 13 to 17 September. Figure 3 shows SO_2 VCD observations during this period within the region between 20 W – 30 E, and 15 S – 5 N with SO_2 VCD larger than 2.5×10^{16} molecules cm^{-2}. Several sets of trajectory calculations were performed. First, three to seven starting locations were selected within

Atmos. Chem. Phys. Discuss., https://doi.org/10.5194/acp-2017-1152
Manuscript under review for journal Atmos. Chem. Phys.
This is just a preview and not the published paper.

Atmospheric Chemistry and Physics Discussions

the SO_2 plumes detected by OMI on 12–17 September 2014. At each location, 15-day (360 hours) forward trajectories were started at the time of the satellite overpass (11 – 14 UTC) at seven altitudes spaced equally between 1 and 7 km. The resulting trajectories initialized at 4 km altitude on 13 September are in best agreement with the satellite data and are shown in Fig. 3. All starting parameters were systematically varied and very consistent patterns were found. The trajectories are superimposed on the map presenting all SO_2 plumes detected by OMI between 12 and 17 September. Trajectories started within the leading edge of the plume are in good agreement with the OMI data, as after 24 hours (second marker) both trajectories are located within the plume detected on 14 September, and after 48 hours (third marker) both trajectories are located within the plume detected on 15 September. The two southernmost trajectories make a sharp turn after 15 September, which is in agreement with the observed pattern, although there is no longer an exact match with the respective OMI observations (in red and maroon). This discrepancy may be due to inaccuracy of the individual trajectories, or the SO_2 plumes might have been below OMI's detection limit. The southernmost trajectories reach South America and come within several hundreds of kilometers of ATTO within 15 days. One of them reached ATTO on 25 September at 1.8 km altitude, whereas the other one passed at an altitude of 1.5 km at the point nearest to ATTO on 24 September.

In addition to the plume forward trajectory analysis, backward trajectories initiated at the ATTO site at an altitude of 300 m (approximately 170 m above ground) were calculated for 360 hours. These trajectories were initiated every hour from 20 September 0:00 UTC up to 30 September 23:00 UTC. The results, presented as a trajectory density plot in Fig. 4, indicate that although during this time period essentially all air masses come from southern Africa, they usually come from further south. Nevertheless, a significant number of trajectories originates close to the volcano and its plume.

3.2 Airborne observation of the volcanogenic aerosol particles

Enhanced sulfate aerosol mass concentrations were observed above 3 km height over the Amazon Basin during the ACRIDICON-CHUVA campaign compared to lower altitudes. A map including all airborne observations on the different flights can be found in the supplementary material (Fig. S4). However, given the multiple sulfate aerosol sources, sulfate itself can not be used as a tracer of volcanic

Atmos. Chem. Phys. Discuss., https://doi.org/10.5194/acp-2017-1152
Manuscript under review for journal Atmos. Chem. Phys.
This is just a preview and not the published paper.

Atmospheric Chemistry and Physics Discussions

emissions. In order to distinguish the volcanogenic sulfate from additional aerosol sources like BB, which is important during this time of the year, we examined the $M_{sulfate}$ vertical profiles together with their sulfate-to-OA mass ratio ($M_{sulfate}$ / M_{org}). A list of the ACRIDICON-CHUVA flights and $M_{sulfate}$ vertical profiles are presented as supplementary information in Table S1 and Fig. S5, respectively. From the different airborne observations, flight AC14 showed the highest sulfate-to-OA mass ratio, indicating the strongest volcanogenic influence. The $M_{sulfate}$ vertical profile measured on 21 September 2014 (AC14) is presented in Fig. 5. The observations show a sulfate-enhanced layer between 4 and 5 km height. The average $M_{sulfate}$ observed during flight AC14 was 1.1 ± 0.5 µg m^{-3} between 3 and 6 km height. This sulfate-enhanced layer exhibits a sulfate-to-OA ratio generally larger than 1. It can be distinguished from lower layers, below 3 km height, which are characteristically rich in OA due to BB and biogenic emissions. Usually, BB aerosol particles have been shown to have higher OA mass concentrations than other aerosol particles (McNaughton et al., 2011; Saturno et al., 2017). Therefore, the high sulfate-to-OA ratio is an indication of the volcanic origin of the probed aerosol. Backward trajectories were calculated from several points along the flight paths. Figure 6 shows backward trajectories started at nine points along the AC14 flight track where sulfate-to-OA ratios larger (colored lines) or smaller than 1 (gray lines) were detected; the flight and aerosol data measured at each point are presented in Table 1. Figure 6 clearly shows that the (colored) trajectories, with one exception, initialized within the sulfate plume originate from central Africa, whereas the gray trajectories, started outside of the sulfate plume, appear to originate from South America or from more southern regions over or across the Atlantic Ocean. The air mass trajectory analysis indicates that the AC14 observations were likely the result of probing the volcanic plume emitted on 7 September, the first one detected by OMI (see Fig. S3). For flight AC17 a similar pattern is observed, with three out of four (colored) trajectories started within the sulfate plume originating from central Africa and half of the other trajectories clearly coming from regions more to the South (see supplement, Fig. S6 and Table S2).

Figures 3, 4, and 6 show that the trajectories agree well, but not perfectly with the ground-based, airborne, and satellite measurements, which is mainly caused by the uncertainty of such long trajectories. Nevertheless, the fact that forward and backward trajectories calculated from various starting points and times agree on the sulfate source is a strong indication that the sulfate plumes

observed at and near ATTO originate from the Nyamuragira volcano. Combined with the westward transport pattern derived from SO_2 satellite data and the lack of an alternative strong sulfate source makes this a quite convincing case.

3.3 Volcanic emission effects on the aerosol particle properties

The arrival of the African volcanic emissions over the Amazon rain forest affected the aerosol physical and chemical properties measured at the ATTO site. The most evident effect was the significant increase in $M_{sulfate}$. The 90th percentile of $M_{sulfate}$ measured at the ATTO site during the dry season 2014 was used as a threshold to define the volcanic influence event (Nya2014) as the time when this threshold was exceeded. By this criterion, the Nya2014 event spanned from 21 September 2014 at 02:00 UTC to 1 October 2014 at 01:00 UTC. Figure 7 shows different aerosol parameters measured before, during and after the Nya2014 event. The N_{CN}, shown in Fig. 7a, did not vary greatly from the values typical of the season (Pöhlker et al., 2016). The average N_{CN} during the dry season in 2014 was $(1.3 \pm 0.6) \times 10^3$ particles cm^{-3}, whereas during the Nya2014 event, there were three peaks lasting for few hours with particle number concentrations higher than 3.0×10^3 particles cm^{-3} on 27, 29, and 30 September 2014.

During the Nya2014 period, $M_{sulfate}$ averaged 1.7 ± 0.6 µg m^{-3}, which was significantly above the dry season 2014 average of 0.7 ± 0.3 µg m^{-3}, see Fig. 7b. The highest $M_{sulfate}$ value observed at the ATTO site was 3.6 µg m^{-3} (hourly mean) on 26 September 2014. For comparison, during the SAMBBA campaign in southern Amazonia, $M_{sulfate}$ barely exceeded 1.0 µg m^{-3}, despite organics nearly reaching 100 µg m^{-3}, M_{BCe} of 5 µg m^{-3} and N_{CN} above 25×10^3 particles cm^{-3} during the peak of biomass burning (Brito et al., 2014). A long-term measurement study, also conducted in southern Amazonia, reported $M_{sulfate}$ of 1.1 ± 0.7 µg m^{-3} during the dry season, with a maximum of 3.3 µg m^{-3} for aerosol particles with mobility diameters smaller than 2 µm (Artaxo et al., 2002). It is important to note that Artaxo et al.'s (2002) sulfate observations were done under strong BB influence with average elemental carbon (EC) mass concentrations, M_{EC}, of 3.8 ± 4.2 µg m^{-3}, with a maximum of 25 µg m^{-3}. In contrast, the BC_e measurements at the ATTO site during the Nya2014 event had an average of 0.4 ± 0.1 µg m^{-3}, with a maximum of 0.8 µg m^{-3}, indicating that the BB influence was relatively weak during the period of

Atmos. Chem. Phys. Discuss., https://doi.org/10.5194/acp-2017-1152
Manuscript under review for journal Atmos. Chem. Phys.
This is just a preview and not the published paper.

Atmospheric Chemistry and Physics Discussions

interest, with some short (few hours) spikes due to the influence of near-by fire events, see Fig. 7b. At a sampling site impacted by Manaus emissions, the sub-micron $M_{sulfate}$ was about 0.2 µg m^{-3} during the wet season, rarely exceeding 0.6 µg m^{-3} (de Sá et al., 2017). Therefore, even considering a range of pollution sources, our measurements at ATTO during the Nya2014 event are the highest sub-micron sulfate concentration ever reported in the Amazon Basin; see Martin et al. (2010) for a summary of wet and dry season aerosol observations. For comparison, the ACRIDICON-CHUVA airborne measurements are also included in Fig. 7b. The $M_{sulfate}$ measured on flight AC14 was significantly enhanced between 3 to 6 km altitude, reaching a median of 1.0 µg m^{-3} and a 75th percentile of 1.6 µg m^{-3}. Previous aircraft measurements during the SAMBBA campaign reported a $M_{sulfate}$ flight average of 0.48 µg m^{-3} (Allan et al., 2014).

The increased $M_{sulfate}$ period was accompanied by an enhanced sulfate-to-OA mass ratio, according to the ATTO observations (Fig. 7c). The Ny2014 sulfate-to-OA average over about 10 days was 0.38 ± 0.09, significantly higher than the dry season average of 0.18 ± 0.15. During some BB pulses, decreased sulfate-to-OA ratios were observed, but the whole Nya2014 period was exceptionally high compared to the typical dry season conditions. The sulfate-to-OA values measured at ground level were usually lower than the airborne values observed between 3 and 6 km height because the OA sources (BB and biogenic emissions) are located at ground level and the LRT sulfate that arrives at higher altitudes is diluted upon vertical mixing. The possibility of fossil-fuel (FF) burning was ruled out as an important sulfur source during the event discussed here because of the particularly high dry-aerosol ω_0 measured during the event (0.89 ± 0.04), as can be observed in the color code data in Fig. 7c. Usually FF emissions, rich in BC, present characteristically low ω_0 (0.2 – 0.3) (Bond and Bergstrom, 2006) and its addition would have lowered the value of ω_0. Instead, an increase in ω_0 was observed to values higher than 0.90 during the period of maximum $M_{sulfate}$ (26 – 27 September 2014).

The effects of the volcanic sulfur plume on the aerosol hygroscopicity was explored by analyzing the κ values measured at different supersaturations. Higher κ values were measured for the accumulation mode aerosol (particles with diameter greater than 100 nm) (Fig. 7d; note the color-coded particle activation diameter, D_a). During the Nya2014 event, the κ values increased significantly, especially when the maximum $M_{sulfate}$ was observed. For example, the average κ for a supersaturation of 0.10 %

(D_a = 167 – 179 nm, 25th and 75th percentile, respectively) was 0.26 ± 0.04 during the Nya2014 event, with a maximum of 0.36. The Nya2014 κ average was slightly higher than the 2014 dry season average of 0.21 ± 0.03 for 0.10 % supersaturation (excluding the volcanic event), and significantly higher than a strong BB event average of 0.18 ± 0.01 for 0.10 % supersaturation, whose high OA content (sulfate-to-OA < 0.04) caused a significant drop in the hygroscopicity parameter (Pöhlker et al., 2017b).

Summary and conclusions

Satellite SO_2 observations showed two explosive events at the Nyamuragira volcano on 7 and 12 September 2014. These emissions were observed to be transported over the South Atlantic Ocean. Air mass trajectory modeling from the plume location showed that the plume was transported towards South America, likely over the ATTO site and its surroundings in central Amazonia. Airborne observations during the ACRIDICON-CHUVA campaign showed a sulfate-enhanced layer between 4 and 5 km height on 21 September 2014 (flight AC14). Additionally, this layer exhibited an increased sulfate-to-OA mass ratio with medians higher than 1 for measurements between 3 and 6 km height.

The ground-based $M_{sulfate}$ measured at the ATTO site reached an hourly mean of 3.6 µg m^{-3} on 26 September 2014, the highest values ever reported in the Amazon Basin. The sulfate-to-OA mass ratio increased from a dry-season average of 0.18 ± 0.15 to 0.38 ± 0.09 during the volcanic influence event, which spanned for a period of about 10 days. Increased sulfate-to-OA and single scattering albedo (ω_0) were assumed as an indication of the low influence of BB and FF sources, respectively. In terms of aerosol hygroscopicity, the values of κ (for 0.10 % supersaturation) measured during the volcanic event reached an average of 0.26 ± 0.04 (and a maximum of 0.36), slightly higher than the dry season average of 0.21 ± 0.03.

The evidence presented here shows one particular event of volcanic SO_2 emissions in Africa influencing the aerosol particles' chemical composition, hygroscopicity, and optical properties in the Amazon Basin. Therefore, our study indicates that these emissions and their transatlantic transport could potentially affect the Amazonian cloud microphysical properties. However, the extent and relevance of the episodic volcanic influence on the Amazonian atmosphere would require more extensive studies. Beyond the

effects and implications of this particular event, the results of our study represent a reference case of the dynamics and conditions of transatlantic aerosol transport from southern Africa to South America. This could help to understand the inter-continental advection of other aerosol species, such as combustion aerosol particles that are more difficult to trace.

Data availability. The data presented in this paper can be accessed via e-mail request to Jorge Saturno (j.saturno@mpic.de) or Christopher Pöhlker (c.pohlker@mpic.de). OMI data are available online at https://disc.gsfc.nasa.gov/.

Competing interests. The authors declare that they have no conflict of interest.

Acknowledgements

This work has been supported by the Max Planck Society (MPG) and the Paul Crutzen Graduate School (MPGS). For the operation of the ATTO site, we acknowledge the support by the German Federal Ministry of Education and Research (BMBF contract 01LB1001A) and the Brazilian Ministério da Ciência, Tecnologia e Inovação (MCTI/FINEP contract 01.11.01248.00) as well as the Amazon State University (UEA), FAPEAM, LBA/INPA and SDS/CEUC/RDS-Uatumã. We acknowledge the generous support of the ACRIDICON-CHUVA campaign by the Max Planck Society, the German Aerospace Center (DLR), FAPESP (São Paulo Research Foundation), and the German Science Foundation (Deutsche Forschungsgemeinschaft, DFG). This study was also supported by EU Project HAIC under FP7-AAT-2012-3.5.1-1 and by the German Science Foundation within DFG SPP HALO by contract no VO1504/4-1 and contract no JU 3059/1-1. The ACRIDICON-CHUVA aircraft measurements presented here were supported by BMBF, grant No. 01LG1205E (ROMIC-SPITFIRE) and by DFG (SCHN1138/1-2). This paper contains results of research conducted under the Technical/Scientific Cooperation Agreement between the National Institute for Amazonian Research, the State University of Amazonas, and the Max-Planck-Gesellschaft e.V.; the opinions expressed are the entire responsibility of the authors and not of the participating institutions. We highly acknowledge the support by the Instituto Nacional de Pesquisas da Amazônia (INPA). We would like to especially thank all the people involved in the technical, logistical, and scientific support of the ATTO project, in particular Reiner Ditz, Jürgen Kesselmeier, Alberto Quesada, Niro Higuchi, Susan Trumbore, Matthias Sörgel, Thomas Disper, Andrew Crozier, Uwe Schulz, Steffen Schmidt, Antonio Ocimar Manzi, Alcides Camargo Ribeiro, Hermes Braga Xavier, Elton Mendes da Silva, Nagib Alberto de Castro Souza, Adi Vasconcelos Brandão, Amaury Rodrigues Pereira, Antonio Huxley Melo Nascimento, Feliciano de Souza Coehlo, Thiago de Lima Xavier, Josué Ferreira de Souza, Roberta Pereira de Souza, Bruno Takeshi, and Wallace Rabelo Costa. J. Saturno thanks the PhD scholarship funding from Fundación Gran Mariscal de Ayacucho (Fundayacucho) and acknowledges Loreto Donoso, Martin Brüggemann, and David Cabrera for support and stimulating discussions. Moreover, we appreciate the support by Jošt V. Lavrič, Tobias Könemann,

Atmos. Chem. Phys. Discuss., https://doi.org/10.5194/acp-2017-1152
Manuscript under review for journal Atmos. Chem. Phys.
This is just a preview and not the published paper.

Atmospheric Chemistry and Physics Discussions

Luciana V. Rizzo, Henrique M. Barbosa, Patrick Schlag, Florian Dinger, Hang Su, Yafang Cheng, and Stephan Borrmann. We thank the GoAmazon2014/5 team, in particular Scot T. Martin. We also thank the ACRIDICON-CHUVA campaign team.

We acknowledge the NOAA Air Resources Laboratory (ARL) for the provision of the HYSPLIT transport and dispersion model and READY website (http://www.ready.noaa.gov) used in this publication. We also acknowledge NASA for providing the OMI/SO_2 total column level 2 data available online by the Goddard Earth Sciences Data and Information Services Center (GES DISC).

Atmos. Chem. Phys. Discuss., https://doi.org/10.5194/acp-2017-1152
Manuscript under review for journal Atmos. Chem. Phys.
This is just a preview and not the published paper.

Atmospheric Chemistry and Physics Discussions

References

Allan, J. D., Morgan, W. T., Darbyshire, E., Flynn, M. J., Williams, P. I., Oram, D. E., Artaxo, P., Brito, J., Lee, J. D. and Coe, H.: Airborne observations of IEPOX-derived isoprene SOA in the Amazon during SAMBBA, Atmos. Chem. Phys., 14(20), 11393–11407, doi:10.5194/acp-14-11393-2014, 2014.

Andreae, M. O. and Andreae, T. W.: The cycle of biogenic sulfur compounds over the Amazon Basin: 1. Dry season, J. Geophys. Res., 93(D2), 1487, doi:10.1029/JD093iD02p01487, 1988.

Andreae, M. O. and Rosenfeld, D.: Aerosol–cloud–precipitation interactions. Part 1. The nature and sources of cloud-active aerosols, Earth-Science Rev., 89(1–2), 13–41, doi:10.1016/j.earscirev.2008.03.001, 2008.

Andreae, M. O., Browell, E. V., Garstang, M., Gregory, G. L., Harriss, R. C., Hill, G. F., Jacob, D. J., Pereira, M. C., Sachse, G. W., Setzer, A. W., Dias, P. L. S., Talbot, R. W., Torres, A. L. and Wofsy, S. C.: Biomass-burning emissions and associated haze layers over Amazonia, J. Geophys. Res., 93(D2), 1509, doi:10.1029/JD093iD02p01509, 1988.

Andreae, M. O., Berresheim, H., Bingemer, H., Jacob, D. J., Lewis, B. L., Li, S.-M. and Talbot, R. W.: The atmospheric sulfur cycle over the Amazon Basin: 2. Wet season, J. Geophys. Res., 95(D10), 16813, doi:10.1029/JD095iD10p16813, 1990.

Andreae, M. O., Anderson, B. E., Blake, D. R., Bradshaw, J. D., Collins, J. E., Gregory, G. L., Sachse, G. W. and Shipham, M. C.: Influence of plumes from biomass burning on atmospheric chemistry over the equatorial and tropical South Atlantic during CITE 3, J. Geophys. Res., 99(D6), 12793, doi:10.1029/94JD00263, 1994.

Andreae, M. O., Acevedo, O. C., Araùjo, A., Artaxo, P., Barbosa, C. G. G., Barbosa, H. M. J., Brito, J., Carbone, S., Chi, X., Cintra, B. B. L., da Silva, N. F., Dias, N. L., Dias-Júnior, C. Q., Ditas, F., Ditz, R., Godoi, A. F. L., Godoi, R. H. M., Heimann, M., Hoffmann, T., Kesselmeier, J., Könemann, T., Krüger, M. L., Lavric, J. V, Manzi, A. O., Lopes, A. P., Martins, D. L., Mikhailov, E. F., Moran-Zuloaga, D., Nelson, B. W., Nölscher, A. C., Santos Nogueira, D., Piedade, M. T. F., Pöhlker, C., Pöschl, U., Quesada, C. A., Rizzo, L. V, Ro, C.-U., Ruckteschler, N., Sá, L. D. A., de Oliveira Sá, M., Sales, C. B., dos Santos, R. M. N., Saturno, J., Schöngart, J., Sörgel, M., de Souza, C. M., de Souza, R. A. F., Su, H., Targhetta, N., Tóta, J., Trebs, I., Trumbore, S., van

Eijck, A., Walter, D., Wang, Z., Weber, B., Williams, J., Winderlich, J., Wittmann, F., Wolff, S. and Yáñez-Serrano, A. M.: The Amazon Tall Tower Observatory (ATTO): Overview of pilot measurements on ecosystem ecology, meteorology, trace gases, and aerosols, Atmos. Chem. Phys., 15(18), 10723–10776, doi:10.5194/acp-15-10723-2015, 2015.

Artaxo, P., Martins, J. V., Yamasoe, M. A., Procópio, A. S., Pauliquevis, T. M., Andreae, M. O., Guyon, P., Gatti, L. V. and Cordova Leal, A. M.: Physical and chemical properties of aerosols in the wet and dry seasons in Rondônia, Amazonia, J. Geophys. Res., 107(D20), 8081, doi:10.1029/2001JD000666, 2002.

Bobrowski, N. and Platt, U.: SO2/BrO ratios studied in five volcanic plumes, J. Volcanol. Geotherm. Res., 166(3–4), 147–160, doi:10.1016/j.jvolgeores.2007.07.003, 2007.

Bobrowski, N., Giuffrida, G. B., Arellano, S., Yalire, M., Liotta, M., Brusca, L., Calabrese, S., Scaglione, S., Rüdiger, J., Castro, J. M., Galle, B. and Tedesco, D.: Plume composition and volatile flux of Nyamulagira volcano, Democratic Republic of Congo, during birth and evolution of the lava lake, 2014–2015, Bull. Volcanol., 79(12), 90, doi:10.1007/s00445-017-1174-0, 2017.

Bond, T. C. and Bergstrom, R. W.: Light Absorption by Carbonaceous Particles : An Investigative Review, Aerosol Sci. Technol., 40, 27–67, doi:10.1080/02786820500421521, 2006.

Boucher, O., Randall, D., Artaxo, P., Bretherton, C., Feingold, G., Forster, P., Kerminen, V.-M., Kondo, Y., Liao, H., Lohmann, U., Rasch, P., Satheesh, S. K., Sherwood, S., Stevens, B. and Zhang, X. Y.: Clouds and Aerosols, in Climate Change 2013 - The Physical Science Basis, edited by Intergovernmental Panel on Climate Change, pp. 571–658, Cambridge University Press, Cambridge., 2013.

Brito, J., Rizzo, L. V., Morgan, W. T., Coe, H., Johnson, B., Haywood, J., Longo, K., Freitas, S., Andreae, M. O. and Artaxo, P.: Ground-based aerosol characterization during the South American Biomass Burning Analysis (SAMBBA) field experiment, Atmos. Chem. Phys., 14(22), 12069–12083, doi:10.5194/acp-14-12069-2014, 2014.

Campion, R.: New lava lake at Nyamuragira volcano revealed by combined ASTER and OMI SO2 measurements, Geophys. Res. Lett., 41(21), 7485–7492, doi:10.1002/2014GL061808, 2014.

Carbone, S., Brito, J. F., Xu, L., Ng, N. L., Rizzo, L. V., Stern, R., Cirino, G. G., Holanda, B. A., Senna, E., Wolff, S., Saturno, J., Chi, X., Souza, R. A. F., Arana, A., de Sá, M., Pöhlker, M. L., Andreae, M. O., Pöhlker, C., Barbosa, H. M. J. and Artaxo, P.: Long-term chemical composition and source apportionment of submicron aerosol particles in the central Amazon basin (ATTO), Atmos. Chem. Phys. Discuss., in preparation, 2017.

Carn, S. A., Clarisse, L. and Prata, A. J.: Multi-decadal satellite measurements of global volcanic degassing, J. Volcanol. Geotherm. Res., 311, 99–134, doi:10.1016/j.jvolgeores.2016.01.002, 2016.

Carn, S. A., Fioletov, V. E., McLinden, C. A., Li, C. and Krotkov, N. A.: A decade of global volcanic SO2 emissions measured from space, Sci. Rep., 7, 44095, doi:10.1038/srep44095, 2017.

Chin, M. and Jacob, D. J.: Anthropogenic and natural contributions to tropospheric sulfate: A global model analysis, J. Geophys. Res. Atmos., 101(D13), 18691–18699, doi:10.1029/96JD01222, 1996.

Chin, M., Jacob, D. J., Gardner, G. M., Foreman-Fowler, M. S., Spiro, P. A. and Savoie, D. L.: A global three-dimensional model of tropospheric sulfate, J. Geophys. Res. Atmos., 101(D13), 18667–18690, doi:10.1029/96JD01221, 1996.

Draxler, R. R. and Hess, G. D.: Description of the HYSPLIT_4 modeling system, Tech. Rep. NOAA Technical Memo ERL ARL-224, Silver Spring, Maryland, USA., 1997.

Draxler, R. R. and Hess, G. D.: An overview of the HYSPLIT 4 modelling system for trajectories, dispersion and deposition, Aust. Met. Mag., 47(4), 295–308, 1998.

Drewnick, F., Hings, S. S., DeCarlo, P., Jayne, J. T., Gonin, M., Fuhrer, K., Weimer, S., Jimenez, J. L., Demerjian, K. L., Borrmann, S. and Worsnop, D. R.: A New Time-of-Flight Aerosol Mass Spectrometer (TOF-AMS)—Instrument Description and First Field Deployment, Aerosol Sci. Technol., 39(7), 637–658, doi:10.1080/02786820500182040, 2005.

Ebmeier, S. K., Sayer, A. M., Grainger, R. G., Mather, T. A. and Carboni, E.: Systematic satellite observations of the impact of aerosols from passive volcanic degassing on local cloud properties, Atmos. Chem. Phys., 14(19), 10601–10618, doi:10.5194/acp-14-10601-2014, 2014.

Eisinger, M. and Burrows, J. P.: Tropospheric sulfur dioxide observed by the ERS-2 GOME instrument, Geophys. Res. Lett., 25(22), 4177–4180, doi:10.1029/1998GL900128, 1998.

Galle, B., Oppenheimer, C., Geyer, A., McGonigle, A. J. ., Edmonds, M. and Horrocks, L.: A miniaturised ultraviolet spectrometer for remote sensing of SO2 fluxes: a new tool for volcano surveillance, J. Volcanol. Geotherm. Res., 119(1–4), 241–254, doi:10.1016/S0377-0273(02)00356-6, 2003.

Global Volcanism Program: Report on Nyamuragira (DR Congo), in Venzke, E (ed.), Bulletin of the Global Volcanism Network, 42:6. Smithsonian Institution., 2017.

van Hoek, M. and Claas, J.: Possibilities to avoid row anomaly rows Date Signature, TN-OMIE-KNMI-963, 2010.

Holanda, B. A., Wang, Q., Saturno, J., Ditas, F., Ditas, J., Pöhlker, M. L., Klimach, T., Moran-Zuloaga, D., Schulz, C., Ming, J., Cheng, Y., Su, H., Wendisch, M., Machado, L. A. T., Schneider, J., Pöhlker, C., Artaxo, P., Pöschl, U. and Andreae, M. O.: Transatlantic transport of pollution aerosol from Africa to the Amazon rain forest - Aircraft observations in the context of the ACRIDICON-CHUVA campaign, Atmos. Chem. Phys. Discuss., in preparation, 2017.

Ilyinskaya, E., Schmidt, A., Mather, T. A., Pope, F. D., Witham, C., Baxter, P., Jóhannsson, T., Pfeffer, M., Barsotti, S., Singh, A., Sanderson, P., Bergsson, B., McCormick Kilbride, B., Donovan, A., Peters, N., Oppenheimer, C. and Edmonds, M.: Understanding the environmental impacts of large fissure eruptions: Aerosol and gas emissions from the 2014–2015 Holuhraun eruption (Iceland), Earth Planet. Sci. Lett., 472, 309–322, doi:10.1016/j.epsl.2017.05.025, 2017.

Jardine, K., Yañez-Serrano, A. M., Williams, J., Kunert, N., Jardine, A., Taylor, T., Abrell, L., Artaxo, P., Guenther, A., Hewitt, C. N., House, E., Florentino, A. P., Manzi, A., Higuchi, N., Kesselmeier, J., Behrendt, T., Veres, P. R., Derstroff, B., Fuentes, J. D., Martin, S. T. and Andreae, M. O.: Dimethyl sulfide in the Amazon rain forest, Global Biogeochem. Cycles, 29(1), 19–32, doi:10.1002/2014GB004969, 2015.

Khodri, M., Izumo, T., Vialard, J., Janicot, S., Cassou, C., Lengaigne, M., Mignot, J., Gastineau, G., Guilyardi, E., Lebas, N., Robock, A. and McPhaden, M. J.: Tropical explosive volcanic eruptions can trigger El Niño by cooling tropical Africa, Nat. Commun., 8(1), 778, doi:10.1038/s41467-017-00755-6, 2017.

Khokhar, M. F., Frankenberg, C., Van Roozendael, M., Beirle, S., Kühl, S., Richter, A., Platt, U. and Wagner, T.: Satellite observations of atmospheric SO2 from volcanic eruptions during the time-period of 1996–2002, Adv. Sp. Res., 36(5), 879–887, doi:10.1016/j.asr.2005.04.114, 2005.

Kirchner, I., Stenchikov, G. L., Graf, H.-F., Robock, A. and Antuña, J. C.: Climate model simulation of winter warming and summer cooling following the 1991 Mount Pinatubo volcanic eruption, J. Geophys. Res. Atmos., 104(D16), 19039–19055, doi:10.1029/1999JD900213, 1999.

Kleist, D. T., Parrish, D. F., Derber, J. C., Treadon, R., Wu, W.-S., Lord, S., Kleist, D. T., Parrish, D. F., Derber, J. C., Treadon, R., Wu, W.-S. and Lord, S.: Introduction of the GSI into the NCEP Global Data Assimilation System, Weather Forecast., 24(6), 1691–1705, doi:10.1175/2009WAF2222201.1, 2009.

Krueger, A. J. and J., A.: Detection of volcanic eruptions from space by their sulfur dioxide clouds, Am. Inst. Aeronaut. Astronaut. Aerosp. Sci. Meet. 23rd, Reno, NV, Jan. 14-17, 1985. 5 p., 1985.

Kuhn, U., Ganzeveld, L., Thielmann, A., Dindorf, T., Schebeske, G., Welling, M., Sciare, J., Roberts, G., Meixner, F. X., Kesselmeier, J., Lelieveld, J., Kolle, O., Ciccioli, P., Lloyd, J., Trentmann, J., Artaxo, P. and Andreae, M. O.: Impact of Manaus City on the Amazon Green Ocean atmosphere: Ozone production, precursor sensitivity and aerosol load, Atmos. Chem. Phys., 10(19), 9251–9282, doi:10.5194/acp-10-9251-2010, 2010.

Levelt, P. F., van den Oord, G. H. J., Dobber, M. R., Malkki, A., Huib Visser, Johan de Vries, Stammes, P., Lundell, J. O. V. and Saari, H.: The ozone monitoring instrument, IEEE Trans. Geosci. Remote Sens., 44(5), 1093–1101, doi:10.1109/TGRS.2006.872333, 2006.

Li, C., Joiner, J., Krotkov, N. A. and Bhartia, P. K.: A fast and sensitive new satellite SO2 retrieval algorithm based on principal component analysis: Application to the ozone monitoring instrument, Geophys. Res. Lett., 40(23), 6314–6318, doi:10.1002/2013GL058134, 2013.

Li, C., Krotkov, N. A., Carn, S., Zhang, Y., Spurr, R. J. D. and Joiner, J.: New-generation NASA Aura Ozone Monitoring Instrument (OMI) volcanic SO2 dataset: algorithm description, initial results, and continuation with the Suomi-NPP Ozone Mapping and Profiler Suite (OMPS), Atmos. Meas. Tech., 10(2), 445–458, doi:10.5194/amt-10-445-2017, 2017.

Machado, L. A. T., Silva Dias, M. A. F., Morales, C., Fisch, G., Vila, D., Albrecht, R., Goodman, S. J., Calheiros, A. J. P., Biscaro, T., Kummerow, C., Cohen, J., Fitzjarrald, D., Nascimento, E. L., Sakamoto, M. S., Cunningham, C., Chaboureau, J.-P., Petersen, W. A., Adams, D. K., Baldini, L., Angelis, C. F., Sapucci, L. F., Salio, P., Barbosa, H. M. J., Landulfo, E., Souza, R. A. F., Blakeslee, R. J., Bailey, J., Freitas, S., Lima, W. F. A. and Tokay, A.: The Chuva Project: How Does Convection Vary across Brazil?, Bull. Am. Meteorol. Soc., 95(9), 1365–1380, doi:10.1175/BAMS-D-13-00084.1, 2014.

Malavelle, F. F., Haywood, J. M., Jones, A., Gettelman, A., Clarisse, L., Bauduin, S., Allan, R. P., Karset, I. H. H., Kristjánsson, J. E., Oreopoulos, L., Cho, N., Lee, D., Bellouin, N., Boucher, O., Grosvenor, D. P., Carslaw, K. S., Dhomse, S., Mann, G. W., Schmidt, A., Coe, H., Hartley, M. E., Dalvi, M., Hill, A. A., Johnson, B. T., Johnson, C. E., Knight, J. R., O'Connor, F. M., Partridge, D. G., Stier, P., Myhre, G., Platnick, S., Stephens, G. L., Takahashi, H. and Thordarson, T.: Strong constraints on aerosol–cloud interactions from volcanic eruptions, Nature, 546(7659), 485–491, doi:10.1038/nature22974, 2017.

Martin, S. T., Andreae, M. O., Artaxo, P., Baumgardner, D., Chen, Q., Goldstein, A. H., Guenther, A., Heald, C. L., Mayol-Bracero, O. L., McMurry, P. H., Pauliquevis, T., Pöschl, U., Prather, K. A., Roberts, G. C., Saleska, S. R., Silva Dias, M. A., Spracklen, D. V., Swietlicki, E. and Trebs, I.: Sources and properties of Amazonian aerosol particles, Rev. Geophys., 48(2), RG2002, doi:10.1029/2008RG000280, 2010.

Martin, S. T., Artaxo, P., Machado, L. A. T., Manzi, A. O., Souza, R. A. F., Schumacher, C., Wang, J., Andreae, M. O., Barbosa, H. M. J., Fan, J., Fisch, G., Goldstein, A. H., Guenther, A., Jimenez, J. L., Pöschl, U., Silva Dias, M. A., Smith, J. N. and Wendisch, M.: Introduction: Observations and Modeling of the Green Ocean Amazon (GoAmazon2014/5), Atmos. Chem. Phys., 16(8), 4785–4797, doi:10.5194/acp-16-4785-2016, 2016.

Martin, S. T., Artaxo, P., Machado, L., Manzi, A. O., Souza, R. A. F., Schumacher, C., Wang, J., Biscaro, T., Brito, J., Calheiros, A., Jardine, K., Medeiros, A., Portela, B., de Sá, S. S., Adachi, K., Aiken, A. C., Albrecht, R., Alexander, L., Andreae, M. O., Barbosa, H. M. J., Buseck, P., Chand, D., Comstock, J. M., Day, D. A., Dubey, M., Fan, J., Fast, J., Fisch, G., Fortner, E., Giangrande, S., Gilles, M., Goldstein, A. H., Guenther, A., Hubbe, J., Jensen, M., Jimenez, J. L., Keutsch, F. N., Kim, S., Kuang, C., Laskin, A., McKinney, K., Mei, F., Miller, M., Nascimento, R., Pauliquevis, T., Pekour, M., Peres, J., Petäjä, T., Pöhlker, C., Pöschl, U., Rizzo, L., Schmid, B., Shilling, J. E., Dias, M. A. S., Smith, J. N., Tomlinson, J. M., Tóta, J. and Wendisch, M.: The Green Ocean Amazon Experiment (GoAmazon2014/5) Observes Pollution Affecting Gases, Aerosols, Clouds, and Rainfall over the Rain Forest, Bull. Am. Meteorol. Soc., 98(5), 981–997, doi:10.1175/BAMS-D-15-00221.1, 2017.

Mather, T. A., Pyle, D. M. M. and Oppenheimer, C.: Tropospheric volcanic aerosol, in Volcanism Earth's atmosphere, pp. 189–212., 2003.

McNaughton, C. S., Clarke, A. D., Freitag, S., Kapustin, V. N., Kondo, Y., Moteki, N., Sahu, L., Takegawa, N., Schwarz, J. P., Spackman, J. R., Watts, L., Diskin, G., Podolske, J., Holloway, J. S., Wisthaler, A., Mikoviny, T., De Gouw, J., Warneke, C., Jimenez, J., Cubison, M., Howell, S. G., Middlebrook, A., Bahreini, R., Anderson, B. E., Winstead, E., Thornhill, K. L., Lack, D., Cozic, J. and Brock, C. A.: Absorbing aerosol in the troposphere of the Western Arctic during the 2008 ARCTAS/ARCPAC airborne field campaigns, Atmos. Chem. Phys., 11(15), 7561–7582, doi:10.5194/acp-11-7561-2011, 2011.

Müller, T., Laborde, M., Kassell, G. and Wiedensohler, A.: Design and performance of a three-wavelength LED-based total scatter and backscatter integrating nephelometer, Atmos. Meas. Tech., 4(6), 1291–1303, doi:10.5194/amt-4-1291-2011, 2011.

Ng, N. L., Herndon, S. C., Trimborn, A., Canagaratna, M. R., Croteau, P. L., Onasch, T. B., Sueper, D., Worsnop, D. R., Zhang, Q., Sun, Y. L. and Jayne, J. T.: An Aerosol Chemical Speciation Monitor (ACSM) for Routine Monitoring of the Composition and Mass Concentrations of Ambient Aerosol, Aerosol Sci. Technol., 45(7), 780–794, doi:10.1080/02786826.2011.560211, 2011.

Petzold, A. and Schönlinner, M.: Multi-angle absorption photometry—a new method for the measurement of aerosol light absorption and atmospheric black carbon, J. Aerosol Sci., 35(4), 421–441, doi:10.1016/j.jaerosci.2003.09.005, 2004.

Platt, U. and Stutz, J. (Jochen): Differential optical absorption spectroscopy : principles and applications, Springer Verlag., 2008.

Pöhlker, C., Walter, D., Paulsen, H., Könemann, T., Moran-Zuloaga, D., Pickersgill, D., Ditas, F., Saturno, J., Lammel, G., Després, V. R., Artaxo, P. and Andreae, M. O.: Technical Note: Back trajectory analysis, land cover footprints, and future perturbation trends in the upwind fetch of the ATTO site in the central Amazon, Atmos. Chem. Phys. Discuss., in preparation, 2017a.

Pöhlker, M. L., Pöhlker, C., Ditas, F., Klimach, T., Hrabe de Angelis, I., Araújo, A., Brito, J., Carbone, S., Cheng, Y., Chi, X., Ditz, R., Gunthe, S. S., Kesselmeier, J., Könemann, T., Lavrič, J. V., Martin, S. T., Mikhailov, E., Moran-Zuloaga, D., Rose, D., Saturno, J., Su, H., Thalman, R., Walter, D., Wang, J., Wolff, S., Barbosa, H. M. J., Artaxo, P., Andreae, M. O. and Pöschl, U.: Long-term observations of cloud condensation nuclei in the Amazon rain forest – Part 1: Aerosol size distribution, hygroscopicity, and new model parametrizations for CCN prediction, Atmos. Chem. Phys., 16(24), 15709–15740, doi:10.5194/acp-16-15709-2016, 2016.

Pöhlker, M. L., Ditas, F., Saturno, J., Klimach, T., Hrabě de Angelis, I., Araùjo, A., Brito, J., Carbone, S., Cheng, Y., Chi, X., Ditz, R., Gunthe, S. S., Kandler, K., Kesselmeier, J., Könemann, T., Lavrič, J. V., Martin, S. T., Mikhailov, E., Moran-Zuloaga, D., Rizzo, L. V., Rose, D., Su, H., Thalman, R., Walter, D., Wang, J., Wolff, S., Barbosa, H. M. J., Artaxo, P., Andreae, M. O., Pöschl, U. and Pöhlker, C.: Long-term observations of cloud condensation nuclei in the Amazon rain forest - Part 2: Variability and characteristic differences under near-pristine, biomass burning, and long-range transport conditions, Atmos. Chem. Phys. Discuss., 1–51, doi:10.5194/acp-2017-847, 2017b.

Reiner, T. and Arnold, F.: Laboratory investigations of gaseous sulfuric acid formation via SO 3 +H 2 O+M→H 2 SO 4 +M: Measurement of the rate constant and product identification, J. Chem. Phys., 101(9), 7399–7407, doi:10.1063/1.468298, 1994.

Richter, A. and Wagner, T.: The Use of UV, Visible and Near IR Solar Back Scattered Radiation to Determine Trace Gases, in The Remote Sensing of Tropospheric Composition from Space, Physics of Earth and Space Environments, ISBN 978-3-642-14790-6. Springer-Verlag Berlin Heidelberg, 2011, p. 67, edited by J. P. Burrows, P. Borrell, and U. Platt, pp. 67–121., 2011.

de Sá, S. S., Palm, B. B., Campuzano-Jost, P., Day, D. A., Newburn, M. K., Hu, W., Isaacman-VanWertz, G., Yee, L. D., Thalman, R., Brito, J., Carbone, S., Artaxo, P., Goldstein, A. H., Manzi, A. O., Souza, R. A. F., Mei, F., Shilling, J. E., Springston, S. R., Wang, J., Surratt, J. D., Alexander, M. L., Jimenez, J. L. and Martin, S. T.: Influence of urban pollution on the production of organic particulate matter from isoprene epoxydiols in central Amazonia, Atmos. Chem. Phys., 17(11), 6611–6629, doi:10.5194/acp-17-6611-2017, 2017.

Saturno, J., Holanda, B. A., Pöhlker, C., Ditas, F., Wang, Q., Morán-Zuloaga, D., Brito, J., Carbone, S., Cheng, Y., Chi, X., Ditas, J., Hoffmann, T., Hrabě de Angelis, I., Könemann, T., Lavrič, J. V., Ma, N., Ming, J., Paulsen, H., Pöhlker, M. L., Rizzo, L. V., Schlag, P., Su, H., Walter, D., Wolff, S., Zhang, Y., Artaxo, P., Pöschl, U. and Andreae, M. O.: Black and brown carbon over central Amazonia: Long-term aerosol measurements at the ATTO site, Atmos. Chem. Phys. Discuss., submitted, 2017.

Stein, A. F., Draxler, R. R., Rolph, G. D., Stunder, B. J. B., Cohen, M. D. and Ngan, F.: NOAA's HYSPLIT Atmospheric Transport and Dispersion Modeling System, Bull. Am. Meteorol. Soc., 96(12), 2059–2077, doi:10.1175/BAMS-D-14-00110.1, 2015.

Stephens, M., Turner, N. and Sandberg, J.: Particle Identification by Laser-Induced Incandescence in a Solid-State Laser Cavity, Appl. Opt., 42(19), 3726, doi:10.1364/AO.42.003726, 2003.

Stevens, B. and Feingold, G.: Untangling aerosol effects on clouds and precipitation in a buffered system., Nature, 461(7264), 607–613, doi:10.1038/nature08281, 2009.

Talbot, R. W., Andreae, M. O., Andreae, T. W. and Harriss, R. C.: Regional aerosol chemistry of the Amazon Basin during the dry season, J. Geophys. Res., 93(D2), 1499, doi:10.1029/JD093iD02p01499, 1988.

Wang, Q., Saturno, J., Chi, X., Walter, D., Lavric, J. V., Moran-Zuloaga, D., Ditas, F., Pöhlker, C., Brito, J., Carbone, S., Artaxo, P. and Andreae, M. O.: Modeling investigation of light-absorbing aerosols in the Amazon Basin during the wet season, Atmos. Chem. Phys., 16(22), 14775–14794, doi:10.5194/acp-16-14775-2016, 2016.

Wendisch, M., Pöschl, U., Andreae, M. O., Machado, L. A. T., Albrecht, R., Schlager, H., Rosenfeld, D., Martin, S. T., Abdelmonem, A., Afchine, A., Araùjo, A. C., Artaxo, P., Aufmhoff, H.,

Barbosa, H. M. J., Borrmann, S., Braga, R., Buchholz, B., Cecchini, M. A., Costa, A., Curtius, J., Dollner, M., Dorf, M., Dreiling, V., Ebert, V., Ehrlich, A., Ewald, F., Fisch, G., Fix, A., Frank, F., Fütterer, D., Heckl, C., Heidelberg, F., Hüneke, T., Jäkel, E., Järvinen, E., Jurkat, T., Kanter, S., Kästner, U., Kenntner, M., Kesselmeier, J., Klimach, T., Knecht, M., Kohl, R., Kölling, T., Krämer, M., Krüger, M., Krisna, T. C., Lavric, J. V., Longo, K., Mahnke, C., Manzi, A. O., Mayer, B., Mertes, S., Minikin, A., Molleker, S., Münch, S., Nillius, B., Pfeilsticker, K., Pöhlker, C., Roiger, A., Rose, D., Rosenow, D., Sauer, D., Schnaiter, M., Schneider, J., Schulz, C., de Souza, R. A. F., Spanu, A., Stock, P., Vila, D., Voigt, C., Walser, A., Walter, D., Weigel, R., Weinzierl, B., Werner, F., Yamasoe, M. A., Ziereis, H., Zinner, T. and Zöger, M.: ACRIDICON–CHUVA Campaign: Studying Tropical Deep Convective Clouds and Precipitation over Amazonia Using the New German Research Aircraft HALO, Bull. Am. Meteorol. Soc., 97(10), 1885–1908, doi:10.1175/BAMS-D-14-00255.1, 2016.

Yang, Y., Wang, H., Smith, S. J., Easter, R., Ma, P., Qian, Y., Yu, H., Li, C. and Rasch, P. J.: Global source attribution of sulfate concentration and direct and indirect radiative forcing, Atmos. Chem. Phys., 17(14), 8903–8922, doi:10.5194/acp-17-8903-2017, 2017.

Yuan, T., Remer, L. A. and Yu, H.: Microphysical, macrophysical and radiative signatures of volcanic aerosols in trade wind cumulus observed by the A-Train, Atmos. Chem. Phys., 11(14), 7119–7132, doi:10.5194/acp-11-7119-2011, 2011.

Atmos. Chem. Phys. Discuss., https://doi.org/10.5194/acp-2017-1152
Manuscript under review for journal Atmos. Chem. Phys.
This is just a preview and not the published paper.

Atmospheric Chemistry and Physics Discussions

Table 1. Measurements at points along track of the flight AC14 (21 September 2014) selected as starting points for backward trajectories presented in Fig. 6. Data points with sulfate-to-OA > 1 are emphasized by bold font.

Time (UTC)	Latitude [°N]	Longitude [°E]	Altitude [km]	$M_{sulfate}$ [μg m^{-3}]	Sulfate-to-OA	Color in Fig. 6
15:14	-2.75	-60.34	1.61	1.2	0.5	Gray
16:19	**-3.19**	**-60.21**	**4.50**	**1.0**	**1.1**	**Blue**
16:36	**-4.00**	**-59.50**	**4.50**	**3.0**	**2.9**	**Green**
16:54	**-5.20**	**-59.25**	**4.49**	**3.1**	**7.8**	**Red**
17:11	-6.45	-58.98	6.45	0.6	0.8	Gray
17:46	-4.52	-59.40	6.43	0.5	0.8	Gray
19:40	-4.44	-59.41	7.68	1.2	1.0	Gray
21:41	**-3.79**	**-59.55**	**4.79**	**1.8**	**2.2**	**Light blue**
21:59	-3.04	-60.20	0.90	1.2	0.3	Gray

Atmos. Chem. Phys. Discuss., https://doi.org/10.5194/acp-2017-1152
Manuscript under review for journal Atmos. Chem. Phys.
This is just a preview and not the published paper.

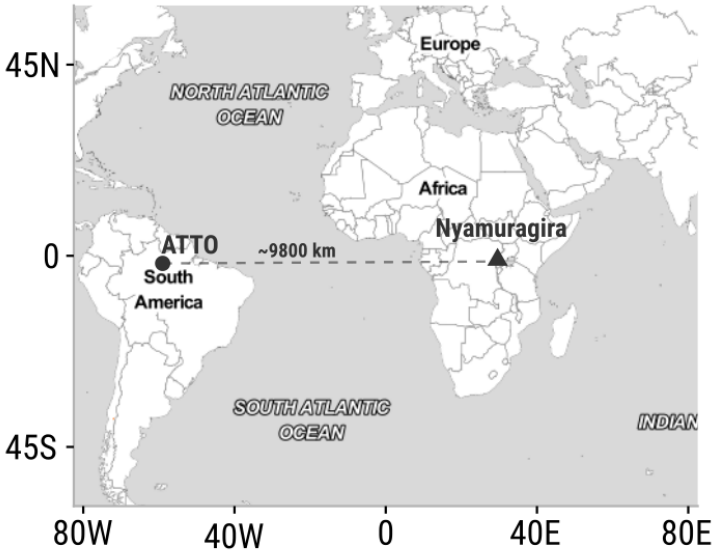

Figure 1. ATTO site and Nyamuragira volcano locations.

Atmos. Chem. Phys. Discuss., https://doi.org/10.5194/acp-2017-1152
Manuscript under review for journal Atmos. Chem. Phys.
This is just a preview and not the published paper.

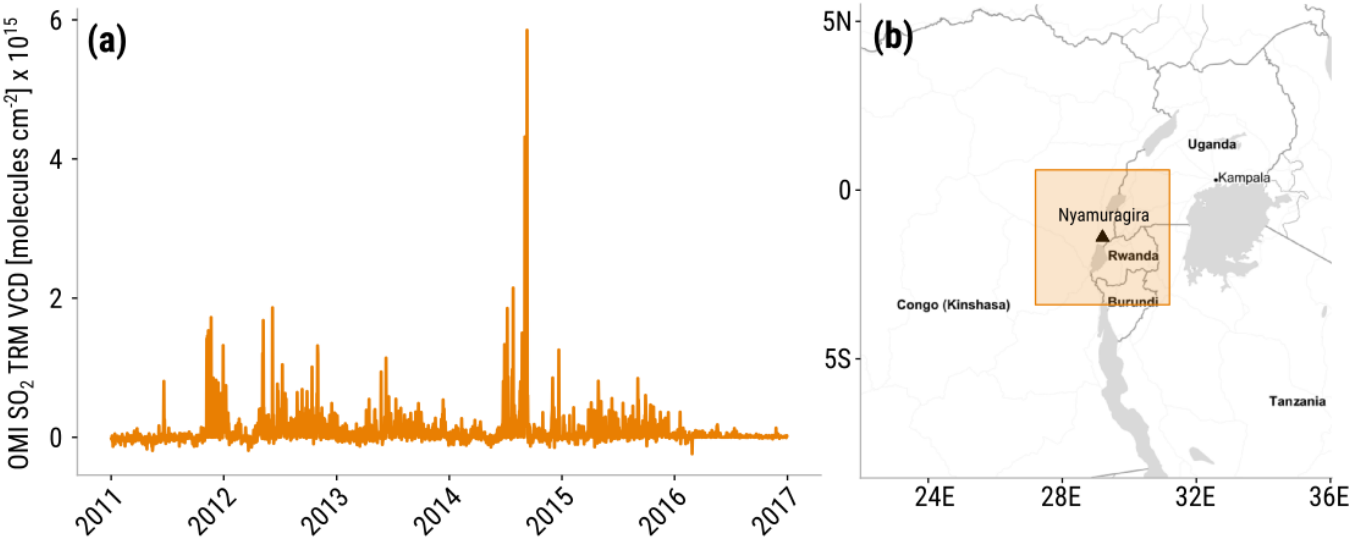

Figure 2. (a) Time series of daily-averaged OMI SO_2 TRM VCD observations corresponding to the averages over the area delimited by 27.2° E, 3.4° S, 31.2° E, and 0.6° N (b). Map of eastern Africa showing the averaging area (orange square). The location of Nyamuragira is represented by a black triangle.

Atmos. Chem. Phys. Discuss., https://doi.org/10.5194/acp-2017-1152
Manuscript under review for journal Atmos. Chem. Phys.
This is just a preview and not the published paper.

Atmospheric Chemistry and Physics Discussions

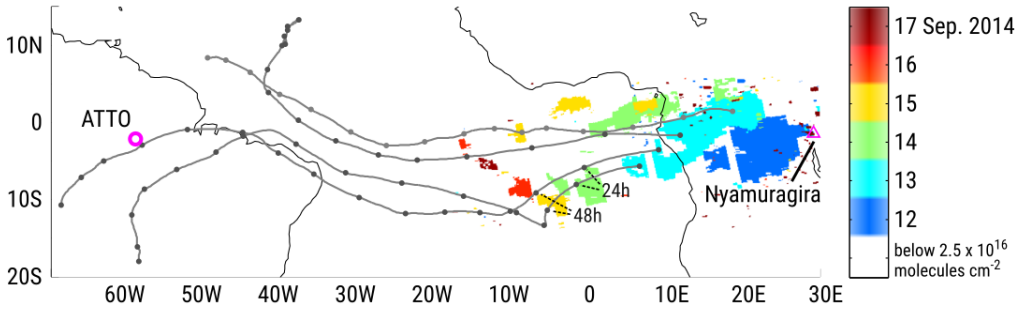

Figure 3. Map of SO_2 plumes with VCD > 2.5 × 10^{16} molecules cm^{-2} color-coded by date of observation. Forward trajectories started at 4 km (above mean sea level, a.m.s.l.) at four locations within the plume detected on 13 September 2014 (light blue) are indicated by black lines with markers at 24-hour intervals. The ATTO site is marked by a pink circle; the location of Nyamuragira is indicated by a pink triangle.

Atmos. Chem. Phys. Discuss., https://doi.org/10.5194/acp-2017-1152
Manuscript under review for journal Atmos. Chem. Phys.
This is just a preview and not the published paper.

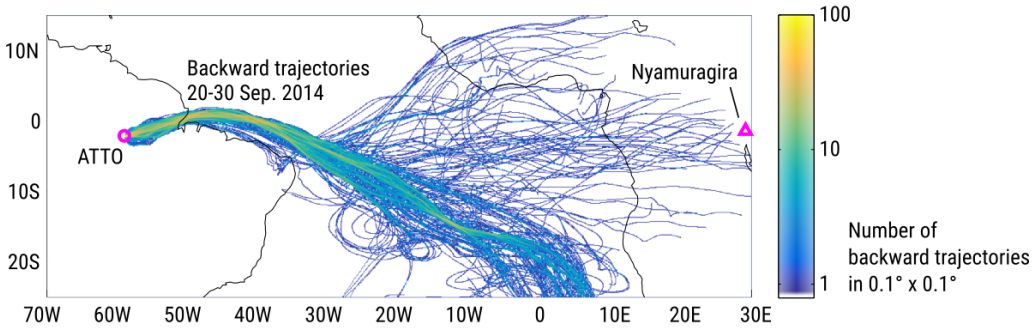

Figure 4. Density of backward trajectories started from ATTO at an altitude of 300 m a.m.s.l. on every hour starting at 0:00 UTC on 20 September 2014 up to 23:00 UTC on 30 September 2014. The locations of the ATTO site and Nyamuragira are shown on the map.

Atmos. Chem. Phys. Discuss., https://doi.org/10.5194/acp-2017-1152
Manuscript under review for journal Atmos. Chem. Phys.
This is just a preview and not the published paper.

Atmospheric Chemistry and Physics Discussions

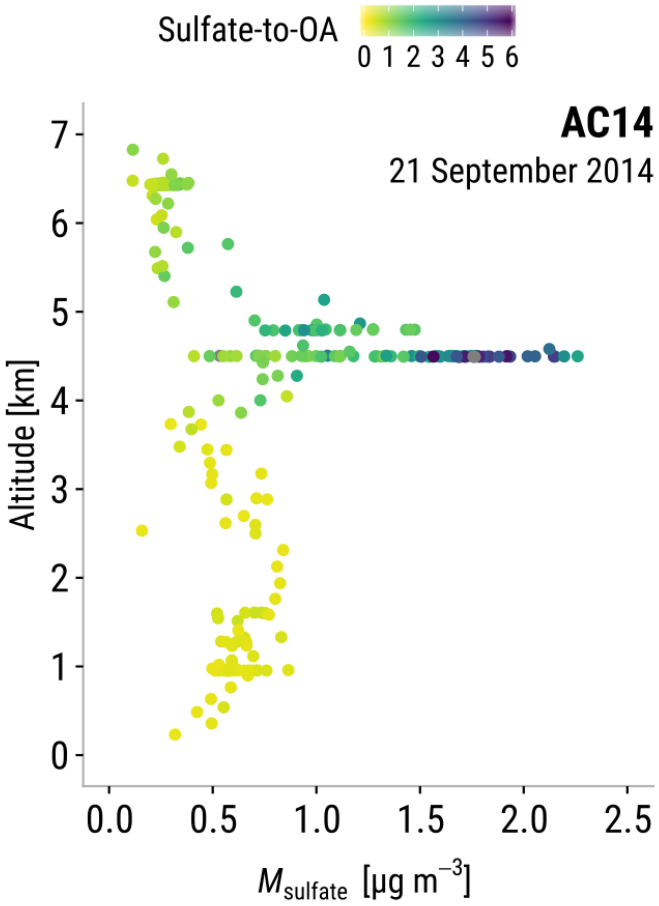

Figure 5. Sulfate layer observations over the Amazon rain forest. The figure shows the $M_{sulfate}$ vertical profile observed during flight AC14 (21 September 2014). Color-coded sulfate-to-OA values are truncated at a maximum of 6.

Atmos. Chem. Phys. Discuss., https://doi.org/10.5194/acp-2017-1152
Manuscript under review for journal Atmos. Chem. Phys.
This is just a preview and not the published paper.

Atmospheric Chemistry and Physics Discussions

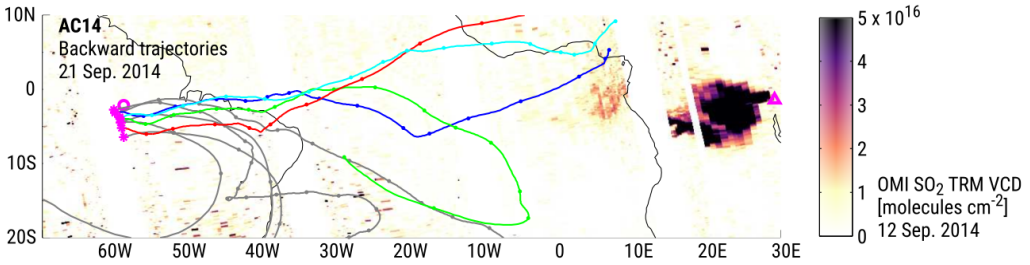

Figure 6. Map of gridded OMI SO_2 VCD, observed on 12 September 2014. Backward trajectories were started at several points along track of the flight AC14 (21 September 2014) at flight altitude. Trajectories starting at points where sulfate-to-OA > 1 are shown in color (see Table 1 for details), all other trajectories are shown in gray; dots are placed at 24-hour intervals. The path of flight AC14 is marked in pink, with stars denoting the starting points of the backward trajectories. The locations of the ATTO site and Nyamuragira are marked with a pink circle and triangle, respectively.

Atmos. Chem. Phys. Discuss., https://doi.org/10.5194/acp-2017-1152
Manuscript under review for journal Atmos. Chem. Phys.
This is just a preview and not the published paper.

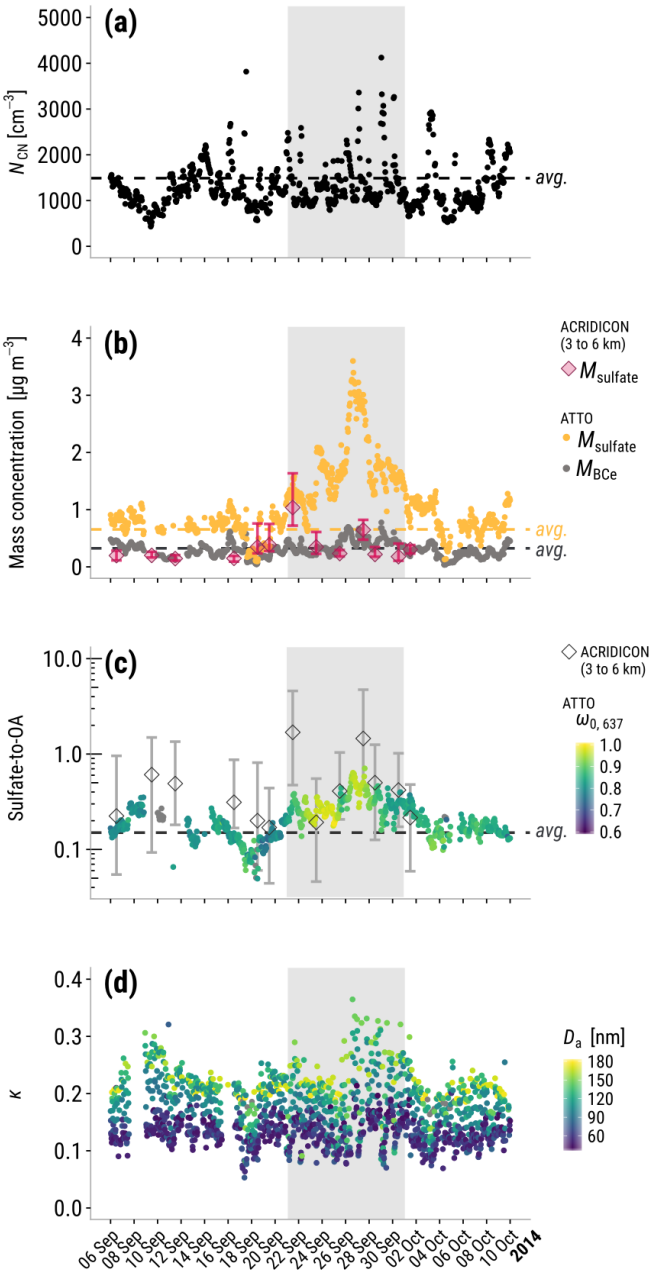

Figure 7. Different aerosol properties measured during the Nya2014 event (gray shaded area), These time series include ATTO hourly averages of (a) aerosol particle number concentration, N_{CN}, (b) sulfate and BC_e mass concentration, (c) sulfate-to-OA mass ratio with color-coded aerosol particle single scattering albedo at 637 nm wavelength, and (d) hygroscopicity parameter, κ, original time resolution, with color-coded particle activation diameter. Dry season averages are shown as dashed lines. ACRIDICON-CHUVA flight medians and inter-quartile ranges from 3 to 6 km altitude are shown in (b) and (c).

Supplement to

African volcanic emissions influencing atmospheric aerosol particles over the Amazon rain forest

Jorge Saturno[1], Florian Ditas[1], Marloes Penning de Vries[1], Bruna A. Holanda[1], Mira L. Pöhlker[1], Samara Carbone[2,3], David Walter[1], Nicole Bobrowski[4,1], Joel Brito[2,5], Xuguang Chi[6], Alexandra Gutmann[7], Isabella Hrabe de Angelis[1], Luiz A. T. Machado[8], Daniel Moran-Zuloaga[1], Julian Rüdiger[9], Johannes Schneider[1], Christiane Schulz[1], Qiaoqiao Wang[10], Manfred Wendisch[11], Paulo Artaxo[2], Thomas Wagner[1], Ulrich Pöschl[1], Meinrat O. Andreae[1,12], and Christopher Pöhlker[1]

[1]Biogeochemistry, Multiphase Chemistry, and Particle Chemistry Departments, and Satellite Research Group, Max Planck Institute for Chemistry, P. O. Box 3060, 55020 Mainz, Germany
[2]Department of Applied Physics, Institute of Physics, University of São Paulo (USP), Rua do Matão, Travessa R, 187, CEP 05508-900, São Paulo, SP, Brazil
[3]Institute of Agrarian Sciences, Federal University of Uberlândia, Uberlândia, Minas Gerais, Brazil
[4]Institute for Environmental Physics, University of Heidelberg, Heidelberg, Germany
[5]Laboratory for Meteorological Physics, Université Clermont Auvergne, Clermont-Ferrand, France
[6]Institute for Climate and Global Change Research & School of Atmospheric Sciences, Nanjing University, Nanjing, 210093, China
[7]Department of Chemistry, Johannes Gutenberg University, Mainz, Germany
[8]Centro de Previsão de Tempo e Estudos Climáticos, Instituto Nacional de Pesquisas Espaciais, Cachoeira Paulista, Brazil
[9]Atmospheric Chemistry, University of Bayreuth, Dr.-Hans-Frisch-Straße 1–3, 95448 Bayreuth, Germany
[10]Institute for Environmental and Climate Research, Jinan University, Guangzhou, 511443, China
[11]Leipziger Institut für Meteorologie (LIM), Universität Leipzig, Stephanstr. 3, 04103 Leipzig, Germany
[12]Scripps Institution of Oceanography, University of California San Diego, La Jolla, CA 92098, USA

Correspondence to: Jorge Saturno (j.saturno@mpic.de) and Christopher Pöhlker (c.pohlker@mpic.de)

This file includes:

Figures S1 to S6.
Tables S1 to S2.

Supplementary information

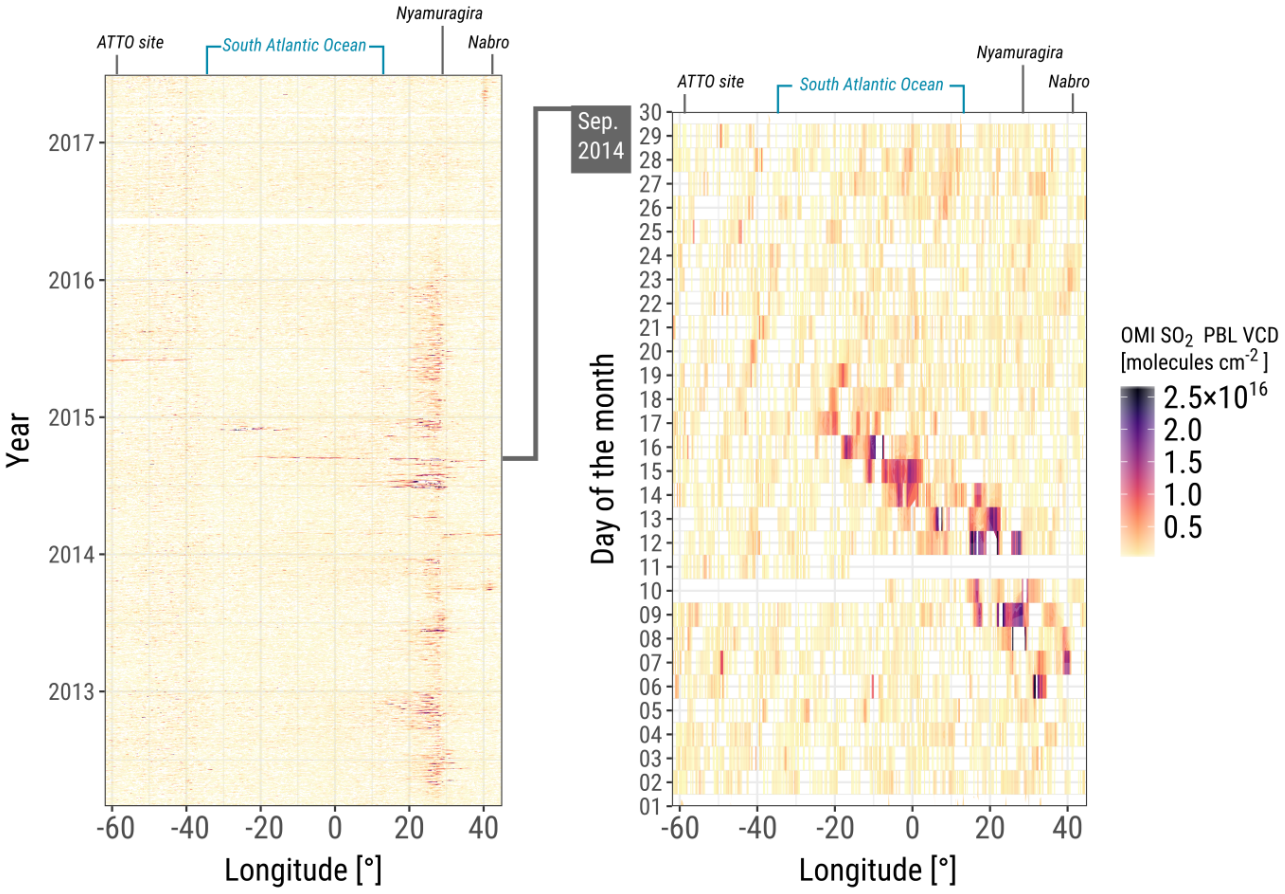

Figure S1. Planetary boundary layer (PBL) OMI SO_2 VCD Hovmöller plots corresponding to a latitude daily average (11° S to 17° N) from March 2012 to July 2017 (left), and September 2014 (right). The VCD color scale was truncated at 2.5×10^{16} molecules cm^{-2} to improve visualization. The longitude location of two active degassing volcanoes in Africa, Nyamuragira and Nabro, the ATTO site, and the approximate west to east extension of the South Atlantic Ocean are indicated at the top of the plots. **Note:** The absolute SO_2 VCD values provided here might be overestimated given that they are calculated for PBL heights and the plume was emitted above 3 km a.m.s.l.

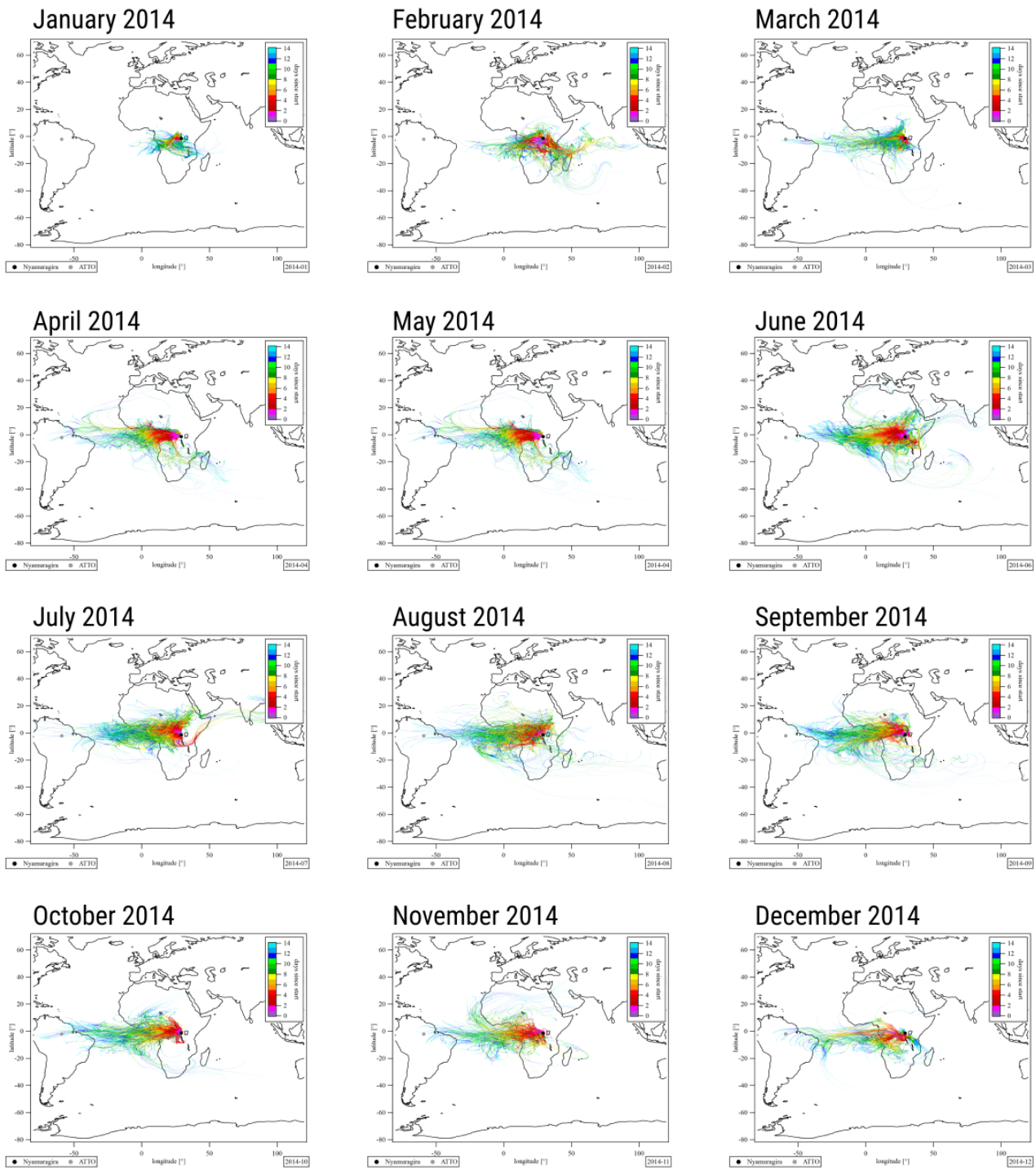

Figure S2. Calculated HYSPLIT 14-day forward trajectories corresponding to each month of 2014. The starting location and height are the Nyamuragira volcano and 3200 m a.m.s.l., respectively.

142

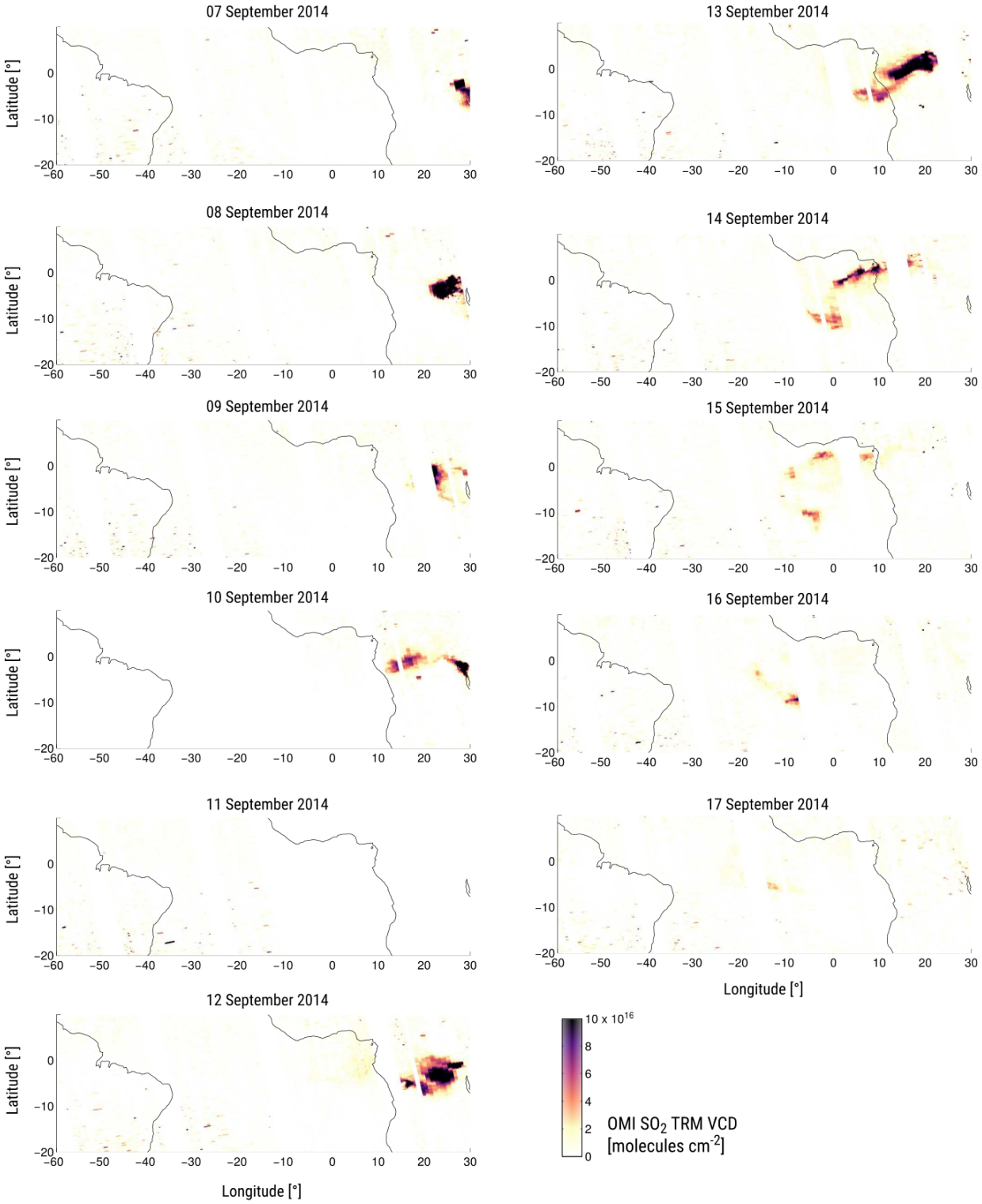

Figure S3. Maps of gridded OMI SO_2 TRM VCD observations corresponding to 7 to 17 September 2014.

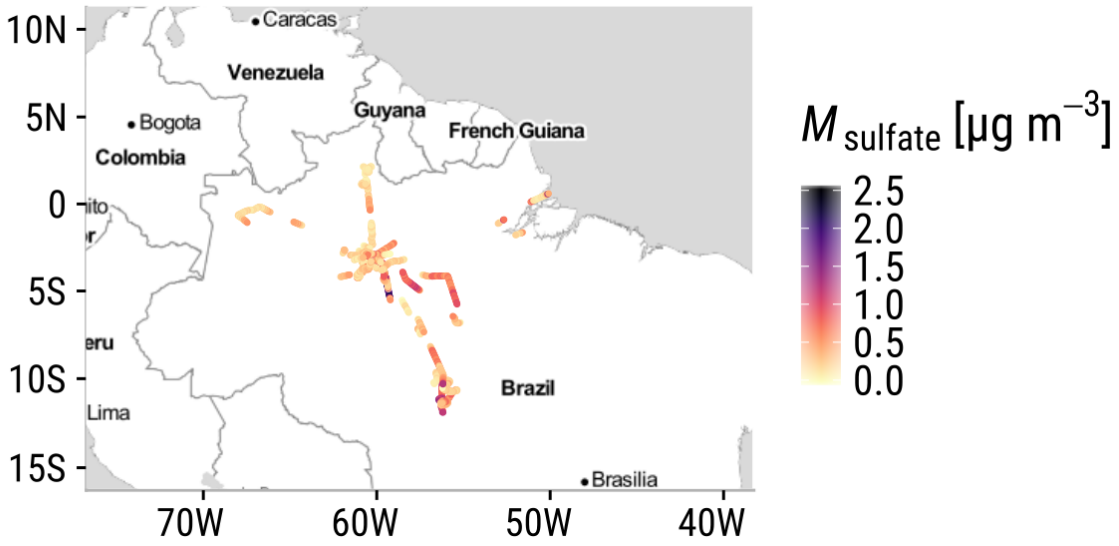

Figure S4. Map of $M_{sulfate}$ observations between 3 and 6 km height during the ACRIDICON-CHUVA campaign over the Amazon Basin. Data from different flights from 6 September to 1 October 2014 are included.

144

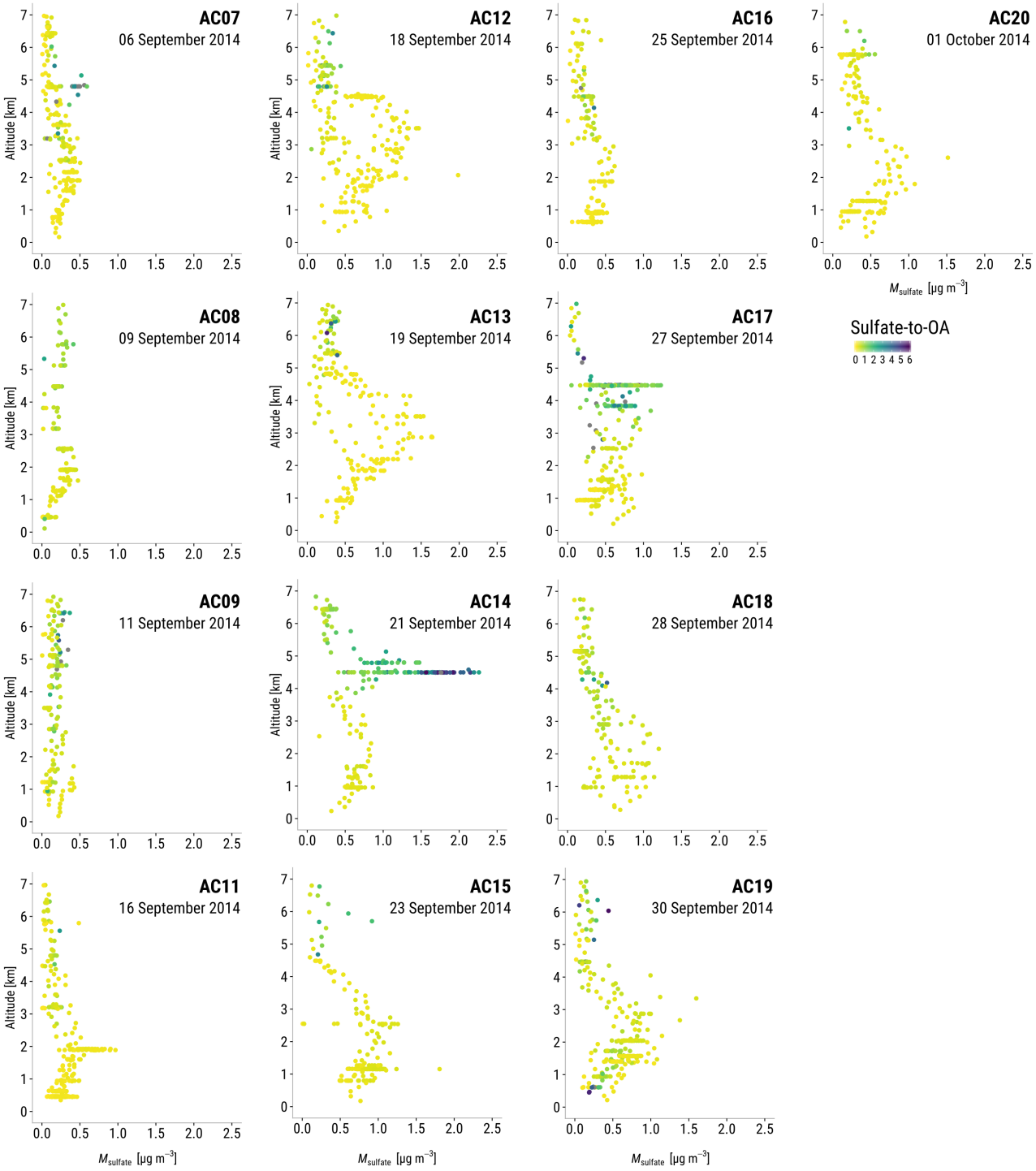

Figure S5. Sulfate mass concentration vertical profiles with color coded sulfate-to-OA mass ratios observed during different ACRIDICON-CHUVA flights over the Amazon Basin.

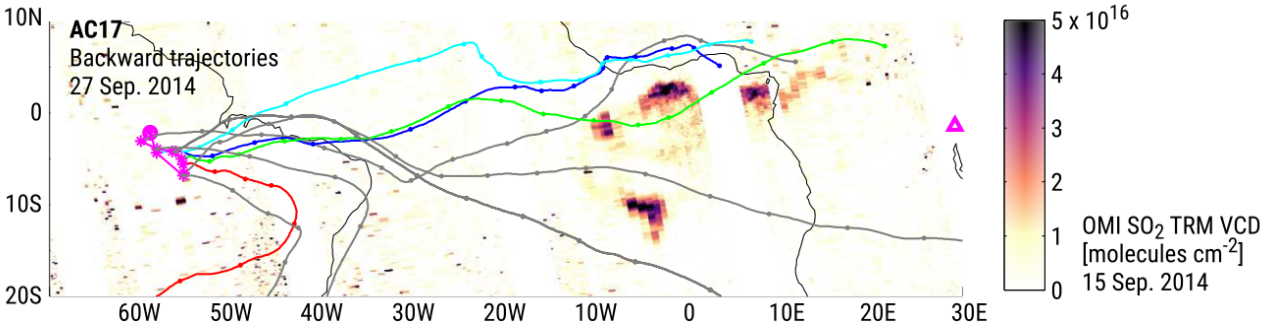

Figure S6. Map of gridded OMI SO_2 VCD, observed on 15 September 2014. Backward trajectories were started at several points along the ACRIDICON-CHUVA flight track AC17 (27 September 2014) at flight altitude. Trajectories starting at points where sulfate-to-OA > 1 are shown in color (see Table S2 for details), all other trajectories are shown in gray; dots are placed at 24-hour intervals. The path of flight AC14 is marked in pink, with stars denoting the starting points of the backward trajectories. The locations of the ATTO site and Nyamuragira are marked with a pink circle and triangle, respectively.

Table S1. List of ACRIDICON-CHUVA campaign flights and their dates.

Flight	Date
AC07	6 Sep 2014
AC08	9 Sep 2014
AC09	11 Sep 2014
AC11	16 Sep 2014
AC12	18 Sep 2014
AC13	19 Sep 2014
AC14	21 Sep 2014
AC15	23 Sep 2014
AC16	25 Sep 2014
AC17	27 Sep 2014
AC18	28 Sep 2014
AC19	30 Sep 2014
AC20	01 Oct 2014

Table S2. Measurements at points along the track of flight AC17 (27 September 2014) selected as starting points for backward trajectories presented in Fig. S6. Data points with sulfate-to-OA > 1 are emphasized by bold font.

Time (UTC)	Latitude [°N]	Longitude [°E]	Altitude [km]	$M_{sulfate}$ [μg m^{-3}]	Sulfate-to-OA	Color in Fig. S6
14:06	-3.04	-60.00	0.93	0.2	0.1	Gray
14:33	-3.90	-58.24	8.07	0.2	0.2	Gray
15:02	-4.20	-56.22	0.94	0.3	0.1	Gray
16:14	**-4.22**	**-56.60**	**3.84**	**1.6**	**1.5**	**Blue**
16:37	**-5.02**	**-55.58**	**4.48**	**1.5**	**11.5**	**Green**
16:45	**-5.61**	**-55.38**	**4.47**	**1.5**	**6.8**	**Red**
16:59	-6.55	-55.29	1.25	0.6	0.1	Gray
18:09	-6.83	-55.41	4.48	0.6	0.9	Gray
18:59	**-4.35**	**-58.31**	**4.47**	**1.5**	**1.7**	**Light blue**
19:54	-2.06	-59.06	1.57	0.8	0.3	Gray

148